PHOTOCHEMICAL FORMATION AND COST-EFFICIENT ABATEMENT OF OZONE: HIGH ORDER SENSITIVITY ANALYSIS

A Dissertation
Presented to
The Academic Faculty

By

Daniel S. Cohan

In Partial Fulfillment
Of the Requirements for the Degree
Doctor of Philosophy in the
School of Earth and Atmospheric Sciences

Georgia Institute of Technology

December, 2004

Photochemical Formation and Cost-efficient Abatement of Ozone:
High Order Sensitivity Analysis

Approved by:

William L. Chameides

Armistead G. Russell

Michael E. Chang

Yuhang Wang

Doug Noonan

September 3, 2004

To my wife and family for their support on this journey

ACKNOWLEDGEMENT

I am deeply appreciative of tremendous support from numerous people during my Ph.D. studies. My advisor, Professor Ted Russell, has provided insightful guidance and fostered a collegial and productive environment in his research group. Current and former members of that group—especially Amir Hakami, Yongtao Hu, Alper Unal, Talat Odman, Michelle Bergin, Jim Boylan, Maudood Khan, Amit Marmur, Di Tian, and others—greatly assisted this research, and their friendship enriched my graduate school experience. I thank Professors Bill Chameides, Yuhang Wang, Michael Chang, and Douglas Noonan for taking the time to serve on my thesis committee and for helpful discussions along the way. My research has also benefited from conversations with Larry Sorrels (U.S. EPA), Steve Ewald (Georgia Power), Allen Greenberg (U.S. Federal Highway Administration), Roderick Duncan, Randy Guensler, and staff members of the Georgia Environmental Protection Division. I also thank Professor Daniel Jacob (Harvard University), whose mentorship brought me to this field. Above all I have been blessed by the tremendous love, patience, support, and even copyediting of my wife, Sandi, and by the continual encouragement of my family.

Research for this dissertation was conducted with funding from the Environmental Protection Division of the Georgia Department of Natural Resources through the Fall-Line Air Quality Study, and from the U.S. Environmental Protection Agency (grants R-82897601 and RD-83096001). My graduate studies were also supported by a National Science Foundation Graduate Research Fellowship, a Georgia Tech Presidential Scholarship, and a Georgia Air & Waste Management Association Scholarship.

TABLE OF CONTENTS

LIST OF TABLES

LIST OF FIGURES

LIST OF NOMENCLATURE

Abbreviations

CMAQ	Community Multiscale Air Quality Model
EPA	Environmental Protection Agency
FAQS	Fall-Line Air Quality Study
(H)DDM-3D	(high-order) Decoupled Direct Method in Three Dimensions
IPCC	Intergovernmental Panel on Climate Change
NAAQS	National Ambient Air Quality Standards
NO_x	nitrogen oxides ($NO + NO_2$)
NO_x SIP Call	NO_x State Implementation Plan Call
NO_y	total reactive, oxidized nitrogen
NO_z	reaction products of NO_x ($NO_z = NO_y - NO_x$)
NRC	National Research Council
SC	source contribution
SIP	state implementation plan
VOC	volatile organic compounds

Symbols

A	surface area
C	concentrations of atmospheric constituents
d	distance
E	emissions
OAE	ozone accumulation efficiency
OPE	ozone production efficiency
p	a sensitivity parameter
P	unperturbed (base case) value of parameter p
ppb	parts per billion
ppm	parts per million
ppt	parts per trillion
$\mathbf{S}_j^{(1)}$	first-order semi-normalized sensitivity coefficients
$\mathbf{S}_{j,k}^{(2)}$	second-order semi-normalized sensitivity coefficients
$\alpha_{i,j}$	non-linearity index
ε	scaling variable for a sensitivity parameter (nominal value 1)
$\Delta\varepsilon$	fractional change in a sensitivity parameter

CHAPTER 1

INTRODUCTION

1.1. Context and Motivation

Though most ozone resides in the stratosphere providing a shield against ultraviolet solar radiation, tropospheric ozone is a significant constituent of photochemical smog, harming human health (Brunekreef and Holgate, 2002) and vegetation (Fuhrer, 2002) while acting as a greenhouse gas (IPCC, 2001). Exposure to high concentrations of ozone may foster or exacerbate asthma and cause inflammation and reduced air capacity of the lungs (Koren, 1995; Brunekreef and Holgate, 2002; McConnell *et al.*, 2002). Ozone is also a source of regulatory headaches, as large sections of California and the eastern United States exceed federal standards despite years of costly abatement efforts (Lin *et al.*, 2001; Bell and Ellis, 2003). Implementing more stringent 8-hour National Ambient Air Quality Standards (NAAQS) for ozone, the U.S. Environmental Protection Agency in 2004 designated non-attainment status to 474 counties (U.S.-EPA, 2004b), including many small and mid-sized metropolitan areas that never before had been found to violate air quality standards. Federal requirements and other economic costs associated with non-attainment are substantial, as are the costs of emissions abatement (Henderson, 1996).

The complexity of ozone formation complicates the development of control strategies. Ozone is not emitted directly but instead forms from complex nonlinear interactions involving its precursor gases, principally nitrogen oxides (NO_x) and volatile

organic compounds (VOC) (Figure 1.1). The responsiveness of ozone to precursor controls varies in both time and space depending on meteorological conditions, emissions densities, and other factors. In NO_x-limited regions with high VOC and low NO_x concentrations (point B in Figure 1.1), such as forested rural areas with abundant biogenic emissions of VOC, ozone may decline with reductions in NO_x emissions but show little responsiveness to VOC. By contrast, urban centers with intense NO_x emissions may be sensitive primarily to VOC emissions and may experience adverse responsiveness to NO_x controls (VOC-limited or "NO_x-inhibited" regime, point A). Transitional conditions of dual sensitivity also occur, and a location's regime may shift with meteorological conditions (Jacob *et al.*, 1995). Even among NO_x-limited locations, the propensity of NO_x to form ozone can vary by source (Liu *et al.*, 1987; Ryerson *et al.*, 2001). Costs of emission control

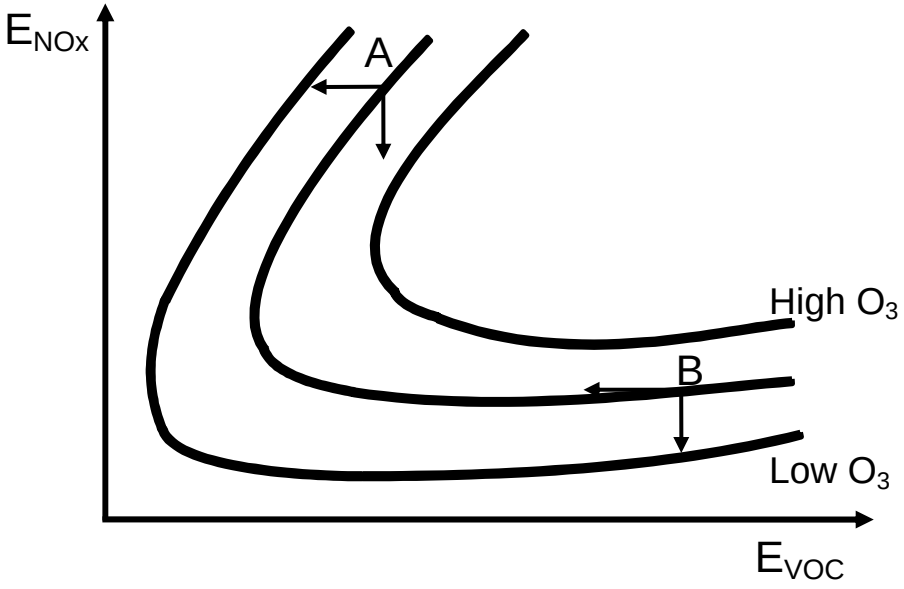

Figure 1.1. Schematic of ozone concentrations under various NO_x and VOC emissions. The isopleths represent constant ozone concentrations. Point A represents a VOC-limited and NO_x-inhibited ozone production regime, whereas Point B is NO_x-limited.

vary widely as well (e.g, Pechan, 2002), and political realities and other considerations can constrain the feasibility of control options (NRC, 2004).

The combination of scientific and economic complexities suggests that integrated approaches may be necessary to inform the identification of sensible ozone abatement policies. Too often, however, scientific and economic analyses of ozone abatement have been conducted in vacuums. Many atmospheric modeling studies have examined how pollutant concentrations would respond to large uniform reductions in domain-wide emission rates, neglecting to examine the percentage of reduction that is feasible. Given the nonlinearity and spatial heterogeneity of ozone formation, these modeling results are not necessarily applicable to state and regional policy makers choosing strategies from limited local control options. This is particularly true as the regulatory structures focus on local controls to be added to regional and nationwide regulations.

The Fall-Line Air Quality Study (FAQS), conducted by the Georgia Institute of Technology with funding from the Georgia Department of Natural Resources and Georgia Department of Transportation, was motivated in part by the desire to break down some of the barriers between science and policy considerations. Public meetings with stakeholders and ongoing communication between scientists and state officials have been incorporated along with cutting-edge observational and model-based scientific exploration throughout the project. FAQS focuses on air quality in the Georgia cities of Columbus, Macon, and Augusta, all of which appeared to be in jeopardy of violating the impending 8-hour ozone NAAQS when the project was initially launched; the Atlanta

region is considered as well because of its own history of air quality violations and to investigate its potential to influence the nearby cities. Since the onset of FAQS, ozone concentrations within Columbus and Augusta have fallen sufficiently to attain NAAQS, but Macon was designated non-attainment in 2004. Regaining attainment status in Macon and Atlanta and maintaining attainment in Columbus and Augusta have important consequences for human and ecological health and economic growth.

The FAQS region and surrounding states also represent an interesting laboratory for scientific investigation, given the sharp contrast between urban and rural emissions densities against a backdrop of rich biogenic VOC emissions. The warm climate of the southeastern U.S. is conducive to ozone formation, especially during stagnant summertime episodes (Altshuller, 1978). Thus the region has long attracted scientific interest as a case study for examining ozone formation (e.g., Sillman *et al.*, 1995; Meagher *et al.*, 1998), although rarely have small and mid-sized cities been the focus of examination.

1.2. Sensitivity Analysis

For policy-oriented applications, one must consider not only ozone concentrations but also the sensitivity of those concentrations to changes in emission rates. A variety of tools have been applied to address ozone sensitivity, with observational studies and photochemical modeling serving as complementary approaches. On the observational side, a large body of research has sought to identify species indicator ratios which signal whether ozone formed under NO_x- or VOC-limited conditions (Sillman, 1999). Other studies have followed the photochemical evolution of plumes of air either through flight-

based measurements (e.g., Ryerson *et al.*, 2001) or smog chamber experimentation (e.g., Paulson *et al.*, 1992).

Because continually changing meteorological conditions negate the possibility of a controlled atmospheric experiment to directly test ozone responsiveness, scientists use photochemical models to simulate the likely impacts of emission perturbations. Traditionally, responsiveness or "sensitivity" has been determined by a "brute force" method in which pollutant concentrations are compared across multiple photochemical model simulations which are identical except for a change in emission rates (Figure 1.2). However, this method becomes cumbersome when sensitivities to a large number of emissions sources must be calculated. Further, because ozone response to emission perturbations is nonlinear (Lin *et al.*, 1988), it may be inappropriate to scale ozone response computed for one fractional perturbation to other perturbations.

The Decoupled Direct Method in Three Dimensions (DDM-3D) (Dunker, 1981; Yang *et al.*, 1997) enables sensitivities to multiple emission rates or other parameters to be computed within a single model simulation, applying the same model formulations used to calculate concentrations. The recent extension of DDM-3D to compute higher-order sensitivity coefficients (Hakami *et al.*, 2003a) has enabled exploration of the nonlinearity of ozone responsiveness. Consideration of first- and higher-order sensitivity coefficients in Taylor expansions has been demonstrated as a method for simulating ozone response to a wide range of perturbations (Hakami *et al.*, 2003a). However, given the short tenure of HDDM-3D, its power has only begun to be applied to scientific investigation of pollutant formation and to informing policy development.

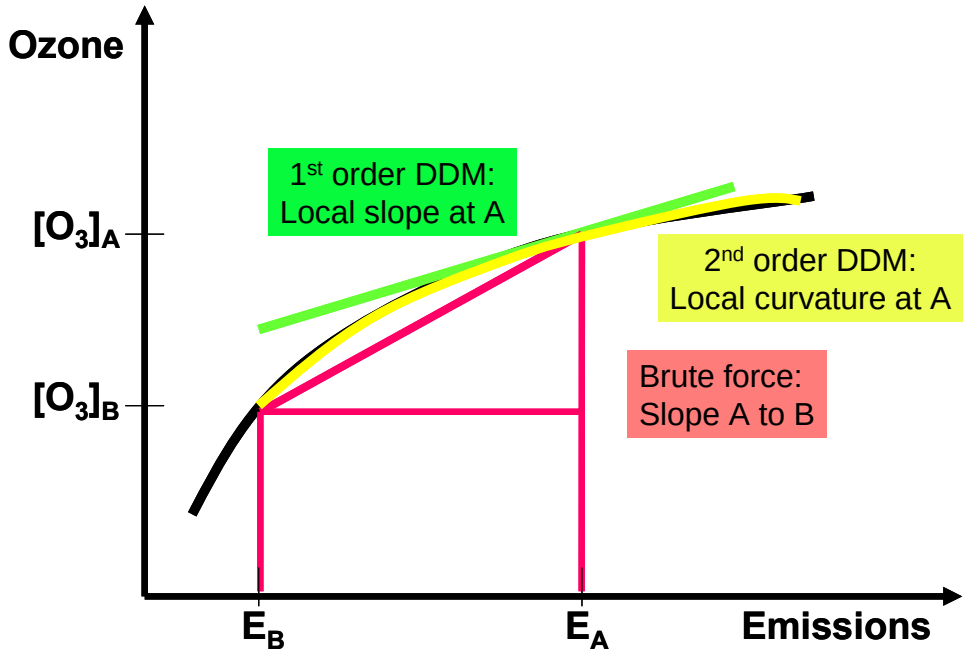

Figure 1.2. Brute force and decoupled direct method sensitivity analysis of ozone response to emissions. Given the typically concave-down response, the brute force slope of response to large reductions in emissions is steeper than the local sensitivity at Point A computed by first-order DDM. Taylor expansions of first- and second-order DDM coefficients enable approximation of response to various perturbations.

1.3 Scope of This Work

Building upon the implementation of high-order DDM-3D into a widely used regional air quality model (Appendix A; Cohan *et al.*, 2002), this dissertation demonstrates how high-order sensitivity analysis can be applied to examine ozone formation and potential options for its abatement. Summertime episodes of high ozone in the southeastern U.S. are considered as case studies.

Though this thesis derives results for specific regions and episodes, the methods developed herein are presented in general terms for wide applicability to other conditions and, in some cases, other pollutants. Tools are developed for a variety of investigations of ozone sensitivity and for assessing the uncertainty of sensitivity estimates. The

dissertation culminates in a demonstration of how sensitivity analysis can be linked with cost estimates to inform the development of cost-optimized pollution control strategies.

Specifically, the chapters are organized as follows.

- **Chapter 2, "Source apportionment and nonlinear sensitivity analysis of ozone response to precursor emissions,"** establishes the accuracy of second-order DDM-3D as implemented in a regional air quality model. A nonlinearity index is introduced to quantify the importance of high-order sensitivity coefficients, and a method is developed to apply these high-order terms to assess the uncertainty of source apportionment and sensitivity estimates arising from error in the underlying emissions inventory.
- **Chapter 3, "Diagnosing ozone production regime and its relevance for control strategy formulation,"** applies HDDM-3D to assess NO_x and VOC limitation of ozone in the southeastern U.S., and compares HDDM-3D sensitivities to modeled values of species indicator ratios. Two complicating factors are investigated which may hinder the relevance of bipartite ozone regime classification.
- **Chapter 4, "Importance of emission location in determining ozone yield from nitrogen oxides,"** examines the relative propensity of various NO_x sources in Georgia to enhance ozone concentrations.
- **Chapter 5, "Grid resolution considerations in ozone sensitivity analysis,"** examines how ozone sensitivity estimates vary with model grid resolution to explore tradeoffs between computational efficiency and accuracy.
- **Chapter 6, "Cost-optimized air pollution controls for different goals: Case study for ozone in Macon, Georgia,"** demonstrates how air quality model results can be

integrated with cost estimates to inform control strategy formulation. A comprehensive menu is developed containing estimates of the cost and effectiveness of various options for reducing NO_x and VOC emissions in Georgia. This menu is linked with HDDM-3D sensitivity estimates to develop least-cost strategies for attaining ozone standards in Macon. These strategies are compared to those optimized for alternative metrics such as reducing regionally-averaged ozone concentrations or potential population exposure to ozone.

- **Chapter 7** provides conclusions and recommendations for further research.
- **Appendices** contain a programmer's guide that describes the implementation of HDDM-3D into a regional air quality model and two chapters from the FAQS report (Hu *et al.*, 2004) that provide additional detail of sensitivity analysis for the Fall-Line cities.

CHAPTER 2

SOURCE APPORTIONMENT AND NONLINEAR SENSITIVITY ANALYSIS OF OZONE RESPONSE TO PRECURSOR EMISSIONS*

2.1 Introduction

Air quality modeling has long been applied not only to simulate ambient concentrations of air pollutants, but also to explore their sensitivity to changes in emission rates and meteorology. Sensitivity analysis is especially vital for secondary pollutants such as ozone, whose sensitivity to emissions of its precursors—primarily nitrogen oxides (NO_x) and volatile organic compounds (VOC)—changes in magnitude and sign depending upon spatio-temporally varying factors (Sillman, 1999).

The responses of pollutant concentrations to perturbations in emission rates are pertinent to both scientific investigation and policy formulation. The manner in which these responses are considered depends on the context. Scientific investigation of air pollutant formation may seek to quantify the "local" sensitivities of concentrations, i.e., their rates of change with respect to infinitesimal perturbations in emission rates. For control strategy development, the relevant question is how concentrations would respond to fractional changes in emissions associated with abatement measures. Source attribution seeks to determine the total contribution of each emission source to ambient

* This chapter is an extension of "Nonlinear response of ozone to emissions: Source apportionment and sensitivity analysis," submitted to Environmental Science & Technology in August 2004. Co-authors are Amir Hakami, Yongtao Hu, and Armistead Russell.

concentrations; this is equivalent to the reduction in concentrations that would occur if an emission source no longer existed.

When atmospheric response is linear, control strategy impact and source contribution can both be scaled directly from local sensitivity. Linear response will tend to be a reasonable approximation for many primary pollutants such as lead for which atmospheric processing rates are linear in concentration. However, for secondary pollutants generated by nonlinear interactions of various precursor substances, atmospheric response is more complex. In the case of ozone, daytime concentrations typically exhibit a concave-down response to NO_x emissions (Lin *et al.*, 1988). This reflects that as NO_x emissions are reduced, ozone production becomes more sensitive to remaining NO_x. Thus, ozone may be more responsive to large reductions in NO_x emissions than would be suggested by a linear scaling of local sensitivity. Conversely, interpolating from the response of ozone to large reductions in emissions may overestimate local sensitivity.

Sensitivity analysis of secondary pollutants may be further complicated by "cross-sensitivity" interactions between the impacts of multiple emission sources. Cross-sensitivity occurs when the sensitivity of ambient concentrations to emissions from one source depends on the emission rate of another source. Because of these interactions, the impact of a multi-part emission control strategy may differ from the sum of the impacts of its component abatement measures. Similarly, the total source contribution of a set of emission sources may differ from the sum of the individual contributions.

For policy applications involving a large number of heterogeneous sources, it would be computationally costly and conceptually cumbersome to assess the nonlinearities and

cross-sensitivities among all of the concentration-emission responses. For simplicity, atmospheric response has often been approximated as linear. Sensitivity analysis can facilitate understanding the relative importance of various nonlinearities and cross-sensitivities and gauge the extent of inaccuracy that may be associated with linear approximation.

Here, we apply a high-order sensitivity analysis technique, the high-order Decoupled Direct Method in Three Dimensions (HDDM-3D) (Yang *et al.*, 1997; Hakami *et al.*, 2003a) to assess the nonlinearity of ozone response to a variety of perturbations in emission rates, and the interactions among sensitivities. Nonlinear response is investigated for an air pollution episode in the southeastern U.S. We identify circumstances that tend to increase the nonlinearity of ozone response to NO_x emissions. We also show that cross-sensitivity relationships can illuminate how sensitivity estimates are affected by inaccuracy in emissions inventories, a key source of uncertainty in atmospheric modeling.

2.2 Method

Sensitivity analysis investigates the response of atmospheric concentrations, $\mathbf{C}_i(\mathbf{x},t)$, to perturbations in a sensitivity parameter, $p_j(\mathbf{x},t)$ where i is a chemical compound, j is a model parameter or input such as an emission rate, initial condition or boundary condition, and $\mathbf{x}$ and t denote space and time. For simplicity, we drop the notations for time, space and species. The unperturbed ("base case") value of the sensitivity parameter is P_j. Perturbations in p_j are considered by defining a scaling variable, ε_j, with a nominal value of 1 such that

$$p_j = \varepsilon_j P_j \tag{2.1}$$

We define the semi-normalized first-order sensitivity coefficients, $\mathbf{S}_j^{(1)}$, of concentration response to parameter p_j by scaling the local sensitivities ($\partial\mathbf{C}/\partial p_j$) by P_j:

$$\mathbf{S}_j^{(1)} = P_j \frac{\partial \mathbf{C}}{\partial p_j} = P_j \frac{\partial \mathbf{C}}{\partial (\varepsilon_j P_j)} = \frac{\partial \mathbf{C}}{\partial \varepsilon_j} \tag{2.2}$$

Similarly, semi-normalized second-order sensitivity coefficients are defined as

$$\mathbf{S}_{j,k}^{(2)} = P_j \frac{\partial}{\partial p_j}\left(P_k \frac{\partial \mathbf{C}}{\partial p_k}\right) = \frac{\partial^2 \mathbf{C}}{\partial \varepsilon_j \partial \varepsilon_k} \tag{2.3}$$

All sensitivity coefficients vary both spatially and temporally and are computed for all modeled constituents, just as the concentration fields. When $j=k$, the second-order sensitivity represents the local curvature of the concentration-parameter relationship. For $j\neq k$, $\mathbf{S}_{j,k}^{(2)}$ represents a "cross-sensitivity" interaction between the sensitivities to two different parameters, p_j and p_k. A cross-sensitivity quantifies the extent to which one sensitivity parameter influences the responsiveness of concentrations to another parameter.

Sensitivity coefficients traditionally have been approximated by "brute force". In this method, finite differencing compares concentrations computed by two chemical transport model (CTM) simulations that are identical except for a perturbation in the sensitivity parameter:

$$\mathbf{S}_j^{(1)} \approx \frac{\mathbf{C}_{+\Delta\varepsilon_j} - \mathbf{C}_{-\Delta\varepsilon_j}}{2\Delta\varepsilon_j} \tag{2.4}$$

The fractional perturbation in the parameter is denoted by $\Delta\varepsilon_j=(\varepsilon_j-1)$. Though most brute force analyses have considered only first-order sensitivities, standard higher-order sensitivity coefficients can be approximated by finite differencing. For example, standard

(*j=k*) second-order sensitivity coefficients can be approximated from the results of three CTM simulations:

$$\mathbf{S}^{(2)}_{j,j} \approx \frac{\mathbf{C}_{(+\Delta\varepsilon_j \cdot p_j)} - 2\mathbf{C}_0 + \mathbf{C}_{(-\Delta\varepsilon_j \cdot p_j)}}{(\Delta\varepsilon_j)^2} \quad \textbf{(2.5)}$$

where $\mathbf{C}_0$ denotes base case concentrations.

The popularity of brute force owes largely to its simplicity and ready application in any CTM. However, the method becomes cumbersome for computing a large number of sensitivities, because it requires additional simulations for each perturbation. Although brute force computes the exact model response to specific perturbations, the accuracy of scaling these results to other perturbations is unclear in the presence of nonlinearity. Further, brute force is prone to numerical error for small perturbations.

HDDM-3D provides a computationally-efficient alternative to brute force for computing sensitivities of concentrations to changes in parameters. DDM-3D calculates sensitivity coefficients by applying the same numerical algorithms and operator splitting used to calculate concentrations (Yang *et al.*, 1997). Whereas the underlying CTM describes pollutant formation and transport by the atmospheric diffusion equation,

$$\frac{\partial C_i}{\partial t} = -\nabla(\mathbf{u}C_i) + \nabla(\mathbf{K}\nabla C_i) + R_i + E_i \quad \textbf{(2.6)}$$

DDM-3D considers auxiliary equations for the sensitivity coefficients. For sensitivity to emission rates, those equations can be written as

$$\frac{\partial S^{(1)}_{i,j}}{\partial t} = -\nabla(\mathbf{u}S^{(1)}_{i,j}) + \nabla(\mathbf{K}\nabla S^{(1)}_{i,j}) + \mathbf{J}_i\mathbf{S}_j + E'_i \quad \textbf{(2.7)}$$

where **u** is the three-dimensional wind field, **K** is the turbulent diffusivity tensor, and R_i and E_i are the chemical reaction rate and emission rate, respectively, of species i. $\mathbf{J}_i$ is the

i^{th} row vector in the Jacobian matrix, **J** ($J_{ik}=\partial R_i/\partial C_k$), which represents photochemical interactions between species. E_i' is the unperturbed emission rate of the sensitivity parameter. This decoupled, direct approach simplifies implementation and provides consistency between sensitivities and concentrations. Similarly, second-order sensitivity coefficients $\mathbf{S}^{(2)}$ are computed by differentiating the governing equations of the first-order sensitivities with respect to the parameters of interest (Hakami *et al.*, 2003a).

DDM-3D sensitivity coefficients represent the responsiveness to infinitesimal perturbations. To project to larger perturbations away from a base case (e.g., significant emissions abatement), we incorporate second-order sensitivity coefficients via Taylor series expansions (Hakami *et al.*, 2003a). In this approach, concentrations for any fractional perturbation in a sensitivity parameter are approximated by:

$$\mathbf{C}_j\Big|_{p_j=P_j+\Delta\varepsilon_j P_j} \approx \mathbf{C}_0\Big|_{p_j=P_j} + \Delta\varepsilon_j \mathbf{S}_j^{(1)} + \tfrac{1}{2}\Delta\varepsilon_j^2 \mathbf{S}_{j,j}^{(2)} + \textit{higher order terms} \qquad \textbf{(2.8)}$$

where $\mathbf{C}_j$ are the concentrations when p_j has been perturbed by an amount $\Delta\varepsilon_j P_j$. Note that the second-order term scales with $\Delta\varepsilon_j^2$, and thus its relative importance increases with the size of the perturbation.

We define the source contribution (SC) of an emitter to be the magnitude of the reduction in concentrations that would occur if that source did not exist. A second-order approximation of SC can be computed by setting $\Delta\varepsilon_j = -1$ in Equation 2.8:

$$\begin{aligned} SC\,(P_j) &\cong \mathbf{C}_0\Big|_{p_j=P_j} - \mathbf{C}_j\Big|_{\{p_j=0;\ i.e.,\ \Delta\varepsilon_j=-1\}} \\ &\approx \mathbf{S}_j^{(1)} - \tfrac{1}{2}\mathbf{S}_{j,j}^{(2)} \end{aligned} \qquad \textbf{(2.9)}$$

If multiple sensitivity parameters are perturbed simultaneously, the approximations of atmospheric response and SC become more complex. Consider fractional perturbations, $\Delta\varepsilon_j$ and $\Delta\varepsilon_k$, to parameters p_j and p_k. When these parameters are perturbed

simultaneously, a second-order Taylor approximation includes the interaction between the two parameters:

$$\mathbf{C}_{j+k} \cong \mathbf{C}\Big|_{\{p_j = P_j + \Delta\varepsilon_j P_j;\quad p_k = P_k + \Delta\varepsilon_k P_k\}}$$
$$\mathbf{C}_{j+k} \approx \mathbf{C}_0 + \Delta\varepsilon_j \mathbf{S}_j^{(1)} + \Delta\varepsilon_k \mathbf{S}_k^{(1)} + \tfrac{1}{2}\Delta\varepsilon_j^2 \mathbf{S}_{j,j}^{(2)} + \tfrac{1}{2}\Delta\varepsilon_k^2 \mathbf{S}_{k,k}^{(2)} + \Delta\varepsilon_j \Delta\varepsilon_k \mathbf{S}_{j,k}^{(2)} + \ldots \quad \textbf{(2.10)}$$

Here, $\mathbf{S}_{j,k}^{(2)}$ is the cross-sensitivity between the two parameters. Because of this term, the change in concentrations for a dual perturbation in sensitivity parameters differs from the sum of two individual changes. Similarly, the source contribution of an aggregate of emitters differs from the sum of the individual contributions:

$$SC(P_j + P_k) \approx \underbrace{(\mathbf{S}_j^{(1)} - \tfrac{1}{2}\mathbf{S}_{j,j}^{(2)})}_{SC\ j} + \underbrace{(\mathbf{S}_k^{(1)} - \tfrac{1}{2}\mathbf{S}_{k,k}^{(2)})}_{SC\ k} - \underbrace{\mathbf{S}_{j,k}^{(2)}}_{cross\ term} \quad \textbf{(2.11)}$$

The extent to which each emitter influences the source contribution of the other is captured by the cross-sensitivity term.

Our implementation of HDDM-3D in the Community Multiscale Air Quality model (Byun and Ching, 1999) v. 4.3 with the SAPRC-99 chemical mechanism (Carter, 2000) provides broad flexibility in the form of the perturbation to model inputs: a static or time-variant change, for an individual species or group of species, from a single grid cell, a region of one or more counties, or the entire domain. The current implementation ignores aerosol and aqueous chemistry processes other than the heterogeneous hydrolysis of N_2O_5, although these processes are applied to the time evolution of concentrations. Comparisons with brute force results, presented later in this chapter, demonstrate that CMAQ-HDDM-3D accurately computes sensitivities for ozone despite this inconsistency.

We model August 11-19, 2000, a period of hot and stagnant conditions over much of the southeastern U.S. Results from the first two days are discarded as model initialization. The nested modeling domain has 13 vertical layers of increasing thickness with height, and covers the eastern U.S. with 36-km resolution (Figure 2.1). This chapter focuses on results in a 12-km resolution sub-domain centered on Georgia, with initial and boundary concentrations supplied by base case simulations of the 36-km domain. Emissions are from the Year 2007 projected inventory of the Fall Line Air Quality Study (FAQS) (Unal et al., 2003) to correspond with a target year for future attainment demonstrations. Modeling of meteorological inputs is detailed elsewhere (Hu et al., 2003). Simulated concentrations for the episode with base year emissions have been extensively evaluated relative to observations, with bias and error shown to be well within U.S. EPA benchmarks (Hu et al., 2004).

2.3 Results and Discussion

2.3.1 Performance of HDDM-3D

We compare CMAQ-HDDM-3D sensitivity coefficients to those approximated by brute force for perturbations in (1) domain-wide (12-km domain) anthropogenic emissions of NO_x, (2) domain-wide anthropogenic emissions of VOC and (3) emissions of NO_x from the 3520 MW Robert W. Scherer coal-fired power plant in Georgia.

Table 2.1 presents brute force and HDDM-3D estimates of first- and second-order local sensitivity coefficients. Brute force approximations are computed by Equations 2.4 and 2.5 using +/- 10% perturbations. Brute force and HDDM-3D results are evaluated over the 8-hour period each day during which base case ozone is maximal in that grid

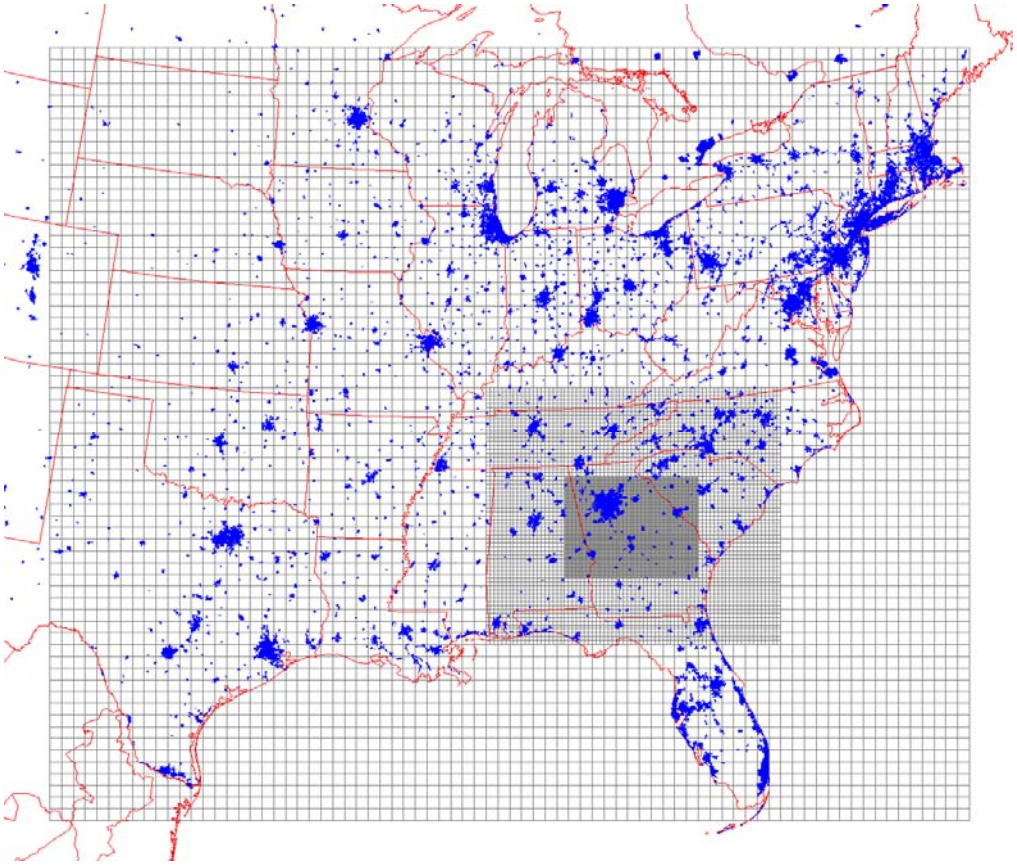

Figure 2.1. Fall-line Air Quality Study nested modeling domain. This chapter focuses on the medium (12-km) resolution domain in the southeastern U.S. (Figure created by Yongtao Hu).

Table 2.1. Sensitivity coefficients, averaged over the domain and episode, of 8-hour ozone to each emissions source.

	Brute Force[a]	DDM	DDM v. B.F.	
Emissions source	**(ppb)**	**(ppb)**	**Bias[b]**	**r^{2} [c]**
1st order domain-wide NO_x	11.90	11.69	-1.8%	0.997
2nd order domain-wide NO_x	-6.85	-6.62	-3.3%	0.967
1st order domain-wide VOC	0.18	0.18	0.2%	0.992
2nd order domain-wide VOC	-0.13	-0.16	25.0%	0.720
1st order Scherer NO_x	0.14	0.14	-1.1%	0.992
2nd order Scherer NO_x	+0.00	-0.04	NA	0.866

[a]Calculated using +/- 10% perturbations.
[b]Normalized mean bias, (DDM – brute force)/(brute force).
[c]Daily r^2 of spatial correlation between DDM and brute force, averaged over episode.

cell, and averaged over the 12-km domain for August 13-19. The r^2 values refer to the 7-day average of the daily spatial correlation between HDDM-3D and brute force coefficients. HDDM-3D coefficients closely match brute force in all cases, especially for first-order terms. The somewhat weaker correlation of second-order coefficients reflects that (1) DDM-3D errors from first-order propagate into the second-order calculations and (2) brute force second-order coefficients are subject to numerical noise, particularly in cases with low sensitivity (e.g., as with the VOCs).

Having examined the accuracy of HDDM-3D for sensitivity coefficients representing responsiveness to infinitesimal perturbations, we proceed to test its applicability to replicate model response to large-scale perturbations in emissions. We consider the reduction in 8-hour ozone that would accompany +/-10%, -50%, and -100% emissions perturbations in each case. Brute force responses are computed by differencing concentrations in base case and perturbed simulations; HDDM-3D estimates are computed by (1) linearly scaling first-order sensitivity coefficients and (2) Taylor expansion of first- and second-order coefficients.

Table 2.2 presents the normalized mean bias and spatial correlation of HDDM-3D-based estimates relative to the reductions in 8-hour ozone simulated to occur by the brute force method.

Table 2.2. Reduction in domain-wide 8-hour ozone, computed by DDM and brute force methods, for each emission perturbation.

	Brute Force[a]	DDM v. B.F.: First-order only[b]		DDM v. B.F.: With second-order[c]	
Emissions Perturbation	**(ppb)**	**Bias[d]**	**r^2 [e]**	**Bias[d]**	**r^2 [e]**
+10% NO_x	-1.156	-1.1%	0.997	1.7%	0.997
-10% NO_x	1.224	-4.5%	0.995	-1.8%	0.997
-50% NO_x	6.949	-15.9%	0.972	-3.9%	0.996
-100% NO_x	16.686	-29.9%	0.891	-10.0%	0.976
+10% VOC	-0.017	-3.9%	0.991	0.7%	0.992
-10% VOC	0.018	-3.2%	0.992	1.1%	0.992
-50% VOC	0.109	-19.3%	0.987	-1.4%	0.990
-100% VOC	0.270	-34.4%	0.974	-5.5%	0.986
+10% Scherer NO_x	-0.014	1.2%	0.991	2.5%	0.993
-10% Scherer NO_x	0.014	-1.1%	0.991	0.2%	0.992
-50% Scherer NO_x	0.075	-7.6%	0.963	-1.5%	0.992
-100% Scherer NO_x	0.167	-16.6%	0.882	-5.5%	0.982

[a]Reduction in ozone relative to base case.
[b]1st order DDM sensitivity coefficient scaled to each perturbation.
[c]Taylor expansion of 1st and 2nd order DDM coefficients.
[d]Normalized mean bias, (DDM – brute force)/(brute force).
[e]Daily r^2 between DDM and brute force, averaged over episode.

The high level of cell-by-cell correlation (r^2) demonstrates that the spatial patterns of response are in close agreement. First-order DDM-3D coefficients are sufficient for accurately predicting response to all +/- 10% perturbations. The widening gap between brute force and first-order DDM-3D for larger reductions reflects nonlinearity. Projected first-order sensitivity underpredicts ozone reduction for large NO_x (VOC) reductions because ozone becomes increasingly sensitive to the remaining NO_x (VOC) as emission

rates decrease. By the same reasoning, linearly interpolating from a large-scale response would underpredict the incremental sensitivity.

Most of the under-prediction of first-order extrapolation can be explained by incorporation of the second-order HDDM-3D coefficients. For the domain-wide NO_x emissions cases, incorporation of second-order coefficients explains most of the under-prediction even in the most extreme (100% reduction) case (Figure 2.2). Some under-prediction remains, with largest biases localized to several cells in which first-order sensitivity to NO_x is negative and the brute force response of ozone to complete removal of NO_x is relatively small.

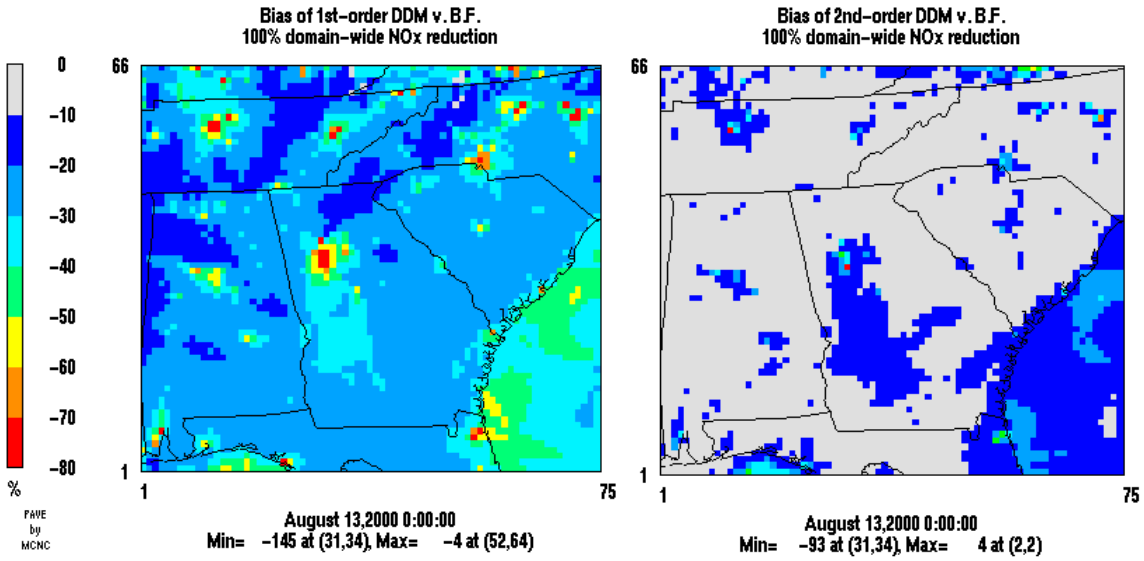

Figure 2.2. Normalized mean bias (%) of Taylor expansions of first-order (left) and first- and second-order (right) HDDM-3D coefficients, relative to brute force, for the episode-average reduction in 8-hour ozone that would accompany complete removal of domain-wide NO_x emissions.

2.3.2 Decomposition of ozone response

We apply HDDM-3D to explore the relationships between ozone and its precursor emissions during the modeled episode, which simulates the air pollution that would occur

if August 2000 meteorology were accompanied by Year 2007 projected emission rates (Figure 2.3). With its abundance of biogenic VOC (Guenther *et al.*, 2000), the southeastern U.S. is predominated by NO_x-limited ozone production (Chameides *et al.*, 1992). For the modeled episode, this is demonstrated by much larger sensitivities to anthropogenic NO_x emissions than to anthropogenic VOC (Figure 2.3). Second-order sensitivity coefficients with respect to NO_x are predominantly negative, reflecting the concave-down response of ozone. In line with the findings of Hakami *et al*. (2003a), greatest nonlinearity occurs where the chemical regime changes between NO_x and VOC limitation and hence spatial gradients in first-order NO_x sensitivity are large.

Figure 2.4 (a) decomposes the source contributions of domain-wide NO_x and VOC emissions to ozone concentrations in the cell corresponding to downtown Atlanta. Significant sensitivity is observed to both NO_x and VOC emissions during the afternoon hours when ozone is highest. The response of Atlanta ozone to NO_x is highly nonlinear, with daytime values reflecting a concave-down response. The situation changes at night, when ozone can be titrated by NO_x in the absence of sunlight and thus display negative sensitivity. The contribution of the cross-sensitivity between NO_x and VOC is negative, reflecting that as NO_x (VOC) emissions are reduced, ozone becomes less sensitive to VOC (NO_x). However, the positive sign of first-order sensitivity to both NO_x and VOC in Atlanta during daytime indicates that 8-hour ozone could be reduced by incremental reductions in either precursor.

Contrasting patterns of ozone formation are modeled to occur for locations less than 50 km from downtown Atlanta and well within the non-attainment region for federal ozone standards. Highest 8-hour ozone concentrations are modeled to occur 36 km south

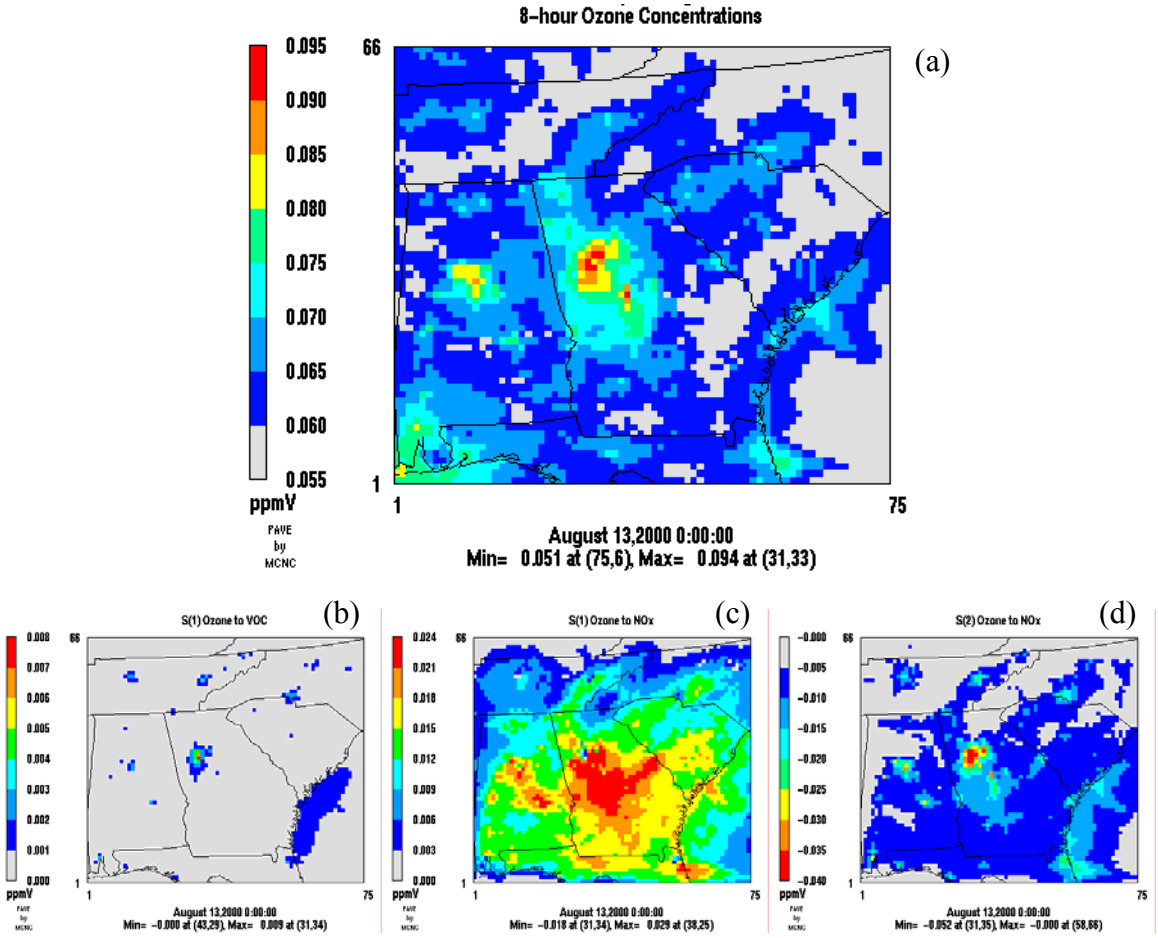

Figure 2.3. Episode-average 8-hour ozone concentrations (a) and their sensitivity to domain-wide emissions of VOC (first-order (b)) and NO_x (first-order (c); second-order (d)).

of downtown in Clayton County (Figure 2.4(b)), as northerly winds predominated during much of the episode. This location experiences somewhat greater sensitivity to NO_x than the downtown location, and similar sensitivity to VOC. However, 50 km north of downtown in Cherokee County, the contribution of VOC is modeled to be negligible and response to NO_x is much more linear (Figure 2.4(c)). With weaker local NO_x emissions, less titration occurs at night and the diurnal cycles of both concentrations and sensitivities are less pronounced.

Outside the Atlanta region, Macon has historically experienced the next highest ozone concentrations in Georgia and is also a non-attainment area for 8-hour ozone. However, our modeling indicates that Macon's ozone exhibits a more linear response to NO_x emissions and virtually no response to anthropogenic VOC (Figure 2.4(d)). The differences between Macon and Atlanta highlight that ozone formation can differ sharply even among nearby non-attainment regions. On the other hand, HDDM-3D results show fairly uniform patterns of sensitivity in less polluted rural regions of the domain. Figure 2.4(e) exemplifies the relatively linear and almost entirely NO_x-limited ozone formation modeled to occur throughout rural regions of the state.

2.3.3 Nonlinearity index

Many studies have assumed that responsiveness of concentrations to one amount of emissions perturbation could be linearly extrapolated or interpolated to estimate response to other amounts of perturbation. The accuracy of these extrapolations and interpolations depends on the nonlinearity of the response. Here we explore how the nonlinearity of ozone response to NO_x emissions varies by source and receptor region.

(a)

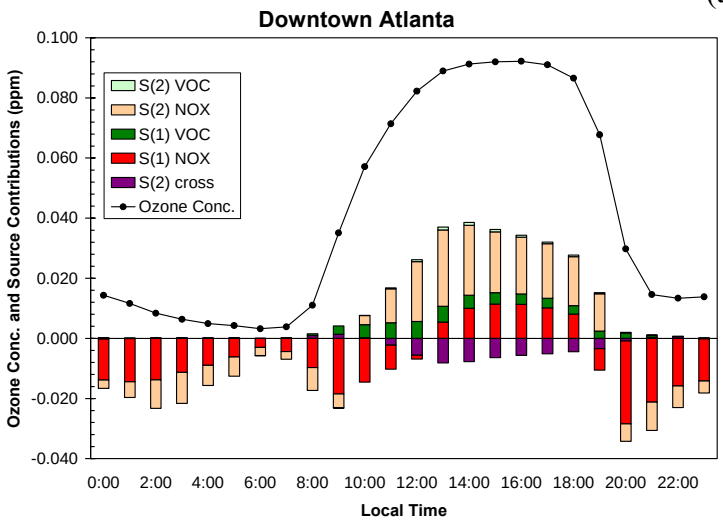
Downtown Atlanta
Ozone Conc. and Source Contributions (ppm)
0.100
0.080
0.060
0.040
0.020
0.000
-0.020
-0.040
S(2) VOC
S(2) NOX
S(1) VOC
S(1) NOX
S(2) cross
Ozone Conc.
0:00 2:00 4:00 6:00 8:00 10:00 12:00 14:00 16:00 18:00 20:00 22:00
Local Time

(b)

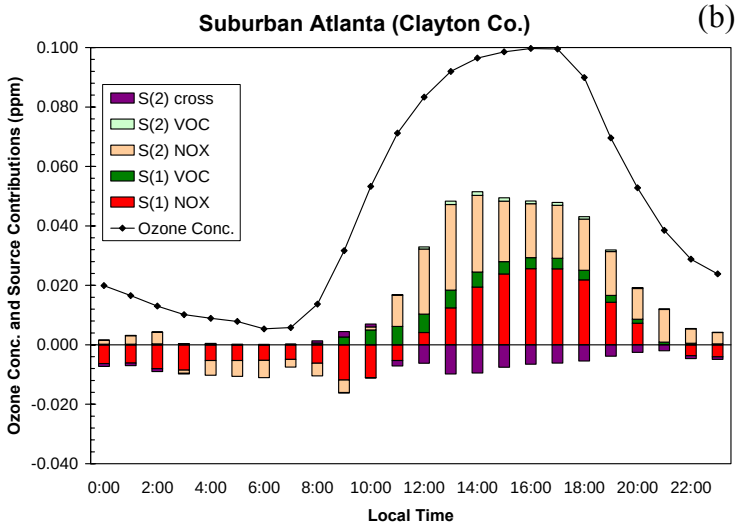
Suburban Atlanta (Clayton Co.)
Ozone Conc. and Source Contributions (ppm)
0.100
0.080
0.060
0.040
0.020
0.000
-0.020
-0.040
S(2) cross
S(2) VOC
S(2) NOX
S(1) VOC
S(1) NOX
Ozone Conc.
0:00 2:00 4:00 6:00 8:00 10:00 12:00 14:00 16:00 18:00 20:00 22:00
Local Time

(c)

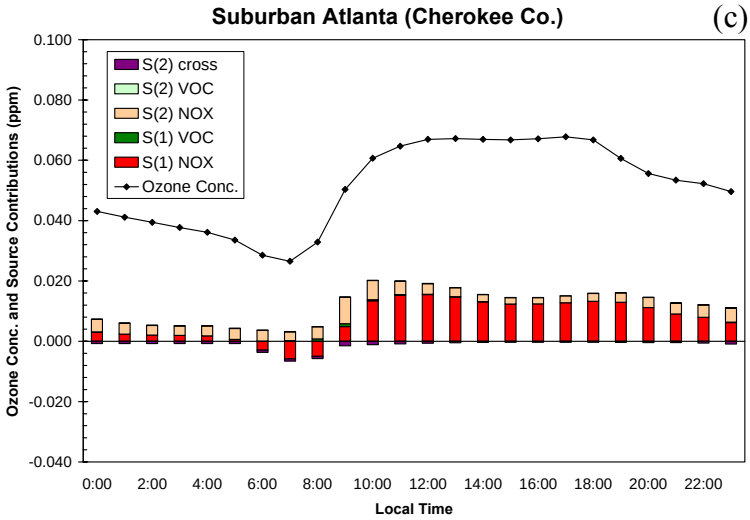
Suburban Atlanta (Cherokee Co.)
Ozone Conc. and Source Contributions (ppm)
0.100
0.080
0.060
0.040
0.020
0.000
-0.020
-0.040
S(2) cross
S(2) VOC
S(2) NOX
S(1) VOC
S(1) NOX
Ozone Conc.
0:00 2:00 4:00 6:00 8:00 10:00 12:00 14:00 16:00 18:00 20:00 22:00
Local Time

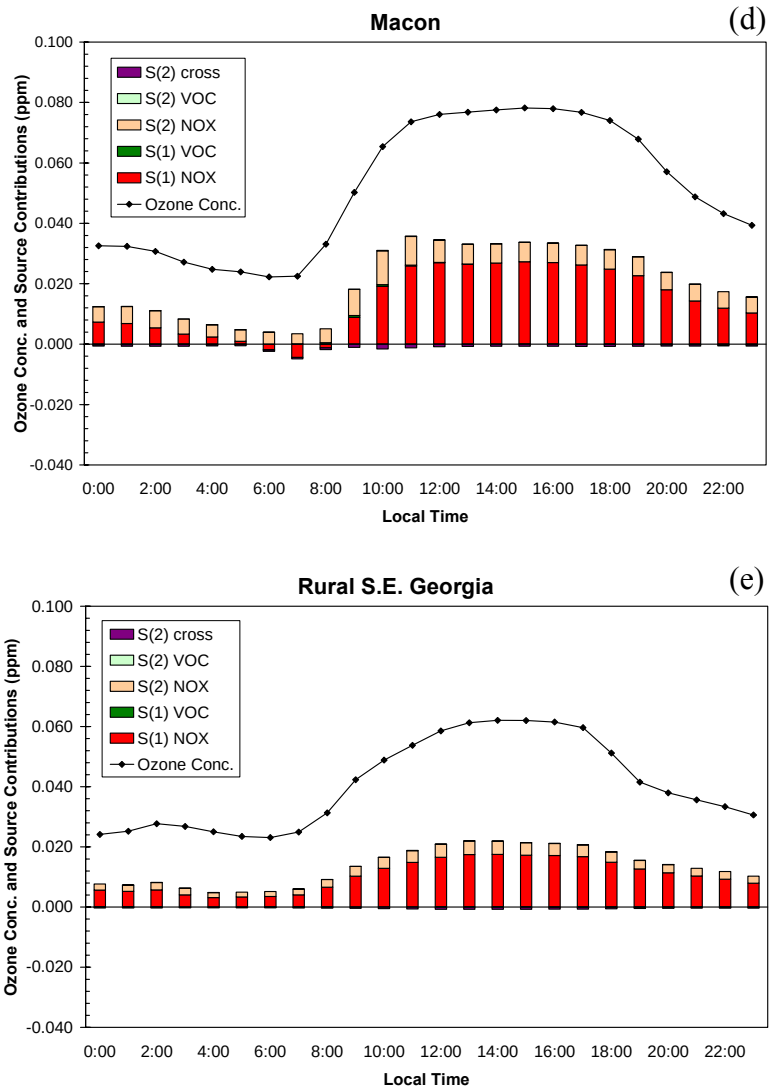

Figure 2.4. Episode-average ozone concentrations (line) and a decomposition of the source contribution of domain-wide NO_x and VOC emissions (see Equation 11). "S(2) cross" is the contribution of the interaction between NO_x and VOC.

We define an index, $\alpha_{i,j}$, to characterize the nonlinearity of response of concentrations of each species i to each sensitivity parameter p_j.

$$\alpha_{i,j} = \left| \frac{0.5 \cdot \overline{S}_{i,j}^{(2)}}{\overline{S}_{i,j}^{(1)}} \right| \qquad \textbf{(2.12)}$$

The overbars represent averaging over the region and time of interest. The nonlinearity index represents the ratio of the second- and first-order terms in a Taylor approximation of the source contribution of p_j (Equation 2.9). For assessing the impact of a partial perturbation in p_j, the ratio of the magnitudes of the second- and first-order terms in the Taylor expansion (Equation 2.8) will equal $\alpha_{i,j}$ multiplied by the fractional amount $\Delta\varepsilon_j$ by which the parameter is perturbed. Thus the larger the nonlinearity index of a sensitivity parameter, and the larger the perturbation of interest, the greater the importance of nonlinearity.

We compute the nonlinearity index for ozone response to NO_x emissions from several regions within Georgia and from the entire 12-km resolution domain. For the purpose of this analysis, CMAQ-HDDM-3D computes first- and second order sensitivity coefficients of ozone with respect to NO_x from each of the following Georgia regions: Atlanta, Macon, Augusta, Columbus, North Georgia, Central Georgia, and South Georgia (Figure 2.5). Emissions from two large point sources of NO_x, Plant Scherer and Plant Harllee Branch, are considered separately. The magnitude and density of NO_x emissions varies sharply across the regions (Table 2.3).

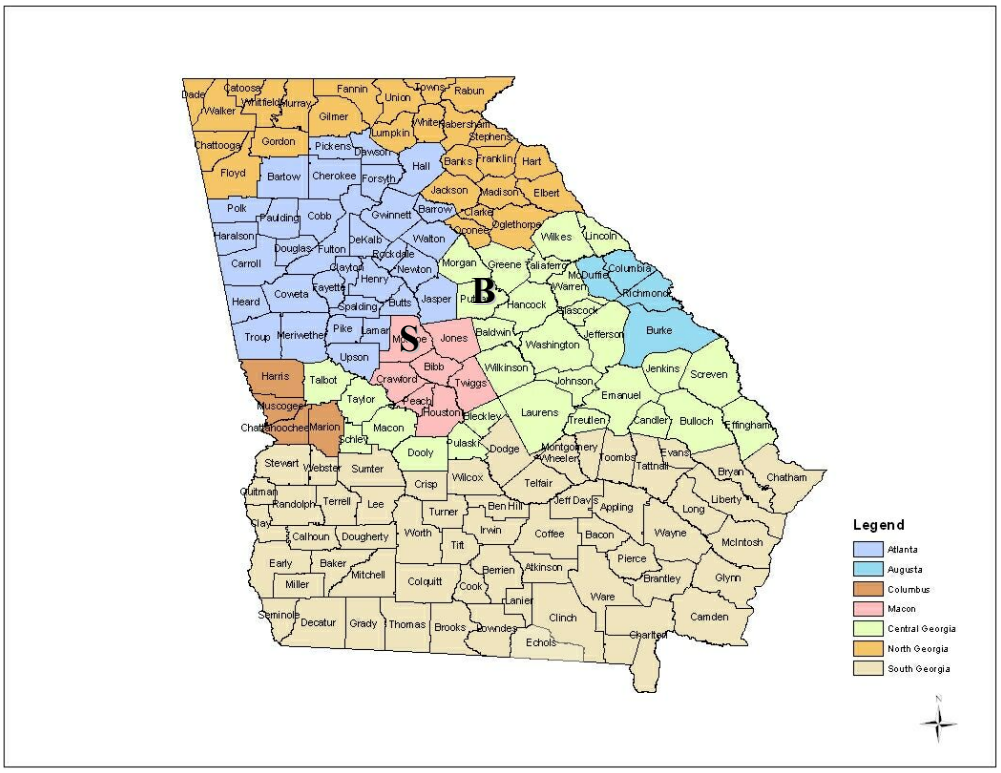

Figure 2.5. Georgia regions for sensitivity analysis. S and B denote Plant Scherer and Plant Branch (Figure created by Alper Unal).

Table 2.3. Episode-average Year 2007 NO_x emissions by region.

	Emissions (tpd)	Area (km^2)	Emissions density ($tpd/10^3km^2$)
Atlanta	591	25168	23.5
Macon	69	5749	12.0
Augusta	46	4385	10.5
Columbus	23	3332	6.9
N. GA	165	19566	8.4
C. GA	111	29261	3.8
S. GA	321	62037	5.2
Scherer	92	144[a]	638.9
Branch	50	144[a]	347.2
Domain	4394	712800	6.2

[a]Reflects 12x12 km model resolution, not facility size.

Table 2.4 presents second-order Taylor approximations of the source contribution (Equation 2.9) of NO_x from each emissions region to 8-hour ozone concentrations in each receptor region and the nonlinearity of each response. Responses averaging less than 0.01 ppb are omitted.

Table 2.4. Source contribution (top) and nonlinearity index (bottom) of each NO_x emission region's impact on episode-average 8-hour ozone in each receptor region.

Emission region	Receptor region							
	Atlanta	**Macon**	**Augusta**	**Columbus**	**N. GA**	**C. GA**	**S. GA**	**Domain**
Atlanta	**15.88 ppb** **0.48**	6.62 ppb 0.16	1.13 ppb 0.12	11.42 ppb 0.31	0.84 ppb 0.11	4.20 ppb 0.20	3.82 ppb 0.25	**1.61 ppb** **0.29**
Macon	0.02 ppb 0.04	**5.75 ppb** **0.19**	0.46 ppb 0.02	0.10 ppb 0.04	0.01 ppb 0.06	1.09 ppb 0.07	0.70 ppb 0.08	**0.21 ppb** **0.09**
Augusta	0.03 ppb 0.03	0.14 ppb 0.05	**5.08 ppb** **0.15**		0.01 ppb 0.01	0.92 ppb 0.07	0.23 ppb 0.06	**0.14 ppb** **0.08**
Columbus	0.01 ppb 0.03	0.16 ppb 0.01	0.06 ppb 0.04	**2.31 ppb** **0.13**		0.23 ppb 0.03		**0.06 ppb** **0.05**
N. GA	2.07 ppb 0.08	1.09 ppb 0.04	0.41 ppb 0.05	1.18 ppb 0.07	**4.25 ppb** **0.13**	1.01 ppb 0.06	0.77 ppb 0.06	**0.54 ppb** **0.08**
C. GA	0.10 ppb 0.06	1.49 ppb 0.09	1.29 ppb 0.05	0.32 ppb 0.02	0.03 ppb 0.07	**2.96 ppb** **0.06**	1.07 ppb 0.06	**0.34 ppb** **0.06**
S. GA		0.05 ppb 0.04	0.29 ppb 0.05	0.04 ppb 0.03		0.70 ppb 0.05	**4.27 ppb** **0.08**	**0.76 ppb** **0.09**
Scherer	0.08 ppb 0.24	4.44 ppb 0.28	0.35 ppb 0.04	0.21 ppb 0.09		0.67 ppb 0.09	0.48 ppb 0.10	**0.16 ppb** **0.13**
Branch	0.04 ppb 0.08	1.17 ppb 0.11	0.24 ppb 0.05	0.03 ppb 0.10		0.71 ppb 0.14	0.29 ppb 0.11	**0.10 ppb** **0.11**
Domain	**25.11 ppb** **0.43**	**32.16 ppb** **0.31**	**24.26 ppb** **0.26**	**26.01 ppb** **0.31**	**14.59 ppb** **0.23**	**23.71 ppb** **0.23**	**21.56 ppb** **0.25**	**15.01 ppb** **0.28**

Several trends in nonlinearity are apparent. For a given emission region, nonlinearity tends to be most significant for ozone within that region (bold entries in Table 2.4) and less significant downwind as the plume dilutes. The most intense source regions, Atlanta and the two power plants, elicit the most nonlinear responses.

To explain why α increases with emissions density (e.g., why Macon yields a more nonlinear response than Central Georgia), we consider a region's emissions to be composed of two components, p_j and p_k. The first- and second-order semi-normalized

sensitivity coefficients with respect to total emissions in the region, $p_{j+k} = p_j + p_k$, can be computed as:

$$\mathbf{S}_{j+k}^{(1)} = \frac{\partial \mathbf{C}}{\partial \varepsilon_j} + \frac{\partial \mathbf{C}}{\partial \varepsilon_k} = \mathbf{S}_j^{(1)} + \mathbf{S}_k^{(1)} \quad \textbf{(2.13)}$$

$$\mathbf{S}_{j+k,j+k}^{(2)} = \frac{\partial^2 \mathbf{C}}{\partial \varepsilon_j^2} + \frac{\partial^2 \mathbf{C}}{\partial \varepsilon_k^2} + \frac{\partial^2 \mathbf{C}}{\partial \varepsilon_j \partial \varepsilon_k} + \frac{\partial^2 \mathbf{C}}{\partial \varepsilon_k \partial \varepsilon_j} = \mathbf{S}_{j,j}^{(2)} + \mathbf{S}_{k,k}^{(2)} + 2 \cdot \mathbf{S}_{j,k}^{(2)} \quad \textbf{(2.14)}$$

The first-order sensitivity coefficient to aggregate emissions equals the sum of the first-order coefficients to each component (Equation 2.13). However, the second-order coefficient to aggregate emissions includes an additional cross-sensitivity term $\mathbf{S}_{j,k}^{(2)}$ (Equation 2.14). The magnitude of the cross-sensitivity interaction increases with the proximity of the two emissions components. If j and k refer to different emitters of the same species, then the cross-sensitivity coefficients will typically have the same sign as the other second-order coefficients. Therefore, the magnitude of $\mathbf{S}_{j+k,j+k}^{(2)}$ increases with the proximity of the component emission sources, while $\mathbf{S}_{j+k}^{(1)}$ is unaffected. Correspondingly, for a given tonnage of emissions α will be greater if the size of the emissions region is smaller.

Equations 2.13 and 2.14 also help explain why domain-wide emissions tend to generate more nonlinear atmospheric response than the individual components. In this case, we re-consider Equations 2.13-2.14 with j and k defined to be two separate emission regions rather than two sources within a region. The first-order sensitivity coefficient of the aggregate region, $\mathbf{S}_{j+k}^{(1)}$, equals the sum of the first-order sensitivity coefficients for the individual regions (Equation 2.13). However, the second-order sensitivity coefficient for the combined region contains an additional term representing the cross-sensitivity interaction (Equation 2.14). The cross-sensitivity term will tend to make an aggregate

emission region have a higher nonlinearity index than would be suggested by its component parts. Because Taylor expansions are less accurate when nonlinearity is most intense, domain-wide emissions (Table 2.2 and Figure 2.2) are likely to represent a worst-case scenario of bias in source attribution.

2.3.4 Cross-sensitivities

Cross-sensitivity interactions can cause the impact of a multi-faceted control strategy, or the source contribution of an ensemble of emission sources, to differ from the sum of its parts. The Atlanta and Macon regions provide interesting case studies of these interactions. It should be noted in the following case studies that source attribution presents an extreme case of the impact of cross-sensitivity, because it represents 100% removal of each source. For assessing the effectiveness of control strategies, the relative impact of all second-order terms, including cross-sensitivities, would be less and would scale by the fractional perturbations of interest.

In the Atlanta region, point source NO_x originates primarily as elevated plumes from several large power plants, whereas other emissions are released over broad areas at ground-level, with greatest intensity near the region center. We separately compute sensitivities and cross-sensitivities to three categories that together comprise Atlanta's anthropogenic NO_x emissions: on-road vehicles, area sources (including non-road vehicles), and point sources.

Figure 2.6 presents each sensitivity term as it appears in a second-order Taylor expansion of average source attribution (Equation 2.11) for 8-hour ozone averaged over the Atlanta region. For both first- and second-order sensitivity, the term for combined

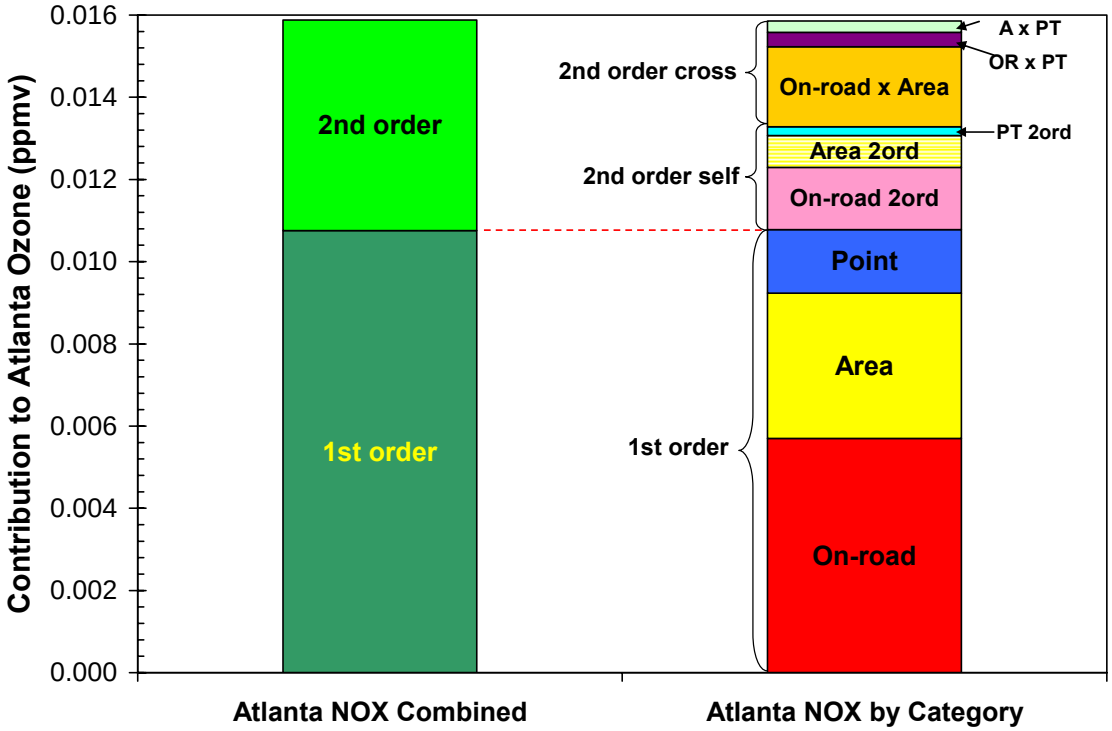

Figure 2.6. Source contribution of Atlanta NO_x emissions, combined and by category, to 8-hour ozone in Atlanta. "OR x PT" is the cross-sensitivity contribution of the on-road and point source second-order term. "A x PT" is the cross-sensitivity contribution of the area (including non-road vehicles) and point source second-order term.

emissions equals the sum of the terms by category (including cross terms in the case of second-order) to within 1 percent, indicative of consistency within HDDM-3D results. However, if source attribution assessed the contribution of each category independently it would neglect the cross-sensitivity terms. This would under-predict the total impact of Atlanta NO_x emissions on Atlanta ozone by more than 2 ppb. The dominant cross-sensitivity term is that between on-road and area sources, consistent with their larger individual contributions and closer spatial proximity to each other than to point sources.

Table 2.5. Decomposition of the source contribution of each NO_x emission region to episode-average 8-hour ozone in the Macon region. The second-order self-sensitivity coefficients have been scaled by -0.5, and the cross-sensitivity coefficients by -1.0, to reflect the source contribution (see Equation 2.11).

		2nd order: Emission region and…			
Emission region	**1st order**	**Macon**	**Atlanta**	**Scherer**	**Branch**
Macon	4.85 ppb	0.90 ppb	0.32 ppb	0.34 ppb	0.06 ppb
Atlanta	5.68		0.94	0.48	0.04
Scherer	3.46			0.98	0.01
Branch	1.05				0.12

Macon provides an illuminating example of how emissions from various regions can interact in their impact on ambient concentrations. Macon ozone can be impacted by NO_x emitted from local sources and from the Atlanta region and Plants Scherer and Branch (Hu *et al.*, 2004). We decompose the source contribution of NO_x emissions from each region to ozone in Macon into first-order impacts and second-order self- and cross-sensitivity impacts (Table 2.5). The first-order terms dominate the source attribution of Macon ozone. For second-order "self-sensitivity," the largest term is that to Scherer emissions, indicative of the tendency of its plume to coincide with high ozone concentrations in the region. Cross-sensitivities are smaller than the other second-order sensitivities because the "footprints" of strongest impact do not always overlap. The largest cross-sensitivity term is between emissions from Atlanta and Scherer, which are aligned to the northwest of Macon. The smallest cross-sensitivity terms are those involving Plant Branch, whose plume does not often align with those of other sources as it is located northeast of Macon whereas Atlanta and Scherer are located to the northwest.

2.3.5 "Sensitivity" of sensitivities to emissions inventory

Second-order self- and cross-sensitivity terms represent not merely complications to scientific and policy analysis, but also storehouses of information regarding how sensitivity analysis results vary with the underlying emissions inventory. Such information is important because inaccuracy in emissions inventories is a leading cause of uncertainty in atmospheric models (Russell and Dennis, 2000; Hanna *et al.*, 2001). When atmospheric response to emissions is nonlinear, errors in an inventory will affect not only concentrations but also the sensitivity of those concentrations to emission perturbations. For example, Plant Scherer switched to a cleaner-burning coal after the FAQS 2007 emissions inventory was developed, reducing its NO_x emission rate. It may be asked how inventory-based estimates of sensitivities and source contributions for both Scherer and other sources should be adjusted to account for the reduction in Scherer emissions. The following section develops a theoretical framework for addressing such questions, and considers the Macon case study as an illustrative example.

Suppose actual emission rate P_j* differs by fraction $\Delta\varepsilon_j$ from the rate P_j assumed in the inventory-based simulation. Any other source k is assumed to emit at its inventoried rate. In other words,

$$\begin{aligned} P_j^* &= P_j + \Delta\varepsilon_j P_j \\ P_k^* &= P_k \end{aligned} \qquad \textbf{(2.15)}$$

We can then apply the second-order sensitivity coefficients from the inventory-based simulation to adjust all first-order sensitivity coefficients to the values they would have under the corrected emission rate.

$$\mathbf{s}_j^{(1)*}(ppb/tpd) = \left.\frac{\mathbf{S}_j^{(1)*}}{P_j^*}\right|_{P_j^*=P_j+\Delta\varepsilon_j P_j} \approx \left(\frac{\mathbf{S}_j^{(1)} + \Delta\varepsilon_j \mathbf{S}_{j,j}^{(2)}}{\mathbf{S}_j^{(1)}}\right)\cdot \mathbf{s}_j^{(1)} \qquad \textbf{(2.16)}$$

$$\mathbf{s}_k^{(1)*}(ppb/tpd) = \frac{\mathbf{S}_k^{(1)*}}{P_k^*}\bigg|_{P_j^*=P_j+\Delta\varepsilon_j P_j} \approx \left(\frac{\mathbf{S}_k^{(1)} + \Delta\varepsilon_j \mathbf{S}_{j,k}^{(2)}}{\mathbf{S}_k^{(1)}}\right)\cdot \mathbf{s}_k^{(1)} \qquad \textbf{(2.17)}$$

In Equations 2.16-2.17, $\mathbf{s}^{(1)}$ (=$\mathbf{S}^{(1)}/P$) and $\mathbf{s}^{(1)*}$ (=$\mathbf{S}^{(1)*}/P^*$) represent the first-order sensitivities on a per-ton basis when source *j* is at its inventoried and actual emission rates, respectively. Equation 2.16 describes the necessary adjustment in the first-order sensitivity to the corrected emission source; Equation 2.17 shows how the cross-sensitivities lead to adjustments in the first-order sensitivities to other sources even though all sources other than *j* are assumed to emit at their inventoried rates.

For ozone-NO_x sensitivity, the daytime second-order sensitivity *coefficients* are typically negative, reflecting concave-down response. Thus, if the actual NO_x emission rate for one source is larger than its inventory rate ($\Delta\varepsilon_j>0$), then the actual first-order ozone-NO_x sensitivities for all sources should be smaller than was modeled (Figure 2.7, dashed lines, and Figure 2.8). Physically, this means that the higher the NO_x emission rates, the less sensitive is ozone to each incremental *ton* of NO_x emissions. It should be noted, however, that if a source is larger than inventoried, each incremental *percentage* change will represent more tons and thus may yield a bigger impact than modeled (this can be seen by multiplying Equation 2.16 by P_j^*). In many control strategy considerations, such as measures for reducing vehicle travel, the *relative* change in emissions may be better-represented than the absolute change.

Note that in the Macon example (Table 2.5), the cross-sensitivity terms are several times smaller in magnitude than the self-sensitivity ($\mathbf{S}_{j,j}^{(2)}$) terms. Thus, uncertainty in the emission rate of one source will primarily impact sensitivity estimates with respect to

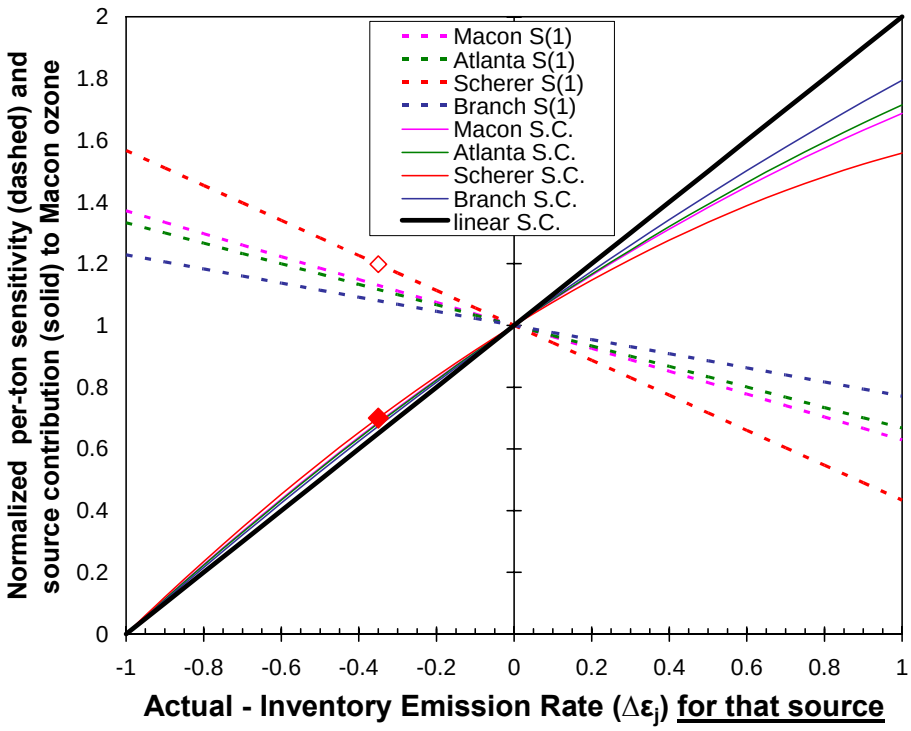

Figure 2.7. Variation in the episode-averaged source contribution (solid) and per-ton sensitivity (dashed) of each NO_x source region to Macon 8-hour ozone, as a function of the fraction by which actual emissions of that source exceed inventory values. Results are normalized to their values when the actual = inventory. For example, if Plant Scherer emits 35% less than inventoried, its overall source contribution decreases by 30% (solid diamond) though the impact of an incremental ton increases by 20% (open diamond).

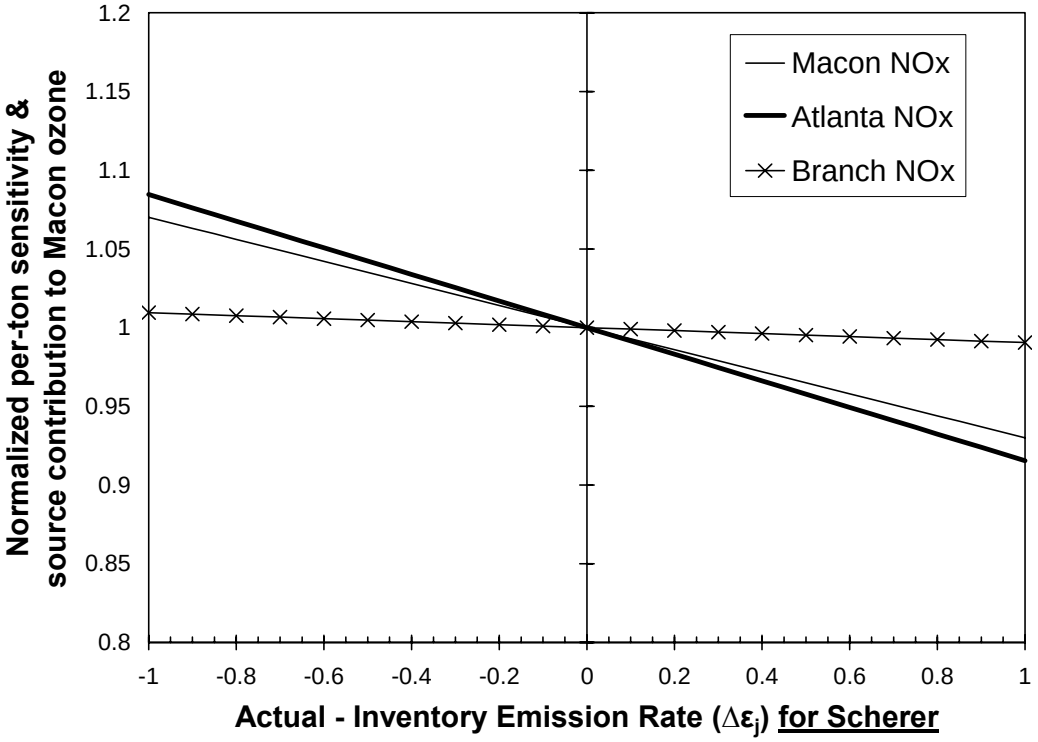

Figure 2.8. Variation in the episode-averaged incremental sensitivity of Macon 8-hour ozone to NO_x emissions from each source region, as a function of the fraction by which actual Scherer emissions may exceed the inventory. Results are normalized to their value when actual = inventory. If Plant Scherer emits 35% less than inventoried, sensitivity to each other region changes by less than 5%.

that source. This is reflected in the much steeper responses to changes in the emission rate at the same source (Figure 2.7) than to changes at another source (Figure 2.8).

How do HDDM-3D estimates of source contribution respond to changes in emission rates? We first consider source attribution when the actual emission rate (P_j*) differs from the inventory emission rate (P_j) *of that source*. The following equations show how Equations 8 and 9 can be applied to adjust the inventory-based estimate of SC to the SC of actual P_j*:

$$SC\ of\ P_j^* = \mathbf{C}\Big|_{p_j=P_j^*} - \mathbf{C}\Big|_{p_j=0} = \left\{\mathbf{C}\Big|_{p_j=P_j} - \mathbf{C}\Big|_{p_j=0}\right\} + \left(\mathbf{C}\Big|_{p_j=P_j^*} - \mathbf{C}\Big|_{p_j=P_j}\right) \quad \textbf{(2.18)}$$

$$SC\ of\ P_j = \left\{\mathbf{C}\Big|_{p_j=P_j} - \mathbf{C}\Big|_{p_j=0}\right\} \approx \mathbf{S}_j^{(1)} - \frac{1}{2}\mathbf{S}_{j,j}^{(2)} \quad (by\ Eqn.\ 9) \quad \textbf{(2.19)}$$

$$\left(\mathbf{C}\Big|_{p_j=P_j^*} - \mathbf{C}\Big|_{p_j=P_j}\right) \approx \Delta\varepsilon_j \mathbf{S}_j^{(1)} + \frac{\Delta\varepsilon_j{}^2}{2}\mathbf{S}_{j,j}^{(2)} \quad (by\ Eqn.\ 8) \quad \textbf{(2.20)}$$

$$Thus\ SC\ of\ P_j^* \approx (1+\Delta\varepsilon_j)\mathbf{S}_j^{(1)} + \frac{(\Delta\varepsilon_j{}^2 - 1)}{2}\mathbf{S}_{j,j}^{(2)} \quad \textbf{(2.21)}$$

Note that in the decomposition of the SC of actual rate P_j* (Equation 2.21), the first-order term scales linearly from the corresponding term for the inventory-based SC (Equation 2.19). However, the second-order term does not scale linearly from the corresponding term in Equation 2.19. Thus SC increases with the actual size of the emission source, but in a nonlinear fashion (Figure 2.7). The deviation from linear response can be observed by comparing each solid curve with the bold diagonal line in Figure 2.7. Scherer exerts the most nonlinear impact on Macon ozone, consistent with Table 2.4 and Table 2.5. It should be noted that reliability of results in Figs. 2.7 and 2.8 declines with the magnitude of inventory error as higher-order terms become more significant.

To estimate how source attribution for one source (k) responds to changes in the emission rate of another source (j), we apply Equation 2.17 to compute $\mathbf{S}_k^{(1)*}$. Lacking direct (third-order) information about how second-order coefficients of one source respond to perturbations in the emission rate of another source, we assume that $\mathbf{S}_{k,k}^{(2)*}$ scales proportionally to $\mathbf{S}_k^{(1)*}$.

$$\begin{aligned} SC\ of\ P_k^* &\approx \mathbf{S}_k^{(1)*} - \frac{1}{2}\mathbf{S}_{k,k}^{(2)*} \\ &\approx \mathbf{S}_k^{(1)} + \Delta\varepsilon_j \mathbf{S}_{j,k}^{(2)} - \frac{1}{2}\frac{\mathbf{S}_k^{(1)} + \Delta\varepsilon_j \mathbf{S}_{j,k}^{(2)}}{\mathbf{S}_k^{(1)}}\mathbf{S}_{k,k}^{(2)} \end{aligned} \quad \textbf{(2.22)}$$

Because Equation 2.22 assumes that second-order self-sensitivity is proportional to first-order sensitivity, the normalized response of source contribution to changes in another source's emission rate equals the normalized response of first-order sensitivity (Figure 2.8).

Our examination of how sensitivities and source attribution respond to inaccuracies in an emissions inventory only scratches the surface of how high-order sensitivities can be applied to uncertainty analysis. Such application is invaluable, as formulation of efficient control strategies depends on accurately simulating not only ambient concentrations, but also their responsiveness to emission perturbations. While atmospheric modeling studies routinely report the level of agreement between simulated and observed concentrations, sensitivity and source apportionment estimates can not be evaluated directly and their uncertainty rarely is examined systematically. Future work could extend the above methods to examine how sensitivity and source apportionment are impacted by uncertainty or error in other parameters such as meteorology, reaction rates, and initial and boundary conditions.

CHAPTER 3

OZONE PRODUCTION REGIME DIAGNOSIS AND ITS RELEVANCE TO CONTROL STRATEGY FORMULATION*

3.1 Introduction

Effective formulation of control strategies requires knowledge of the responsiveness of ozone to emissions of its two main precursors, nitrogen oxides ($NO_x = NO+NO_2$) and volatile organic compounds (VOC). While responsiveness depends nonlinearly on an array of spatially and temporally variable factors, a large body of research has sought to classify ozone formation into categories of chemical regime (Sillman *et al.*, 1990; NRC, 1991; Sillman, 1999). In NO_x-limited regimes, ozone increases with increasing NO_x and exhibits only slight sensitivity to VOC; in VOC-limited (or NO_x-saturated) regimes, ozone increases with VOC and exhibits slight or even negative sensitivity to NO_x. Transitional conditions of dual sensitivity also occur. Classification of ozone production regime helps determine whether NO_x or VOC emissions should be targeted more aggressively in strategies to reduce ozone.

In addition to photochemical modeling of ozone responsiveness, "indicator ratios" have been sought to diagnose ozone production regime based on observable concentrations and to corroborate atmospheric models (Sillman *et al.*, 1995; Lu and

* This chapter will be submitted to Journal of Geophysical Research, with co-authors Armistead G. Russell and Yongtao Hu. It is an extended version of "Alternative approaches to diagnosing ozone production regime," in press in Air Pollution Modeling and Its Application XVII, NATO/CCMS International Technical Meeting, Banff, Canada, October 2004. Copyright permissions have been granted from Kluwer Academic Publishers.

Chang, 1998; Kleinman, 2000; Sillman and He, 2002). Recent work has also suggested that ozone production regime can be diagnosed by satellite observations (Martin *et al.*, 2004). Regardless of diagnosis method, two factors hinder the usefulness of any single classification. First, because ozone production is nonlinear, response to large changes in emissions may not scale linearly from incremental sensitivity. Second, because ozone forms downwind of emission sources, response to domain-wide emissions may not reflect response to local emissions.

Here, we compare modeled ozone sensitivities to NO_x and VOC during a summertime air pollution episode in the southeastern U.S. with modeled values of three widely used indicator ratios. By modeling the response of ozone to both large and infinitesimal perturbations of both local and region-wide emissions, we examine how ozone sensitivity depends on the size and scope of the emission perturbation. Lessons are drawn regarding the usefulness of ozone production regime diagnosis.

3.2 Method

3.2.1 Direct, high-order sensitivity analysis

The Decoupled Direct Method in Three Dimensions (DDM-3D) provides a computationally efficient method for computing the sensitivity of modeled concentrations to perturbations in input parameters such as initial conditions, boundary conditions, or emission rates (Yang *et al.*, 1997). The method computes sensitivity coefficients simultaneously with concentrations, utilizing the transport and chemistry mechanisms of the underlying model. Hakami *et al*. (2003a) recently extended DDM-3D to compute higher-order sensitivity coefficients.

We have implemented second-order HDDM-3D into the Community Multiscale Air Quality (CMAQ) model v. 4.3 (Byun and Ching, 1999), with the SAPRC-99 chemical mechanism (Carter, 2000). First-order sensitivity coefficients, $s_{ij}^{(1)} = \partial C_i/\partial p_j$, represent the local sensitivity or "slope" of species i with respect to input parameter p_j whose unperturbed value is P_j. Perturbations in p_j are considered by defining a scaling variable, ε_j, with a nominal value of 1 such that

$$p_j = \varepsilon_j P_j = (1 + \Delta\varepsilon_j) P_j \qquad \textbf{(3.1)}$$

Second-order sensitivities, $s_{i,j1,j2}^{(2)} = \partial^2 C_i/(\partial p_{j1} \partial p_{j2})$, represent the second-derivative or local "curvature" of the species-parameter relationship. In this chapter we present sensitivity coefficients S_{ij} semi-normalized to the size of the unperturbed input field:

$$S_{ij}^{(1)} = P_j \frac{\partial C_i}{\partial p_j} = P_j \frac{\partial C_i}{\partial (\varepsilon_j P_j)} = \frac{\partial C_i}{\partial \varepsilon_j} \qquad \textbf{(3.2)}$$

For certain comparisons, we divide S by the coincident ozone concentrations; thus, for example, a concentration-normalized ozone-to-NO_x sensitivity of 0.15 (unitless) means that a 1% reduction in NO_x emissions would reduce ozone by 0.15%.

Due to nonlinearity, accurate approximation of response to a large perturbation requires consideration of the second-order sensitivity coefficients via Taylor expansion (Hakami *et al.*, 2003a):

$$(\mathbf{C}\Big|_{p_j=(1+\Delta\varepsilon_j)P_j} - \mathbf{C}\Big|_{p_j=P_j}) \approx \Delta\varepsilon_j \mathbf{S}^{(1)} + \tfrac{1}{2}\Delta\varepsilon_j^2 \mathbf{S}^{(2)} + \textit{higher order terms} \qquad \textbf{(3.3)}$$

Note that the second-order term scales with $\Delta\varepsilon^2$, so its relative importance increases with the fractional perturbation from the base case. The accuracy of CMAQ-HDDM has been rigorously demonstrated by comparison to finite difference calculations for a variety of

brute force perturbations (Chapter 2). Thus, we have high confidence in the ability of HDDM-3D to capture response of the underlying model.

3.2.2 Species indicator ratios

Numerous studies have suggested metrics by which the relative concentrations of certain chemical compounds at a receptor could indicate whether ozone was formed under primarily NO_x- or VOC-limited conditions. Here we focus on three indicator ratios that were introduced by Sillman *et al.* (1995) and have been further considered by others including Lu and Chang (1998), Kleinman (2000), and Sillman and He (2002): (1) H_2O_2/HNO_3, (2) $HCHO/NO_y$ (where NO_y is total reactive nitrogen), and (3) O_3/NO_z (where NO_z is the sum of NO_x reaction products, or NO_y-NO_x).

All three ratios are expected to be higher in NO_x-limited regimes and lower in VOC-limited regimes. The first ratio compares the concentration of H_2O_2, the major sink for odd hydrogen radicals (OH and HO_2) in NO_x-limited regimes (via the reaction $HO_2+HO_2 \rightarrow H_2O_2+O_2$), with the concentration of HNO_3, the major sink for odd hydrogen in VOC-limited regimes (via the reaction $OH+NO_2 \rightarrow HNO_3$) (Sillman *et al.*, 1995). The ratio $HCHO/NO_y$ serves as a reactivity-weighted proxy for the VOC/NO_x ratio, because HCHO is a product of reactions of VOC with OH (Sillman *et al.*, 1995). The rationale for considering O_3/NO_z is more complex, and supposes that the quantity is approximately proportional to the photochemical production rate of odd hydrogen divided by the loss rate of odd nitrogen (Sillman *et al.*, 1995; Kleinman *et al.*, 1997). The ability of O_3/NO_z to diagnose ozone sensitivity is expected to weaken when reactions other than ozone photolysis provide significant sources of odd hydrogen (Sillman and He, 2002).

3.2.3 Model episode

CMAQ-HDDM is applied to model ozone and its sensitivity to precursor emissions in the southeastern United States during the August 11-20, 2000 air pollution episode. Results from the first two days are ignored to allow model initialization. Modeling methodology and evaluation of simulated relative to observed concentrations during the episode are presented extensively elsewhere (Hu *et al.*, 2004), with performance well within U.S. EPA benchmarks. Meteorology for the episode is simulated with the fifth-generation Pennsylvania State University / National Center for Atmospheric Research Mesoscale Model (MM5) version 3.3.4 (Grell *et al.*, 1994) as described by Hu et al. (2003). Emissions are taken from the Year 2000 emissions inventory developed for the Fall-Line Air Quality Study (FAQS) (Unal *et al.*, 2003).

We focus on modeling results from the 12-km resolution nest of the FAQS domain, which covers Georgia and surrounding states in the southeastern United States. We define "domain-wide emissions" as anthropogenic emissions occurring within the outer 36-km domain that covers the eastern United States from Texas to Maine. Sensitivities to domain-wide emissions are modeled by using 36-km resolution results to provide boundary concentrations and sensitivities for the 12-km nest; sensitivities to local emissions are modeled on the 12-km domain only, with boundary concentrations provided by the 36-km domain but boundary sensitivities set to zero.

3.3 Results and Discussion

3.3.1 Spatial and temporal variability of sensitivity

CMAQ-DDM simulations indicate significant spatial and temporal variability in the sensitivity of peak-hour ozone to domain-wide anthropogenic emissions. August 14 and August 17 typify the range of conditions during the episode. On August 14, a day with moderate temperatures relative to the otherwise hot episode, ozone concentrations were correspondingly low. While CMAQ-DDM results indicate significant sensitivity ($S^{(1)} \geq 5$ ppb) of peak-hour ozone to NO_x but not VOC emissions for most of the domain, the localized areas of significant VOC sensitivity had some of the highest ozone concentrations on this day (Figure 3.1). Near the location of peak ozone in Atlanta, the first-order sensitivity coefficient to VOC reached 25 ppb (i.e., a 1% reduction in VOC would reduce ozone by 0.25 ppb) in a cell with negative sensitivity to NO_x.

On August 17, temperatures above 35°C and relatively stagnant winds contributed to the highest ozone concentrations of the episode (Hu *et al.*, 2004). CMAQ-DDM results indicate that sensitivity to NO_x was more pronounced on this day, while sensitivity to VOC diminished despite the higher ozone concentrations. Except for isolated locations of NO_x-inhibition, sensitivity to NO_x exceeded VOC sensitivity throughout the domain, including areas with especially high ozone. That VOC sensitivity was more prevalent on the days with lower ozone concentrations contrasts with Roselle and Schere (1995), who found greatest VOC sensitivity during the most severe events. However, our results could reflect that high temperatures, by enhancing biogenic emissions of VOC (Guenther *et al.*, 1996), reduced the relative importance of anthropogenic VOC.

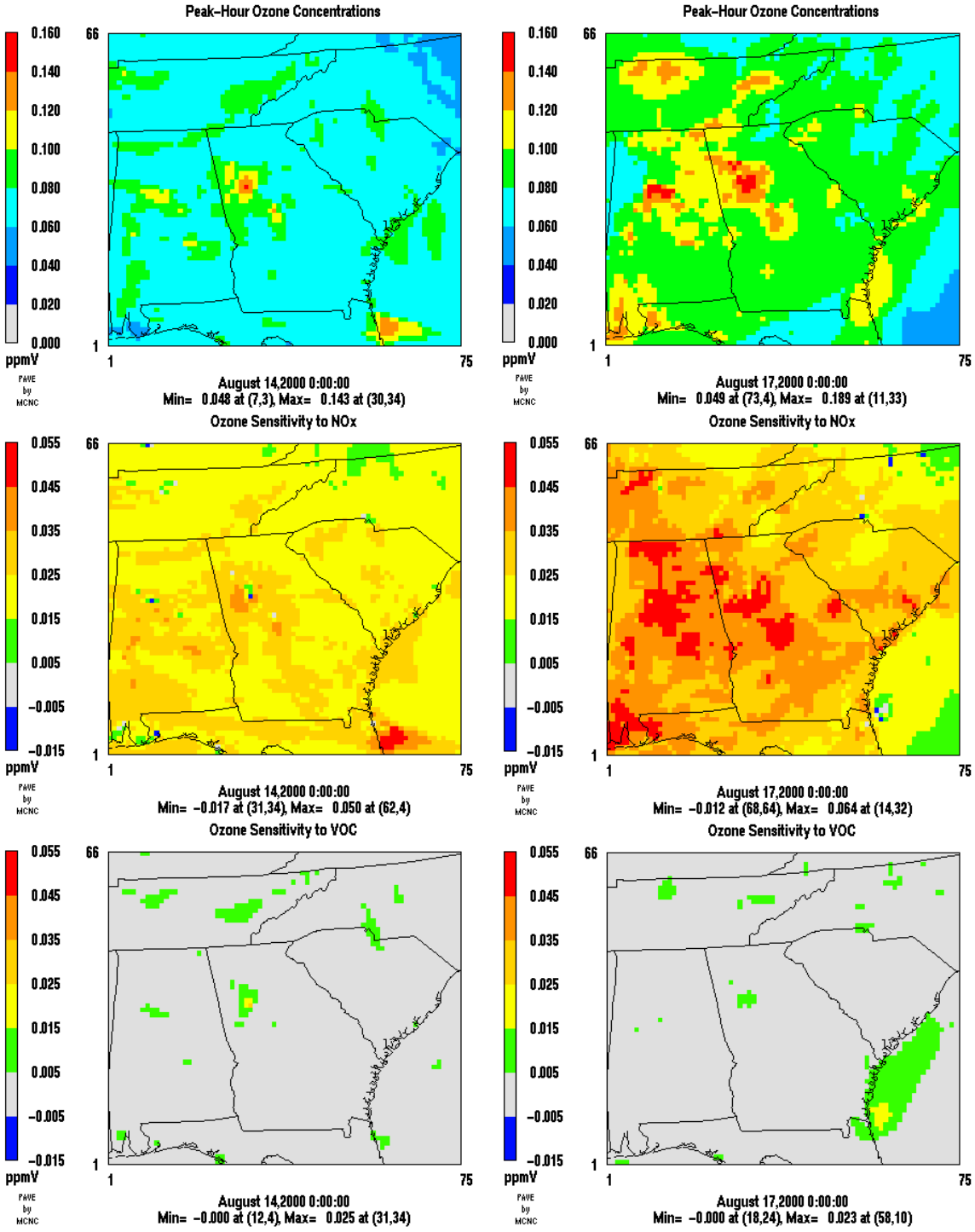

Figure 3.1. Peak-hour ozone concentrations (top) and their sensitivity to NO_x (middle) and VOC (bottom) on August 14 (left) and August 17 (right).

To explore the temporal variability of ozone sensitivity, we focus on conditions in Atlanta and Macon. Though both cities are in non-attainment of federal ozone standards and experienced some of the highest concentrations during the episode, CMAQ-DDM shows that ozone in Atlanta and Macon was characterized by very different sensitivities to emissions during the episode. At a grid cell containing downtown Atlanta, DDM-3D results indicate that afternoon ozone was more sensitive to VOC than to NO_x on the first three days of the episode but primarily limited by NO_x on later days (Figure 3.2). At night, ozone at this location exhibited strong negative sensitivity to NO_x, as titration by NO_x pushed ozone concentrations to near zero in the shallow nocturnal boundary layer. In Macon, the city with the second-highest ozone concentrations in Georgia, daytime ozone was consistently sensitive to domain-wide NO_x emissions and sensitivity to VOC emissions was almost always negligible. Day-to-day variability in ozone sensitivity was much more subdued in Macon than in Atlanta.

3.3.2 Species indicator ratios

For each day and ground-level grid cell, the DDM-3D first-order sensitivities and the corresponding species indicator ratios were evaluated based on concentration-normalized sensitivities at the time of peak hourly ozone concentrations. As expected, sensitivity to NO_x tends to increase with the H_2O_2/HNO_3 and $HCHO/NO_y$ indicator ratios, and VOC sensitivity tends to decrease (Figures 3.3 and 3.4). The response of NO_x sensitivity can be described as asymptotic in each case, as NO_x-inhibition (i.e., negative sensitivity) occurs only at low values of the ratios but sensitivities plateau as the ratios increase. Normalized sensitivity to NO_x peaks at about 0.5, whereas VOC sensitivity peaks at less than 0.15, indicative of the predominance of NO_x-limited ozone conditions during the episode.

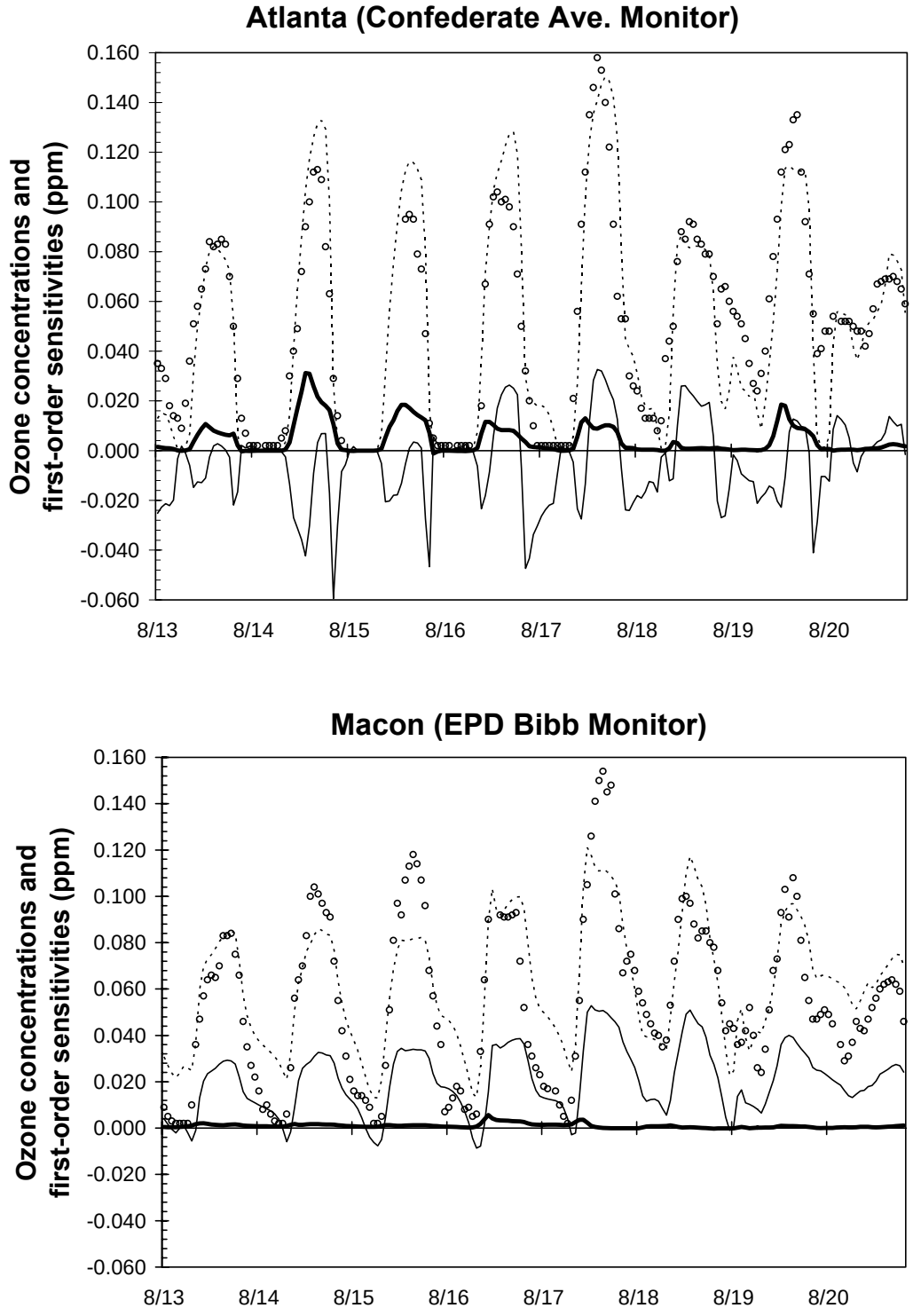

Figure 3.2. Modeled (dashed line) and observed (open circles) ozone concentrations and their first-order sensitivity coefficients to NO_x (thin line) and VOC (bold line), in downtown Atlanta (top) and Macon (bottom). All units are ppm. Date labels indicate local midnight.

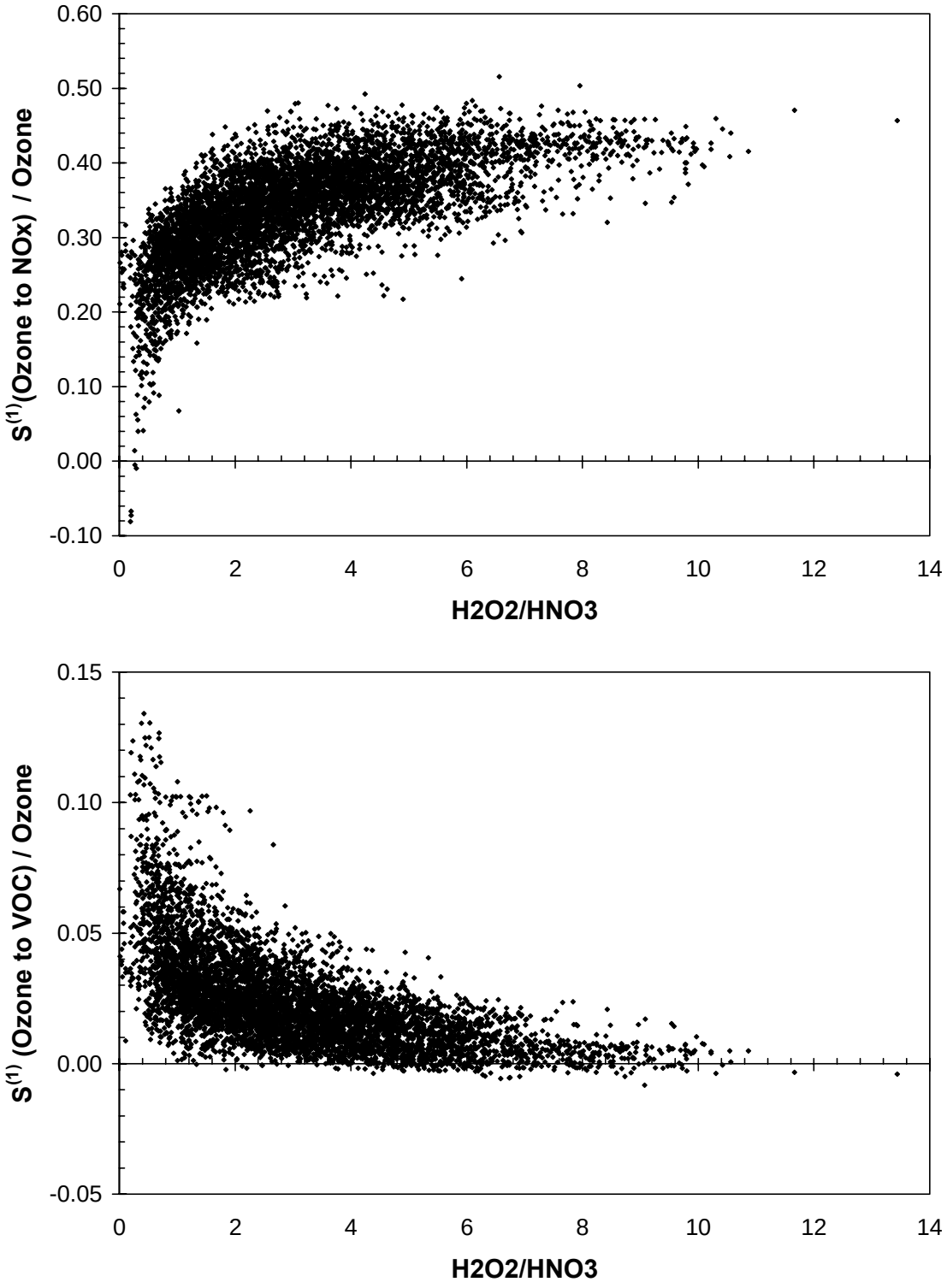

Figure 3.3. First-order sensitivity coefficients, normalized by ozone concentrations, of ozone response to anthropogenic NO_x (top) and VOC (bottom), plotted against concurrent concentration ratio H_2O_2/HNO_3 in CMAQ-DDM simulations. Each data point corresponds to a grid-cell-day at the hour of its daily peak ozone. For plotting purposes, only every fourth point is shown.

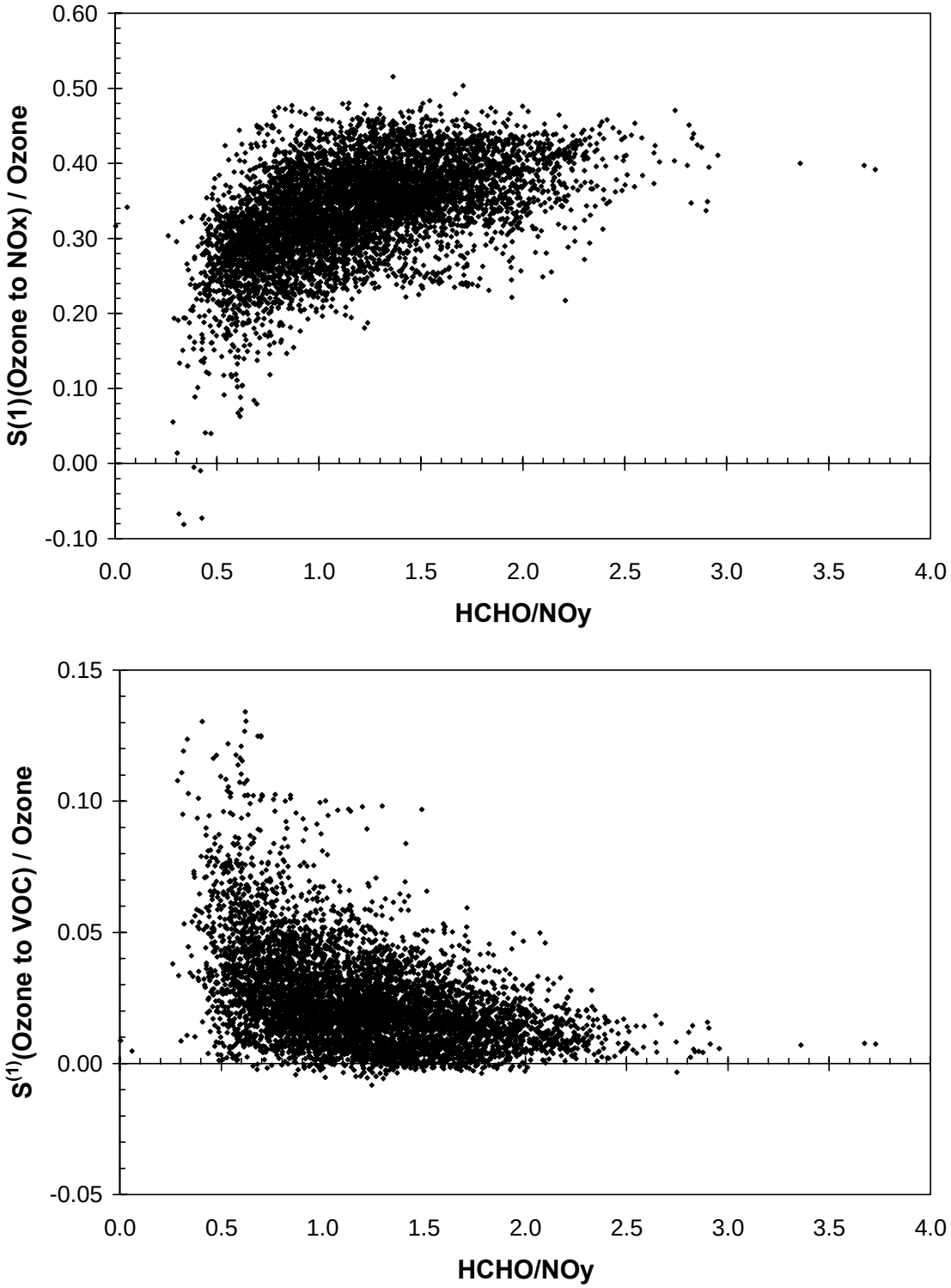

Figure 3.4. Normalized sensitivity (as in Figure 3.3) of peak-hour ozone to NO_x (top) and VOC (bottom), plotted against concurrent $HCHO/HNO_3$ ratios.

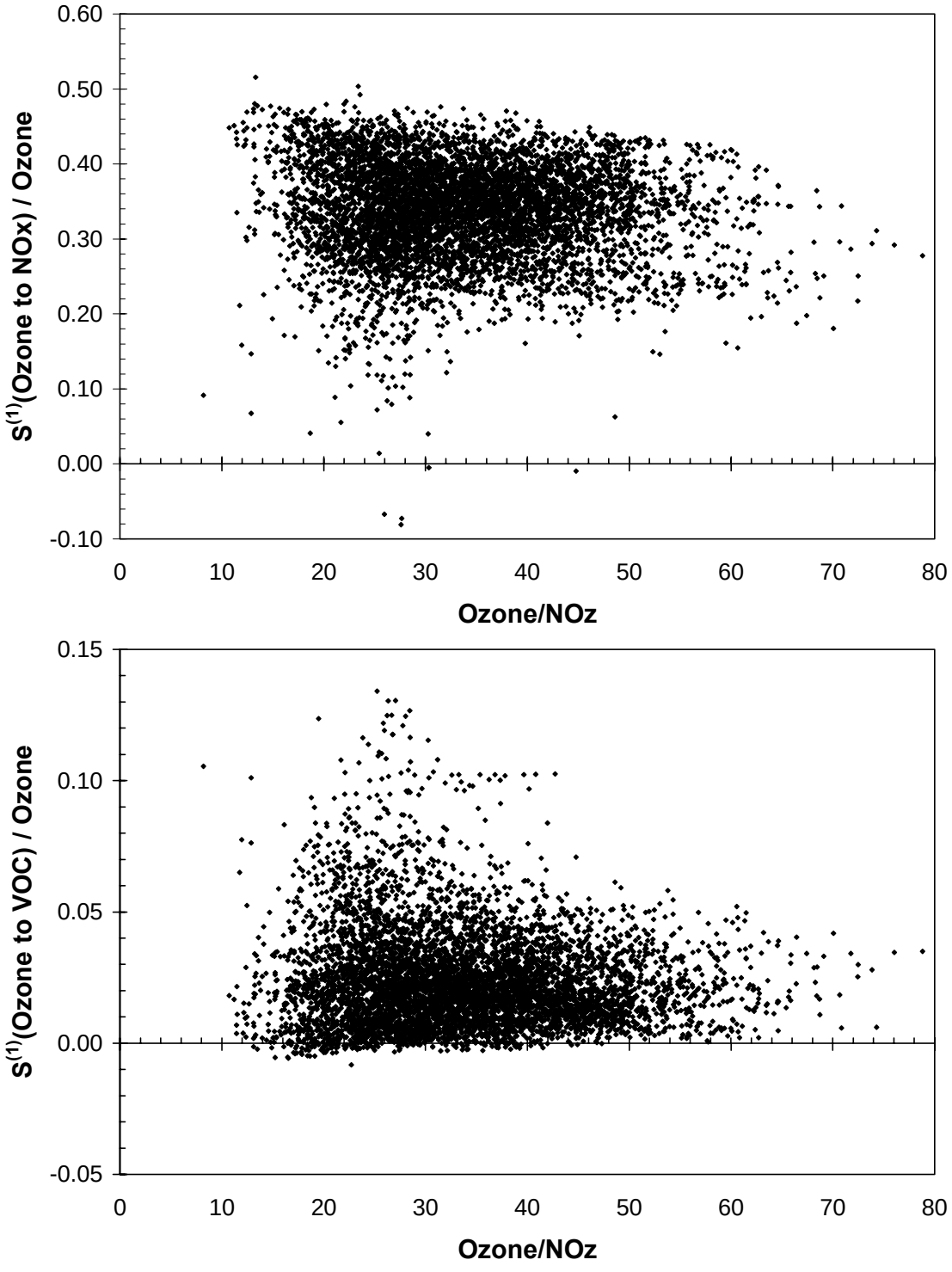

Figure 3.5. Normalized sensitivity (as in Figure 3.3) of peak-hour ozone to NO_x (top) and VOC (bottom), plotted against concurrent Ozone/NO_z ratios.

NO_x-inhibition is confined to locations with H_2O_2/HNO_3 less than 0.3 and $HCHO/NO_y$ less than 0.5 (Table 3.1). NO_x sensitivity consistently exceeds VOC sensitivity whenever H_2O_2/HNO_3 is greater than 0.7 or $HCHO/NO_y$ is greater than 0.8. The paucity of VOC-limited locations in the FAQS domain precludes clear definition of regime thresholds. However, the approximate transition zones indicated by the bounds on NO_x inhibition and greater VOC sensitivity are consistent with the thresholds suggested by earlier studies (Sillman *et al.*, 1995; Lu and Chang, 1998; Sillman and He, 2002). It should be noted in our results that even when indicator ratios are below the bounds defined by NO_x-inhibition, a majority of grid cells have greater sensitivity to NO_x than to VOC. Close inspection of the points in Figure 3.3 with exceptionally low values of H_2O_2/HNO_3 (ratio<0.15) but moderate sensitivity to NO_x and VOC reveals that they correspond to anomalous conditions when peak ozone occurred overnight concurrent with low concentrations of H_2O_2. Even neglecting these points, there is no firm lower bound of H_2O_2/HNO_3 in our simulations below which ozone sensitivity is consistently VOC-limited and insensitive to NO_x.

Table 3.1. Maximal indicator ratios in our simulations corresponding to (1) NO_x inhibition and (2) VOC sensitivity exceeding NO_x sensitivity, and ozone regime threshold values suggested by other studies. Ozone tends to be NO_x-limited above thresholds, and can be VOC-limited below.

	Max. ratio for NO_x-inhibition	Max. ratio for $S^{(1)}(O_3 \text{ to VOC}) > S^{(1)}(O_3 \text{ to } NO_x)$	*Sillman* (1995)	*Lu and Chang* (1998)	*Sillman and He* (2002)
H_2O_2/HNO_3	0.3	0.7	0.25-0.67	0.8-1.0	0.23-0.54
$HCHO/NO_y$	0.5	0.8	0.2-0.39	0.5-0.7	NA
O_3/NO_z	NA	NA	6-14	25-30	8-20

The ratio O_3/NO_z fails to define any clear distinction between ozone production regimes in our simulations (Figure 3.5). Grid cells with NO_x-inhibition or with strongest sensitivity to VOC correspond to a wide range of O_3/NO_z. This is consistent with studies that have found that the O_3/NO_z ratio is a weaker indicator of sensitivity than the other ratios (Sillman and He, 2002). Two factors hinder the usefulness of the O_3/NO_z ratio here. First, the ratio almost always exceeds 10 at the time of peak-hour ozone in our simulations, which is within the ranges of thresholds reported elsewhere (Table 3.1). Second, abundant biogenic VOC provides additional sources of odd hydrogen other than ozone photolysis, undermining the premise of the O_3/NO_z ratio.

While the indicator ratios are intended to provide metrics for applying observed concentrations to the diagnosis of ozone production regime, few observations of the necessary species are available for the episode. Measurements of H_2O_2 and HNO_3 are not available, and HCHO was measured only sporadically at two stations. The ratio O_3/NO_z could be computed only from observations at the two suburban Atlanta PAMS stations which concurrently measured NO_x, NO_y, and O_3. At the time of daily peak ozone, observed O_3/NO_z at these stations ranged from 11-35 during the episode, consistent with or exceeding the modeled range of 11-19 at the corresponding grid cells.

3.3.3 Size of perturbation

Although we have so far considered sensitivity to incremental perturbations, regimes have traditionally been characterized by the response of ozone to arbitrary percentage reductions in emissions of each precursor. For example, Lu and Chang (1998) considered 50% reductions in anthropogenic emissions, and Sillman *et al.* (1995) and Sillman and He (2002) considered 25-35% reductions. Such large perturbations were considered in

part to reduce computational noise, but in practice one can expect only modest NO_x reductions across a region. Given the concave-down response of daytime ozone to NO_x, greater nonlinearity increases the extent to which ozone reductions from large NO_x reductions exceed those indicated by scaling from incremental sensitivity.

Chapter 2 introduced an index, α, to characterize the nonlinearity of concentration response to emissions:

$$\alpha = \left| \frac{0.5 \cdot S^{(2)}}{S^{(1)}} \right| \qquad \textbf{(3.4)}$$

The product of the nonlinearity index and the fraction by which emissions are perturbed (i.e., $\alpha \cdot \Delta\varepsilon$) represents the relative importance of the second-order term in a Taylor approximation of the associated reduction in concentrations (Equation 3.3). Given the concave-down response of daytime ozone to NO_x (i.e., $S^{(2)}$ is typically negative), α indicates for a large reduction in emissions the extent to which the actual reduction in ozone would exceed that predicted by linearly scaling the incremental sensitivity.

We focus on the nonlinearity of ozone response to NO_x during times of daily peak ozone. Highest values of the nonlinearity index occur where values of H_2O_2/HNO_3 (Figure 3.6) and $HCHO/NO_y$ (not shown) are low. This reflects that ozone response to NO_x tends to be most nonlinear near the spatial peak in ozone concentrations and just downwind of intense NO_x emissions (Hakami *et al.*, 2003a) where HNO_3 and NO_y are highest. Since high α also coincides with low or negative first-order sensitivity, the range of response to NO_x indicated by Figures 3-5 narrows as greater fractional perturbations are considered. Thus, the relationships between NO_x sensitivity and the two ratios, though consistently positive, becomes more muddled as larger perturbations are considered. In fact, second-order Taylor approximations of HDDM-3D coefficients

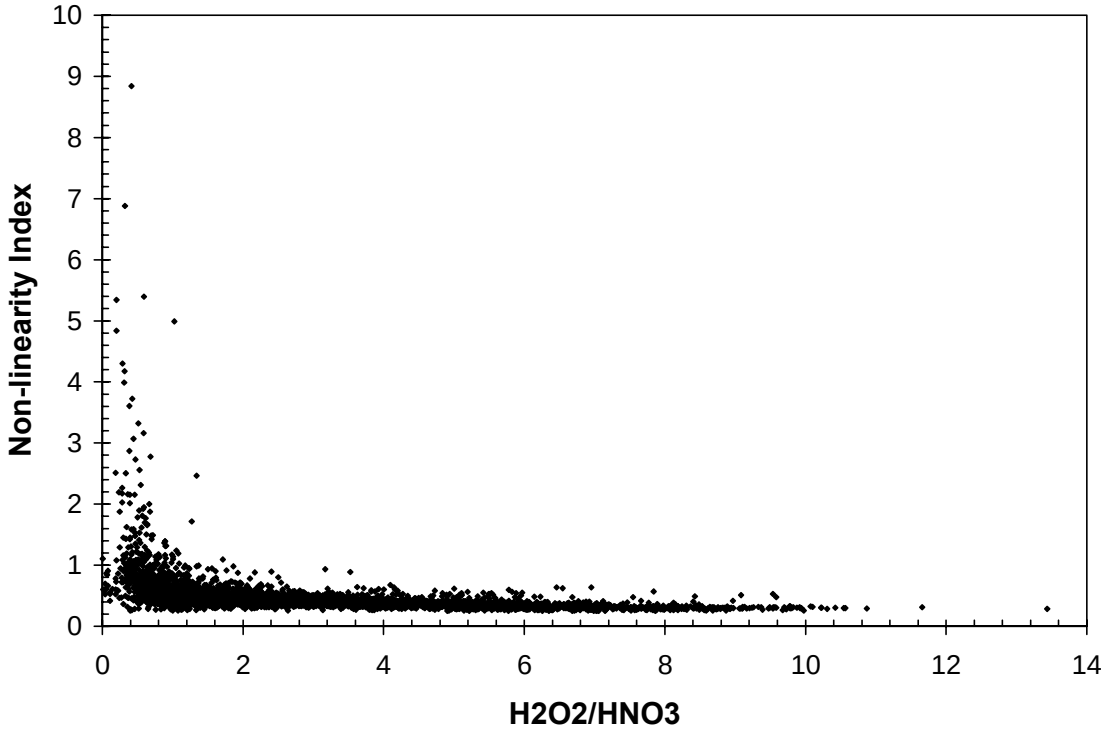

Figure 3.6 Nonlinearity index (Equation 3.4) of ozone response to NO_x plotted against concurrent H_2O_2/HNO_3 ratios.

indicate that in all grid cells with negative sensitivity to NO_x, ozone concentrations would decline if domain-wide NO_x emissions were reduced by 50% or more.

3.3.4 Location of perturbation

For urban and regional pollution control strategy formulation, ozone sensitivity to local emissions can be more pertinent than its response to domain-wide emissions. If a receptor is diagnosed as NO_x- (VOC-) limited with respect to domain-wide emissions, will NO_x (VOC) controls necessarily be the most effective local response? We investigate this question by applying DDM-3D to compute the sensitivity of ozone to emissions from two regions: the Atlanta region, defined here as the 13 non-attainment counties at the time of the episode, and the 7-county Macon-Warner Robbins Combined Statistical Area.

VOC emissions enhance ozone production primarily within 100 km of the source, so sensitivity to local VOC closely tracks sensitivity to domain-wide emissions (not shown). Intense NO_x emissions, however, often generate an initial decline in ozone concentrations before forming ozone downwind (e.g., Gillani and Pleim, 1996; Ryerson *et al.*, 2001). Figure 3.7 compares the first-order sensitivities of ozone in downtown Atlanta and Macon to domain-wide NO_x emissions and to emissions from within the respective regions. Sensitivity to domain-wide emissions is consistently higher than sensitivity to regional emissions, and the gap between the lines indicates the positive sensitivity to emissions from outside the region. In Atlanta, sensitivity to local emissions on August 16 and 17 is a sizable fraction of domain-wide sensitivity during the afternoon hours when ozone was highest. However, on the final three days of the episode DDM-3D indicates that local NO_x reduction would increase ozone concentrations, even though domain-wide sensitivity indicates primarily NO_x-limited ozone production. In Macon, sensitivities to

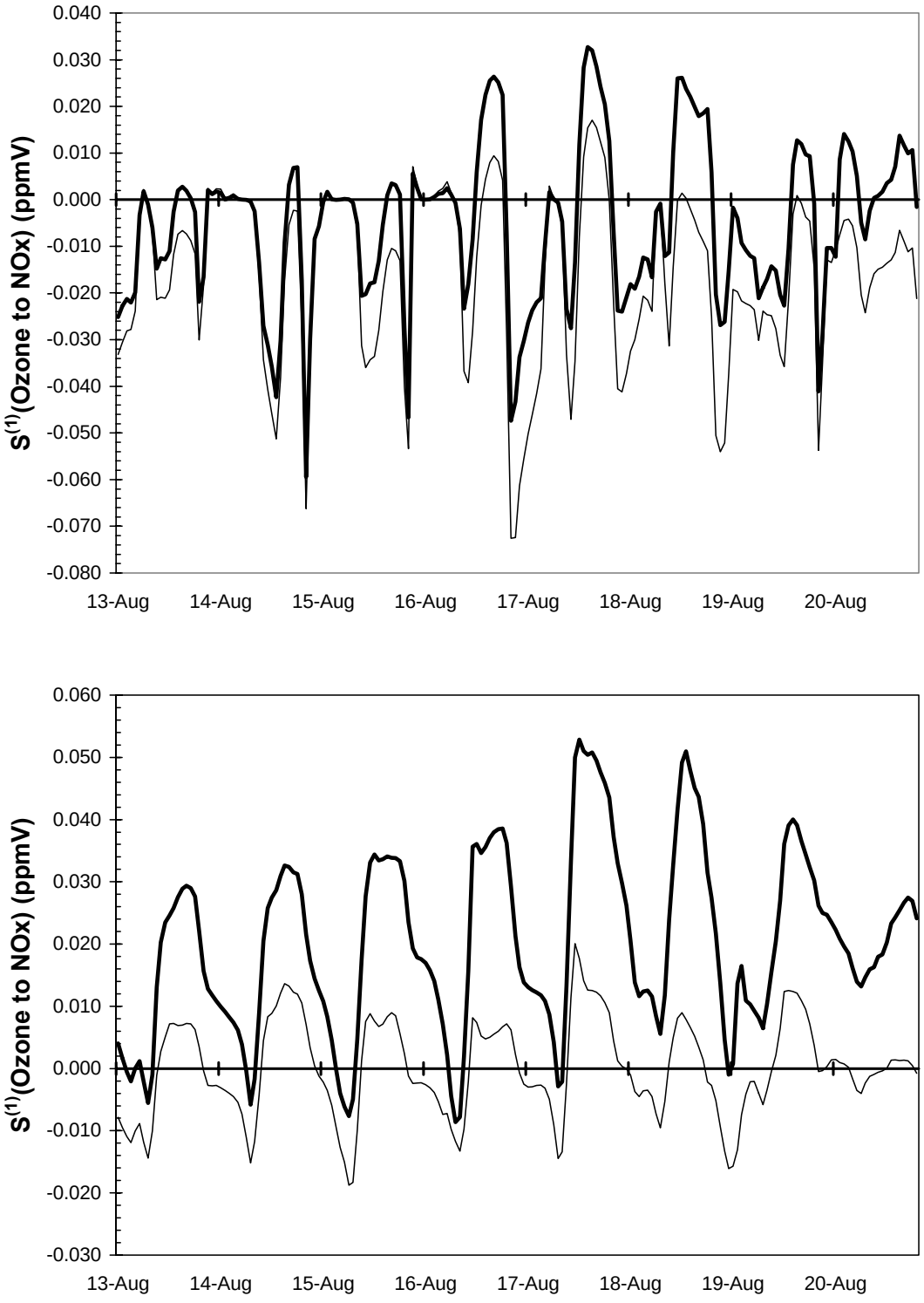

Figure 3.7. First-order sensitivity of ozone in downtown Atlanta (top) and Macon (bottom) to domain-wide (bold line) and local (thin line) NO_x emissions.

local emissions remain positive during the afternoon hours when ozone was highest. On a 24-hour average basis, however, the sensitivity to local emissions is virtually zero in Macon despite strongly positive sensitivity to domain-wide emissions.

Within the Atlanta region, sensitivity of peak-hour ozone at a particular location and day to domain-wide emissions is a poor predictor of that location's sensitivity to Atlanta emissions (Figure 3.8). While sensitivity to domain-wide emissions provides an upper-bound for sensitivity to local emissions, the local emissions impact is often negative or negligible at locations with positive sensitivity to domain-wide emissions. Since spatio-temporal patterns of response to local and domain-wide emissions are not well correlated, what is the meaning of indicator ratios in the context of local emissions? As shown in Figure 3.9, sensitivity to non-Atlanta NO_x emissions exhibits an asymptotic response to the H_2O_2/HNO_3 ratio analogous to Figure 3.3, but sensitivity to local emissions declines to near zero as the ratio increases. These patterns suggest an additional meaning of indicator ratios—a signal of the origin of ozone in urban areas. As before, high H_2O_2/HNO_3 ratios signify NO_x-limited ozone production and low ratios signify NO_x-saturation. Because the Atlanta plume has a much higher NO_x/VOC ratio than the biogenic VOC-laden domain (Guenther *et al.*, 2000), ozone would more likely have formed under NO_x-limited conditions if it originated upwind of the region rather than from Atlanta emissions, and high H_2O_2/HNO_3 serves as a proxy for such conditions.

3.4 Conclusion

CMAQ-DDM results have shown that ozone in the southeastern United States is predominately governed by NO_x-limited conditions during the episode, consistent with earlier studies of the VOC-rich region (e.g., Chameides *et al.*, 1992). Significant

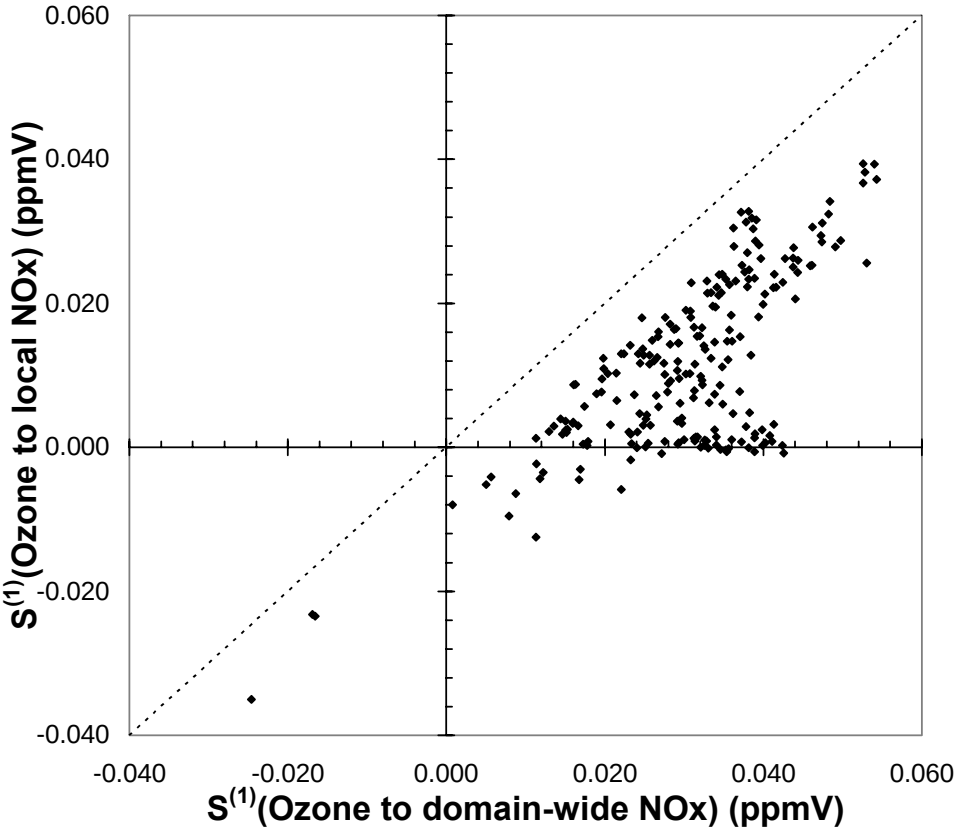

Figure 3.8. First-order sensitivity of daily peak-hour ozone to Atlanta region NO_x emissions plotted against concurrent sensitivity to domain-wide emissions. Each point represents a grid-cell-day within the Atlanta region.

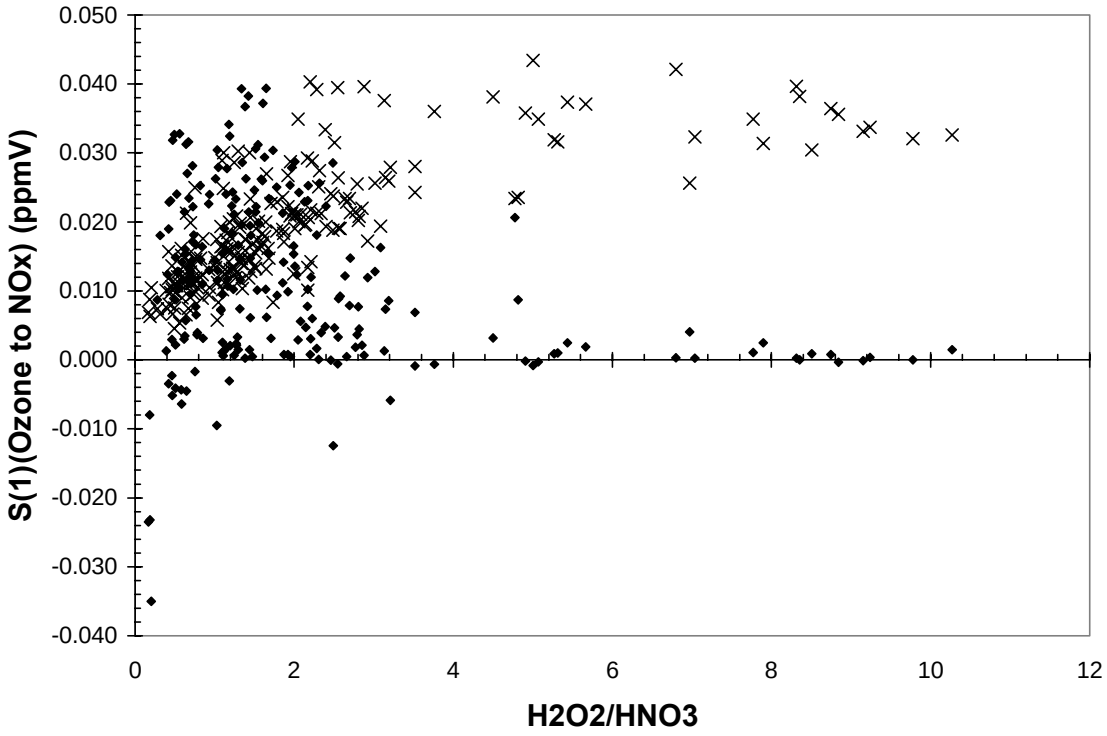

Figure 3.9. First-order sensitivity of daily peak-hour ozone at Atlanta region grid cells to local NO_x emissions (diamonds) and to other-than-local NO_x emissions (crosses), plotted against concurrent H_2O_2/HNO_3 ratios.

sensitivity to VOC occurs only in urban centers, but the dense populations and high ozone concentrations of these areas make them important from a policy perspective. The importance of anthropogenic VOC decreases with temperature, as hotter weather fosters biogenic VOC emissions and shifts ozone production toward greater NO_x limitation.

The concentration ratios H_2O_2/HNO_3 and $HCHO/NO_y$ have been shown to be useful but not definitive indicators of ozone sensitivity to domain-wide emissions. Ozone sensitivity to NO_x tends to increase asymptotically with each ratio, and significant sensitivity to VOC is confined to low values of the ratios. The ratio O_3/NO_z is not a meaningful predictor of ozone sensitivity during this episode. The associations between ozone sensitivities and species indicator ratios are consistent with those reported in earlier studies (Sillman *et al.*, 1995; Lu and Chang, 1998; Sillman and He, 2002), but the paucity of VOC-limited conditions hinders definitive quantification of threshold values here.

We have identified and explored two factors which complicate the usefulness of categorizing locations by ozone production regime. First, ozone production is nonlinear and the degree of nonlinearity varies spatially and temporally. We have shown that ozone tends to be most nonlinear when H_2O_2/HNO_3 and $HCHO/NO_y$ are low, so correlations of sensitivity with these ratios will diminish as the size of perturbation increases. Second, and more significant for air pollution policy, are the distinctions between response to domain-wide and local emissions. For VOC, domain-wide sensitivity is strongly indicative of the impact of local controls. For NO_x, however, local control may elicit a positive, negative, or neutral impact even when ozone exhibits strong positive sensitivity to domain-wide NO_x. Diagnosing the ozone production regime at a given receptor, whether by indicator ratio or by modeled sensitivity to domain-wide emissions, is

therefore insufficient to determine whether local NO_x control would be beneficial. In localities whose NO_x/VOC emissions ratios differ markedly from surrounding areas, species ratios may be recast as indicators of the upwind-versus local character of ozone formation.

CHAPTER 4

VARIABILITY OF OZONE YIELD WITH EMISSION LOCATION FOR NITROGEN OXIDES IN GEORGIA

4.1 Introduction

Given the abundance of summertime biogenic emissions of volatile organic compounds (VOC) in the eastern United States (Guenther *et al.*, 2000), numerous studies have suggested that effective control of regional ozone pollution will primarily require reduction of ozone's other principal precursor, nitrogen oxides ($NO_x \equiv NO+NO_2$) (e.g., Trainer *et al.*, 1987; McKeen *et al.*, 1991; Chameides *et al.*, 1992). Recognizing the central role of NO_x, the U.S. Environmental Protection Agency enacted the NO_x State Implementation Plan (SIP) Call (U.S.-EPA, 1998; U.S.-EPA, 2004b), mandating overall NO_x emissions reductions in eastern states but allowing trading among sources to reduce total costs to industry. As in many trading mechanisms (Tietenberg, 1980; Farrell, 2001), each ton of NO_x emissions is treated equally, regardless where in a state it originates. Similarly, many attainment plans for individual metropolitan regions have adopted a "bubble" approach, setting a target for NO_x emissions but offering flexibility regarding where the reductions occur.

Are all tons equal? As with any short-lived pollutant, the location of impact depends on the location of NO_x origin. However, because ozone response to NO_x is known to be nonlinear (e.g., Lin *et al.*, 1988), the emission origin may influence not only the location of impact but also the amount of ozone that forms from a given amount of NO_x. The

propensity of a NO_x source to form ozone can vary by orders of magnitude with time and location, increasing with ambient VOC and decreasing with ambient NO_x (Liu *et al.*, 1987; Lin *et al.*, 1988). For example, a small power plant plume amidst rich biogenic sources of VOC will produce ozone far more efficiently than a more intense plume in a VOC-poor region (Ryerson *et al.*, 2001). If pollutant yield varies with emission location, accounting for spatial heterogeneity may improve the cost-effectiveness of controls arising from trading and other mechanisms (Mendelsohn, 1986; Nobel *et al.*, 2001).

Here, we examine the extent of variability within small spatial scales of emission origin that would often be treated as homogeneous in NO_x abatement policies. Considering a summertime air pollution episode in Georgia as a case study, we examine how ozone yield and distance of impact depend on the intensity of a source and its elevation above ground level. We compare the impacts of NO_x from a variety of source regions in Georgia, and for an ensemble of locations near Atlanta.

4.2 Method

4.2.1 Modeling methodology

We assess the responsiveness of ozone to NO_x emissions by applying the high-order Decoupled Direct Method in Three Dimensions (HDDM-3D) (Yang *et al.*, 1997; Hakami *et al.*, 2003a) as implemented in version 4.3 of the Community Multiscale Air Quality (CMAQ) model (Byun and Ching, 1999; Cohan *et al.*, 2002). As detailed by Yang *et al.* (1997), DDM-3D efficiently and accurately computes the sensitivities of modeled concentrations to perturbations in input parameters such as initial conditions, boundary conditions, or emission rates, utilizing the same transport and chemistry mechanisms as

the underlying model. Hakami *et al.* (2003a) presented the extension of DDM-3D to compute higher-order coefficients.

The application of Taylor expansions to first- and second-order HDDM-3D sensitivity coefficients, which represent the local slope and curvature respectively of concentration response to an emission rate, enables the approximation of how concentrations would respond to large perturbations in that rate (Hakami *et al.*, 2003a). Here we are specifically interested in quantifying the contribution of each source, which is the increment by which ozone concentrations are higher because that source exists. Source contribution (SC) can be approximated by second-order Taylor expansions of sensitivity coefficients:

$$\begin{aligned} SC_{i,j} &\cong \mathbf{C}_{i,with\ j} - \mathbf{C}_{i,without\ j} \\ &\approx \mathbf{S}^{(1)}_{i,j} - \tfrac{1}{2}\mathbf{S}^{(2)}_{i,j,j} \end{aligned} \qquad \textbf{(4.1)}$$

$\mathbf{C}_i$ represents concentrations and $\mathbf{S}_{i,j}^{(1)}$ and $\mathbf{S}_{i,j,j}^{(2)}$ represent the semi-normalized first- and second-order sensitivity coefficients of species concentration *i* response to emission source *j* (see Hakami *et al*. (2003a) for the theoretical basis of HDDM-3D coefficients). Chapter 2 showed that computing source contribution from HDDM-3D coefficients by Equation 4.1 replicates to within 10% the average response indicated by the underlying model, even for very large NO_x sources.

We apply CMAQ-HDDM-3D to simulate ozone concentrations and sensitivities to NO_x during the August 11-20, 2000 air pollution episode. Our modeling domain, developed for the Fall-Line Air Quality Study (FAQS), covers the southeastern United States with 12-km horizontal resolution and 13 vertical layers (Hu *et al.*, 2003). Initial and boundary concentrations are supplied by an outer domain, which covers the eastern United States from Texas to Maine with 36-km resolution. The FAQS Year 2000

emissions inventory, meteorological modeling, and air quality modeling are described extensively elsewhere (Hu *et al.*, 2003; Unal *et al.*, 2003; Hu *et al.*, 2004). Model evaluation finds ozone simulation performance well within U.S. EPA benchmarks (Hu *et al.*, 2004).

Table 4.1. Anthropogenic NO_x emissions in each region during the August 2000 episode.

	E_{NOx} (kg N d^{-1})	Area (km^2)	E_{NOx} Density (kg N d^{-1} km^{-2})
Atlanta	132600	10140	13.1
Macon	24900	5750	4.3
Augusta	17180	4380	3.9
Columbus	7780	3330	2.3
Scherer[a]	35300	144[a]	245.1
Branch[a]	23000	144[a]	159.8

[a]Point source emissions are modeled as uniformly emitted over a single cell. Actual density at point of emission is much greater.

Response of ozone has been computed with respect to emissions from each of six NO_x source regions within Georgia representing a broad range of NO_x emissions intensity (Table 4.1). The regions are a large urban area, Atlanta, defined here as the 13 counties that were in non-attainment of federal ozone standards at the time of the episode; three mid-sized cities in central Georgia: Macon (the 7-county Macon-Warner Robins Combined Statistical Area), Augusta (the four Georgia counties of the Augusta Metropolitan Statistical Area (MSA)) and Columbus (the four Georgia counties of the Columbus MSA); and two large coal-fired power plants in central Georgia: Plant Robert W. Scherer in Monroe County, and Plant Harllee Branch in Putnam County. Though Plant Scherer falls within the Macon region, its emissions are considered separately. The spatial proximity of the regions and their location in the interior of the model domain

facilitates comparison of ozone yield. To explore the spatial variability of responsiveness within an emissions region, we also compute the sensitivity of ozone to incremental NO_x from each of 13 cells in or near Atlanta.

4.2.2 Metrics of ozone accumulation efficiency

Traditional metrics of ozone production efficiency (OPE) (Liu et al., 1987) divide the amount of ozone that has been photochemically produced by the amount of NO_x that has been photochemically consumed. However, for many policy applications the more important quantity is the amount of ambient ozone attributable to a source on a per-kg of NO_x basis. We therefore focus on metrics of ozone accumulation efficiency (OAE), which differ from OPE in that they consider only ozone remaining in the atmosphere and ignore ozone that has been produced but then lost to deposition or photochemical processing.

We quantify OAE by three metrics. The first divides ozone source contribution (Equation 4.1) by the emission rate of the corresponding NO_x source.

$$OAE(per-kg\ metric) = \frac{SC_{O_3,j}(ppbv) \cdot A(km^2)}{E_j\ (kg\ N\ d^{-1})} \qquad \textbf{(4.2)}$$

Here, E_j and $SC_{O3,j}$ refer to the daily emission rate of source *j* and its source contribution to ozone, and *A* is the surface area over which *SC* has been evaluated. This metric is especially relevant for policy considerations, as it computes the per-kg contribution of a source to ambient ozone concentrations.

The other two metrics divide ozone source contribution by the amount of NO_x consumed to compute unitless OAEs that are more directly comparable to traditional OPE metrics but less directly applicable to policy considerations. In the "NO_z method," the summed concentrations of reaction products of NO_x, known as NO_z (NO_z=NO_y –

NO_x, where NO_y is total reactive, oxidized nitrogen), serves as a proxy for NO_x consumption. The contribution of a source to NO_z concentrations in an air parcel, computed by Equation 4.1, indicates the amount of emitted NO_x that has been photochemically converted to NO_z and remains in the parcel. We compute a unitless ratio to indicate the number of ozone molecules formed per NO_x molecule oxidized.

$$OAE(NO_z\ metric) = \frac{SC_{O_3,j}\ (ppbv)}{SC_{NO_z,j}(ppbv)} \qquad \textbf{(4.3)}$$

This NO_z-based metric is comparable to many observational studies which approximate OPE by comparing enhancements of ozone and NO_z (Trainer *et al.*, 1993). However, NO_z-based estimates are known to over-estimate ozone yield when NO_z loss is unaccounted for (Trainer *et al.*, 2000), so this method will not be a focus here.

In the "tracer NO_x" method, akin to the OPE calculation method of Sillman (2000), we apply Equation 4.1 to compute the source contribution of a NO_x source both to NO_x concentrations and to concentrations of a NO_x "tracer" which is identical to NO_x except that it is not subject to chemical reactions. Differencing the two source contributions approximates the amount of NO_x that has been oxidized since emission origin, giving rise to a unitless metric for OAE.

$$OAE(tracer\ NO_x\ metric) = \frac{SC_{O_3,j}(ppbv)}{\{SC_{tracerNO_x,j} - SC_{NO_x,j}\}\ (ppbv)} \qquad \textbf{(4.4)}$$

In Equation 4.4, $SC_{tracerNOx,j}$ is computed directly from the first-order DDM-3D sensitivity coefficient because response is linear in the absence of chemistry.

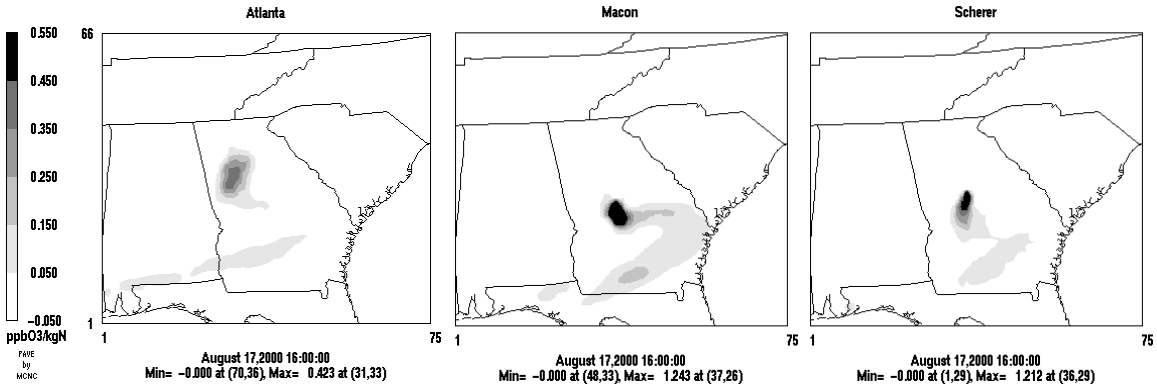

Figure 4.1. Contribution of Atlanta (left), Macon (center), and Scherer (right) NO_x to ground-level ozone at 4 p.m. EDT on August 17, 2000 on a per-kg basis.

4.3 Results and discussion

4.3.1 Spatio-temporal patterns of ozone accumulation

The impact of NO_x on ozone at 4 p.m. EDT on August 17 (Figure 4.1), the hour of peak domain-wide ozone for the episode, is illustrative of spatial patterns of daytime source contribution. Each NO_x source most enhances ozone concentrations near the emission region, and exerts less influence downwind. The spatial spread of ozone accumulation attributable to each source can be quantified by the first moment.

$$moment_{O_3,j} = \frac{\sum_{\mathbf{x}} d_j(\mathbf{x}) \cdot SC^{+}_{O_3,j}(\mathbf{x})}{\sum_{\mathbf{x}} SC^{+}_{O_3,j}(\mathbf{x})} \qquad \textbf{(4.5)}$$

Here, $d_j(\mathbf{x})$ is the distance from the center of mass of emissions j to grid cell $\mathbf{x}$, and $SC^{+}_{O3,j}(\mathbf{x})$ is the source contribution of j to ozone at $\mathbf{x}$ (cells with negative impacts, which primarily reside in the immediate vicinity of a source, are ignored in Equation 4.5). Though the smaller regions exhibit the most intense peak impacts (Figure 4.1), overall the spatial scales of impact for afternoon ozone as quantified by the moments are remarkably consistent across the NO_x source regions (Table 4.2). The moments indicate

ground-level ozone accumulation extends a few hundred kilometers downwind while most NO_x is consumed closer to the source.

Table 4.2. First moments of ozone, NO_x, and NO_z accumulation attributed to NO_x from each source region, averaged over 4 p.m. periods during the episode.

	First Moment (km)		
	Ozone	NO_x	NO_z
Atlanta	183	63	152
Macon	147	62	127
Augusta	144	56	122
Columbus	144	55	122
Scherer	167	107[a]	158
Branch	202	325[a]	216

[a]Only a small fraction of elevated point source NO_x reaches ground-level as NO_x.

Diurnal and vertical patterns of ozone response are similar across source regions (Figure 4.2). During the daytime, NO_x catalyzes the photochemical production of ozone, with ground-level impact peaking at about 4 p.m. Consistency of afternoon impact throughout the first 8 layers (Figure 4.3), which represent the lowest 1440m of the atmosphere, reflects vigorous mixing in the daytime boundary layer. Greatest ozone accumulation occurs in layer 8, corresponding to altitudes of about 970-1440 m above the surface, but impact declines sharply in layer 10 (~3030-5010 m) as this layer is typically above the daytime boundary layer. When the boundary layer collapses at night, ozone near the surface is subject to deposition and titration by NO_x but residual ozone persists in higher layers. Thus, the amplitude of the diurnal cycle diminishes with height. The small values for ground-level accumulation efficiency at night reflect a balance between strongly negative impacts from titration near the source and residual ozone in the aged plume downwind.

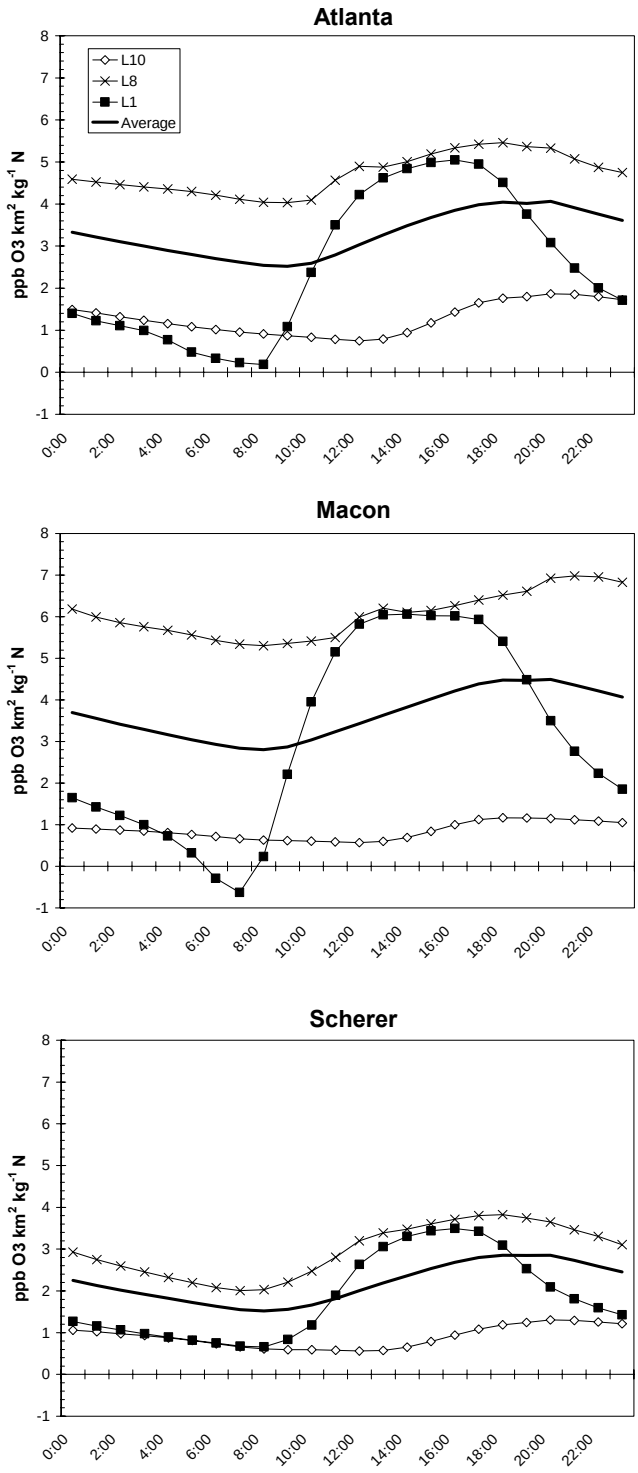

Figure 4.2. Contribution of Atlanta (top), Macon (middle) and Scherer (bottom) NO_x emissions to ozone concentrations, for vertical layers 1 (squares), 8 (crosses) and 10 (open diamonds), and a mass-weighted average of the lowest 10 layers (bold line).

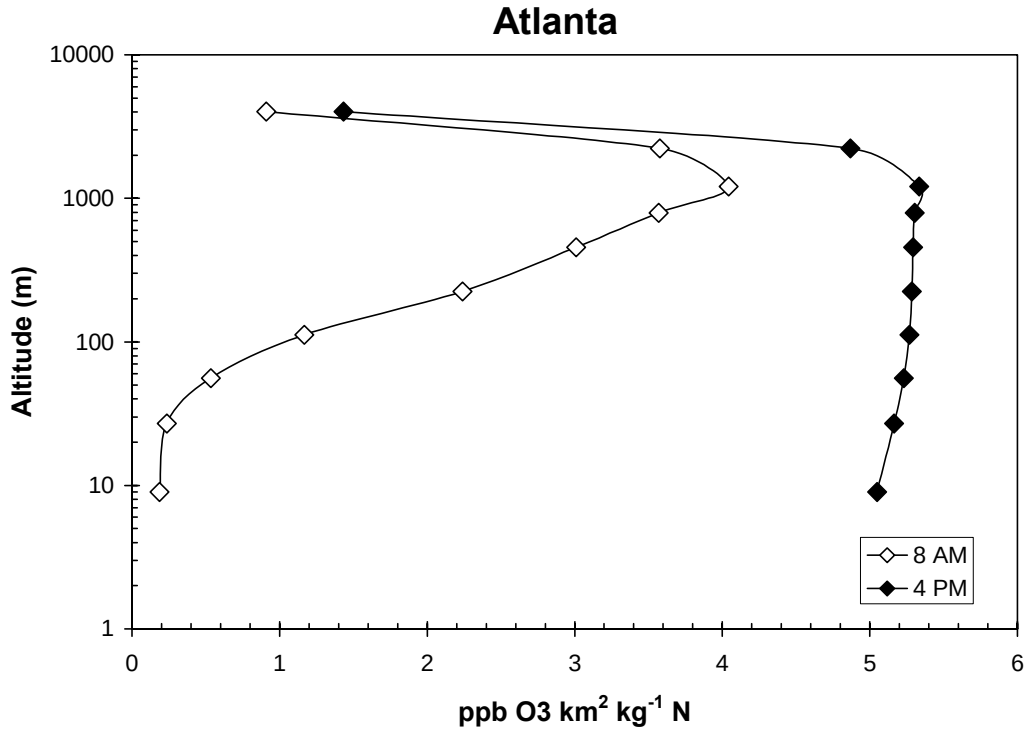

Figure 4.3. Vertical profile of Atlanta NO_x impact on domain-wide ozone at 8 a.m. (open symbols) and 4 p.m. (closed symbols).

The NO_z and tracer NO_x metrics for OAE (Equations 4.3 and 4.4), which both represent ozone accumulation per NO_x consumed (in contrast to the per-emissions metric (Equation 4.2)), exhibit similar vertical and diurnal patterns despite differences in magnitude. Thus for simplicity, only the tracer NO_x metric is plotted in Figures 4.4 and 4.5. The layer averages of domain-wide OAE are computed by separately averaging the numerator and the denominator of Equation 4.4 before division. Vertical and diurnal patterns of the tracer NO_x metric (Figure 4.4 and Figure 4.5) are similar to those simulated on a per-kg basis (Figures 4.2 and 4.3). The exception is that in the NO_x consumption based metrics, daytime OAE remains high even in layer 10. This indicates that the sharp drop in ozone accumulation on a per-kg basis above the daytime boundary layer results from little of the plume reaching these altitudes within the domain, rather than from weak ozone production efficiency there. The daytime patterns of tracer NO_x-based OAE shown for Atlanta are similar to those for all the other sources considered. However, at night the elevated point sources continue to exhibit significant positive values of OAE even at ground level (Figure 4.4b). Fresh emissions from the elevated sources are injected above the shallow nocturnal boundary layer, so nighttime impact on ground-level ozone reflects residual ozone formed during daytime without titration by fresh NO_x.

4.3.2 Magnitude of ozone yield

As discussed above, the distance of impact and spatio-temporal patterns of ozone accumulation are very similar across the NO_x source regions considered. We now compare magnitudes of accumulation efficiencies across Georgia source regions.

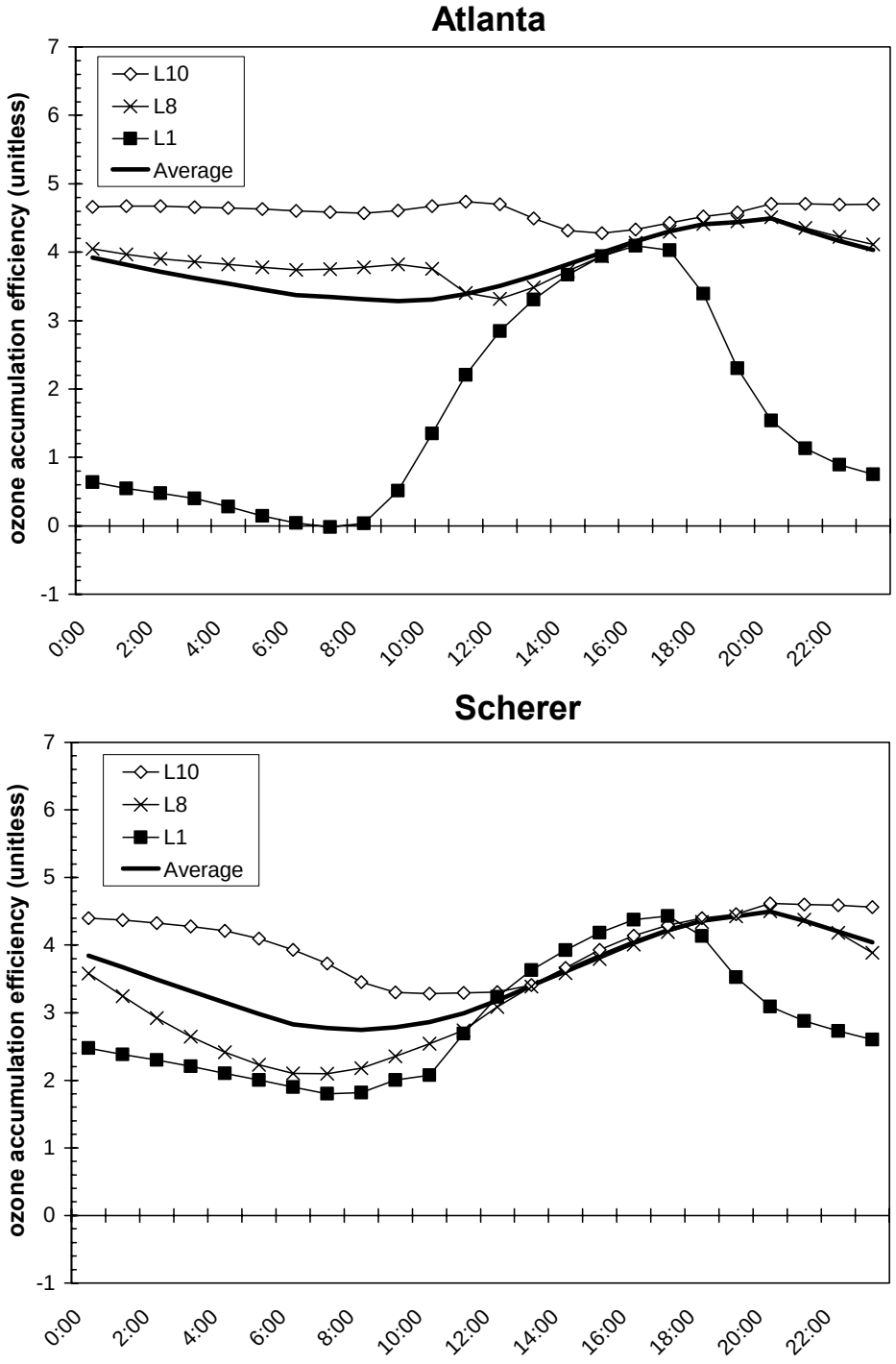

Figure 4.4. Ozone accumulation efficiency (tracer NO_x method) of Atlanta (top) and Scherer (bottom) NO_x emissions, for vertical layers 1 (squares), 8 (crosses) and 10 (open diamonds), and a mass-weighted average of the lowest 10 layers (bold line).

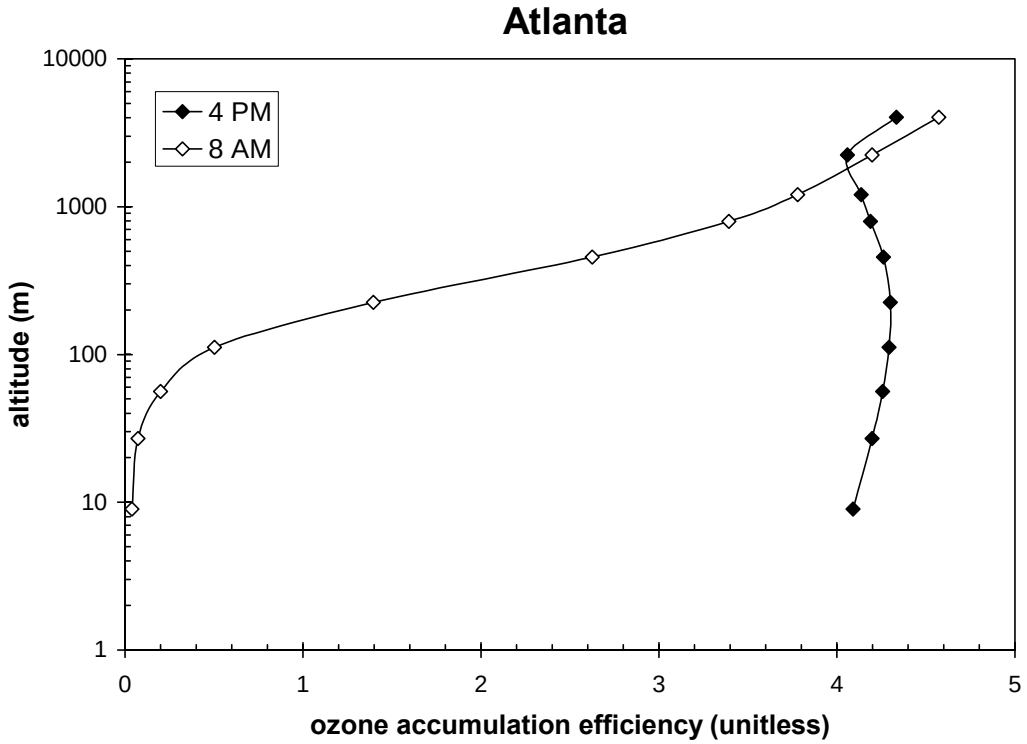

Figure 4.5. Vertical profile of domain-wide ozone accumulation efficiency (tracer NO_x method) of Atlanta emissions at 8 a.m. (open symbols) and 4 p.m. (closed symbols).

Table 4.3. Ground-level ozone accumulation efficiency at 4 p.m, averaged over the episode. Parentheses show the range of the daily values.

	Per-kg Metric (ppb O_3 km^2 kg^{-1} N) Average (min, max)	Tracer NO_x Metric (unitless) Average (min, max)	NO_z Metric (unitless) Average (min, max)
Atlanta	5.1 (3.0, 6.3)	4.1 (3.1, 4.8)	9.6 (6.6, 11.7)
Macon	6.0 (3.8, 8.4)	5.0 (4.2, 5.4)	10.8 (8.3, 12.5)
Augusta	6.0 (3.5, 9.9)	4.8 (3.3, 5.8)	10.5 (6.8, 13.7)
Columbus	5.5 (3.6, 6.9)	5.8 (5.2, 6.2)	12.5 (10.6, 14.4)
Scherer	3.5 (2.0, 5.2)	4.4 (3.2, 5.2)	8.8 (5.8, 11.5)
Branch	4.1 (2.3, 6.6)	4.9 (3.0, 5.7)	9.4 (6.1, 10.6)

Table 4.3 presents the averages and ranges of the daily accumulation efficiencies for ground-level ozone at 4 p.m. as computed by each metric. On a per-kg basis, the three mid-sized cities each yield more ozone than Atlanta, which in turns yields more ozone than either power plant. This generally follows a trend of increasing per-kg OAE with decreasing NO_x emissions density (Tables 4.1 and 4.3). A slight exception is that Columbus yields less ozone per kg of NO_x than do Macon and Augusta, despite having the lowest emissions density of any region. Because Columbus is the westernmost source region, its plume extends beyond the domain boundary during periods of northeasterly wind flow, reducing its modeled OAE on a per-kg basis. Measured by the other metrics, Columbus has the highest OAE.

Though the direction of the relationship between emissions density and yield is as expected, episode average OAE on a per-kg basis varies by only a factor of 1.7 across sources despite the differences in emissions density and altitude of emissions. By contrast, the range of the daily OAE for each source is a factor of 2-3 and is driven by changing meteorological conditions.

As shown in Table 4.3, NO_z-based estimates of OAE are twice as high as tracer NO_x based estimates, even though both metrics seek to define the amount of ozone accumulation per NO_x consumed. As discussed in a review by Trainer *et al.* (2000), NO_z-based methods tend to overestimate production efficiencies by failing to account for loss of NO_z. The tracer NO_x method may provide a more reliable measure of NO_x oxidation.

Kasibhatla *et al.* (1998) suggested that per-kg OAE could be estimated by dividing the build-up of regional peak-hour ozone during a multi-day episode with the NO_x emissions of the corresponding period and region. That study reported regional average ground-level OAE of 1-2 ppbv km^2 O_3 kg^{-1} N for summertime episodes in the eastern United States, lower than the 5-6 ppbv km^2 O_3 kg^{-1} N indicated for Georgia regions in Table 4.3. Applying the Kasibhatla method to a five-day period (August 13-17) of steadily rising modeled ozone concentrations during the FAQS episode, we estimate OAE of 1.0 ppbv km^2 O_3 kg^{-1} N for the Atlanta region and 1.8 for the state of Georgia, within the range reported by Kasibhatla *et al.* (1998). OAE estimates would be about one-fifth higher if the Kasibhatla method was applied to observed rather than modeled ozone concentrations during the FAQS episode, but still well below Table 4.3 results. Thus, the higher per-kg ozone yields estimated by Equation 4.2 than by Kasibhatla *et al.* (1998) primarily reflect differences in method rather than differences between the episodes considered. The Kasibhatla method considers only the impact of NO_x on the day-to-day increase in ozone concentrations, not on background ozone concentrations, and considers only impact within the emission region rather than over a larger domain. Both of these factors lead to lower estimates than in Equation 4.2.

Table 4.4. NO_x emissions density and population in the 144 km^2 grid cell at the center of mass of Atlanta NO_x emissions, and in cells 24, 48, and 72 km away.

Distance from Atlanta center	E_{NOx} Density (kg N d^{-1} km^{-2}) Average (min, max)	Population per grid cell (U.S. Census 2000) Average (min, max)
0 km	62.2 (NA)	206270 (NA)
24 km	24.6 (12.6, 52.4)	107950 (61530, 126918)
48 km	2.4 (2.0, 2.9)	11550 (7890, 14980)
72 km	1.0 (0.6, 1.8)	4350 (2910, 5910)

4.3.3 Variability within Atlanta

Implicit in our consideration of source regions is the assumption that NO_x emissions from a region exert a homogeneous impact. We now examine the validity of this assumption within the Atlanta region.

Atlanta NO_x emissions exhibit a nuclear pattern, with density declining sharply with distance from the city center. For example, the 12x12 km cell corresponding to the center of mass of Atlanta emissions contains 20 times more NO_x emissions than any cell 48 km away (Table 4.4). Population density is also greatest near the center of Atlanta.

CMAQ-DDM is applied to simulate the sensitivity of ozone to a marginal unit of ground-level NO_x from each of 13 emitting points. One grid cell is the center of mass of Atlanta NO_x emissions, and the others are located 24, 48, and 72 km away in each of the cardinal directions. The 72-km points reside just outside the 13-county region, but all other points are within. Sensitivities are computed to NO_x emitted from both ground-level and from layer 6 (~300-610 m), the height of maximal emissions from power plants following plume rise. The unit emissions are weighted to occur with the same diurnal cycle as domain-wide anthropogenic NO_x emissions.

Emissions of NO_x from the center of the Atlanta region yield less ground-level peak-hour ozone over the domain than any other point (Figure 4.6). The height of the emissions has little impact on ozone yield, as the well-mixed boundary layer extends well above layer 6 during the afternoons. Considering only the ozone impact occurring within the Atlanta region, points an intermediate distance from the city center tend to yield the greatest impact. Among emitting points equidistant from the center, those to the north yield greater impacts within the region than those to the south, due to the predominately northerly flow during the episode. This explains the height of the bars in Figure 4.6b, which show that direction from the city center is more important than distance in determining the within-region impact of emissions during this short-term episode. Considerable day-to-day variability of ozone yield is also modeled to occur (Figure 4.7).

On a population-weighted basis, afternoon ozone exhibits negative sensitivity to NO_x emissions from the center of Atlanta and greatest sensitivity to emissions an intermediate distance away (Figure 4.8). In areas of intense NO_x emissions, NO_x-inhibition can occur in the immediate vicinity of a source, with ozone forming tens of kilometers downwind (e.g., Gillani and Pleim, 1996; Ryerson *et al.*, 2001).

4.4 Conclusion

CMAQ-HDDM-3D results for Georgia regions during a summertime air pollution episode show that ozone accumulation efficiency varies inversely with NO_x emissions density, consistent with earlier studies (e.g., Liu *et al.*, 1987). Macon and Augusta are found to yield 40-70% more ground level ozone per ton of emissions than two large power plants, and about 20% more than Atlanta. Significant day-to-day and spatial

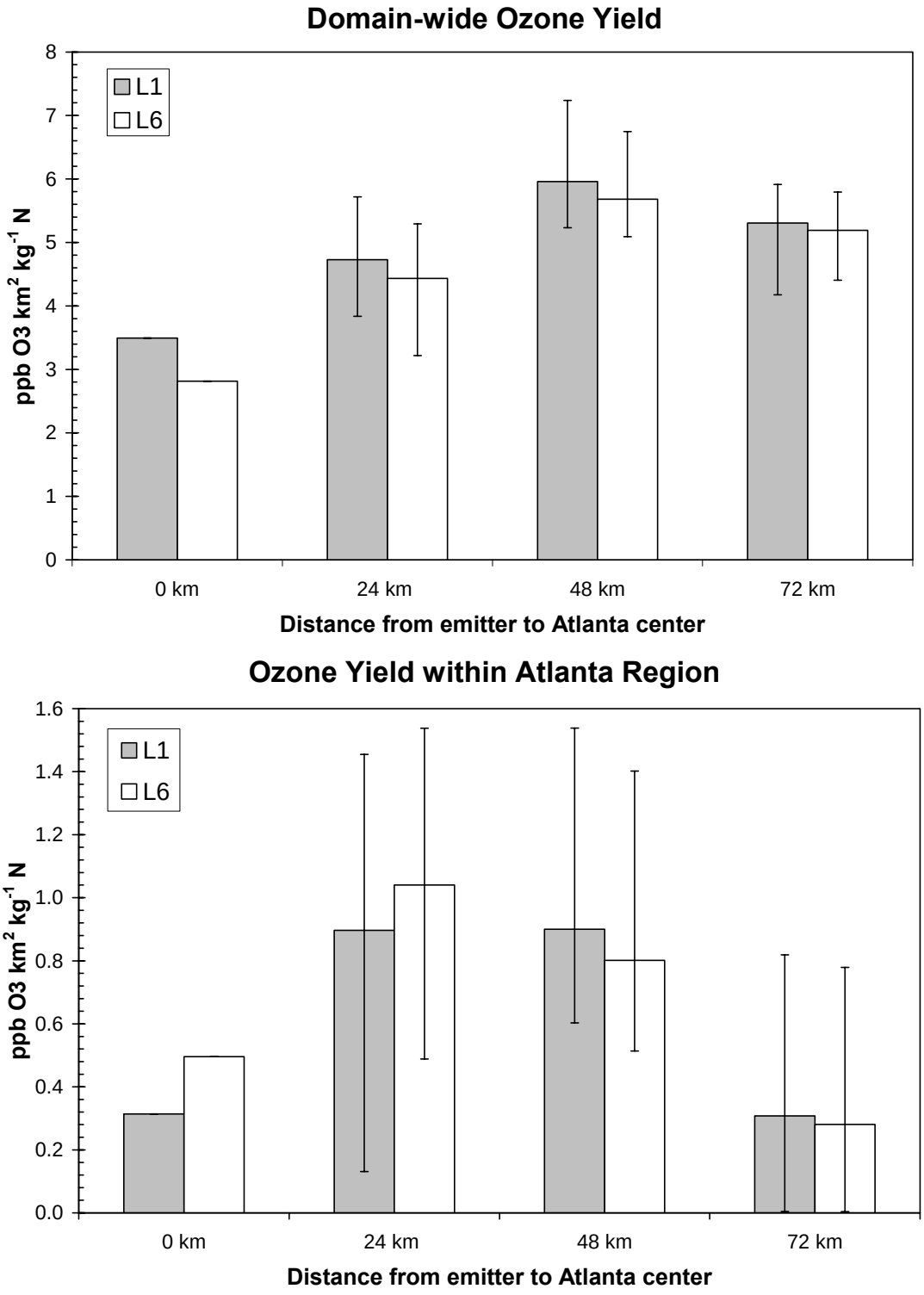

Figure 4.6. Sensitivity of peak-hour ground-level ozone throughout the domain (top) and in the Atlanta region (bottom) to Layer 1 (shaded) and Layer 6 (white) NO_x emissions originating from points 0, 24, 48, and 72 km from the center of Atlanta. Bars show the range of the 4 emitting points that comprise each average.

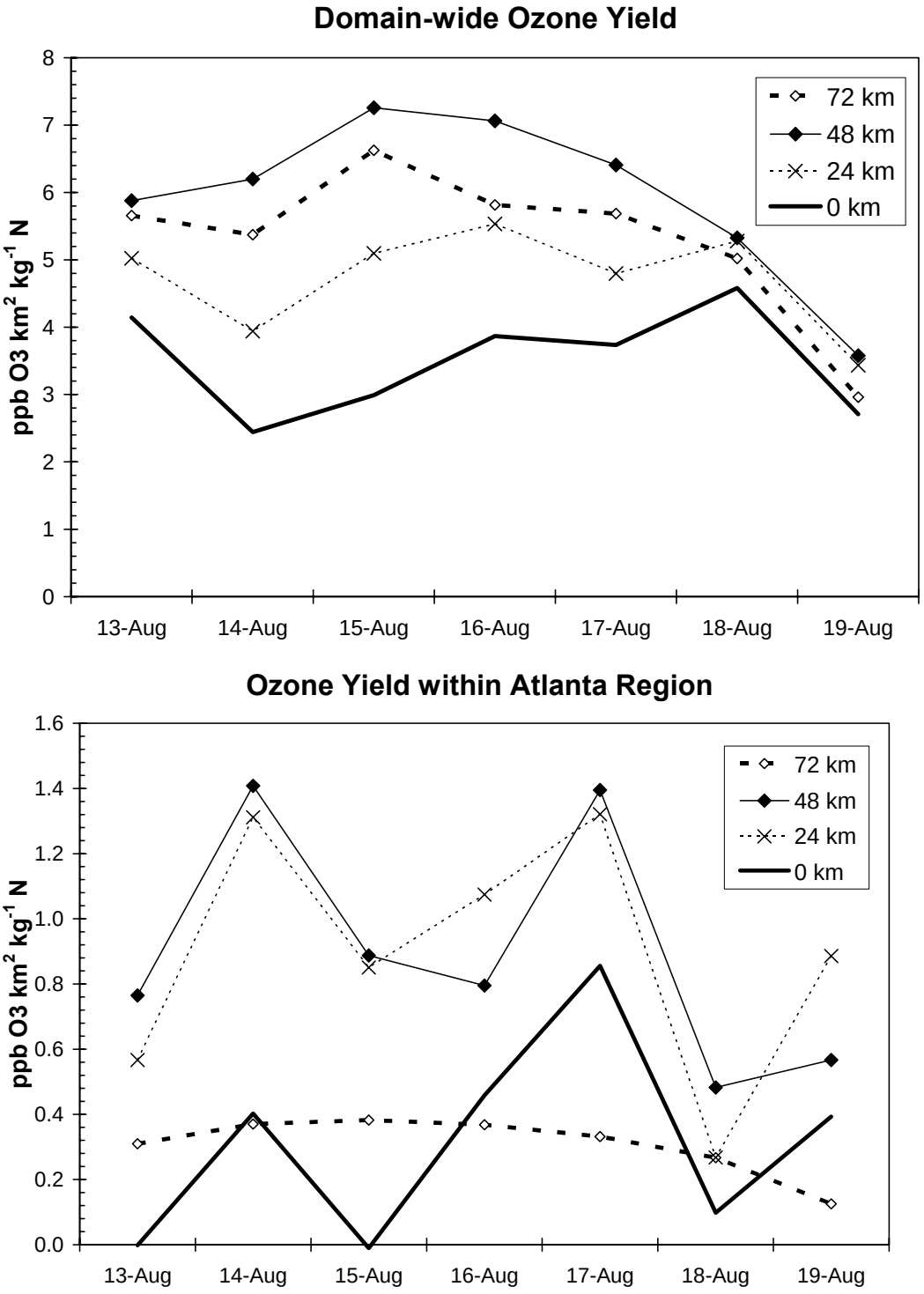

Figure 4.7. Day-to-day variability of the sensitivity of domain-wide (top) and Atlanta region (bottom) peak-hour ground-level ozone to ground-level emissions of NO_x originating from points 0, 24, 48 and 72 km from the center of Atlanta.

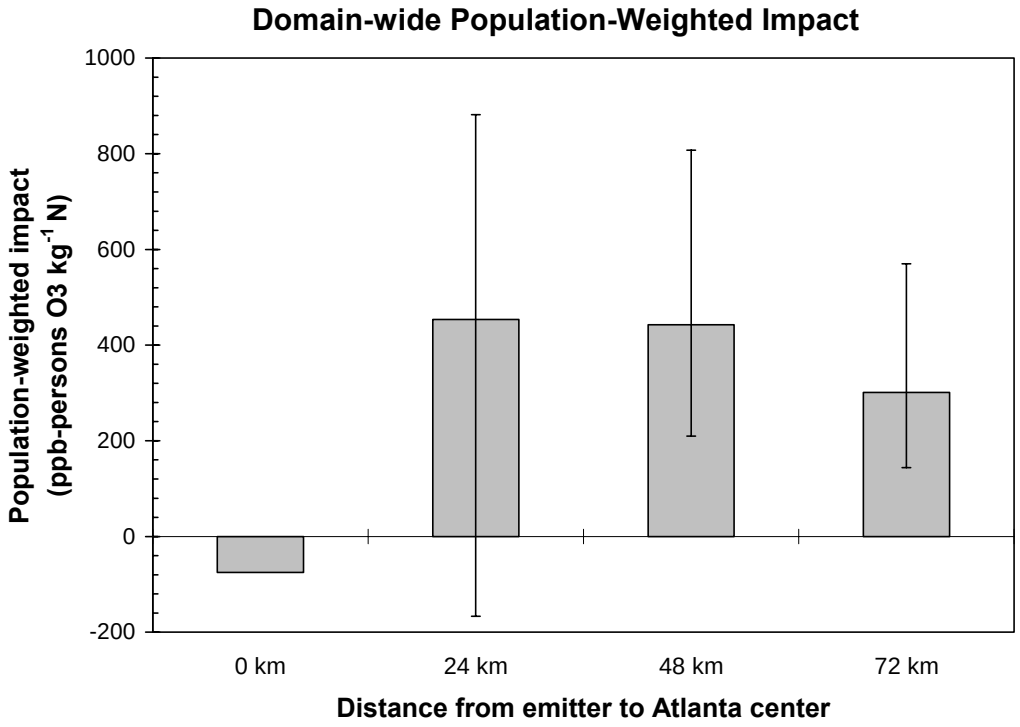

Figure 4.8. Sensitivity of 4 p.m. ozone to NO_x emitted 0, 24, 48, and 72 km from the center of Atlanta, weighted by the population of each grid cell. Bars show the range of the 4 emitting points that comprise each average.

variability is found for ozone yield of NO_x emitted in and near the Atlanta region. Ozone yield is found to be lowest for emissions at locations of highest NO_x density, but to be insensitive to the altitude of origin. The interplay of emission location and wind conditions strongly influences how much of the ozone accumulation occurs within the Atlanta region. Longer term studies would be needed to examine whether some of the spatial variability found here is smoothed out on a climatological basis.

The finding of greater variability in ozone yield within a region than across regional averages is an unexpected result with significant policy implications, and is consistent with the larger variability of NO_x emissions density within the Atlanta region than among regional averages (compare Table 4.1 and Table 4.4). In devising zones for emissions trading or regulation, there is often thought to be a trade-off: small zones limit opportunities for cost-saving trades, but large zones increase the possibility of adverse trades and fail to account for heterogeneous impacts in abatement decisions (Mendelsohn, 1986; Nobel *et al.*, 2001). The finding of substantial heterogeneity of emissions impact even on small spatial scales complicates the establishment of sensible zones. One alternative approach to traditional zone creation would be to assign weights to emissions sources based on their expected impact. However, doing so would result in more complex emissions trading and regulatory mechanisms that may be heavily reliant on debatable modeling assumptions and episode selection. Additional study is merited to further investigate the heterogeneity of pollutant impacts and to consider implications for the development of sensible control policies.

CHAPTER 5

GRID RESOLUTION CONSIDERATIONS IN OZONE SENSITIVITY ANALYSIS*

5.1 Introduction

Eulerian grid models of the atmosphere are frequently applied to inform the development of air pollution abatement policies. In such applications, photochemical models must accurately simulate not only concentrations of air pollutants, but also how those concentrations would respond to changes in emissions.

Grid resolution choice represents a perennial dilemma in photochemical modeling due to the associated trade-off between accuracy and efficiency. Finer grid scales are better able to resolve inhomogeneities in emission rates, land cover and dispersion. However, very fine resolution substantially increases computational cost. Each halving of grid dimension quadruples the number of grid cells required to cover a given domain, and can double the number of time steps needed to satisfy stability constraints.

The impact of grid resolution has attracted particular attention in the photochemical modeling of tropospheric ozone (Jang *et al.*, 1995a; Jang *et al.*, 1995b; Liang and Jacobson, 2000; Chock *et al.*, 2002; Tang, 2002), a gas that is harmful to human health and vegetation and whose concentrations exceed National Ambient Air Quality Standards (NAAQS) in many regions of the United States. Modeling of ozone is particularly prone

* This chapter is intended for submission to Atmospheric Environment with Yongtao Hu and Armistead G. Russell as co-authors.

to vary with grid resolution because ozone both forms from and reacts with its precursors, nitrogen oxides (NO_x) and volatile organic compounds (VOC), in nonlinear and locally variable fashions. Failure to properly account for inhomogeneities in concentrations of precursor gases and their oxidants can lead to errors in estimates of ozone concentrations and their sensitivities to control strategies (Gillani and Pleim, 1996).

Sophisticated sensitivity analysis techniques within Eulerian models have made possible the direct and efficient computation of ozone sensitivity to precursor emissions. The Decoupled Direct Method in Three Dimensions (DDM-3D) (Yang *et al.*, 1997) has been shown to accurately compute the local sensitivity of concentrations to perturbations in input parameters, including emission rates. Recent advances have extended DDM-3D to also compute the nonlinearity, or curvature, of concentration response to perturbations (Hakami *et al.*, 2003a).

Here, we apply high-order HDDM-3D on a three-level nested domain to examine the grid-scale dependence of model results for two key features of ozone: whether its formation is limited primarily by emissions of NO_x or VOC (ozone production regime), and the sensitivity of concentrations to an incremental unit of emissions (ozone production efficiency). The nonlinearity of ozone response will also be compared across grid resolutions. Ozone sensitivities to both domain-wide and local perturbations are considered.

5.2 Method

All simulations are conducted using HDDM-3D in the Community Multiscale Air Quality (CMAQ) model (Byun and Ching, 1999; Cohan *et al.*, 2002). Emissions are those

projected for 2007 by the Fall Line Air Quality Study (FAQS) (Unal *et al.*, 2003; Hu *et al.*, 2004). We choose a projected emissions inventory to correspond to control strategy development for future year scenarios.

Here, thirteen vertical layers of increasing thickness with height are used with three one-way nested horizontal domains with grid resolutions of 36, 12 and 4 km (Figure 5.1). This chapter compares model sensitivity and emission control responses over the shared inner domain, which is centered on northern Georgia, for August 13-19, 2000, an episode of elevated ozone concentrations in this region. August 11-12 are used as initialization days. Results for each day are assessed for the 8-hour interval when ozone concentrations are maximal, corresponding to the U.S. NAAQS for ozone (U.S.-EPA, 2004b). We focus particular attention on August 17, the day of highest ozone concentrations.

Meteorology for the FAQS episode is simulated with version 3.3.4 of the PSU/NCAR Mesoscale Model (MM5) (Grell *et al.*, 1994), using 34 vertical layers and horizontal resolution corresponding to each of the photochemical domains (Hu *et al.*, 2003). Four dimensional data assimilation (FDDA) is applied on the 36- and 12-km domains (but not on the 4-km domain) to "nudge" fields of winds, temperature and moisture toward values derived from NCEP Eta analysis data and ADP observational data archived by NCAR. At the surface, only winds are nudged. FDDA is not typically applied on the fine-scale nest in meteorological models because nudging to inadequate observational data may degrade simulation results (Stauffer and Seaman, 1994). For the FAQS domain, three-dimensional analysis nudging is not practical within the 4-km nest, which contains only one vertical sounding station. Attempts to conduct observation nudging, an alternative to analysis nudging in which surface winds are nudged toward

(a)

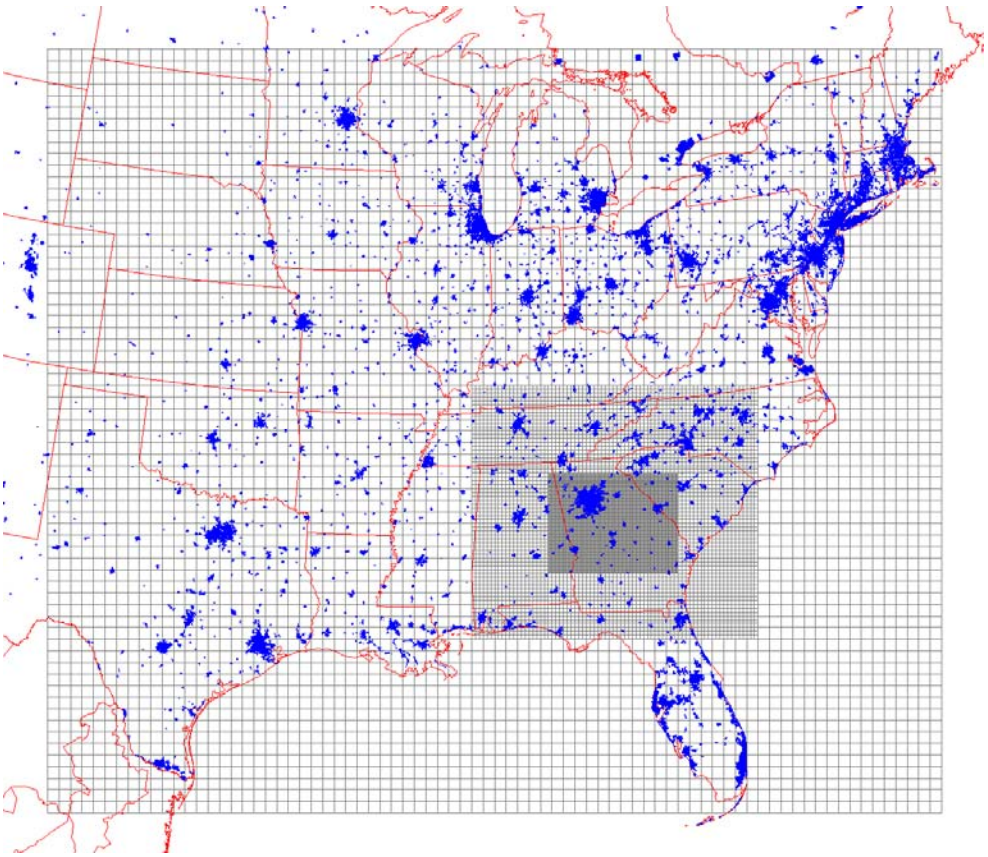

(b)

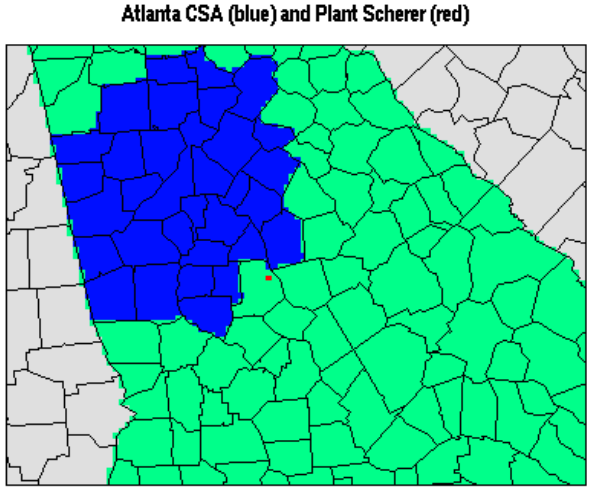

Figure 5.1. (a) The Fall-Line Air Quality Study modeling domain, with grids of 36, 12, and 4-km resolution, and (b) the locations of the Atlanta region (blue) and Plant Scherer (red) in Georgia.

values observed at ground-level meteorological stations, failed to improve model performance at 4-km resolution. As will be discussed, inconsistencies in meteorological modeling across grid resolutions can have a significant impact when comparing spatial patterns of photochemical model response to emissions changes.

5.3 Results and Discussion

FAQS simulations of ozone concentrations in the three domains and the correspondence of those results (for modeling with a Year 2000 emissions inventory) to observed concentrations have been evaluated and discussed extensively elsewhere (Hu *et al.*, 2004). Briefly, we note that spatially-averaged 8-hour ozone concentrations over the shared region vary by only a few percent with grid resolution, but the range and spatial heterogeneity of concentrations increase with finer resolution. Model bias and error relative to observations are well within U.S. EPA established bounds; average performance is virtually identical on the 12- and 4-km nests, and slightly weaker for the 36-km results.

Here we focus on the grid-scale dependence of estimates of ozone sensitivity to perturbations in Year 2007 emission rates. We first consider the sensitivity of ozone concentrations on the shared domain to perturbations in emissions throughout the medium-resolution (12-km) domain. Sensitivities are quantified by first-order DDM-3D sensitivity coefficients, $S_{O3,j}^{(1)}$, which represent the local slope of ozone response to emission source j. Coefficients are semi-normalized to the unperturbed emission rate; thus, for example, $S_{O3,ENOx}^{(1)} = 19$ ppb would mean that a 1% increase in E_{NOx} would increase 8-hour ozone concentrations by 0.19 ppb.

For domain-wide NO_x emissions, average values of $S^{(1)}$ are similar across domains—18 ppb on the coarse domain and 19 ppb on the fine domain (Table 5.1).

Table 5.1. Episode-average concentrations and sensitivities (ppb) of 8-hour ozone over the shared region, and correlation across grid resolution.

	Average (stdev) in ppb			Correlation (R^2)		
	36-km	12-km	4-km	36 v 12	36 v 4	12 v 4
Ozone Concentration	69.41 (10.5)	67.15 (11.1)	70.57 (11.3)	0.892	0.786	0.792
1st-order sensitivity to:						
Domain[a] NO_x (6234 tpd)	18.10 (6.4)	18.44 (7.2)	18.99 (7.5)	0.856	0.711	0.770
Domain[a] VOC (6131 tpd)	-0.07 (0.36)	0.03 (0.73)	0.05 (0.79)	0.741	0.607	0.566
Atlanta NO_x (591 tpd)	5.03 (6.28)	4.83 (6.48)	5.03 (6.33)	0.877	0.692	0.707
Scherer NO_x (92 tpd)	0.58 (1.48)	0.45 (1.39)	0.43 (1.19)	0.717	0.271	0.328

[a] "domain" denotes anthropogenic emissions within the middle (12-km) domain, much of which originates outside the shared region.

This indicates that average ozone production efficiency (OPE) is only weakly dependent on grid resolution over the range of scales considered here. Spatio-temporal variability and correlation across domains can be assessed by comparing the sensitivity in each grid cell on a coarser domain with the average of results in corresponding grid cells on a finer domain (Figure 5.2, Table 5.1). Bars (Figure 5.2) span the minimum and maximum sensitivities in the finer-scale cells that comprise the coarser-scale cell, and the diamonds represent the average 8-hour ozone sensitivity for each day. Finer resolution yields a more textured image of ozone sensitivity to NO_x (Figure 5.3b), but does not significantly change average results. On the 4-km domain, extreme values of $S_{O3,ENOx}^{(1)}$ range from locations with strongly positive sensitivities indicative of NO_x-limited ozone formation, to locations where negative sensitivities reflect NO_x-inhibition and a disbenefit to NO_x control. NO_x-inhibition of daytime ozone occurs primarily in small "hotspots" in the

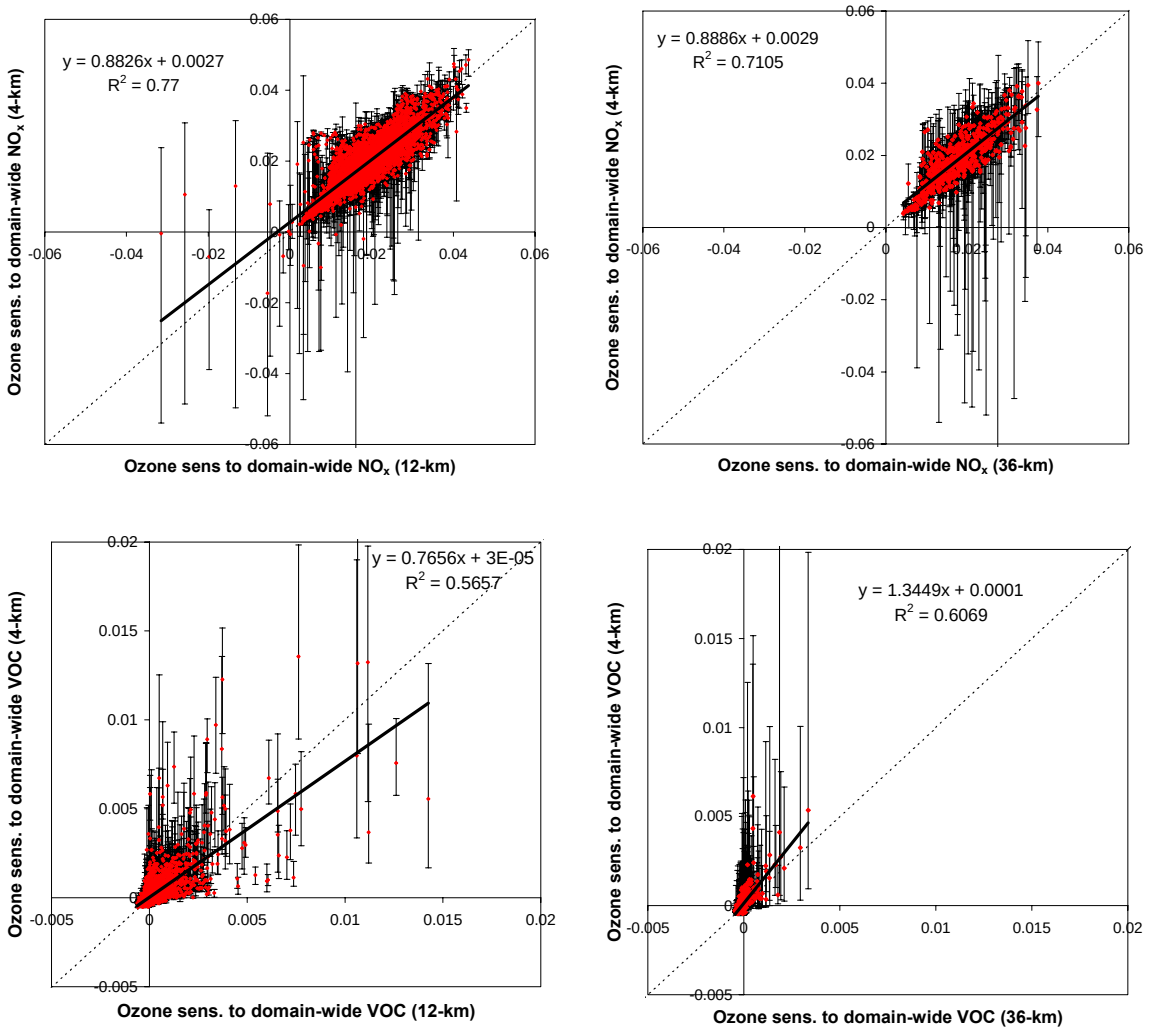

Figure 5.2. First-order sensitivity coefficient (ppm) of daily 8-hour ozone to NO_x (top) and VOC (bottom) emissions. Results in 12-km (left) and 36-km (right) cells are compared with average and extreme values in corresponding 4-km cells over the shared region. Solid line and equations show linear fit, and dashed line shows 1-to-1 correspondence. Vertical bars show the range of values in the 4-km cells within each larger cell.

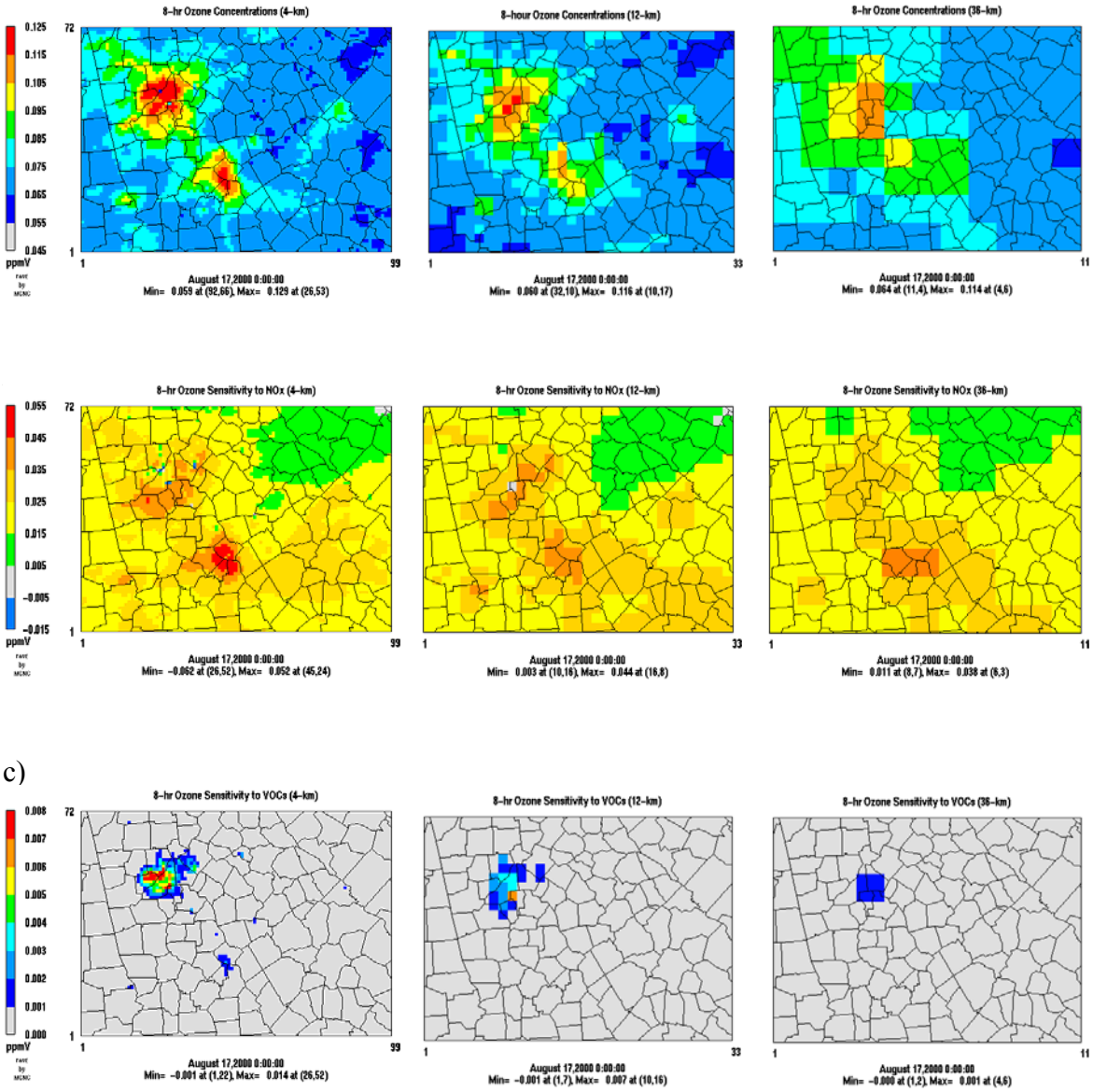

Figure 5.3, Part 1 (caption on next page).

d)

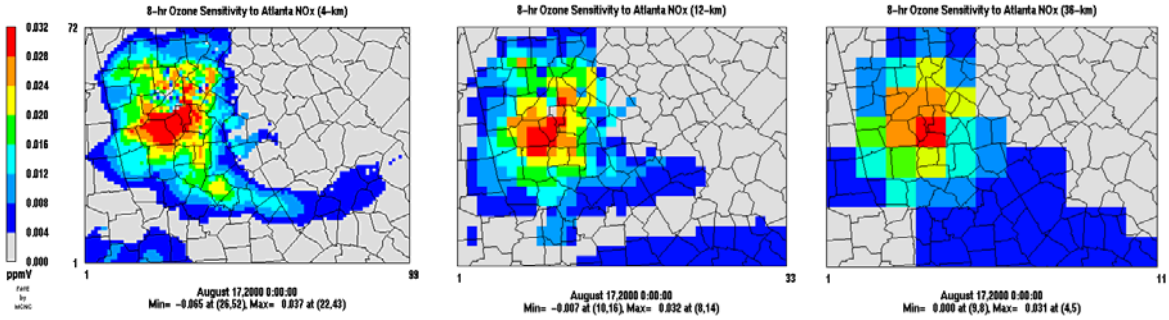

e)

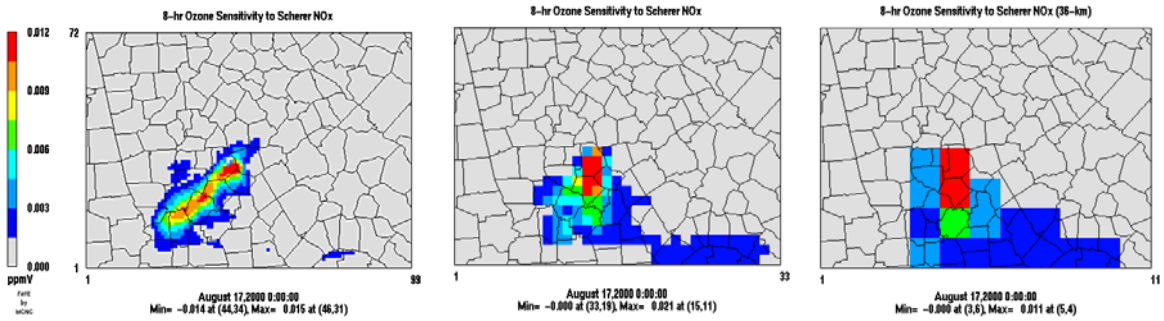

Figure 5.3. 8-hour ozone concentrations on August 17 (a) and their sensitivity to domain-wide NO_x (b), domain-wide VOC (c), Atlanta NO_x (d), and Scherer NO_x (e) emissions. In each row, results are shown for 4-km (left), 12-km (center), and 36-km (right) grid resolution.

immediate vicinity of intense emissions; averaging 4-km results up to the corresponding 36-km grid cells yields no locations of negative sensitivity.

Results differ more sharply with grid resolution for sensitivity to domain-wide VOC than to NO_x. All domains show negligible or slightly negative sensitivity to VOC in rural regions where NO_x concentrations are especially low. However, the 36-km simulation significantly underpredicts the extent and magnitude of positive VOC sensitivity indicated by 12- and 4-km resolution (Figures 5.2, 5.3c). With 36-km resolution, sensitivity to VOC never tops 3.3 ppb, while 12- and 4-km resolution results show a handful of points with sensitivities as high as 14 and 20 ppb on some days (Figure 5.2). Thus, the coarsest resolution fails to capture the extent to which local areas may benefit from VOC controls. Many of the VOC-sensitive areas are densely populated and therefore potentially important for population based exposures despite their small size.

For many policy applications, such as the formulation of emissions abatement strategies for State Implementation Plans (SIPs), sensitivity to domain-wide emissions is less important than responsiveness to local controls. We consider ozone sensitivity to NO_x emissions from two sources: the Atlanta region, defined here as the 32 Georgia counties of the Atlanta-Sandy Springs-Gainesville Combined Statistical Area, and Plant Scherer, a coal-fired power plant in central Georgia projected to be the state's largest point source of NO_x in 2007 (Figure 5.1). Unlike our fully-nested modeling of sensitivity to domain-wide emissions, in this case we model sensitivity independently on each domain, passing boundary concentrations but not boundary sensitivities from coarser to finer domain.

For Atlanta NO_x emissions, each nest yields similar estimates of average sensitivity (Table 5.1) and thus of ozone production rate. Spatial correlation of impact is high across all domains, especially between 36- and 12-km results. The plume of Atlanta's impact on ozone shows similar spatial extent across grid resolution, though with greater spatial heterogeneity in the finer resolution (Figure 5.3d). On the day of peak concentrations, 4-km resolution modeling finds first-order ozone sensitivity coefficients to Atlanta NO_x ranging from NO_x inhibition as strong as -65 ppb to NO_x sensitivity as high as 37 ppb. The extreme values are separated by a distance of less than 40 km as they occur in the immediate vicinity (negative sensitivities) and close downwind (positive sensitivities) of densest Atlanta emissions. Coarser resolution predicts a narrower range of sensitivity to Atlanta emissions.

By prematurely diffusing intense plumes over large volumes, coarse grids are known to unrealistically dilute emissions, thus masking NO_x-inhibition and titration of ozone near the source and increasing ozone production efficiency over intermediate scales downwind (Gillani and Pleim, 1996; Liang and Jacobson, 2000; Chock *et al.*, 2002). For the Scherer plume, coarsest resolution yields about 30% higher estimates of average ozone sensitivity than is estimated at either medium or fine resolution (Table 5.1). The results indicate that 12-km resolution is sufficient to simulate average sensitivity to the plume. Only at the 4-km resolution is there evidence of strong negative sensitivity to Scherer NO_x, and this is limited to a few cells nearest the facility.

Though the spatial extent and average magnitude of the Scherer plume are similar across the nests, the plume's predicted location differs at times (Figure 5.3e). As explained earlier, FDDA nudging was applied to the coarser two domains but not to the

finest domain. Thus, wind speed and direction tend to be more similar between the two coarser resolution results than in comparison with the finest resolution. On August 17, for example, the coarser simulations model the Scherer plume to be advected by northerly winds, whereas the finest-scale plume reflects northeasterly flow (Figure 5.3e). Similarly, a much higher spatial correlation of Scherer sensitivity is found between the 36- and 12-km results than between either and the 4-km results (Table 5.1).

Given the extreme heterogeneity of population density within the inner domain (Figure 5.4), ranging from 1 to more than 2000 people per square kilometer, discrepancies in winds could potentially cause discrepancies in population-weighted sensitivities even if spatially averaged sensitivities are similar. Population-weighted sensitivities are indicative of the likely impact of emission control strategies on potential exposure to pollutants. To examine the importance of grid resolution on exposure-based studies, we compute population-weighted averages of sensitivities:

$$population\ weighted\ \overline{S} = \frac{\sum_{\mathbf{x}} S(\mathbf{x})P(\mathbf{x})}{\sum_{\mathbf{x}} P(\mathbf{x})} \qquad \textbf{(5.1)}$$

where $S(\mathrm{x})$ and $P(\mathrm{x})$ are the sensitivity and population in each cell.

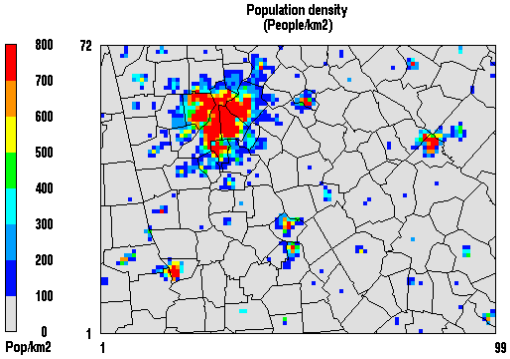

Figure 5.4. Population density in shared domain (U.S. Census 2000).

Averaged over the entire episode, population-weighted sensitivities show similar consistency across grid resolution (Table 5.2) as was found for spatially averaged sensitivities (Table 5.1). Note that across all resolutions, weighting by population increases the average sensitivity to VOC and to Atlanta NO_x because the impacts of these emissions are greatest where population is highest. In terms of day-to-day variability, consistent results are observed across resolution for population-weighted sensitivity to domain-wide NO_x (not shown) and to Atlanta NO_x (Figure 5.5). For these emissions, all resolutions predict highest per capita sensitivities on the day with the most stagnant and hot conditions (August 17) and lowest sensitivities on the coolest day of the episode (August 13). For daily sensitivity to Scherer NO_x, however, the temporal patterns are inconsistent, with 4-km resolution predicting the largest per capita sensitivities on August 14 and 15, and coarser resolutions predicting peak values on August 17 and 18 (Figure 5.5). Whereas Atlanta emissions originate from a broad area with high population density, Plant Scherer resides in a rural area between Macon and Atlanta and thus the number of people in the path of its plume will vary enormously with wind direction and speed and vertical mixing.

Table 5.2. Episode-average concentrations and sensitivities (ppb) of 8-hour ozone over the shared region, weighted by population.

	36-km	12-km	4-km
Ozone Concentration	76.19	75.10	76.06
1st-order sensitivity to:			
Domain NO_x	18.32	17.88	17.84
Domain VOC	0.42	0.91	1.18
Atlanta NO_x	8.94	7.10	7.06
Scherer NO_x	0.26	0.25	0.33

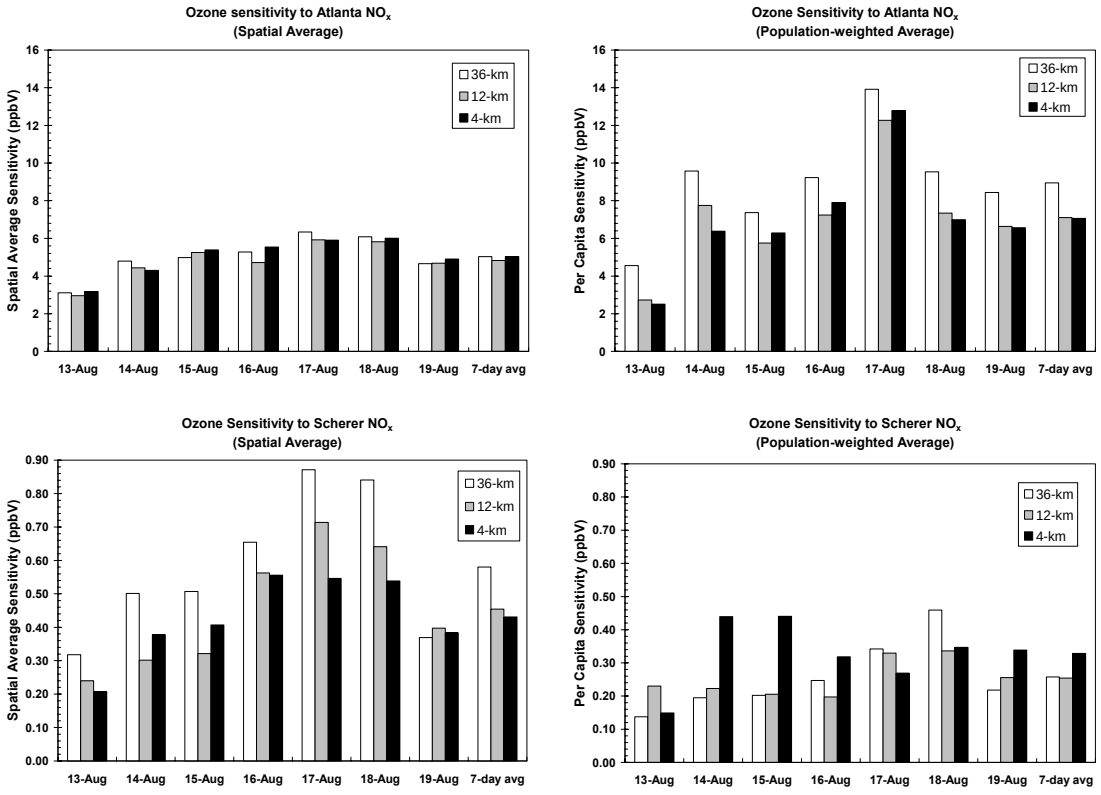

Figure 5.5. Spatial (left) and population-weighted (right) average first-order sensitivity coefficient of 8-hour ozone to NO_x emissions from Atlanta (top) and Scherer (bottom), averaged over the 4-km domain.

The extent to which linear scaling of local first-order sensitivities can accurately predict atmospheric response to large perturbations (or alternatively, the extent to which interpolation of large-scale brute force response can accurately predict incremental sensitivity) depends on the nonlinearity of the response. However, characterizing nonlinear response requires more complex and time-consuming approaches such as high-order HDDM-3D or multiple brute force runs to characterize the field of response. Understanding the relative significance of nonlinearity therefore helps calibrate modeling and analysis tools to most appropriately address the problem at hand.

Chapter 2 introduced an index, $\alpha_{i,j}$, to characterize the nonlinearity of atmospheric response of concentration C_i to emission rate p_j.

$$\alpha_{i,j} = \left| \frac{0.5 \cdot S^{(2)}_{i,j,j}}{S^{(1)}_{i,j}} \right| \qquad \textbf{(5.2)}$$

In Equation 5.2, $S_{i,j,j}^{(2)}$ is the second-order local sensitivity coefficient (curvature) of C_i to p_j, semi-normalized to the base emission rate. For the daytime response of ozone concentrations to emissions of either NO_x or VOC, $S^{(2)}$ will typically be negative, reflecting a concave-down response as greater NO_x (VOC) emissions decrease the degree to which the ozone production regime is NO_x- (VOC-) limited. First- and higher-order local sensitivity coefficients can be applied in Taylor expansions to accurately approximate concentration response to large perturbations in emissions (Hakami *et al.*, 2003a; Hu *et al.*, 2004). In such approximations, the relative importance of second-order terms (and the associated error of linear approximations ignoring these terms) is proportional to the nonlinearity index.

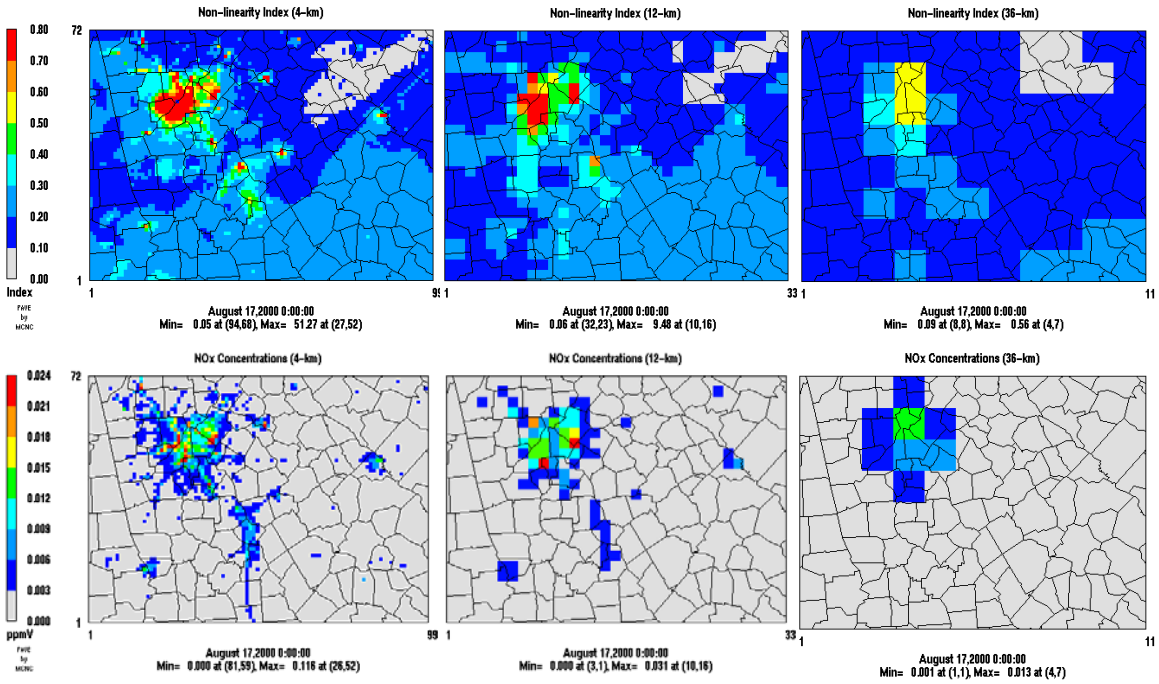

Figure 5.6. Nonlinearity index (top) and NO_x concentrations (bottom) on August 17 at the time of peak 8-hour ozone. In each row, results are shown for 4-km (left), 12-km (center), and 36-km (right) grid resolution.

Here, the nonlinearity index of ozone to domain-wide NO_x emissions is compared across the three nests. With 36-km resolution, the index rarely exceeds 0.4 outside Atlanta's urban core (Figure 5.6, top). Finer resolution yields much higher indices in Atlanta and in the immediate vicinity of Macon, Augusta, and the largest power plants.

The reason for the higher indices becomes apparent by examining model estimates of NO_x concentrations (Figure 5.6, bottom). Though NO_x concentrations differ by only a few percent when averaged across the domains, the heterogeneous texture of concentrations is better resolved at finer resolution. Photochemical production of ozone is most nonlinear when NO_x and ozone concentrations are high (Chapter 2; Hakami *et al.*,

2003a). Thus by smearing out high NO_x concentrations, coarse resolution exhibits more linear production of ozone.

5.4 Conclusion

The impact of grid resolution has been investigated for the sensitivity of ozone to its precursor emissions. In all cases examined, finer grid scales better resolve the texture of small-scale inhomogeneities in ozone response. However, from a regional perspective, the importance of grid resolution depends on the issue at hand.

For first-order sensitivities to NO_x emissions, results are largely consistent across domains when fine scale results are aggregated up to the corresponding coarse grid cells. Thus on a regionally averaged basis, estimates of ozone production efficiency are not strongly dependent on grid resolution over the range examined. Two caveats must be noted. First, ozone production may be overestimated, and local NO_x-inhibition undetected, when coarse domains are applied to intense emitters such as power plant plumes, as has been observed elsewhere (e.g. Gillani and Pleim, 1996). Here we find that 12-km resolution is sufficient to predict ozone production efficiency, but that 4-km resolution is required to identify localized pockets of NO_x-inhibition. Second, the common practice of conducting FDDA nudging on all but the finest domain may lead to discrepancies in wind fields that will shift the location of sensitivities. The spatial shifts may greatly affect estimates of exposure-based impacts, especially for sources such as certain power plants located in areas of heterogeneous density of population. For domain-wide emissions or emissions from broad regions such as Atlanta, potential population exposure depends less on wind direction because the impact is more dispersed.

For VOC sensitivities and the identification of locations with VOC-sensitive ozone production, much more significant grid scale dependence is observed. In the shared FAQS domain, the coarsest (36-km) resolution underpredicts the extent and magnitude of VOC-sensitivity indicated by the finer nests, especially in the center of the Atlanta region. The medium (12-km) resolution is sufficient to capture the extent of VOC-sensitivity in Atlanta but underestimates its peak intensity by a factor of 2. Despite the discrepancies, it must be noted that all nests agree that extent and magnitude of sensitivity to anthropogenic VOC is much less than that for NO_x sensitivity, reflecting the abundant biogenic emissions of VOC in the region (Guenther *et al.*, 2000).

The nonlinearity of ozone production with respect to NO_x emissions is found to increase with finer resolution, reflecting the premature diffusion of emissions on coarser nests. For concave-down ozone-NO_x response, higher nonlinearity means that greater underestimation will occur if incremental linear sensitivities are extrapolated to determine the ozone reductions associated with major reductions in emissions. The importance of using high-order sensitivity tools in air pollution policy and scientific applications may therefore depend in part on the grid resolution being used.

We note again that base year modeling of the FAQS episode showed performance of modeled relative to observed ozone concentrations was similar for the 4- and 12-km resolution simulations and only somewhat worse at 36-km resolution (Hu *et al.*, 2004). This suggests that model error is driven by factors other than grid resolution, at least over the range of resolution considered here. This study has explored the extent to which sensitivities to emissions may differ across resolution despite similar performance with regard to concentrations. We have shown that 12- and for some purposes 36-km

resolution are sufficient to capture many of the broad features of ozone response to emissions, and that finer resolution becomes necessary when localized variability of response is of interest.

CHAPTER 6

COST-OPTIMIZED AIR POLLUTION CONTROLS FOR DIFFERENT GOALS: CASE STUDY FOR OZONE IN MACON, GEORGIA*

6.1 Introduction

Beyond the associated harm to human health (Brunekreef and Holgate, 2002) and vegetation (Fuhrer, 2002), non-attainment of air quality standards can substantially hamper the economy (Henderson, 1996) and prestige (Chang, 2001) of a region and its access to federal transportation funds. The costs of emissions controls are substantial as well and vary greatly among various options (e.g., Pechan, 2002). Thus, much is at stake in reducing air pollution in a cost-effective manner.

Alternative goals can be considered in the optimization of air pollution control strategies. The development of regulatory attainment plans can be abstracted as a constrained optimization problem of attaining air quality standards at minimal cost. One may also consider how to minimize regional pollutant concentrations or potential population exposure subject to a budget constraint. Ozone forms from complex nonlinear interactions involving nitrogen oxides (NO_x) and volatile organic compounds (VOC) (Sillman, 1999), so the impact of a control measure will depend on which pollutant is reduced, the location of reduction, and variable factors such as meteorology. Thus, there

* This chapter is intended for submission to Environmental Science and Technology, with co-authors Di Tian, Yongtao Hu, and Armistead Russell. It is an extended version of "Cost-optimized air pollution control using high-order sensitivity analysis," in press in Air Pollution Modeling and Its Application XVII, NATO/CCMS International Technical Meeting, Banff, Canada, October 2004. Copyright permissions have been granted from Kluwer Academic Publishers.

is the potential to improve overall cost-effectiveness by considering ozone sensitivity along with control costs in strategy formulation.

With the onset of more stringent National Ambient Air Quality Standards (NAAQS) for ozone (U.S.-EPA, 2004b), many mid-sized metropolitan regions have been designated non-attainment and for the first time must develop control plans. Here we consider Macon, Georgia, as a case study of the options facing one such area. The U.S. Environmental Protection Agency (EPA) in 2004 designated Bibb County and portions of Monroe County as non-attainment based on ozone observations in Bibb County, Macon's only regulatory monitor. Under its "basic" level designation, Macon is mandated to attain ozone standards by 2009. Given that date, we use 2007 as our analysis year as it represents when most of the currently planned controls are expected to be in place, it is far enough in the future to allow for implementation of additional measures, and it falls within the three-year interval of observations (2006-2008) that will be considered in 2009 for attainment demonstration. We develop a comprehensive menu of potential control measures, and link this menu with concentration-emission sensitivities computed by a photochemical model to determine the least-cost approach to ozone attainment in Macon. We compare the least-cost attainment strategies with those optimized for other goals, such as reducing regional concentrations or potential population exposure to elevated ozone.

6.2 Methods

6.2.1 Emissions abatement options

We developed a menu of NO_x and VOC control measures that could be implemented in Macon and other areas of Georgia on a 2007 time horizon. Where possible, estimates of the costs and emissions reductions associated with each control measure were obtained from AirControlNET v. 3.2, a control technology analysis tool developed by E.H. Pechan & Associates for the EPA (Pechan, 2003a). AirControlNET software links a database of cost and effectiveness estimates (Pechan, 2003b; Table 6.1 contains a partial list of measures) to an inventory of emission sources. Annual costs in AirControlNET represent the sum of operational costs plus the amortized value of capital costs, and do not consider indirect effects on the economy.

We applied AirControlNET to a projected 2010 National Emissions Inventory, the closest available inventory in the software for our 2007 target year. Control measures were excluded from consideration if they could not be implemented at the state or local level (e.g., federal vehicle standards), if they were no longer applicable (e.g., facilities known to have already implemented the control measure), or if another measure could achieve greater emission reduction at the same source for lower cost per ton.

Because AirControlNET focuses primarily on emissions from area and point sources, separate analysis was conducted for potential controls on mobile sources, both on-road and non-road. Table 6.2 summarizes the assumptions that were made regarding the cost and emission reduction for each non-AirControlNET measure. Estimates of cost per ton were taken from available sources (see Table 6.2 footnotes), and emissions reductions were computed by applying percentage reductions to the corresponding categories in the

Table 6.1. Sampling of the 258 NO_x control measures in U.S. EPA AirControlNET[a].

Source Category	Control Measure	Typical Effectiveness	Cost per ton NO_x (Year 2000$)
Cement manufacturing	Mid-kiln firing	25%	$62
	SCR	80%	$3947
Coal-fired utility boilers	SCR	80%	$1,200-$1,900
ICI boilers (coal)	SNCR	40%	$1,151-$1,426
	SCR	70%	$959-$1,726
ICI boilers (natural gas)	OT + WI	65%	$932
	SCR	80%	$3,055
ICI boilers (residual oil)	LNB	50%	$548
	SCR	80%	$2,029
ICI boilers (wood bark)	SNCR	55%	$1,275
Industrial natural gas combustion	RACT to 25tpy	31%	$1,055
Internal combustion engines	L-E (low-speed)	87%	$863-$2,302
Lime kilns	Mid-kiln firing	30%	$630
	SCR	80%	$4,618
Natural gas water heaters	Replacement	7%	$0
Sulfate-piping recovery furnaces	OT + WI	65%	$932
	SCR	80%	$3,055

[a]Cost and effectiveness assumptions in AirControlNET are documented by Pechan 2003b. Costs shown here are for application to Georgia sources in the Year 2010 AirControlNET inventory.
Abbreviations: ICI = industrial, commercial, and institutional; LNB = low-NO_x burners; OT + WI = oxygen trim + water injection; RACT = Reasonably Available Control Technologies; SCR = selective catalytic reduction; SNCR = selective non-catalytic reduction

Table 6.2. Additional control options considered outside AirControlNET. Estimates based on available literature and other approaches as described below and in the text. Costs and impacts may vary greatly under alternative assumptions.

Control Measure	Emissions Reduction	Cost (Year 2000 $) per ton NO_x
Parking pricing	2% of light-duty vehicle emissions (Bibb & Houston County and Atlanta only) [a]	$0 [a]
Open and prescribed burning ban	90% where not already implemented [b]	$0 [b]
Discourage idling by school buses	0.016% on-road NO_x, 0.005% on-road VOC [c]	$0 [c]
Electric airport ground support equipment	50% replacement	$0 [d]
Powder River Basin coal at Scherer	35% NO_x reduction [e]	$0 [e]
Closure of Brown & Williamson Tobacco	100% reduction (Bibb County facility already slated for closure)	$0
Selective catalytic reduction: Branch	Reduce NO_x to 0.07 lb/mmBtu (from 0.50lb/mmBtu permitted rate)[e]	$1,282-$1,717 [e]
Truck-stop electrification	2.6% of heavy-duty vehicle emissions [c]	$1,591 [c]
Locomotives (various options)	78-98% of locomotive NO_x [f]	$2,584-$3,655 [f]
Cetane additive to diesel	0.3% of heavy-duty vehicle NO_x [c]	$3,923 [c]
Distance-based car insurance pricing	10% of light-duty vehicle emissions [g]	$4,086 [g]
Selective catalytic reduction: Scherer	Reduce NO_x to 0.07 lb/mmBtu (from 0.14-0.17 lb/mmBtu PRB coal rate)[e]	$4,104-$5,638 [e]
Traffic signal synchronization	0.17% mobile NO_x, 0.55% mobile VOC [c] (Bibb & Houston County and Atlanta only)	$4,593 [c]
Low-NO_x aircraft	10% reduction in aircraft NO_x [h]	$4,768 [h]
Cleaner non-road vehicles	9.6% NO_x, 8.4% VOC from affected categories, based on 30% replacement of vehicles[h] and EPA NONROAD model[c]	$9,572 [c]
Transportation demand management	0.5-3.0% light-duty vehicle emissions [i]	$9,970-$109,660 [i]
Smoking vehicle ordinance	0.07% NO_x, 0.20% VOC from on-road [c]	$10,144 [c]
Inspection & maintenance	6% NO_x, 12% VOC from mobile sources where not already implemented [j]	$18,660 [c]
Cap freeway speeds at 65 mph	varies [k]	$18,602 [l]
Electric lawn and garden equipment	15% replacement [h]	$1,317/ton VOC [h]

Table 6.2 (continued): Footnotes

[a]Commuting travel declines 12% at firms which apply parking cash out on a revenue-neutral basis (Shoup, 1997). Assumed unfeasible outside urban areas.
[b]Burning ban already implemented in 45 counties surrounding Atlanta (GA-DNR, 2001). Zero-cost assumes burning would be shifted to low-ozone days. Davis and Miller (2004) estimated a cost of at least \$20,000/ton NO_x if burning is instead replaced by alternative disposal.
[c]Davis and Miller 2004 estimates for Nashville in 2007.
[d]Pechan (2002) shows that electric equipment has lower net costs than diesel. However, Davis and Miller 2004 compute \$8200/ton NO_x based on airport projects funded by Texas Emissions Reduction Program.
[e]Selective catalytic reduction at Branch and Scherer boilers are costed individually because of their size, proximity to Macon, and known controls already in place. The 0.07 lb/mmBtu rate equals the permitted rate which has been achieved at other large Georgia power plants. Costs are the range of each plant's 4 units and are computed by the method of U.S. EPA (2001). We assume operation during only 5-month ozone season (thus on \$/ozone-season-ton basis used in strategy selection, these SCRs are relatively more cost-effective than this table suggests). Powder River Basin coal has already been implemented at Scherer but is not accounted for in the FAQS 2007 inventory, which is based on permitted rate. Higher transport costs are balanced by the lower cost of PRB coal (Steve Ewald, Georgia Power, personal communication).
[f]CARB (1995), average of original and industry estimates.
[g]Litman (1997) estimates per-mile insurance premiums could reduce vehicle travel 5-15% (Baker and Barrett (1999) estimate 10-20%). Additionally, revenue-neutral distance-based or emission-based pricing could be applied via vehicle registrations, leasing rates, fuel taxes or tolls (U.S.-EPA, 1997). Cost assumes \$5 annual odometer check, 12,200 miles/vehicle/yr (U.S.-EIA, 2004).
[h]Pechan (2002). Percentage reductions based on SAMI "bold" strategy.
[i]Costs are assumed to increase linearly from \$0.00-\$0.40/mile with the percent of reduction, up to 10% reduction in mileage, based on typical ranges in Kuzmyak (2002) and Pansing *et al*., (1998). Per-mile costs converted to per-ton based on MOBILE-6 light-duty vehicle 2007 average emission rates (1 ton NO_x, 1.18 tons VOC per 996,900 miles). We consider only mileage reduction up to 3% (in ½% increments) in strategy development menu as further control is cost-prohibitive under these costing assumptions.
[j]Based on MOBILE-6 applied to 2007 Georgia on-road fleet.
[k]Computed by MOBILE-6 for the 2007 Georgia on-road fleet, with average speeds on rural interstates reduced from 65 to 55 mph.
[l]Tolley and Smith (2001). Others have estimated lower or even zero net costs based on reduced accident severity and fuel consumption.

Fall-Line Air Quality Study (FAQS) 2007 inventory (Unal *et al.*, 2003). Costs were converted to Year 2000 U.S. dollars based on the consumer price index. Controls not considered here include: land use modification (Ang-Olson *et al.*, 2000), because it could not be reliably quantified and significant modification is unlikely on a 2007 time horizon; vehicle scrappage (Hahn, 1995), because its impact in 2007 could not be reliably quantified; and delayed operation of construction equipment (e.g., no use before noon on ozone alert days) because preliminary modeling indicated that 8-hour ozone is more sensitive to afternoon NO_x emissions.

Taken together, the menu of measures represents the potential to control 20-35% of NO_x and VOC in Georgia regions, but with marginal costs increasing rapidly beyond 15-20% reductions (Figure 6.1). VOC tends to be slightly cheaper to control than NO_x, but marginal costs depend much more on the fraction reduced than on the precursor category.

6.3.2 Photochemical model simulations

Two summertime air pollution episodes in Georgia—August 1-19, 1999, and August 11-19, 2000—were simulated with the Community Multiscale Air Quality (CMAQ) model v. 4.3 (Byun and Ching, 1999). Both episodes contain several days representative of ozone exceedances in Macon, according to classification and regression tree analysis of historical meteorological conditions and ozone observations (ICF-SAI, 2002). The first two days of results from each episode were discarded as model initialization periods. The nested modeling domain has 13 vertical layers and covers the southeastern United States at 12-km resolution and northern Georgia at 4-km resolution (Figure 6.2). Initial and boundary conditions were supplied by simulations on a 36-km resolution grid covering the eastern United States from Texas to Maine. Modeling of meteorological conditions

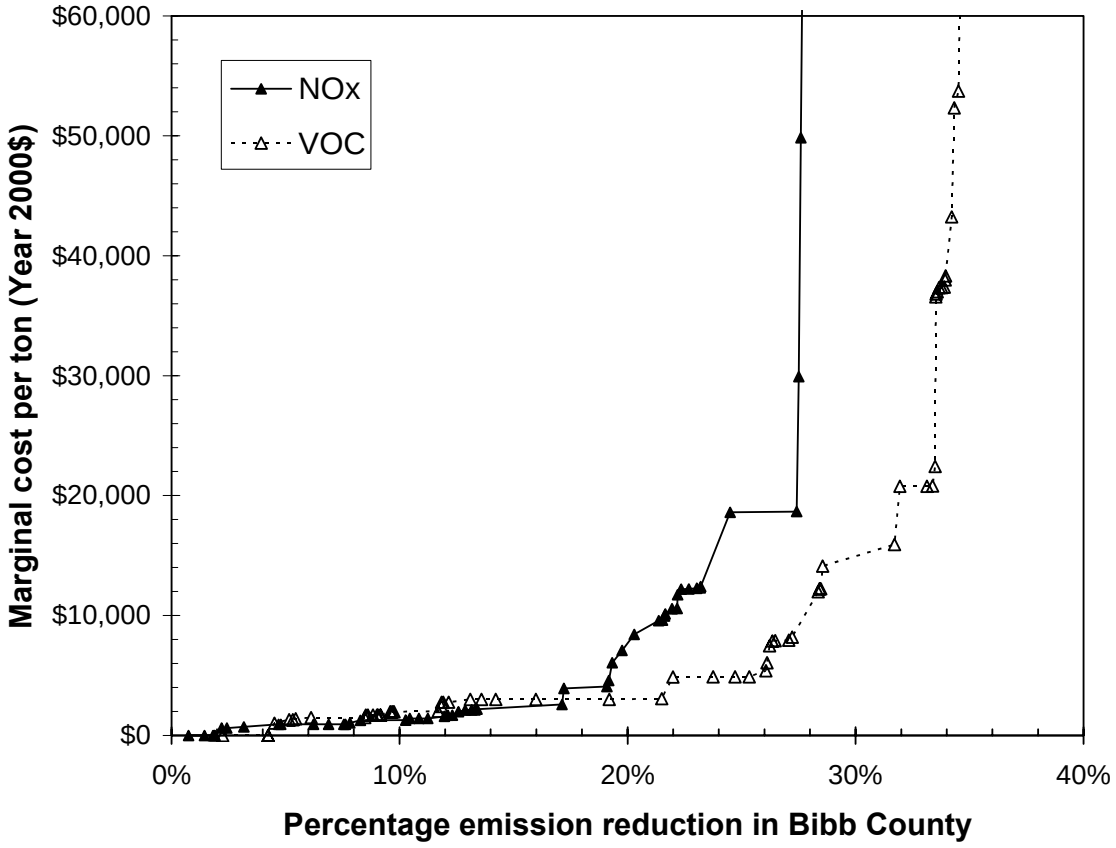

Figure 6.1. Marginal cost per ton of NO_x and VOC reduction by application of control options (Tables 6.1 and 6.2) in Bibb County, indicative of cost curves for other regions.

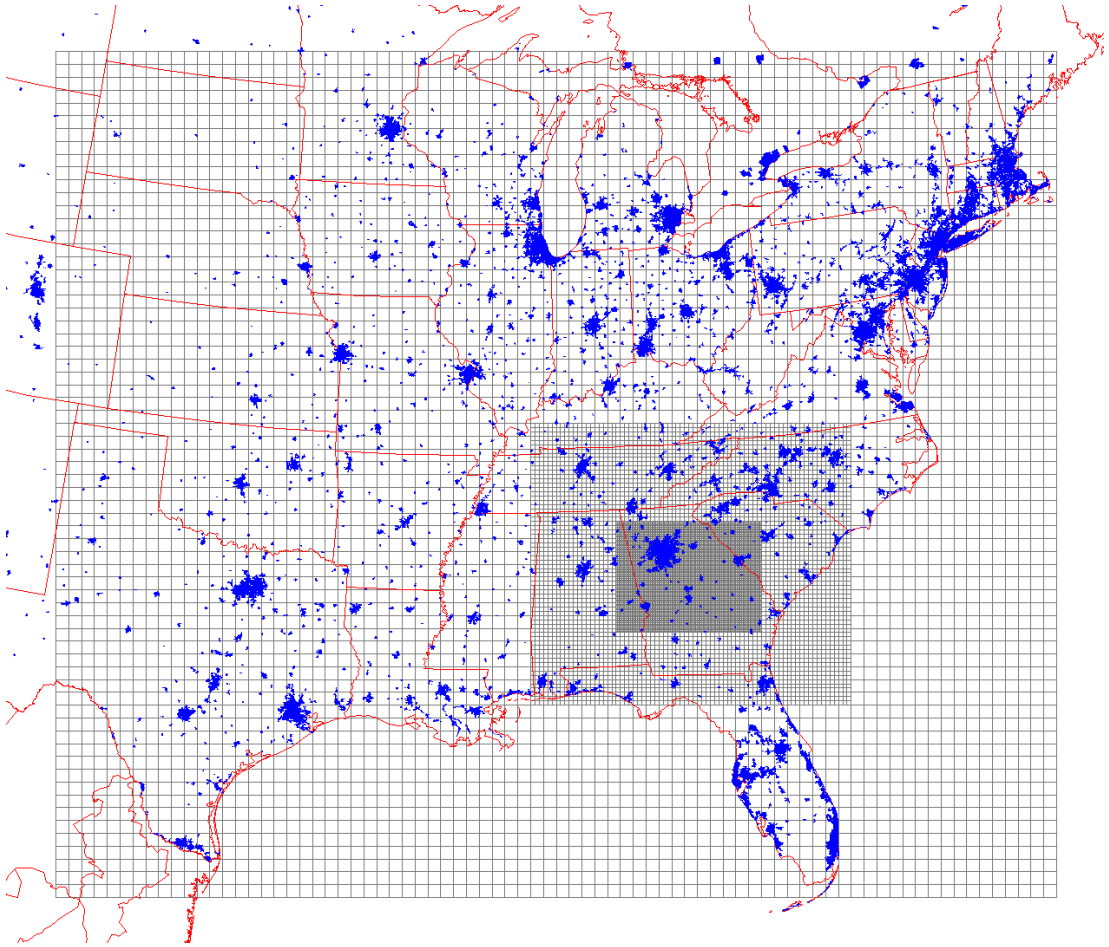

Figure 6.2. Fall-line Air Quality Study nested modeling domain.

for the episodes is described in detail elsewhere (Hu *et al.*, 2003; Tian *et al.*, 2004). Separate simulations were conducted using base year and Year 2007 emissions inventories developed for FAQS (Unal *et al.*, 2003). Base year modeling results have been evaluated extensively relative to observations and shown to be well within EPA performance benchmarks for ozone (Hu *et al.*, 2004).

To evaluate the impact of Year 2007 emissions controls on ozone concentrations, we used a high-order sensitivity analysis feature, the Decoupled Direct Method in Three Dimensions (HDDM-3D) (Dunker, 1981; Yang *et al.*, 1997; Hakami *et al.*, 2003a). DDM-3D computes the sensitivity of pollutant concentrations to perturbations in model parameters and inputs such as emissions rates, utilizing the same equations that compute concentrations in the underlying model. Although the response of ozone to emissions perturbations is nonlinear (Liu *et al.*, 1987; Lin *et al.*, 1988), Taylor expansions of first- and second-order HDDM-3D sensitivity coefficients (Hakami *et al.*, 2003a) accurately capture the concentration-emission response of the underlying model even for perturbations of 50% or more (see Chapter 2).

CMAQ-HDDM-3D was applied with 4-km resolution to compute the sensitivity of ozone to Year 2007 projected emissions of NO_x and VOC from each of 9 Georgia regions (Figure 6.3 and Table 6.3): the 7 counties (each considered separately) which comprise the Macon-Warner Robins Combined Statistical Area (CSA); the "Macon Buffer," defined here as the 12 mostly rural counties which border the Macon region; and the Atlanta region, defined here as the 20 counties designated in 2004 as non-attainment for 8-hour ozone (U.S.-EPA, 2004b). Sensitivities to NO_x from two coal-fired power plants that are the largest point sources near Macon, Plant Robert W. Scherer in Monroe County

(Macon region) and Plant Harllee Branch in Putnam County (Macon Buffer), were computed separately. Sensitivities were computed on the 12-km resolution grid with respect to NO_x emissions from the "Rest of Georgia", consisting of all other counties in the state, and from Alabama, South Carolina, and the within-domain portions of Tennessee and North Carolina. Preliminary modeling showed anthropogenic VOC from these regions negligibly impacts Macon ozone so their sensitivities are not considered here.

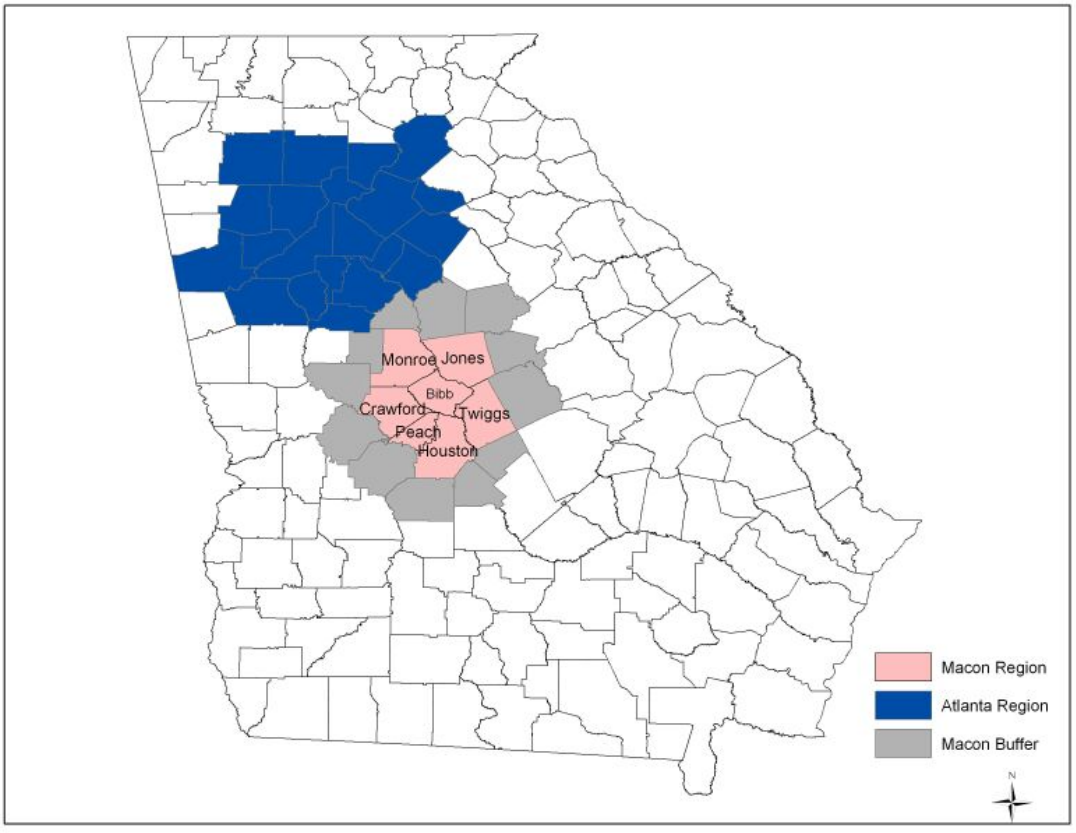

Figure 6.3. Georgia emissions regions considered in control strategy analysis. Each county of the Macon region is modeled separately (Figure created by Alper Unal).

Table 6.3. Average anthropogenic emission rates (tpd) during the episodes.

	1999 and 2000 (avg.)		2007	
Emission Region	NO_x	VOC	NO_x	VOC
Macon Region				
Bibb County	36.7	34.0	24.5	26.5
Crawford County	1.8	2.1	1.6	1.9
Houston County	21.5	17.6	20.7	14.8
Jones County	9.6	5.4	5.4	4.6
Monroe County[a]	10.7	6.6	8.1	5.3
Peach County	6.5	6.9	5.3	5.3
Twiggs County	5.0	3.2	4.3	2.5
Plant Scherer	136.9		99.0	
Macon Buffer (12 counties)[b]	52.0	50.2	48.3	41.3
Plant Branch	101.1		60.3	
Atlanta (20 counties)	766.8	509.3	537.3	400.6
Rest of Georgia	865.5		705.8	
Alabama	1470.8		948.6	
North Carolina[c]	1313.0		944.0	
South Carolina	998.4		701.9	
Tennessee[c]	1285.6		849.8	

[a]Excluding Scherer.
[b]Excluding Branch.
[c]Portion of state within 12-km resolution modeling domain.

6.3 Results and Discussion

6.3.1 Ozone attainment in Macon

The new NAAQS (U.S.-EPA, 2004b) mandate that yearly 4th highest 8-hour ozone concentrations, averaged over 3 years, must remain below 85 ppb. Under the EPA attainment demonstration method (U.S.-EPA, 1999), concentrations are simulated near non-attaining monitors for historical episodes under base year and projected emission rates. The ratio of future to base modeled ozone is known as the "relative reduction factor (RRF)." Sufficient emission reductions must be identified such that the product of RRF (evaluated in 4-km modeling based on the daily maximal 8-hour ozone within a 7x7 cell box around the monitor) and the design value (computed from ozone observations in the three years straddling the base year) is below 85 ppb. We deviate slightly from the EPA method (U.S.-EPA, 1999) by not rounding or truncating model results because the sensitivities considered in subsequent analysis are continuous.

Because control measures may reduce NO_x, VOC, or both, and because impact depends on emission location, a common metric was developed to facilitate comparison. Measures were ranked based upon their annual cost per change in ozone as approximated by first-order sensitivities:

$$cost-effectiveness(\$ / ppbO_3) = \frac{Annual\ Cost}{s^1_{O_3,NO_x} \cdot R(NO_x) + s^1_{O_3,VOC} \cdot R(VOC)} \quad \textbf{(6.1)}$$

In Equation 1, s^1 is the first-order sensitivity of ozone to an incremental short ton per day (tpd) of emissions, and R is the reduction in emissions associated with a measure. This accounts for the impact of reductions in both VOC and NO_x without the use of an arbitrary ratio or scaling. When multiple control technologies were available for a single source, the option with lowest cost-per-ton was ranked highest and its impact was input

to the ranked list. The net costs and net *R* of subsequent measures with larger emissions impacts were re-evaluated based upon that measure being applied instead of the more cost-effective measure. Thus, for example, the net cost per ton of selective catalytic reduction (SCR) at a cement plant would be larger than it appears in Table 6.1 because it would negate cheaper mid-kiln firing. Second-order terms for NO_x slightly enhance ozone impact in the final analysis, but cannot be considered in the initial ranking because their importance in Taylor expansions depends on the cumulative reduction (Hakami *et al.*, 2003a). Total impact on ozone is computed as the sum of impacts from controls in each region, ignoring cross-sensitivities.

The cost-effectiveness metric is driven both by the net cost of a measure, which varies from zero to tens of thousands of dollars per ton (Tables 6.1 and 6.2; Figure 6.1), and by the sensitivity to emissions from that region (Table 6.4). Sensitivities depend strongly on the chemical compounds emitted and on the proximity of the source to the monitor. Macon ozone is much more sensitive to NO_x than to VOC as is typical in the biogenic VOC-rich southeastern U.S. (Sillman, 1999). Ozone near the Bibb monitor is several times more sensitive to emissions from within Bibb County than to neighboring counties, and far less sensitive to emissions from elsewhere in the state. It is also 40% less sensitive to each ton of NO_x from the two elevated point sources, Scherer and Branch, than to other emissions from the corresponding regions, reflecting lower ozone production efficiencies in concentrated NO_x plumes (Ryerson *et al.*, 2001). Despite its relatively small per-ton impacts on Macon, Atlanta's large emission rates and its own non-attainment status lead to high interest in control options there. Macon ozone is relatively insensitive to emissions from neighboring states (Table 6.4), and control

Table 6.4. Sensitivity of 8-hour ozone to emissions in 2007.

	Sensitivity near Macon monitor[a] (10^{-3}ppb/tpd)		Spatial-average sensitivity[b] (10^{-3}ppb/tpd)	Population-weighted sensitivity[b] (10^{3}ppb-persons/tpd)
Emission Region	$s^1_{O3,NOx}$	$s^1_{O3,VOC}$	$s^1_{O3,NOx}$	Ψ_{NOx}
Macon Region				
Bibb County	295.3	17.3	8.3	25.0
Crawford County	36.7	5.5[c]	10.0	10.8
Houston County	60.4	1.8	10.0	14.0
Jones County	80.7	5.5[c]	8.3	16.3
Monroe County[d]	84.3	5.5[c]	7.0	12.8
Peach County	115.2	4.0	11.2	20.2
Twiggs County	44.5	5.5[c]	10.0	10.0
Plant Scherer	49.4	NC	3.9	7.1
Macon Buffer (12 counties)[e]	16.8	0.7	9.6	7.4
Plant Branch	9.4	NC	3.8	3.8
Atlanta (20 counties)	8.8	0.7	7.2	46.1
Rest of Georgia	3.5	NC	5.9	5.1
Alabama	2.3	NC	2.8	1.9
North Carolina	0.7	NC	0.9	0.5
South Carolina	1.1	NC	2.0	0.8
Tennessee	2.1	NC	2.1	6.3

NC: not computed.
[a]Sensitivity of daily maximal cell in 7x7 box around Macon monitor, averaged over 2 episodes (days with O_3<70ppb excluded).
[b]Evaluated over 4-km resolution domain, averaged over all days.
[c]4 counties grouped together for VOC sensitivity calculations.
[d]Excluding Scherer.
[e]Excluding Branch.

measures from these states are not considered. All sensitivities exhibit large day-to-day variability driven by meteorological conditions.

We apply the EPA attainment demonstration method (U.S.-EPA, 1999) to the two episodes, with 2007 as the target year. NO_x and VOC emissions are projected to decline about 20-30% between the base years and 2007 as stationary source controls associated with an earlier Atlanta State Implementation Plan (SIP) (GA-DNR, 2001) and the NO_x SIP Call (U.S.-EPA, 1998; U.S.-EPA, 2004a) along with cleaner on-road and non-road vehicles more than offset growth during the period. Thus, ozone is modeled to be 12-15% lower in 2007. Although the two episodes are only one year apart and have similar emission rates, the base year design value for the 1999 episode (based on 1998-2000 observations) is 7 ppb higher than the 2000 episode (based on 1999-2001), reflecting much higher ozone in 1998 than 2001. Thus, a hypothetical Year 2007 demonstration for the 2000 episode would indicate attainment, whereas the 1999 episode would indicate the need for 6.4 ppb of additional controls, even though ozone concentrations are modeled to be lower in the 1999 episode (Table 6.5). Joint consideration with equal weight for each episode indicates that 2.7 ppb of ozone reduction is needed.

Control measures were selected in order of cost-effectiveness until cumulative ozone reduction near the Macon monitor achieved the threshold. Total impact on ozone was computed as the sum of the impacts from controls in each region, including second-order self-sensitivities but ignoring cross-sensitivity interactions across regions. For the combined episodes, the necessary 2.7 ppb of reduction would require annual expenditures of $750,000 according to our optimization (Figure 6.4), mostly for low-cost NO_x

Table 6.5. Year 2007 attainment modeling for 8-hour ozone in Macon.

Episode	Peak Modeled 8-hour Ozone Near Monitor		RRF[a]	Design Value		
	Base Year (ppb)	2007 (ppb)		Base Year[b] (ppb)	2007[c] (ppb)	Required Further Reduction[d] (ppb)
Aug. 3-19, 1999	96.6[e]	84.6[e]	0.876	105	92.0	6.4
Aug. 13-19, 2000	112.6	96.0	0.853	98	83.6	0
Average	104.6	90.3	0.863	101.5	87.6	2.7

[a]Relative reduction factor is the ratio of Year 2007 and Base Year modeled concentrations.
[b]Annual 4th highest 8-hour ozone observations, averaged over three years straddling the episode base year.
[c]Product of RRF and the observed design value.
[d]Minimal reduction in Year 2007 modeled concentrations for which RRF*DesignValue < 85 ppb.
[e]Excludes three days with modeled Base Year O_3 < 70 ppb, in accordance with EPA methodology.

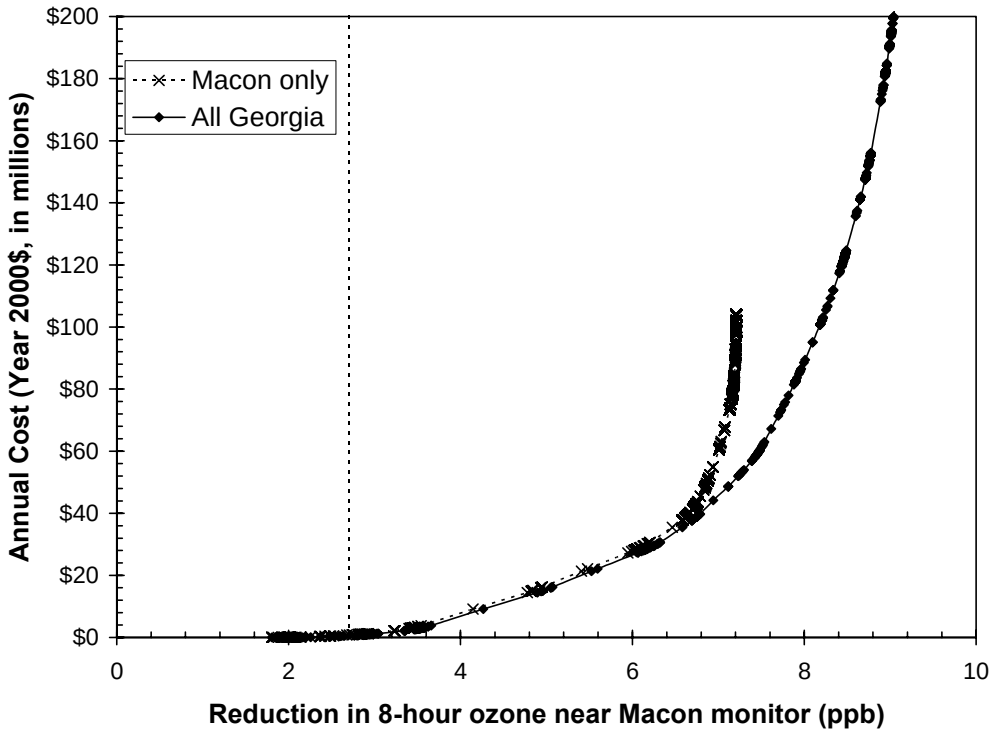

Figure 6.4. Cost-optimized reduction of daily maximal 8-hour ozone near Macon monitor, based on the 2-episode average sensitivities. Dashed curve assumes controls are applied only within the Macon region (including Scherer), and solid curve allows controls anywhere in Georgia. Vertical line denotes 2.7 ppb reduction target for attainment demonstration (Table 6.5). Applying all measures statewide results in 9.84 ppb reduction at an annual cost of $1.14 billion.

controls for industrial sources and local locomotives in the Macon region. Measures assumed to have zero net cost—continuation of lower-emitting Powder River Basin (PRB) coal at Scherer, a seasonal burning ban, parking pricing (Shoup, 1997), replacement of water heaters, and the planned closure of Brown & Williamson Tobacco—achieve 2.1 ppb of the reduction, 1.8 ppb of which is due to the PRB coal. Because almost all ozone reduction results from controls within the Macon region, excluding extra-regional controls only marginally raises the costs. In practice, policy makers may choose to implement controls beyond the threshold to provide a safety margin for attainment. Modest reductions beyond the 2.7 ppb threshold could be achieved through additional controls on local industrial sources and locomotives.

Demonstrating attainment based solely upon the August 1999 episode would be tremendously more costly. Based on sensitivities during the 1999 episode, the least-cost approach to reduce Macon ozone by the necessary 6.4 ppb would be an ensemble of measures totaling $72.6 million annually (Figure 6.5). Note that costs are two orders of magnitude higher than in the dual-episode scenario, reflecting sharply increasing marginal costs as cost-effective options are exhausted (Figure 6.1). Also contributing to increased costs is the fact that ozone is modeled to be somewhat less sensitive to nearby NO_x emissions during the 1999 episode than in the 2-episode average, lowering the amount of ozone reduction that could be achieved by a given measure. Participation from neighboring Georgia regions would be essential, as full implementation of all considered control measures within the Macon region would not quite achieve the necessary reduction. The least-cost approach (Table 6.6, Figure 6.7) would achieve nearly half its

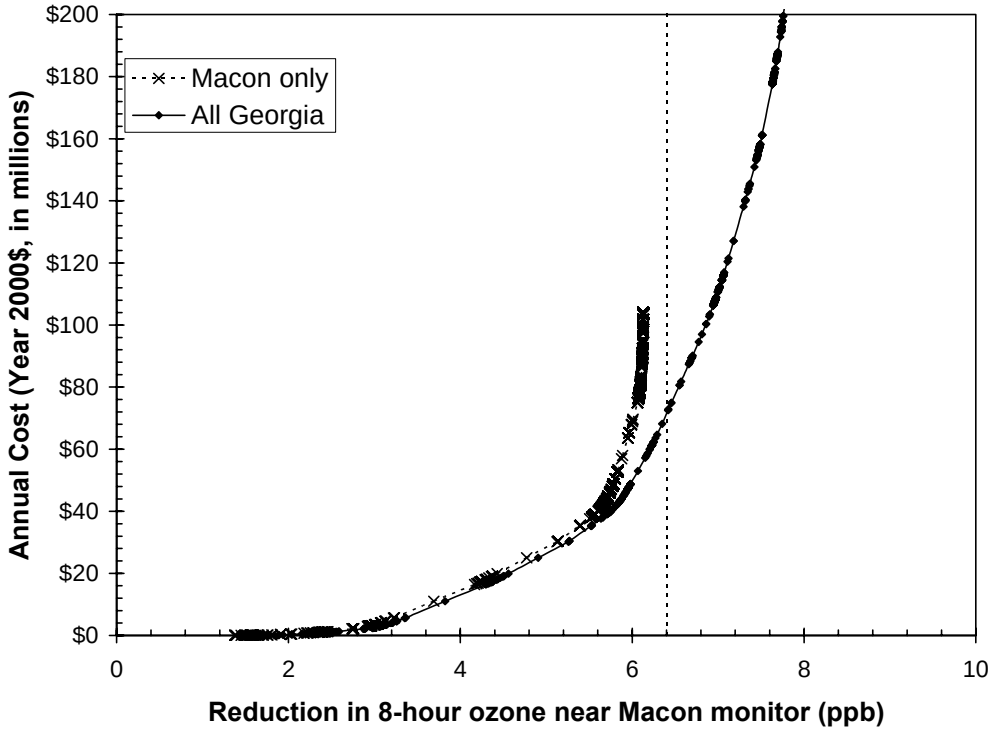

Figure 6.5. As in Figure 4, except based on the August 1999 episode only. Control options within the Macon region identified in this study would be insufficient to achieve the 6.4 ppb target.

Table 6.6. Major components of least-cost Macon attainment strategy, August 1999 episode.

Control measures	O_3 Reduction near Macon (ppb)	Annual Cost ($10^6)	Effectiveness ($10^6/ppb)
Zero-cost options (PRB coal at Scherer, burning ban, parking pricing, water heater replacement, airport ground support equipment, school bus anti-idling, emulsified asphalts)	1.72	$0	$0
Various industrial NO_x controls (Bibb Co.)	0.82	$2.6	$3.2
Truck-stop electrification (all Macon counties & buffer)	0.09	$0.5	$5.6
Distance-based pricing (all Macon counties)	0.23	$2.0	$8.9
Locomotive controls (all Macon counties & Atlanta)	0.77	$7.3	$9.4
SCRs on all 4 units at Plant Scherer	1.63	$20.9	$12.8
Cement plant controls (Houston Co.)	0.07	$1.0	$14.6
Non-road vehicle replacement (6 Macon counties)	0.11	$2.0	$18.5
Freeway speed reduction (Bibb Co.)	0.11	$2.1	$19.1
Inspection & maintenance (Bibb Co.)	0.25	$4.9	$19.6
Internal combustion engine controls (Atlanta)	0.05	$1.0	$20.5
Power plant controls (Atlanta)	0.25	$12.6	$51.2
SCR on 1 unit at Plant Branch	0.07	$4.4	$63.9
TOTAL STRATEGY	**6.42**	**$72.6**	**$11.3**

impact through PRB coal and installation of SCRs at Scherer, at an annual cost of $20.9 million computed by EPA costing methodology (see Table 6.2 footnotes). The least-cost approach would also entail $15.3 million in annual expenditures in Bibb County and $15.7 million in the Atlanta region on a wide array of measures, and $4.4 million for an SCR on one unit at Branch. Significant VOC-specific controls would be applied only in Bibb County because of the slight sensitivity to VOC from elsewhere (Table 6.4). As may be expected for an attainment-optimized strategy, largest resultant ozone reductions would occur within the Macon region.

6.3.2 Alternative metrics

Is the attainment demonstration approach well suited to reducing population and vegetation exposure to ozone? While a plethora of metrics have been developed for evaluating the relative effectiveness of control measures (e.g., Georgopoulos *et al.*, 1997; Nobel *et al.*, 2002), for simplicity we consider only two metrics averaged over all modeled days: (1) the domain-wide average sensitivity of 8-hour ozone, and (2) a potential exposure metric, Ψ, which weights sensitivities by the population of each cell where 8-hour ozone is modeled to be at least 85ppb under default 2007 emissions.

$$\Psi(ppb - persons\ of\ O_3 / tpd) = \sum_{O_3 \geq 85\ ppb} s_{O_3,E}(i,j) \cdot Population(i,j) \qquad \textbf{(6.2)}$$

Here, $s_{O3,E}(i,j)$ is the per-ton sensitivity of 8-hour ozone in cell (i,j) to emission source E. Population is taken from the 2000 U.S. Census. The spatial metric is a proxy for the propensity of a source to yield ozone, and $\Psi_{O3 \geq 85ppb,E}$ quantifies contribution to high ozone concentrations in populated areas.

Spatially-averaged sensitivity tends to be higher where NO_x emissions are less intense (Table 6.4), reflecting that ozone production becomes less NO_x-limited as

NO_x:VOC ratios increase (Sillman, 1999). However, the range of spatially-averaged sensitivity among northern Georgia source regions is narrow relative to the variation in emissions density. Sensitivities to the "Rest of Georgia" region and other states are lower because their impact occurs mainly outside the 4-km resolution domain. On a population-weighted basis, Atlanta emissions are far more important per-ton than those from other source regions (Table 6.4), reflecting Atlanta's denser population and higher ozone.

We re-rank emission control measures by applying Ψ in place of s^1 in Equation 6.1. As before, total impact for each level of cumulative emission reduction is assessed by incorporating 2nd-order NO_x sensitivities in Taylor expansions(Hakami *et al.*, 2003a). Given an annual budget constraint of $72.6 million, the minimal Macon attainment cost for the 1999 episode, the maximal impact on Ψ would be 6.32 million ppb-persons (Figure 6.6). This Ψ-optimized strategy would devote 98% of control expenditures to Atlanta NO_x (Table 6.7, Figure 6.7), largely for control technologies at coal-fired power plants. Correspondingly, its greatest impact on ozone would occur in the densely populated Atlanta region. By contrast, the optimal Macon attainment strategy (Table 6.6) achieves a 3.23 million ppb-persons impact. The gap between population-based impacts would be more pronounced except that both strategies include all zero-cost options, which account for 0.60 million ppb-persons of total impact. On the other hand, the gap is accentuated by the case-specific situation of mid-sized city attainment near a much larger city.

Similar consideration of the spatial-average metric shows that the $72.6 million strategy for Macon attainment developed for the August 1999 episode would reduce

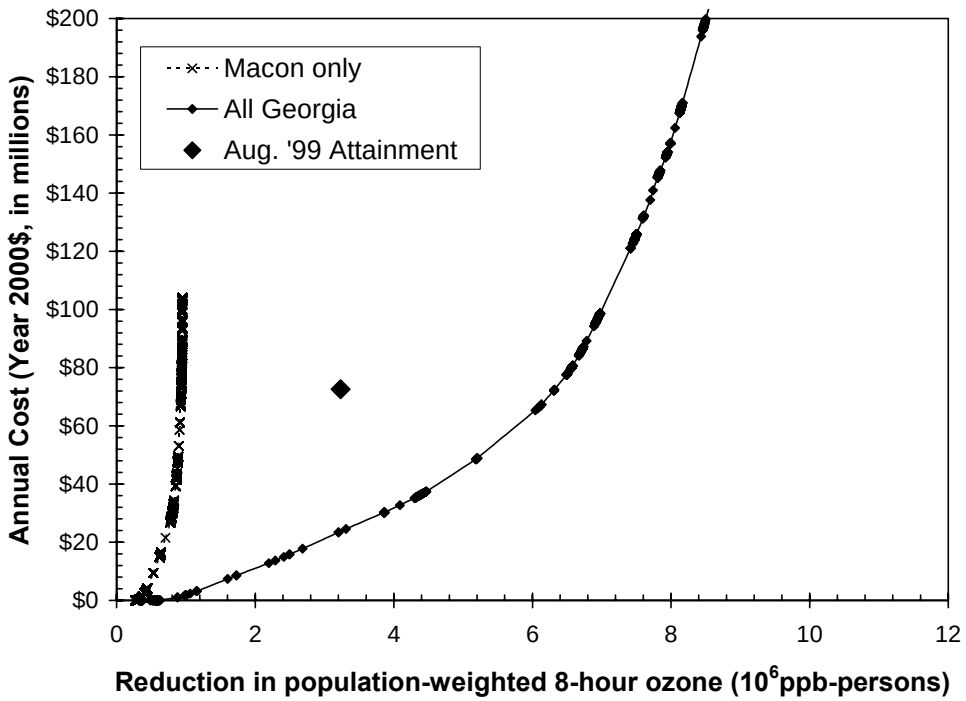

Figure 6.6. Least-cost reduction in Ψ (population-weighted 8-hour ozone above 85 ppb threshold), averaged over all modeled days, by emission controls anywhere in Georgia (solid curve, diamonds) or within the Macon region only (dashed curve, x's). The large diamond denotes the least-cost attainment strategy for the August 1999 episode. Applying the entire statewide control menu yields 11.1 million ppb-persons reduction at an annual cost of $1.14 billion.

Table 6.7. Measures to maximally reduce population-weighted 8-hour ozone (85 ppb threshold) with $72.6 million budget constraint.

Control measures	Impact (10^6ppb-persons)	Annual Cost ($10^6$$)	Effectiveness ($/ppb-person)
Zero-cost options (see Table 6.6)	0.60	$0	$0
Internal combustion engine controls (Atlanta)	0.26	$1.0	$3.8
Power plants controls (Atlanta)	3.15	$30.7	$9.7
Truck-stop electrification (Atlanta and Bibb & Peach Counties)	0.20	$2.1	$10.6
New residential space heaters (Atlanta)	0.13	$1.6	$12.9
Locomotive controls (Atlanta & Macon)	0.92	$12.4	$13.5
Distance-based pricing (Atlanta)	0.83	$16.4	$19.7
Cleaner aircraft (Atlanta)	0.18	$4.8	$27.0
TOTAL STRATEGY	**6.32**	**$72.4**	**$11.5**

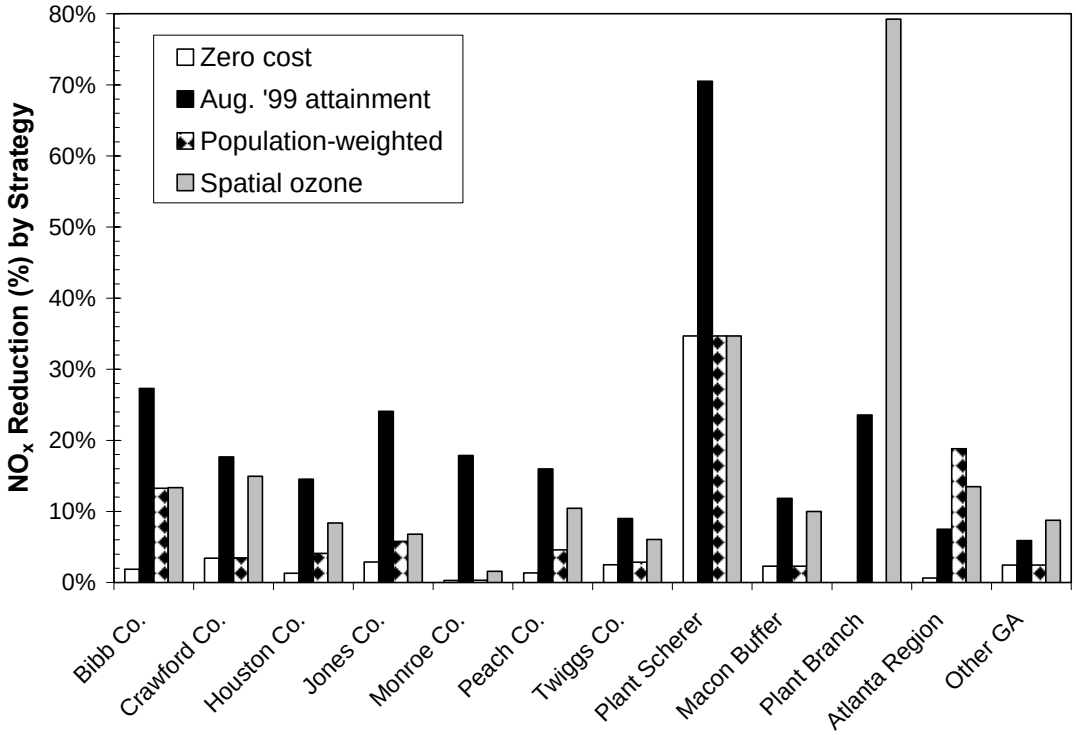

Figure 6.7. NO_x reductions for implementation of zero-cost measures (white), least-cost Macon attainment strategy (Aug. 1999 episode; black), and the strategies that would achieve maximal reduction in population-weighted (checkered) and spatially-weighted (gray) ozone at the same cost as the attainment strategy.

domain-wide 8-hour ozone by 1.04 ppb when averaged over all days of the two episodes, compared with a 1.38 ppb reduction that could be achieved at the same cost by optimizing for this metric (Figure 6.7). Statewide adoption of zero-cost measures accounts for 0.30 ppb of the domain-wide reduction in each case. Because per-ton spatial impacts have a narrower range than the other metrics (Table 6.4), rankings under this metric are driven more by per-ton NO_x control costs than by the region in which it occurs. For example, the strategy optimized for domain-wide ozone would call for SCRs at all 4 Plant Branch units (Table 6.2), even though these controls are not cost-effective in terms of Macon and population-weighted impact (Figure 6.7) because of Branch's rural location.

6.3.3 Other considerations

Rankings by cost-effectiveness should not be the only criterion for selection of attainment strategies, a process in which informed policy makers must also consider political will, regulatory structure, and other factors (NRC, 2004). Cost estimates are inherently subject to alternative assumptions and some measures yield ancillary impacts. For example, though transportation demand management tends to be relatively costly on a per-ton basis, it could help alleviate traffic congestion. Speed reduction may reduce fuel use and accident severity but impose opportunity costs on motorists. Some measures may help reduce fine particulate matter, a potentially greater health threat than ozone (Brunekreef and Holgate, 2002).

The deterministic optimization approach adopted above ignores considerable uncertainty in both the control menu and the concentration-emission responses and the unknown nature of future meteorological conditions. In Macon and elsewhere, observed

ozone design values historically have fluctuated on the order of 10 ppb even over years with similar emissions rates and despite the 3-year smoothing that these values represent (Chock *et al.*, 1997). Such meteorology-driven fluctuations are comparable to the modeled impact of the entire control menu considered here, complicating attainment in cities such as Macon whose ozone concentrations hover near regulatory limits. With attainment impossible to guarantee, stochastic analysis (e.g., Wang and Milford, 2001; Liu *et al.*, 2003) may be needed to help assess the *probability* of attainment under various controls.

Nevertheless, the process and results outlined in this chapter could provide helpful insights into the formulation of cost-effective ozone control strategies. The linkage of cost estimates with pollutant-emission sensitivities for different pollutants, regions and source characteristics has been shown to be a valuable approach for informing policy decisions. Cost-optimized strategies such as the ones developed here provide a starting point from which a region can discuss appropriate actions, conduct additional cost-benefit assessments, and identify viable strategies given the broad range of considerations.

For Macon we have shown that modest improvements in air quality are achievable through local controls, but larger change would require regional action. Sensitivities have been shown to differ widely even among nearby source regions, and thus that it would be inappropriate to consider only "costs per ton" in the decision-making process. Our results show that strategies designed for attainment demonstration can be less cost-effective at reducing regional or population-weighted ozone than strategies designed explicitly for those goals. Matching strategies to goals is therefore a key component in the development of sensible policies for air pollution.

CHAPTER 7

CONCLUSION

This thesis has applied a high-order sensitivity method to yield important insights into photochemical ozone formation in the southeastern United States, and demonstrated how those insights can be linked with economic analysis to inform the development of sensible control strategies. In doing so, a variety of major findings were developed, along with directions for further study.

7.1 Major Findings

7.1.1 High-order sensitivity method

Analysis was conducted using high-order Decoupled Direct Method in Three Dimensions (HDDM-3D) in the Community Multiscale Air Quality (CMAQ) model. For first- and second-order sensitivity coefficients, comparisons with brute force showed that CMAQ-HDDM-3D very accurately captured the magnitudes and spatial patterns of incremental sensitivity in the underlying model. For larger perturbations in emission rates, incorporation of second-order HDDM-3D coefficients in Taylor expansions accounted for most of the nonlinearity of response, though the absence of third- and higher-order coefficients caused second-order HDDM-3D Taylor expansions to underpredict modeled ozone reduction by about 10% in the extreme case of complete removal of domain-wide anthropogenic NO_x.

Assessment of high-order terms showed that nonlinearity increases in importance with the intensity of an emission source and the fraction by which it is perturbed. High-order terms were shown to offer important insights into the uncertainty of sensitivity and source apportionment results arising from uncertainty in the underlying emissions inventory. In a case study of Macon ozone, it was shown that sensitivity estimates for a source were several times more responsive to inventory error in the emission rate of that source than to error in other sources. Cross-sensitivity interactions may cause an ensemble of nearby NO_x emission sources to contribute more to ozone than would be indicated by the sum of the individual source contributions. For example, the sum of the individual contributions of Atlanta NO_x emissions by category was about 15% less than the total impact of Atlanta NO_x on ozone in the region, because each category affected the impacts of the others.

Despite the complicating role of second-order and cross sensitivities in source attribution (which considers the impact of 100% removal of the source), it must be emphasized that their importance is proportional to the fraction of perturbation and thus is several times smaller in typical control strategy consideration. Thus, high confidence is merited in the application of CMAQ-HDDM-3D to the analysis of incremental sensitivity and moderate control strategies, and the technique remains useful but merits some caution in application to source apportionment of large emitters. Given the concave-down nature of daytime ozone-precursor response, earlier studies which linearly extrapolated first-order sensitivities likely underpredicted the impact of large-scale emission reductions; similarly, brute force estimates based on large emission reductions tend to overpredict sensitivities of ozone to incremental perturbations. It is recommended that

HDDM-3D and brute force be applied in complementary roles for control strategy formulation: HDDM-3D is highly accurate for small perturbations and offers a computationally efficient method for scouting the likely impacts of a large number of potential control measures as shown in the control strategy case study (Chapter 6); however, given the complicating presence of high-order terms including cross-sensitivity interactions, brute force should be applied to verify the total impact of an ensemble of control measures.

7.1.2 Ozone Formation in the Southeastern U.S.

Ozone in mid-sized cities and rural and suburban areas of the southeastern U.S. was shown to be consistently NO_x-limited during the two summertime air pollution episodes. Polluted urban centers displayed more variable ozone sensitivity that was at times VOC-limited and NO_x-inhibited. Despite their small size, the high ozone concentrations and dense populations of these areas make them important on the basis of potential population exposure. Modeling at 36-km resolution may be too coarse to capture these "hotspots" of sensitivity to VOC, but 12-km resolution is sufficient for replicating general patterns of NO_x and VOC sensitivity found at finer resolution.

DDM-3D sensitivities to domain-wide NO_x and VOC emissions were found to correlate with modeled values of the species indicator ratios H_2O_2/HNO_3 and $HCHO/NO_y$ in a manner consistent with earlier studies (Sillman *et al.*, 1995; Lu and Chang, 1998; Sillman and He, 2002). The ratio O_3/NO_z does not provide a reliable indicator of ozone regime for the conditions examined here. Classification of a receptor as NO_x- or VOC-limited with respect to domain-wide emissions is not sufficient to determine whether local NO_x or VOC controls would be advisable. Some receptors that appear NO_x-limited

with respect to domain-wide emissions may exhibit negligible or even negative sensitivity to local NO_x emissions. In cities such as Atlanta whose NO_x/VOC ratios differ substantially from surrounding regions, species indicator ratios may be recast as signals of the local versus upwind origin of ozone.

Despite the pervasiveness of NO_x-limited conditions in most of the southeastern U.S., the propensity of a ton of NO_x emissions to foster ozone accumulation varies with emission location. Two large power plants were found to yield about two-thirds as much ground-level ozone per ton of NO_x as sources in surrounding regions. Interestingly, wide variation in ozone yield was also found for NO_x emissions from points within and near the Atlanta region. NO_x originating 24-72 km away from the city center was on average about 50% more efficient at yielding ground-level ozone than NO_x emitted from central Atlanta. Considering only ozone accumulation within the Atlanta region, ozone yield varied by an order of magnitude among Atlanta emitting points, depending strongly on the location of an emitter in relation to prevailing winds during the episode. On both a domain-wide and within Atlanta basis, ground-level ozone impact from the test points did not depend strongly on whether emissions originate at ground-level or at an elevation of 300-600 m. This reflects a well-mixed daytime boundary layer and suggests that the weaker ground-level ozone yield of power plants resulted more from the high NO_x/VOC ratios of their plumes than from the elevation of their origin.

The possibility of greater variation of ozone yields for points within a metropolitan region than among regionally-averaged yields across regions poses important challenges for policy formulation. If per-ton ozone impact is heterogeneous even for nearby emission sources, then sensitivities to region-wide emissions such as those computed

throughout this thesis may not accurately reflect the impact of control measures that affect only part of a region. In modeling to support control strategy formulation, care should be taken to define source regions for sensitivity analysis that are consistent with potential control measures. Spatial heterogeneity in ozone yield also complicates the creation of appropriate zones for emission trading. Trading mechanisms can reduce the overall cost of achieving emission reduction objectives, allowing market forces to seek out cost-effective controls (Tietenberg, 1980). However, trading across regions with different yields has the potential to increase pollutant concentrations (Nobel *et al.*, 2001). With ozone yields varying even among nearby source locations, it may be impractical to create zones of uniform per-ton impact. Reducing the size of trading zones could reduce the potential for cost-saving trades (Mendelsohn, 1986). Trading could be established with different weights for each emission source, but doing so would be cumbersome for a large number of sources and could be heavily reliant on model assumptions and episode selection.

7.1.3 Cost-optimization of Control Strategies

A comprehensive menu of potential NO_x and VOC control options in Georgia was developed for a 2007 time horizon, with estimates of the cost and emission reduction associated with each measure. Many of the control measures with lowest cost per ton were those targeting stationary sources, with on-road and non-road vehicles being more expensive to control except for a handful of low-cost measures. In sum, the control menu offers the potential to control about 20-35% of emissions in most Georgia regions, but marginal costs increase rapidly beyond 15-20% reductions.

A method was demonstrated for linking high-order ozone sensitivities with the control menu to develop cost-optimized strategies. Macon was considered as a case study because the Georgia city was recently designated non-attainment of 8-hour ozone NAAQS and mandated to reduce its ozone concentrations. Following U.S. EPA ozone attainment demonstration methodology (U.S.-EPA, 1997), the necessary amount of ozone reduction necessary to demonstrate attainment depends heavily on the historical episode being considered. A Year 2007 demonstration based upon the August 2000 episode indicates attainment without the need for additional controls, whereas attainment based on the August 1999 episode would cost at least $72.6 million according to this optimization.

The control measures that would be chosen for this least-cost attainment strategy differ markedly from those that would be chosen to minimize spatially- or population-weighted ozone at the same cost. The least-cost Macon attainment strategy relies heavily upon emission controls at a power plant (Scherer) and other sources in the Macon region, whereas potential population exposure to elevated ozone could be reduced twice as efficiently by heavier emphasis on controls in the densely populated Atlanta region. Although these comparisons highlight the importance of matching methods to objectives in air pollution control, the contrasts in strategies between metrics may be unusually pronounced in this case study of mid-sized city attainment in the vicinity of a much more populated city.

Rankings by cost-effectiveness should not be the only criterion for selection of attainment strategies. Political will and regulatory structure play major roles in the ability to implement cost-optimized strategies (NRC, 2004). Cost estimates are inherently

subject to alternative assumptions and some measures yield ancillary impacts. The unknown nature of future meteorological conditions complicates the choice of how large of a safety margin should be designed into attainment plans. All of these nuanced considerations require the oversight of informed policymakers and cannot be decided based on cost-effectiveness alone. However, the linkage of costs with sensitivities has been shown to be a valuable starting point to discuss appropriate actions, conduct additional assessments, and identify viable strategies.

7.2 Recommendations for Future Research

This dissertation has only begun to tap the potential of high-order sensitivity analysis for scientific investigation and policy guidance. The following recommendations point the direction toward fruitful avenues for potential research.

7.2.1 Application to other regions and episodes

Methods developed in this thesis are readily applicable to other locations and time periods. Analysis of other regions could help determine whether patterns of ozone production regime and yield heterogeneity noted above are specific to the southeastern U.S. or hold similarly elsewhere, which is hypothesized to be the case. It could also be examined whether the pervasiveness of NO_x-limitation in the southeastern U.S. persists during cooler periods when biogenic VOC would be less abundant and chemical reaction rates reduced. The control strategy optimization method applied here to Macon could be applied to help inform policy decisions in the many regions nationwide which have recently been designated non-attainment of ozone NAAQS. The method could also be

extended to address optimization subject to multiple constraints, such as the multi-state control strategies that would be needed to bring an ensemble of monitors into attainment.

7.2.2 Further application of uncertainty analysis using high-order coefficients

Chapter 2 introduced a method for applying high-order sensitivity coefficients to assess the uncertainty in source apportionment and in first-order sensitivity coefficients arising from uncertainty in the emissions inventory of the underlying model. Emissions inventories are thought to be a leading source of uncertainty in air quality modeling (NRC, 1991; Bergin *et al.*, 1999; Russell and Dennis, 2000), and the analysis presented in Chapter 2 could be extended to other situations and coupled with comprehensive assessments of the uncertainty of various components of emissions inventories (e.g., Frey and Zheng, 2002). An analogous method could also be readily applied to examine the dependence of sensitivity results on other uncertain model inputs such as initial and boundary conditions, meteorological conditions, and chemical reaction rates. Other studies have found that in addition to emissions inventories, meteorological conditions and certain reaction rates also contribute significantly to uncertainty (Hanna *et al.*, 1998; Bergin *et al.*, 1999; Hanna *et al.*, 2001).

7.2.3 High-order sensitivity analysis of aerosol processes

Work is nearly completed to incorporate first-order aerosol processes into CMAQ-DDM-3D (S. Napelenok, personal communication). Future work could further extend CMAQ-DDM-3D to higher-order sensitivities of aerosols. Such extension may be complicated by discontinuities in the formulations of some aerosol processes and by difficulties in accurately simulating sensitivities through complex CMAQ cloud mechanisms, which affect aerosols more strongly than ozone in sensitivity simulations.

If these hurdles could be overcome, high-order sensitivity analysis for aerosols would provide tremendous opportunities for fruitful research. Even in the absence of high-order HDDM-3D for aerosols, analysis could be conducted by an ensemble of brute force simulations. Fine particulate matter is thought to be far more damaging to public health than ozone, especially in terms of potential mortality (Brunekreef and Holgate, 2002). Composed of numerous primary and secondary constituents, fine particulate concentrations depend on the interactions of multiple precursor emissions. Source apportionment of particulate matter has attracted much attention recently and sensitivity analysis could provide important insights regarding which emission sources should be targeted for control. Assessments of cross-sensitivity interactions analogous to those conducted in Chapter 2 could provide important insights into the trade-offs that may be involved in multi-species control strategies for secondary particulate matter.

7.2.4 Uncertainty analysis of control strategy optimization

Chapter 6 conducted control strategy optimization in a deterministic fashion, assuming that costs and sensitivities were perfectly known. In reality, of course, there is considerable uncertainty in both the control menu and the concentration-emission responses. Uncertainties in cost and sensitivity estimates and unknown future meteorological conditions negate the ability to guarantee attainment in cities such as Macon whose ozone concentrations hover near regulatory limits. With certain attainment impossible to assure, stochastic analysis (e.g., Wang and Milford, 2001; Liu *et al.*, 2003) can help assess the *probability* of attainment under various controls.

Rigorous uncertainty analysis would be quite challenging, because it is difficult to quantify the uncertainty in each component. Some cost estimates, such as those for

industrial source controls that are in widespread use, are well-established, but others range by orders of magnitude depending on various assumptions. For example, Davis and Miller (2004) consider speed limit reduction to be a zero-cost measure because of fuel economy and accident mitigation benefits, whereas Tolley and Smith (2001) estimate costs of more than $18,000 per ton based on opportunity costs to truckers and commuters. Uncertainty in concentration-emission sensitivity estimates is also difficult to quantify. Whereas modeled concentrations can be compared to observations, there is no direct way to validate sensitivity results.

Beyond attempting to quantify uncertainty in cost and sensitivity estimates, much could be learned by comparing previously determined optimal strategies with those that would be chosen if costs or sensitivities were ignored. For example, ignoring sensitivities is equivalent to a bubble approach in which all tons are assumed to have equal impact and control options are selected solely on the basis of cost per ton. Ignoring costs is analogous to a command-and-control approach in which measures are mandated solely based on their per-ton effectiveness. Strategies could also be optimized in a Monte Carlo approach with specific uncertainty ranges assigned to each cost and sensitivity. Examining how costs increase as uncertainty intervals grow would help determine the value of obtaining accurate information about sensitivities and costs.

7.2.5 Area of Influence

The demonstrated ability of CMAQ-DDM-3D to accurately track the impact of small perturbations to individual sources and avoid the numerical error associated with brute force makes possible the implementation of the “area of influence” method proposed by Wilkinson and Yang (2000). The AOI approach inverts traditional DDM-3D sensitivities

computed for unit emissions from an ensemble of test points to quantify the impact of upwind sources in a location-specific fashion, providing an estimate of the response of any receptor to any emission. Preliminary testing has demonstrated the ability of AOI to capture the response of ozone to NO and of CO concentrations to CO emissions. The AOI method could provide a powerful complement to the source apportionment methods described in Chapter 2 by spatially resolving how emissions from anywhere in the domain impact a receptor.

7.2.6 Integration with observational approaches

For credibility with policy makers and for demonstrating scientific validity, it is important that atmospheric models complement and be verified by observable reality. Whereas modeled concentrations can be directly compared to observations, the "ground truthing" of model sensitivity analysis is difficult because we cannot conduct real world experiments holding all other conditions constant while emissions are perturbed. Creative approaches could identify instances such as large-scale blackouts, holidays, or other events that caused emission rates to differ. The species indicator ratios discussed in Chapter 3 offer an additional approach to linking models with observations, but more extensive observations of the relevant species would be needed to move beyond comparing modeled sensitivities to modeled ratios.

7.3 Closing Remarks

While much work remains, important insights have been derived from this thesis regarding the photochemical formation of ozone in the southeastern U.S., the optimization of ozone control strategies, and the potential role of high-order sensitivity

analysis in such investigations. Specific results have been derived to inform ozone abatement efforts in the region, with methodology developed in a general sense for ready application to other conditions. The findings of this thesis along with the above recommendations open numerous avenues for potentially fruitful future investigation.

APPENDIX A

CMAQ-DDM-3D PROGRAMMER'S GUIDE: IMPLEMENTATION OF DECOUPLED DIRECT METHOD SENSITIVITY ANALYSIS INTO THE COMMUNITY MULTISCALE AIR QUALITY MODEL

A.1 Overview of decoupled direct method

The Decoupled Direct Method in 3 dimensions (DDM-3D) is a sensitivity analysis technique for computing sensitivity coefficients simultaneously while air pollutant concentrations are being computed (Dunker, 1981; Dunker, 1984; Yang *et al.*, 1997; Dunker *et al.*, 2002; Hakami *et al.*, 2003a). The sensitivity coefficients represent the change in concentration, of any modeled species at any modeled time, associated with a change in a model input (e.g., an initial condition, boundary condition or emission rate) or a parameter (e.g., a reaction rate).

We have implemented DDM-3D for gas-phase processes (i.e., aerosol & aqueous processes not considered in our initial release) into the Community Multiscale Air Quality model by modifying the code from the September 2003 release (v. 4.3). The code in CMAQ-DDM-3D is the work of Daniel Cohan in Professor Ted Russell's group at Georgia Tech, and is based upon existing CMAQ code and code from previous implementations of DDM-3D into other air quality models by members of Professor Russell's group, especially Yueh-Jiun Yang and Amir Hakami.

CMAQ-DDM-3D generates concentration outputs that are essentially identical to normal CMAQ results, while simultaneously computing sensitivity coefficients for any

species concentration to a change in initial conditions, boundary conditions, or emission rate. We have attempted to adhere to CMAQ programming conventions, with the implementation discussed later in this programmer's guide. Some changes have been made to the input and output of data to keep the sensitivity output files to a reasonable size and to facilitate the necessary passing of information from mother domains to daughter domains for nested runs (see "Output of Data").

This guide is intended to assist users of our implementation of DDM sensitivity analysis into CMAQ. We acknowledge that our implementation is a work in progress and list cautionary notes (see "Shortcomings and Unimplemented Features") that should be considered when using CMAQ-DDM. However, we have tested that for ozone chemistry CMAQ-DDM gives results in good agreement with sensitivities calculated by differencing multiple "brute-force" runs of CMAQ, at a significant savings of computational time.

A.2 Conventions used in incorporating DDM into CMAQ

To the extent possible, the programming style is intended to be compatible with the CMAQ code from the May 2003 release (i.e., with allocatable arrays and other FORTRAN 90 conventions). Code added to existing subroutines is incorporated within #ifdef sens / #endif constructs. Most new subroutines begin with the letter s or s_ (e.g., s_tridiag.F). Sensitivity data is held in an allocatable array SENGRID (similar structure and same units as CGRID), with dimensions of (rows, columns, layers, sensitivity parameter, species). The sensitivity parameters are described by the allocatable pointers IPARM, IPT, IREGION, IDATE, ITIME, and SEN_PAR, whose values are determined when sinput.F reads sensinput.dat.

A.3 How sensitivity is implemented in each module

DDM has been implemented by modifying existing subroutines and adding additional subroutines when necessary. The implementation approach as well as the modifications and additions are listed below:

- **INITSCEN**:
    - call **SINPUT** (sinput.F) to read sensinput.dat, which contains information about the sensitivity parameters
    - if we're doing sensitivity to an intial condition, the IC is read into SENGRID
    - call **OPSENS** (opsens.F) to open sensitivity output file and write initial sensitivities
- **COUPLE/DECOUPLE** (couple.F): convert units of SENGRID analogous to treatment of CGRID
- **XADV, YADV, ZADV (**xadvppm.F, yadvppm.F, zadvppm.F): advect sensitivities using the same algorithms used for concentrations; if we're looking at sensitivity to a boundary condition, BC data is passed in here. DDM-3D has also been implemented for bot scheme, but bot scheme was omitted from the v. 4.3 release of CMAQ and thus is no longer available.
- **ADJADV** (adjadv.F): multiplies SENGRID by same adjustment factors used for CGRID
- **HDIFF** (hdiff.F): diffuses SENGRID using same algorithms as for CGRID
- **VDIFF** (vdiffim.F): Vertically diffuses SENGRID analogous to CGRID, using **STRIDIAG** (stridiag.F). If we're looking at sensitivity to an emission, then the

emission is added into SENGRID in this subroutine (we assume emissions occur in vertical diffusion).

- **CHEM** (hrdriver.F): Using CGRID from the middle of the timestep and rate constants, create a Jacobian matrix (jac.F). Solve it using Gaussian elimination (s_lu.F), and update SENGRID accordingly. Sensitivity has been implemented for the MEBI solver for all variations of cb4, radm2, and saprc99. Note that jac.F will be different depending which chemical mechanism is used.
- **CLDPROC** (cldproc.F): SENGRID is passed through the dynamic processes of the cloud, including scavenging, analogous to the handling of CGRID. However, aqueous chemistry is not considered.
- **AERO** (aero_driver.F): aerosol processes are not yet handled by CMAQ-DDM. SENGRID contains aerosol and non-reactive species and they are advected and diffused, but they are not emitted and do not undergo any aerosol processes.
- **WR_CONC** (wr_conc.F, wr_aconc.F, wr_asens.F, etc.): hourly-averaged and end-of-hour SENGRID data is output analogously to CGRID. If wrall is not set, then end-of-hour data is only saved for the final hour. The wrbsen and wrisen options allow BC and IC data to be written for use by a daughter domain.

A.4 New and modified files

CMAQ-DDM was implemented as a modification of the July 2002 release of CMAQ. The following lists indicate which files were modified, and which new files were added.

A.4.1 Modified files

- Adjadv.F: adjust SENGRID by same factor as CGRID for that species
- Cldproc.F: pass SENGRID through cloud processes analogous to CGRID
- Couple.F: scale SENGRID by same factor as CGRID for that species; pass SENGRID through radmcld and rescld
- Decouple_a.F: scale SENGRID by same factor as CGRID for that species
- Driver.F: create SENGRID analogous to CGRID; adjust calls to modules so that SENGRID, sensitivity parameters (IREGION, SEN_PAR, etc.) are passed as necessary
- Flcheck.F: skip over checking certain sensitivity files
- Hbot.F: modified to handle SENGRID and CGRID simultaneously, with special care in the handling of non-linearities
- Hdiff.F: diffuse SENGRID with same algorithms as CGRID
- Hrdriver.F: use the concentrations and reaction rates from the middle of the timestep to set up a Jacobian matrix, then solve it by Gaussian elimination to update SENGRID for the effects of chemistry
- Initscen.F: calls sinput to read sensinput.dat for user-defined information about the sensitivity parameters; if we're using a restart file, reads in initial sensitivities; otherwise, sets SENGRID to (a) 0, if not an initial condition sensitivity or (b) the relevant initial condition. Then opens the sensitivity output file and writes the initial results.
- Radmcld.F: passes SENGRID through, analogous to CGRID; special care is taken when functions AMIN or AMAX are used on CGRID; bounds are used to

constrain changes in sensitivity; The effects of aqueous chemistry processes are ignored – we will add treatment of aqueous chemistry when we implement sensitivity for aerosols.

- Rescld.F: multiply SENGRID by the ratio for that species of (CGRID_after_rescld) / (CGRID_before_rescld)
- Rdbcon.F: reads in boundary condition file of sensitivity data (typically used in daughter domain, with file passed from mother domain) if the "usebsen" option is set in the bldit script.
- Scavwdep.F: scavenges SENGRID analogous to CGRID
- Vbot.F: modified to handle SENGRID and CGRID simultaneously, with special care in the handling of non-linearities
- Vdiffim.F: special care is taken in inserting emissions into SENGRID if it's an emissions sensitivity parameter; SENGRID is diffused by same algorithms as CGRID
- Wr_conc.F: writes out sensitivity file in addition to concentration file; writes only the final hour for CGRID and SENGRID (by copying over previous hour) unless "wrall" option is set in bldit script
- Xadvppm.F, yadvppm.F, zadvppm.F: advects SENGRID using same algorithms as for CGRID, by passing SENGRID through HADV after CGRID has been passed through; inserts boundary condition data (x & y directions only) if it's a boundary condition sensitivity parameter.
- Xadvbot.F, yadvbot.F, zadvbot.F: advects SENGRID using the same algorithms as for CGRID; CGRID and SENGRID are passed through on the same call of

HBOT so that non-linearities in the bot scheme treatment of CGRID can be handled appropriately for SENGRID; inserts boundary condition data (x & y directions only) if it's a boundary condition sensitivity parameter. This feature is not supported by CMAQ v. 4.3.

A.4.2 New files

- Chektime.F: checks if JTIME is within time interval specified by ITIME
- HGRD_DEFN_IN.F: analogous to HGRD_DEFN.F, this gets the dimensions for the daughter domain
- Jac.F: creates the Jacobian matrix based on the chemical mechanism, middle-of-timestep CGRID, and reaction rates; NOTE: a different jac.F will be needed for each mechanism – I've prepared Jacobians for all mechanisms in the July 2002 release of CMAQ
- Load_bcon.F (includes subroutine load_bsen): loads concentrations (and sensitivities) from mother domain into a buffer that will be output to serve as boundary concentrations (and sensitivities) for the daughter domain. NOTE: NTHIK is assumed to be 1.
- Load_icon.F (includes subroutine load_isen): loads concentrations (and sensitivities) from mother domain into a buffer that will be output as initial conditions for the daughter domain.
- Load_sengrid.F: similar to load_cgrid.F, this reads SENGRID from a file
- Opsens.F: similar to opconc.F, this opens the sensitivity output file.
- Sinput.F: reads sensinput.dat to determine information about the user-defined sensitivity parameters. If "regions" option is set to allow sensitivity to

perturbations from specific regions, reads the REGIONS_1 netcdf file. NOTE: earlier versions of CMAQ-DDM-3D had a separate rdregion.F, which is now incorporated into sinput.

- s_lu.F: written by linpack; contains subroutines sgesl, sgefa, and saxpy which are needed to solve Jacobian by Gaussian elimination
- S_PCGRID_DEFN.F: analogous to PCGRID_DEFN.F, this creates a SENGRID target, S_PCGRID
- s_opemis.F: opens separate emissions files split into area, mobile, non-road, point, and biogenic sources
- s_rdemis.F: reads emissions files split into the 5 categories (see s_opemis)
- s_sciproc.F: analogous to sciproc.F, this has calls adjusted for sensitivity analysis. Also tracks HNO_3 and N_2O_5 before and after AERO to account for N_2O_5 hydrolysis.
- s_tridiag.F: analogous to tridiag.F, this is used in vertical diffusion of SENGRID
- wr_asens.F: outputs hourly-averaged sensitivity file
- wr_bcon.F: writes boundary condition files for concentrations and sensitivities for use by the daughter domain; this replaces the need for the bcon module
- wr_icon.F: writes initial conditions files for concentrations and sensitivities for use by the daughter domain; this replaces the need for the icon module
- conv_sengrid.F: analogous to conv_cgrid.F
- sensinput.dat: user-defined input file to describe the desired sensitivity parameters; note that sensitivity computed relative to a 100% change in an existing emission, initial condition or boundary condition, or to a specified

amount of emissions. The location and time of the change in input can be specified for each parameter**.** Extensive comments at the bottom of this file describe how sensitivity parameter data should be written in the file.

- FILES_CTM.EXT.sens: similar to FILES_CTM.EXT, with additional filenames for sensitivity analysis
- in_out.q.sens(.nosplit): adjusted from in_out.q for to include DDM-3D I/O files
- NR_xxx_SENS.EXT: shorten the names of the vapor species.

NOTE on Jan. '04 update: REGIONS.EXT and SENS.EXT are no longer used in the Jan. 2004 update of the code. The number of sensitivity parameters must now be entered in the runscript, and the ASENS file is written for the same species and levels that are specified in the runscript. Characteristics of the regions file and other information are now determined automatically in the code. These improvements mean that CMAQ-DDM-3D can be compiled once, and then various runs can be formed simply by changing info about sensitivity parameters in sensinput.dat and run-specific parameters in the runscript. Also, sensitivity parameters are now defined as allocatable pointers for compatibility with Intel compilers; the change to pointers does not affect the operation of DDM-3D.

A.5 Execution of CMAQ-DDM

The CMAQ code, as modified for sensitivity analysis, must be compiled with a modified bldit script, and run using a modified runscript. The key changes to the bldit and run scripts and associated files are described below:

- sensinput.dat: user should specify which sensitivity parameters s/he wishes to examine by carefully listing the specifications following the format described in the comments at the bottom of this input file.
- bldit script: add options for:

  sens: if sensitivities are being computed; include FILES_CTM.EXT.sens, and in_out.q.sens

  regions: allows a file specifying regions; need to specify the filename of the netcdf file to be used.

  userst: use a sensitivity initial condition file (i.e., an SGC_IC file); this should be set false for the initial run of an episode, and true for subsequent days so that sensitivity results are continuous

  wrall: write all hours, rather than only final hour, for end-of-hour CGRID & SENGRID

  wricon: write initial condition concentration (& sensivivity) file for daughter domain

  wrbcon: write boundary condition concentration (& sensitivity) file for daughter domain

  usebsen: use sensitivity boundary condition file; this should be set true when running on a daughter domain with BC sensitivity data provided from the mother domain

  split: Use emissions split into multiple files for categories biogenic, mobile, non-road, area, and point; this allows sensitivity to be computed to specific type(s) of emissions. NOTE: in_out.q.xxx file must reflect whether

emissions are split. Code is currently configured to accept either one merged emission file or the merged file plus the 5 category files listed above. By re-writing vdiffim.F, s_rdemis.F and associated EXT files, code could be re-configured for other categories of emissions files.

high: Allow 2nd order sensitivity analysis.

- run script: add parameters for:

  ICONDATE/ICONTIME: specify the initial date and time for the daughter domain (if applicable)

  NPMAX: number of sensitivity parameters

  GRIDNAME_IN: the grid domain that will be used for the daughter domain (if applicable)

  OUTDIR1/OUTDIR2: the user may specify different output directories for different output files if desired.

  additional filenames: extra filenames must be specified for input and output files used in sensitivity analysis

- in_out.q.sens: similar to in_out.q, with additional input and output files for sensitivity
- in_out.q.sens.nosplit: used if we're not splitting emissions
- FILES_CTM_EXT.sens: similar to FILES_CTM.EXT, with additional files needed for sensitivity

A.6 Input and output of data

CMAQ-DDM requires the same input files as a normal CMAQ run. If nested domains are used, we will need an additional file containing boundary condition sensitivity data output from relevant gridcells of the mother domain for use by the daughter domain. If the daughter domain begins later than the mother domain, an additional file will be needed which contains sensitivity data output from relevant gridcells of the mother domain at the time corresponding to the initial time of the daughter domain.

SENGRID is NPMAX (# of sens parameters) times as large as CGRID, so the output file sizes would become prohibitively large if we were to output all of SENGRID for every hour, gridcell, and species. Thus significant changes have been made to the output of data to accommodate sensitivities.

- Output of hourly-averaged concentrations (ACONC) is unchanged. An analogous file (ASENS) is output of hourly-averaged sensitivities for desired species on desired levels. NOTE: The units for sensitivity outputs are the same as those for a given species of concentrations, divided by the change in input (e.g., (ppm O3) / (1 mol/s increase in emis of NO), or (ppm NO2) / (100% increase in emis of NO))
- End-of-hour concentrations (CONC), and an analogous file for end-of-hour sensitivities (SENS), are output to a file which copies over the output from the previous hour. Thus only the final hour of end-of-hour data, for all species and all gridcells (and all NPMAX) is saved, and can be used for a restart. The option "wrall" may be set in the bldit script to output all hours.

- If wrbcon is set in bldit script: Boundary condition files, BCON and BSEN, contain data from CGRID and SENGRID for every hour, species, and sensitivity parameter, but only from the gridcells relevant to the boundary condition of the daughter domain. These files are output using the grid definition of the daughter domain. NOTE: I have assumed NTHIK = 1.
- If wricon is set in bldit script: Initial condition files, ICON AND ISEN, contain data from CGRID and SENGRID for every species and sensitivity parameter, but only for the hour that will be the initial time for the daughter domain. These files are output using the grid definition of the daughter domain.

Table A.1. Output files in CMAQ-DDM

FILE	HOURS	DOMAIN	GRIDCELLS	SPECIES
ACONC / ASENS	All	Mother	All cells, select layers	Specified in runscript
CONC / SENS	Last hour only (unless wrall)	Mother	All cells, all layers	All
BCON / BSEN	All hours, begin with init time for daughter domain	Daughter	Boundary cells, all layers	All
ICON / ISEN	init time for daughter	Daughter	All cells, all layers	All

A.7 Shortcomings and unimplemented features

The implementation of CMAQ-DDM is a work in progress. Features **not** yet implemented in CMAQ-DDM include:

- Tracer species
- Aerosol processes (However, we do account for N_2O_5 hydrolysis on aerosols by tracking N_2O_5 and HNO_3 before and after the call to AERO) and aqueous chemistry. Aerosol and aqueous processes are currently being implemented.

- Allowing emissions in chemistry (they are assumed to occur in vdif, which is more stable. We do not recommend inputting emissions during chemistry.)
- Process analysis (This would be a significant project).
- Plume-in-grid (This would be a significant project).
- ACM method vertical diffusion (We were advised against using ACM because it has not been widely used or tested yet. Making DDM compatible with ACM should not be difficult.)
- SMVGEAR and QSSA solvers (This should be straightforward for EPA to do if desired, by adopting the same approach as we used in hrdriver.F. Our studies suggest QSSA is less accurate and computationally slower than MEBI. SMVGEAR is much slower than MEBI but yields vary similar results.)
- Output files for sensitivity of deposition (This should be straightforward, but it awaits more comprehensive treatment of aqueous chemistry in a future DDM release.)
- User-friendly interface for defining sensitivity parameters (sinput.F / sensinput.dat)
- Some computational time saving could perhaps be achieved by using a sparse matrix routine to solve the Jacobian, rather than Gaussian elimination as implemented now.
- Only sensitivity to emissions, initial conditions, and boundary conditions have been implemented so far; it would be straightforward to extend CMAQ-DDM to handle sensitivities to reaction rate constants, deposition velocities, or windspeed (see Yang *et al.*, 1997).

Caution should also be taken with the following known shortcomings:

- The species names VAP_xxxx in the non-reactive species lists have been changed to V_xxxx to accommodate 16-character names of sens parameters
- Sergey is working on improving our handling of cloud processes and incorporating aerosol and aqueous chemistry processes. Currently, radmcld may cause DDM to go unstable in very rare and obvious instances (results $>10^6$ times as large as normal). For ozone sensitivity, this may be overcome by turning off cloud processes on days when instability occurs, as ozone sensitivity is largely unaffected by cloud processes.

A.8 Summary

DDM has proven to be a very effective tool for air quality studies. This implementation in CMAQ has been done with the intent to provide flexibility and computational efficiency, and also maintain the CMAQ code structure. CMAQ-DDM has been found to accurately simulate sensitivity of ozone to initial conditions, boundary conditions, and emissions of precursor species. However, CMAQ-DDM remains a work in progress with known shortcomings and its accuracy has not been tested for all conceivable applications. Any errors should be reported to the author at dcohan@eas.gatech.edu.

APPENDIX B

MODELING OF SENSITIVITIES*

B.1 Introduction

The air quality modeling presented in the preceding chapters of this report has sought to simulate the August 2000 air pollution episode, and to predict pollutant levels under identical meteorology accompanied by future year emissions. Such modeling is crucial to understanding the spatio-temporal characteristics of the air pollution episode, assessing the reasonableness of models and inventories, and anticipating future conditions.

Many policy applications of air quality modeling require not only the simulation of past and future conditions, but also the probing of various "what if" worlds. What if County A instituted emissions inspections for vehicles, or Power Plant B reduced its NO_x emissions, or Factory C expanded its VOC generating operations? How would ozone concentrations at monitors X, Y, and Z respond to each change in precursor emissions?

Sensitivity analysis, amongst many applications, examines the relationships between emissions and ambient concentrations. This analysis is especially vital in the case of ozone, whose sensitivity to incremental emissions of NO_x or of VOC varies greatly in magnitude and even in sign depending upon meteorological conditions and the relative emission rates of these precursor gases. For example, in some forested rural regions

* Appeared as a chapter in a FAQS report to Georgia Department of Natural Resources
Hu, Y., D. S. Cohan, M. T. Odman and A. G. Russell (2004). Air quality modeling of the August 11-20, 2000 episode for the Fall Line Air Quality Study. Prepared for Environmental Protection Division, Georgia Department of Natural Resources.

where biogenic emissions of VOC dwarf the anthropogenic component, ozone concentrations may depend virtually only on the availability of NO_x (NO_x-limited regime); in a heavily-trafficked urban center or the immediate vicinity of a power plant, NO_x concentrations may be sufficiently high that ozone concentrations are more effectively controlled by reducing the level of VOC (VOC-limited, radical-limited, or "NO_x-saturated", regime), and increasing NO_x might lead to local reductions in ozone. Effective formulation of emission control strategies for ozone attainment requires knowledge of the spatio-temporally variable sensitivity of ozone to its precursor gases, NO_x and VOC.

Traditionally, sensitivity analysis in air quality modeling is conducted by the "brute force method." Ozone concentrations are modeled under "base case" conditions, and differenced from a perturbed run in which emissions rates are altered. However, the brute force method faces key shortcomings: (1) numerical noise for small perturbations, (2) unclear applicability to perturbations other than the size modeled, and (3) burdensome computations when a large number of sensitivity parameters is desired.

For the FAQS project, we utilize an alternative approach to sensitivity analysis, the Decoupled Direct Method in 3D (DDM-3D) (Yang *et al.*, 1997), to efficiently explore the sensitivity of ozone to precursor emissions. This chapter presents the implementation of DDM-3D in a regional air quality model, and assesses its performance relative to the brute force method. The following chapter applies DDM-3D to analyze the sensitivity of ozone concentrations to a broad range of perturbations to the projected inventory of Georgia emissions in 2007.

B.2 DDM-3D Sensitivity Analysis

DDM-3D operates simultaneously with an underlying atmospheric model to compute the local sensitivities of pollutant concentrations to perturbations in input parameters (e.g., initial conditions, boundary conditions, or emission rates). For this report, we focus on the sensitivity of ozone concentrations to emission rates, using DDM-3D as implemented in the Community Multiscale Air Quality (CMAQ) model, v. 4.3 (Byun and Ching, 1999). The implementation of DDM-3D in CMAQ has been presented by Cohan *et al*. (2002).

CMAQ, like other Eulerian models of the atmosphere, computes the evolution of species concentrations by a numerical approximation of the mass balance equation governing reactive transport:

$$\frac{\Delta C_i}{\Delta t} = [advection] + [diffusion] + [deposition] + [chemistry] + [emissions] + [clouds] \qquad \textbf{(B.1)}$$

where [*process*] is the numerical representation of an atmospheric process and C_i is the concentration of species *i*. DDM-3D assesses the sensitivity of *C* to perturbations in model inputs of emissions, by defining:

$$I_j(x,t) = I_{j,0}(x,t) + \varepsilon_j \cdot p_j(x,t) \qquad \textbf{(B.2)}$$

$$S^{(1)}_{i,j}(x,t) = \frac{\partial C_i(x,t)}{\partial \varepsilon_j} \qquad \textbf{(B.3)}$$

Here, $\varepsilon_j p_j$ is a perturbation to a base case model input $I_{j,0}$ (an emission rate, initial condition, or boundary condition); and $S^{(1)}$ is the local first-order (linear) sensitivity of *C* to the perturbation of the model input. *S* varies both spatially and temporally, just as the concentration fields. Our implementation provides broad flexibility in the form of the perturbation to model inputs: a static or time-variant change, for an individual species or

group of species, from a single gridcell, a region of one or more counties, or the entire domain. We present sensitivity coefficients, *S*, semi-normalized to the size of the unperturbed input field. Thus, for example, if the sensitivity coefficient of ozone with respect to domain-wide NO_x emissions is +10 ppbV at a given time and receptor, then a 10% reduction in NO_x would be expected to reduce ozone concentrations by 1 ppbV.

To compute the time variance of *S*, we differentiate Equation 1 with respect to ε:

(B.4)

$$\frac{\Delta S_{i,j}}{\Delta t} = \frac{\partial}{\partial \varepsilon}[advection] + \frac{\partial}{\partial \varepsilon}[diffusion] + \frac{\partial}{\partial \varepsilon}[deposition] + \frac{\partial}{\partial \varepsilon}[chemistry] + \frac{\partial}{\partial \varepsilon}[emissions] + \frac{\partial}{\partial \varepsilon}[clouds]$$

As described in detail by Yang *et al*. (1997), DDM-3D calculates $S^{(1)}$ in the above equation by applying the same numerical algorithms and operator splitting used to calculate *C*. This decoupled direct approach simplifies the implementation of DDM and provides consistency between calculations of sensitivities and concentrations. An exception is that calculations of concentrations reflect the CMAQ aero3 aerosol module, but the current implementation of DDM-3D ignores aerosol and aqueous chemistry processes other than the heterogeneous hydrolysis of N_2O_5. The comparisons of DDM-3D with brute force results, presented later in this chapter, demonstrate that DDM-3D accurately computes sensitivities for ozone despite this inconsistency. DDM-3D in CMAQ has been extended recently to include aerosol processes.

Since $S^{(1)}$ is a local, first-order measure of sensitivity, its accuracy in characterizing model responses to input perturbations will diminish with the size of the perturbation and the nonlinearity of the response. We have extended CMAQ-DDM to compute second-order sensitivity coefficients by the method of Hakami *et al.* (2003a) (Cohan *et al.*, 2003). Essentially, second-order sensitivity coefficients are computed by differentiating the

governing equations of the atmospheric model with respect to a first-order DDM-3D sensitivity coefficient. While first-order sensitivity coefficients represent the local sensitivity or "slope" of species *i* with respect to input parameter *j*, second-order sensitivities, $S_{i,j1,j2}^{(2)} = \partial^2 C_i/(\partial \varepsilon_{j1} \partial \varepsilon_{j2})$, represent the second-derivative or local "curvature" of the species-parameter relationship (Figure B.1). The relationship between ozone concentrations and emissions of precursor gases is typically concave down as depicted in Figure B.1. Thus first-order DDM-3D (slope of green line) will tend to underpredict the reduction in ozone accompanying a large reduction in emissions; conversely, a slope indicated by brute force (red line) will tend to overpredict the steepness of the local response to incremental changes from base case *A*. Second-order DDM-3D measures the local curvature of the relationship at (E_A, $O_{3,A}$).

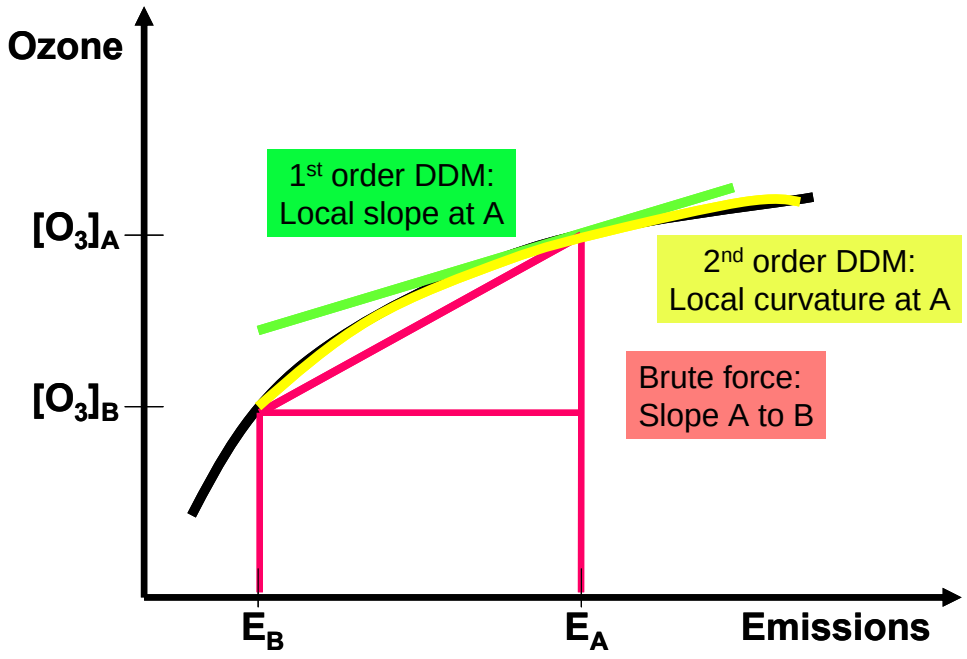

Figure B.1. Schematic ozone response to emissions, and brute force and DDM-3D sensitivities.

By incorporating second-order sensitivity coefficients along with first-order coefficients in Taylor series expansions, the response can more accurately be projected to larger perturbations away from a base case (Hakami *et al.*, 2003a). In this approach, concentrations for a perturbed case are approximated by:

$$C_{i,j}(x,t) = C_{i,0}(x,t) + \varepsilon_j S^{(1)}_{i,j}(x,t) + \tfrac{1}{2}\varepsilon_j^2 S^{(2)}_{i,j,j}(x,t) \qquad \textbf{(B.5)}$$

where $C_{i,0}$ is the concentration of species i under base case conditions, $C_{i,j}$ is the concentration when model input has been perturbed by an amount $\varepsilon_j p_j$, and $S_{i,j}^{(1)}$ and $S_{i,j,j}^{(2)}$ are the first- and second-order semi-normalized sensitivity coefficients of C_i with respect to perturbation p_j. This is illustrated by the following hypothetical scenario:

Table B.1. Hypothetical Taylor expansion of sensitivity coefficients.

Base case concentration ($C_{O3,0}$)	1st order sensitivity to NO_x emissions from Source A ($S_{O3,A}^{(1)}$)	2nd order sensitivity to NO_x emissions from Source A ($S_{O3,A,A}^{(2)}$)	Change in NO_x emissions from Source A
85 ppbV	10 ppbV	-5 ppbV	-30%
First-order approximation of ozone at X for 30% reduction in NO_x from Source A: $C_{O3,-30\%NOx}$ = 85ppbV + (-0.3) * 10 ppbV = 82 ppbV			
Second-order approximation: $C_{O3,-30\%NOx}$ = 85ppbV + (-0.3) * 10 ppbV + 0.5 * $(-0.3)^2$ * (-5 ppbV) = 81.78 ppbV			

The importance of the first-order sensitivity coefficient increases linearly with the size of the perturbation, whereas the second-order term increases with the square of the perturbation. Thus, the relative importance of the second-order term in the Taylor approximations will increase with both the size of the second-order coefficient and the size of the perturbation from the base case.

Note that Taylor expansions utilize only local sensitivity coefficients calculated at the base case to predict concentrations for any size perturbation of the input parameter. Taylor expansions of DDM-3D sensitivity coefficients therefore represent an extremely powerful tool in air quality analysis, to the extent to which the expansions remain accurate for large perturbations. The accuracy of DDM-3D and its applicability to large perturbations are examined in the following section.

B.3 Performance of DDM-3D

B.3.1 Overview and Methodology

The accuracy of sensitivity analysis is inherently difficult to assess. Even if we could turn off power plants, or alleviate traffic volume from the roads, we would be unable to hold meteorology and other conditions constant to truly observe the sensitivity of ambient concentrations to that change in emissions. Sensitivity analysis can be only as accurate as the underlying model, and depends on the model simulating air quality accurately and for the right reasons. Because we cannot directly observe sensitivity in the atmosphere, we assess the accuracy of a sensitivity analysis technique by how well it captures the relationships within the underlying model.

DDM-3D computes the local sensitivity of outputs (concentrations) to changes in inputs (e.g., emission rates), so the most appropriate benchmark for its performance is to compare DDM-3D sensitivity coefficients with those suggested by brute force model runs with small perturbations. We assess the accuracy of CMAQ-DDM sensitivity coefficients by comparing them to finite difference calculations from brute force model runs with +/- 10% perturbations in NO_x and VOC emissions from the entire 12 km

domain and to NO_x emissions from a single point source, Plant Scherer. These comparisons test DDM-3D over the full range of spatial scales to which it could be applied.

The semi-normalized sensitivity coefficients from DDM-3D can be compared with finite differencing of brute force results as shown in Table B.2.

Table B.2. Semi-normalized first- and second-order sensitivity coefficients.

Order of sensitivity	DDM-3D	Brute Force Method
1st order	$S_{i,E\_NOX}^{(1)}$	$5 * (C_{110\%NOx} - C_{90\%NOx})$
2nd order	$S_{i,E\_NOX,E\_NOX}^{(2)}$	$100 * [(C_{110\%NOx} - C_{base}) - (C_{base} - C_{90\%NOx})]$

In this table, $C_{x\%NOx}$ refers to the concentration of ozone in a brute force run with NO_x emissions scaled by x% for the entire domain or Plant Scherer, where appropriate. The normalization scales the sensitivity coefficients to 100% of the NO_x emissions to provide a relevant comparison with the DDM-3D coefficients.

In addition to assessing the *accuracy* of DDM-3D in comparison with small brute force perturbations, we probe the *applicability* of DDM-3D to predicting the impact of larger perturbations in emissions. Through Taylor approximations (Equation B.5 and Table B.1), the local sensitivity coefficients computed by DDM-3D are extended to predict ozone concentrations over a wide range of hypothetical emissions. The DDM-3D Taylor approximations are compared to the results of brute force simulations in which each is reduced by 50% and 100%.

All brute force and DDM-3D simulations discussed in the sensitivity analysis section of this report are conducted using CMAQ version 4.3 with August 2000 meteorology and the FAQS 2007 emissions inventory. The 12-km resolution domain used in these CMAQ simulations is slightly larger (75 columns x 66 rows) than that used in previous chapters, to incorporate the entire states of South Carolina and Alabama and major emissions regions in Tennessee and North Carolina. Otherwise, CMAQ concentrations are computed in identical fashion to simulations detailed in preceding chapters of this report. In particular, initial and boundary conditions are taken from a base case simulation of the 36-km domain covering the Eastern United States, with Year 2007 emissions.

B.3.2 Domain-wide comparisons

To evaluate the performance of DDM-3D for calculating the sensitivity of ozone concentrations to domain-wide emissions, CMAQ simulations with uniform percentage changes in anthropogenic emissions within the 12-km domain are differenced from a standard CMAQ simulation. Each CMAQ simulation incorporates identical meteorology, initial conditions, and boundary conditions to the base case run. Results are evaluated over the 8-hour period each day during which base case ozone concentration was maximal in that grid cell.

Ozone sensitivity to 10%, 50%, and 100% reductions in domain-wide emissions of NO_x is computed by the brute force method and by Taylor expansions of DDM-3D sensitivity coefficients. The level of agreement between brute force and DDM-3D results on August 17 (Figure B.2) is indicative of agreement on other days (not shown).

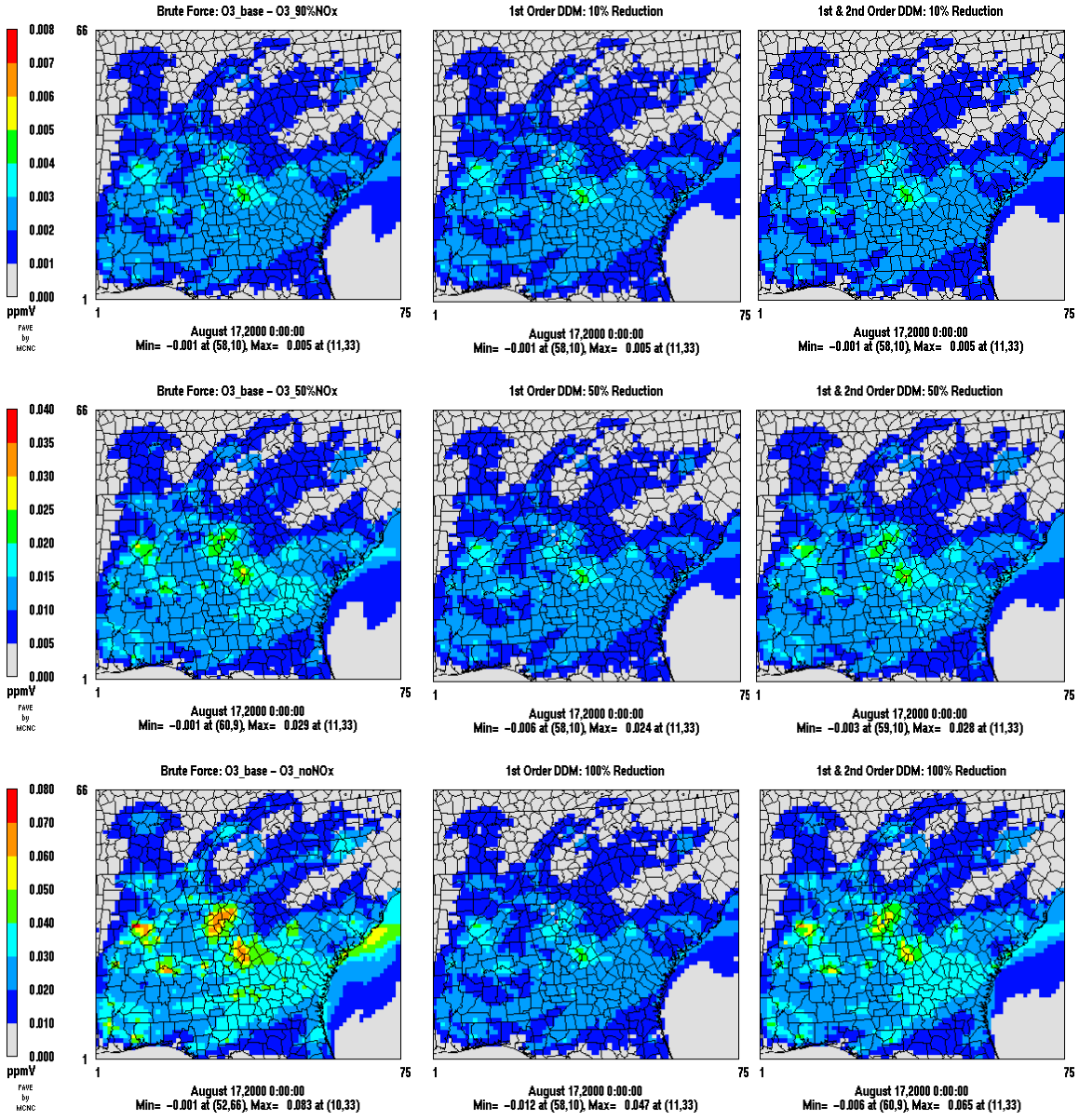

Figure B.2. Reduction in 8-hour ozone on Aug. 17, accompanying a 10% (top), 50% (middle), and 100% (bottom) reduction in NO_x emissions. In each row, the left panel shows the brute force difference, and subsequent panels show Taylor approximations incorporating first-order (C) and first- & second-order (R) DDM-3D coefficients.

Sensitivity to NO_x emissions is strongest near large source regions such as Atlanta and Birmingham, and weakest where inflow from the domain boundary predominates. The color scales among plots are proportional to the reduction in emissions, so the increasing prevalence of yellow and orange in the brute force plots indicates non-linear response to emissions. For 10% reductions in NO_x emissions (Figure B.2, top row), brute force and DDM-3D yield nearly identical results, even if only first-order DDM-3D sensitivity coefficients are considered. For 50% reductions in NO_x emissions (Figure B.2, middle row), the first-order Taylor expansion underpredicts the reduction in ozone, but incorporation of the second-order DDM-3D coefficient yields closer agreement with brute force. For complete removal of anthropogenic NO_x emissions within the domain (Figure B.2, bottom row), the underprediction by first-order Taylor expansion becomes even more severe. Incorporation of the second-order coefficient greatly improves the agreement between DDM-3D and brute force in this case. Some underprediction remains, with the largest discrepancies occurring where sensitivity is highest.

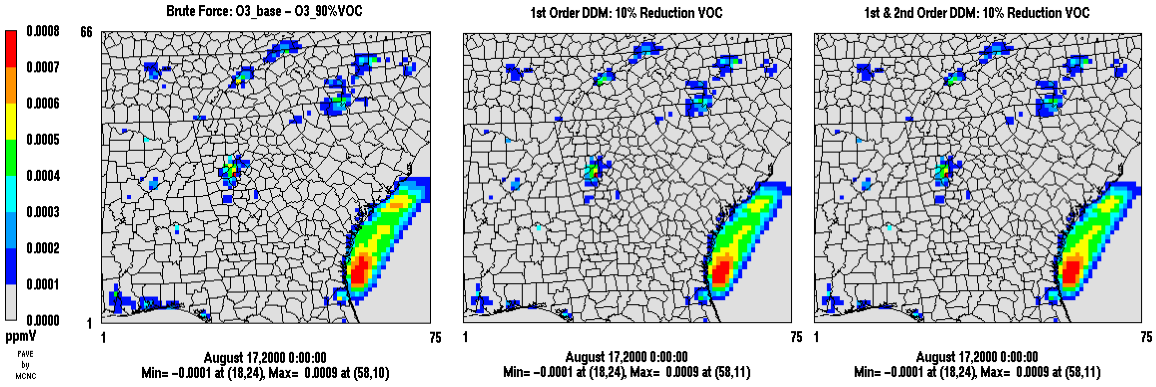

Figure B.3. Reduction in 8-hour ozone on Aug. 17, accompanying a 10% reduction in VOC emissions. The left panel shows the brute force difference, and the subsequent panels show DDM-3D approximations incorporating first-order (C) and first- and second-order (R) coefficients.

As with perturbed NO_x emissions, DDM-3D well reproduces the magnitude and spatial distribution of ozone sensitivity to anthropogenic VOC emissions (Figure B.3). Note that although the color scale in Figure B.3 is a factor of 10 smaller than that used for 10% reduction in NO_x emissions in Figure B.2, the majority of the domain shows almost no sensitivity to anthropogenic VOC emissions. Significant sensitivity of ozone to VOC appears primarily in (1) the centers of urban regions and (2) off the coast where continental outflow is not supplemented with fresh biogenic VOC emissions. These trends are well-captured by DDM-3D.

A statistical comparison of semi-normalized coefficients (Table B.3) demonstrates that for domain-wide perturbations, DDM-3D computes local sensitivities in close agreement with those computed by brute force.

Table B.3. Semi-normalized sensitivity coefficients of 8-hour ozone for domain-wide changes in emissions.

	Brute force* (ppb)	DDM (ppb)	Difference (%)	DDM v. B.F. (r^2)
1st order NO_x	11.90	11.69	-1.8%	0.997
2nd order NO_x	-6.85	-6.62	-3.3%	0.967
1st order VOC	0.18	0.18	0.2%	0.992
2nd order VOC	-0.13	-0.16	25.0%	0.720

* Central-difference estimates computed from simulations with +/-10% perturbations in emissions, as described in Table B.2..

The first two columns present sensitivity coefficients averaged over the domain for the period August 13-19. The r^2 values refer to the daily correlation between DDM-3D and brute force coefficients on a grid cell-by-grid cell basis. The somewhat weaker correlation of second-order coefficients reflects that (1) for DDM-3D these are computed as a "sensitivity of a sensitivity" of first-order coefficients and (2) brute force second-

order coefficients are subject to numerical noise, particularly in the case of the small levels of sensitivity for ozone concentrations with respect to VOC emissions. Further assessment of inaccuracies in DDM-3D and brute force calculations can be found in Hakami *et al*. (Hakami, 2003b).

The applicability of Taylor expansions to replicating a wide range of changes in domain-wide emissions is evaluated in Table and presented visually in Figure B.4. The bold columns in Table B.4 show brute force and DDM-3D calculations of the reduction in 8-hour ozone concentrations, averaged over the domain and the period August 13-19, that would accompany each domain-wide perturbation to emissions. The r^2 values represent the cell-by-cell correlation with respect to brute force.

Table B.4. Reduction in 8-hour ozone accompanying perturbations to domain-wide emissions.

Change in Emissions	**Brute force[+] (ppb)**	**DDM1* (ppb)**	DDM1 v. B.F. (r^2)	**DDM1,2** (ppb)**	DDM1,2 v. B.F. (r^2)	**B.F. Taylor*** (ppb)**	B.F. Taylor v. B.F. (r^2)
-10% NO_x	**1.224**	**1.169**	0.996	**1.202**	0.997		
+10% NO_x	**-1.156**	**-1.169**	0.997	**-1.136**	0.997		
-50% NO_x	**6.949**	**5.846**	0.975	**6.675**	0.996	**6.807**	0.998
-100% NO_x	**16.686**	**11.692**	0.896	**15.006**	0.976	**15.328**	0.977
-10% VOC	**0.018**	**0.018**	0.992	**0.019**	0.992		
+10% VOC	**-0.017**	**-0.018**	0.991	**-0.017**	0.992		

[+] Reduction in mean domain-wide 8-hour ozone concentration relative to base case simulation.
* Taylor expansion of 1st order DDM sensitivity coefficient.
** Taylor expansion of 1st and 2nd order DDM sensitivity coefficients.
*** Taylor expansion of the 1st and 2nd order sensitivity coefficients computed by differencing brute force runs of +/- 10% changes in NO_x emissions.

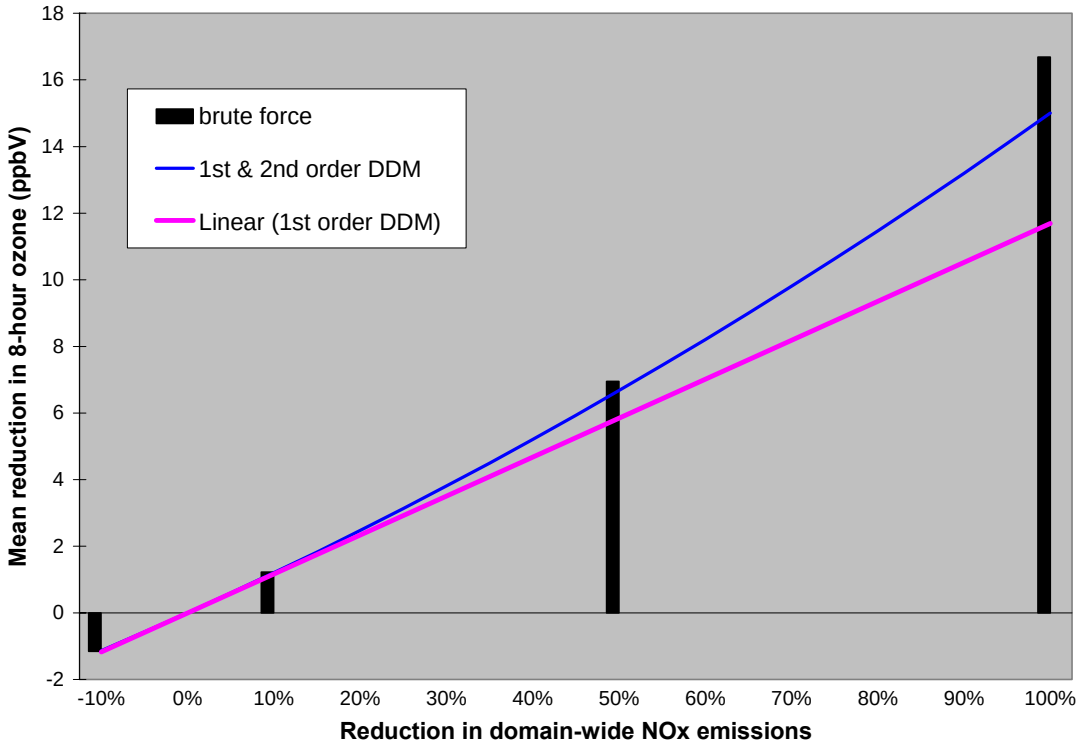

Figure B.4. Response of 8-hour ozone, averaged over the domain for Aug. 13-19, to changes in domain-wide NO_x emissions.

The performance of DDM-3D for all +/- 10% perturbations is very strong. The increasing gap between brute force and first-order DDM-3D as the size of the NO_x perturbation increases reflects non-linearity, with ozone becoming increasingly sensitive to the remaining NO_x as emissions decrease. Incorporation of second-order sensitivity coefficients becomes more significant for reductions beyond about 25% in domain-wide emissions, and enables accurate simulation of the 50% brute force case. For 100% removal of anthropogenic NO_x, the high r^2 value (0.976) demonstrates that second-order DDM-3D reproduces the spatial pattern of changes very well, but magnitudes are underpredicted by an average of 10%.

That the underprediction of the 100% NO_x reduction case is larger than the underprediction of coefficients in Table 2.1 suggests the presence of non-linear responses that cannot be completely characterized even if local slope and curvature at the base case are accurately computed. We test this hypothesis by conducting Taylor expansions of brute force sensitivity coefficients (Table B.4, right columns).Equation B.5 is applied again, but with sensitivity coefficients derived as in Table B.2 from the results of brute force simulations with -10%, 0%, and +10% perturbations to NO_x emissions. Taylor expansion of brute force coefficients underpredicts the response to 100% NO_x removal by a similar amount (8%) as Taylor expansion of DDM-3D coefficients. Therefore, the moderate discrepancy with respect to 100% changes primarily reflects a limitation in the applicability of extending local first- and second-order sensitivity coefficients to predict ozone response to very large changes in emissions, rather than inaccuracy in DDM-3D.

B.3.3 Point source comparisons

In addition to evaluating DDM-3D for domainwide perturbations in emissions, we also check its performance for local perturbations in emissions by examining sensitivities to NO_x emissions from a single point source, Plant Scherer. This coal-fired power plant in Monroe County is projected to be the largest single source of NO_x emissions in Georgia in 2007. Power plant plumes provide an especially rigorous test of DDM-3D, because ozone sensitivity is known to vary greatly as NO_x dilutes over regions with large biogenic emissions (Ryerson *et al.*, 2001), and because tracking sensitivity to a single point tests the ability of DDM-3D to reproduce the advection and diffusion processes of the underlying model.

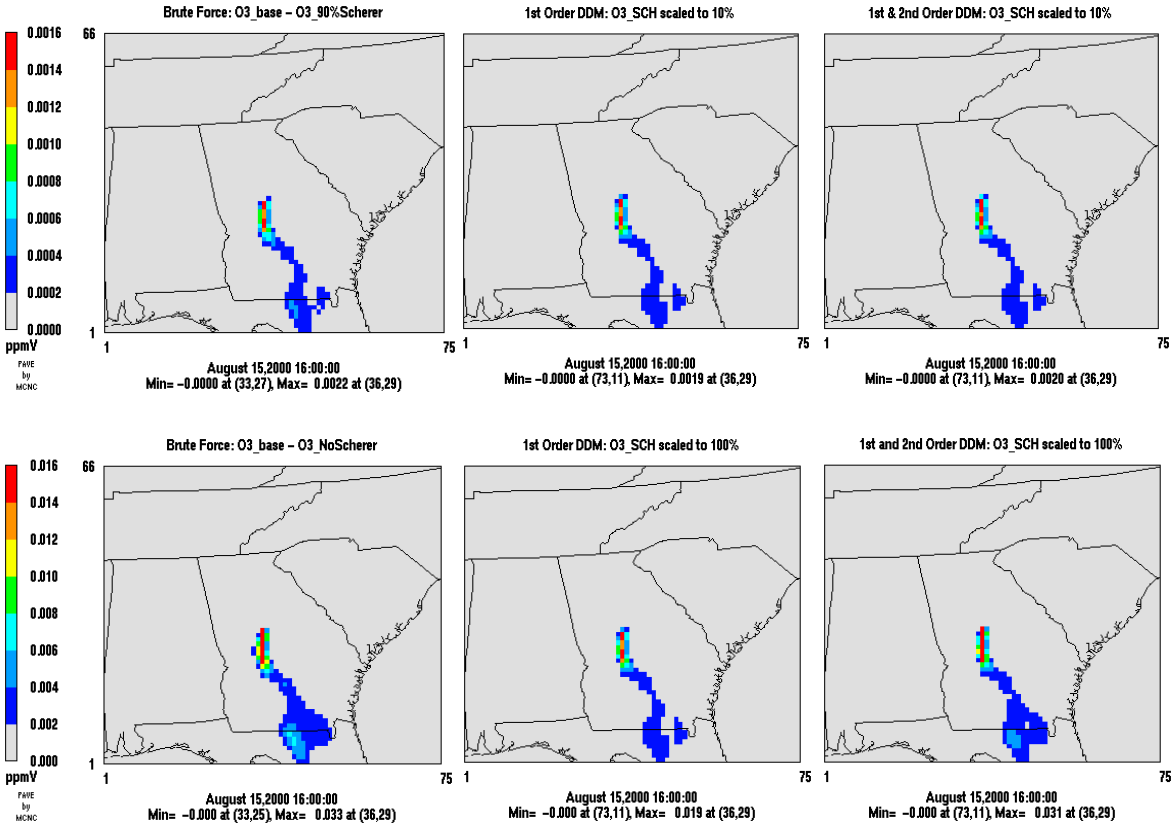

Figure B.5. Reduction in ozone at 4 p.m. EDT, Aug. 15, accompanying a 10% (top) and 100% (bottom) reduction in Year 2007 NO_x emissions from Plant Scherer. In each row, the left panel shows the brute force difference, and the subsequent panels show DDM-3D approximations incorporating first-order (C) and first- and second-order (R) coefficients.

Plant Scherer sensitivity results from 4 p.m. on August 15 are indicative of the level of agreement between DDM-3D and brute force sensitivity results throughout the episode (Figure B.5). Brute force and DDM-3D both show very similar spatial patterns of a plume that is most concentrated within 100 km of the plant and is being blown to the south-southeast. For a 10% reduction in emissions, first-order DDM-3D is sufficient to replicate the spatial patterns and magnitudes indicated by brute force. For a 100% reduction, incorporation of second-order DDM-3D results is very beneficial in capturing the spatial pattern and magnitude of the impact, particularly the magnitude of the maximum impact which is more than 10 times larger than in the 10% case. This non-linearity reflects that as NO_x emissions are reduced, the ozone production regime within the plume becomes NO_x-limited more rapidly and thus more sensitive to further reductions in NO_x.

The statistical performance of DDM-3D for Plant Scherer sensitivities is similar to that found for the domain-wide case (compare Table B.5 with Table B.4).

Table B.5. Reduction in 8-hour ozone accompanying changes in Plant Scherer NOx.

Change in Emissions at Plant Scherer	**Brute force[+] (ppb)**	**DDM1* (ppb)**	DDM1 v. B.F. (r^2)	**DDM1,2** (ppb)**	DDM1,2 v. B.F. (r^2)	**B.F. Taylor*** (ppb)**	B.F. Taylor v. B.F. (r^2)
-10%	**0.0141**	**0.0139**	0.992	**0.0141**	0.992		
+10%	**-0.0141**	**-0.0139**	0.991	**-0.0137**	0.993		
-50%	**0.0752**	**0.0695**	0.966	**0.0741**	0.992	**0.0701**	0.996
-100%	**0.1667**	**0.1390**	0.868	**0.1575**	0.975	**0.1396**	0.963

[+] Reduction in mean domain-wide 8-hour ozone concentration relative to base case simulation.
* Taylor expansion of first-order DDM sensitivity coefficient.
** Taylor expansion of 1st and 2nd order DDM sensitivity coefficients.
*** Taylor expansion of the 1st and 2nd order sensitivity coefficients computed by differencing brute force runs of +/- 10% changes in NO_x emissions.

The bolded columns present the domain-wide average change in 8-hour ozone, averaged over August 13-19, associated with various perturbations to Year 2007 Plant Scherer NO_x emissions. Once again, some underprediction (6%) but very strong spatial representation (r^2=0.975) is found with second-order DDM-3D expansions for the case of 100% reduction in emissions. In the case of Plant Scherer emissions, second-order Taylor expansion of DDM-3D results performs somewhat better than Taylor expansion of brute force results, which are subject to numerical noise because emissions from only a single point source have been perturbed.

For DDM-3D results to be applicable in policy formulation, it is necessary that they be accurate not only in an overall sense but also specifically at the monitors most affected by a given source. Figure B.6 compares DDM-3D and brute force results for the impact of 10% and 100% reductions in Plant Scherer NO_x emissions on ozone concentrations at the Sandy Beach monitor in western Bibb County. Our modeling indicates that Sandy Beach, operated by Georgia Tech during the FAQS study, is the ozone monitor most often impacted by the Scherer plume. The scale of the plots is proportional to the size of the emissions reduction, such that if the ozone response scaled linearly the curves would appear to have the same heights on each chart.

For a 10% reduction, first-order DDM-3D is sufficient to almost identically reproduce the magnitudes and temporal trends found by brute force. For a 100% reduction in emissions, the corresponding reduction in ozone is more than 10 times larger than in the 10% case, especially at times when the plume most directly impacts Sandy Beach. Incorporation of second-order DDM-3D coefficients into a Taylor expansion captures most but not all of this non-linearity of response. The light blue line indicates the

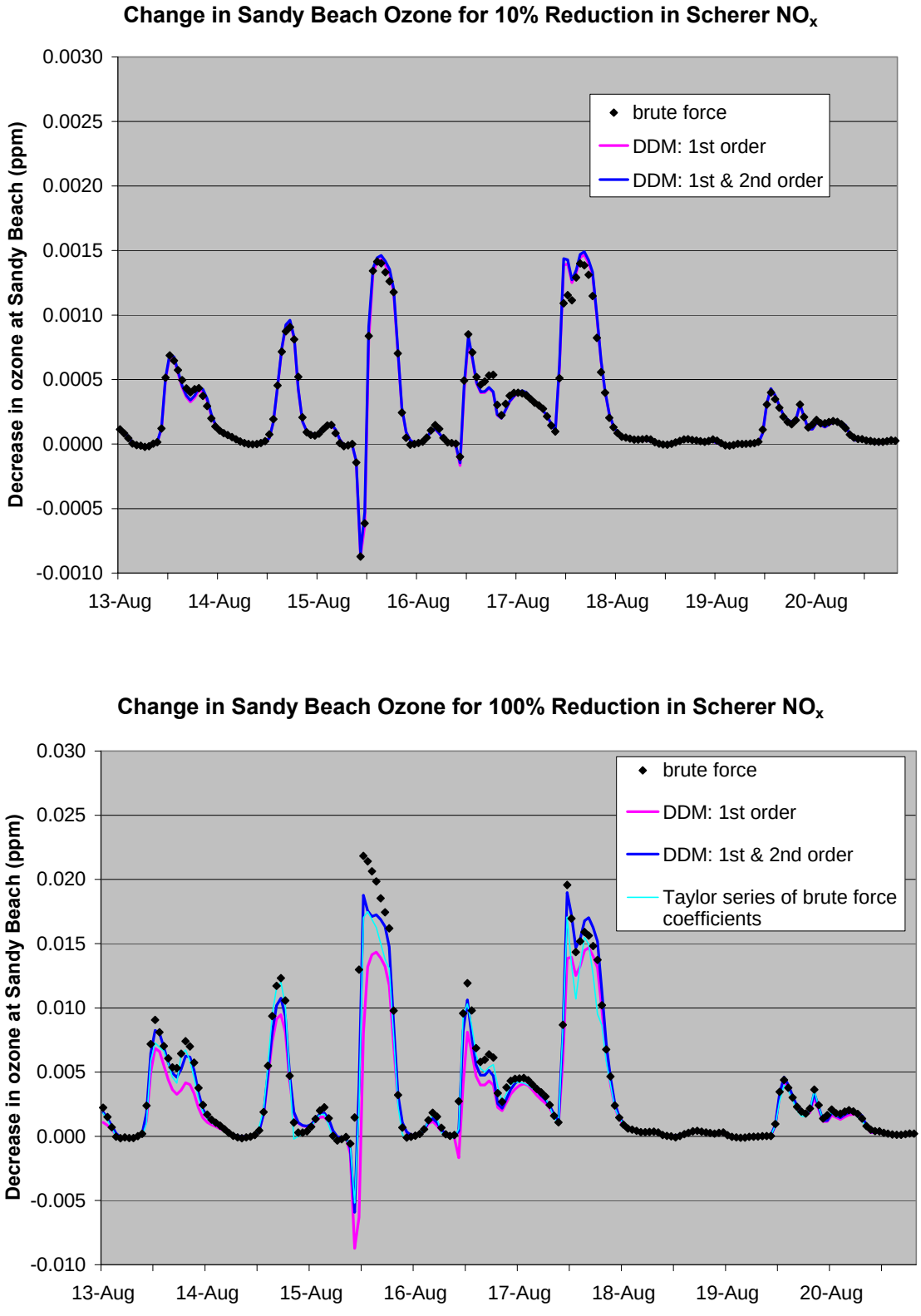

Figure B.6. Reduction in ozone at Sandy Beach accompanying 10% (top) and 100% (bottom) reductions in NO_x emissions from Plant Scherer.

relationship that would be predicted by a Taylor series expansion using sensitivity coefficients derived from brute force runs of -10%, 0%, and +10% changes in emissions. Comparing the brute force Taylor series with that derived from DDM-3D coefficients, there are times when each better predicts the actual modeled impact of removing Scherer, and neither can be said to be consistently more accurate than the other.

B.4 Conclusions

DDM-3D accurately reproduces the spatial and temporal patterns of ozone response to changes in both domain-wide and point source emissions of precursor gases. First and second-order sensitivity coefficients computed by DDM-3D closely match the magnitude and spatial distribution of those computed by the brute force method.

First-order sensitivities are sufficient to replicate the modeled impact of small percentage changes in emissions. Incorporation of second-order coefficients into Taylor expansions becomes increasingly important as the size of the perturbation grows, reflecting the significance of non-linearities. Even in the most extreme case of 100% reduction in emissions, Taylor expansions of first and second-order DDM-3D coefficients reproduce the spatial pattern of ozone response extremely well and underpredict magnitudes by only 5-15%. The underprediction is modest and primarily reflects non-linear responses beyond what can be explained by local second-order sensitivity coefficients, rather than inaccuracy in DDM-3D. The applicability of DDM-3D over a wide range of perturbations is remarkable given that the method computes only local sensitivity coefficients with respect to base case conditions.

The nonlinearities found in the response of ozone to precursor emissions demonstrate the importance of matching model results to policy objectives. The appropriate use of sensitivity analysis results depends on the question being addressed.

- **To assess the change in concentration per incremental change in precursor emissions**, first-order DDM-3D sensitivities will most effectively represent the effect because DDM-3D computes the local slope of response. Brute force estimates, computed as the change in concentration divided by the change in emissions between two simulations, will be accurate only if the size of the brute force perturbation is small. Brute force estimates based on large perturbations (e.g., differencing a base case and a run with the entire emissions source removed) will tend to overestimate the sensitivity to incremental changes due to the concave-down nature of ozone response to precursor emissions.
- **To address the impact of large changes in precursor emissions**, Taylor expansions incorporating second-order DDM-3D coefficients will accurately represent the modeled response over a wide range of changes in emissions levels, with a slight tendency to underpredict for especially large changes. Brute force will provide exact results for the size of perturbation modeled, but applicability to other amounts of perturbation is unclear. Extrapolation of first-order DDM-3D will tend to underestimate ozone response to emissions changes, because it captures only the local linear response.
- **For source attribution, which assesses the impact of each emissions component influencing concentrations**, brute force simulations in which the entire source is removed will provide the most accurate estimates. However, because it would be

computationally burdensome to conduct n+1 brute force simulations for source attribution among n sources, DDM-3D provides a computationally efficient alternative with moderate sacrifice in accuracy. First-order DDM-3D would likely be sufficient to gauge the impact of small sources. Incorporation of second-order DDM-3D coefficients into Taylor expansions is necessary to model the impact of complete removal of sources such as cities and point sources that are sufficiently large to alter the ozone production regime. The concave-down curvature typical of ozone-precursor relationships means that source attribution using only first-order DDM-3D coefficients would significantly underestimate the contribution of large emissions sources. Modest underpredictions may still occur when second-order coefficients are included.

- **For development of implementation plans and control strategies,** DDM-3D, especially as enhanced by second-order computations, provides an accurate and computationally efficient tool for estimating the effectiveness of a wide range of individual options. However, the impact of an overall control strategy may differ from a linear combination of its components. For example, if mobile source NO_x emissions are controlled within a metropolitan area, then NO_x controls at a nearby power plant will become slightly more effective at reducing ozone because the NO_x plume will then be emitted into a more NO_x-sensitive region. Similarly, a mobile source NO_x control may slightly reduce the impact of simultaneous VOC controls. Thus to demonstrate that a multi-faceted control strategy is modeled as achieving its desired goals for ambient concentrations, it is advisable to follow DDM-3D analysis

with a brute force simulation in which the control strategy case is compared to a base case.

Provided that results are used appropriately as described above, DDM-3D represents a powerful tool for the analysis of air pollution and the development of control strategies.

APPENDIX C
SENSITIVITY ANALYSIS OF OZONE IN 2007*

C.1 Introduction

Formulation of efficient air pollution control strategies requires an understanding of the response of ambient concentrations to changes in emissions. This understanding is especially crucial in the case of ozone, which forms from complex non-linear interactions of its precursor gases, nitrogen oxides (NO_x=NO+NO_2) and volatile organic compounds (VOC). A variety of geographic and meteorological features determine how ozone concentrations change in response to changes in each of these precursor emissions, and the relative influence of local and upwind emissions.

This chapter analyzes the sensitivity of ozone concentrations in Georgia to various sources of NO_x and VOC emissions in the Year 2007. Attention is focused on the sensitivity of peak 8-hour ozone concentrations in Atlanta, Macon, Augusta, and Columbus to precursor emissions from within the State of Georgia. The sensitivity analysis seeks to explore (1) the changes in ozone concentrations that would accompany incremental perturbations in emissions, and (2) the contribution of each emission source to ozone concentrations. Incremental sensitivities are invaluable for estimating the amount of emissions reduction needed to attain an air quality goal and for comparing the per-ton effectiveness of controlling emissions from each source category and region.

* Appeared as a chapter in a FAQS report to Georgia Department of Natural Resources (Hu *et al*., 2004)

Source contribution analysis is an aggregate rather than per-ton measure of the impact of each emissions source on ambient concentrations.

C.2 Methodology

All modeling is conducted using CMAQ-DDM-3D v. 4.3 with meteorology from the August 11-20, 2000 air pollution episode, and emissions from the Year 2007 FAQS projected inventory. Simulations presented in this chapter are conducted on the extended 75x66, 12-km resolution domain introduced in the preceding chapter, with initial and boundary conditions taken from the standard 36-km resolution FAQS domain of the Eastern United States. Otherwise, CMAQ is operated in identical fashion to that used for other FAQS modeling of ambient concentrations.

The implementation and accuracy of DDM-3D sensitivity analysis in CMAQ was presented in the preceding chapter. Sensitivity results in this chapter are presented primarily in two forms. For assessing the impact of incremental changes in emissions, we examine the local sensitivity or "slope" of ozone response. In this case, the semi-normalized first-order DDM-3D coefficient, $S_{O3,j}^{(1)}$, is divided by the emission rate of category j.

$$\frac{\partial C_{O_3}}{\partial E_j} = \frac{S_{O_3,j}^{(1)}}{E_j} \qquad \textbf{(C.1)}$$

In this equation, C_{O3} is the concentration of ozone and E_j is the daily average tonnage of emissions from the source j to which the sensitivity coefficient was calculated. These results are presented in units of (pptV of ozone)/(ton/day of emissions) and referred to as incremental sensitivities.

For source attribution and exploring the origin of ozone at a given monitor, a Taylor expansion is applied to semi-normalized first- and second-order DDM-3D coefficients, $S_{i,j}^{(1)}$ and $S_{i,j,j}^{(2)}$, with respect to emissions E_j from one or more regions and source categories.

$$\Delta C_{O_3}(100\%\Delta E) = S^{(1)}_{O_3,E_j} - 0.5 \cdot S^{(2)}_{O_3,E_j,E_j} \quad \textbf{(C.2)}$$

Equation C.2 estimates the reduction in ozone, ΔC_{O3}, that would occur if source j were completely removed. The units for these results are ppmV of ozone.

We examine the sensitivity of peak 8-hour ozone concentrations to NO_x and VOC emissions from 7 source regions within Georgia: Atlanta, Macon, Augusta, Columbus, North Georgia, Central Georgia, and South Georgia (Figure C.1 and Table C.1).

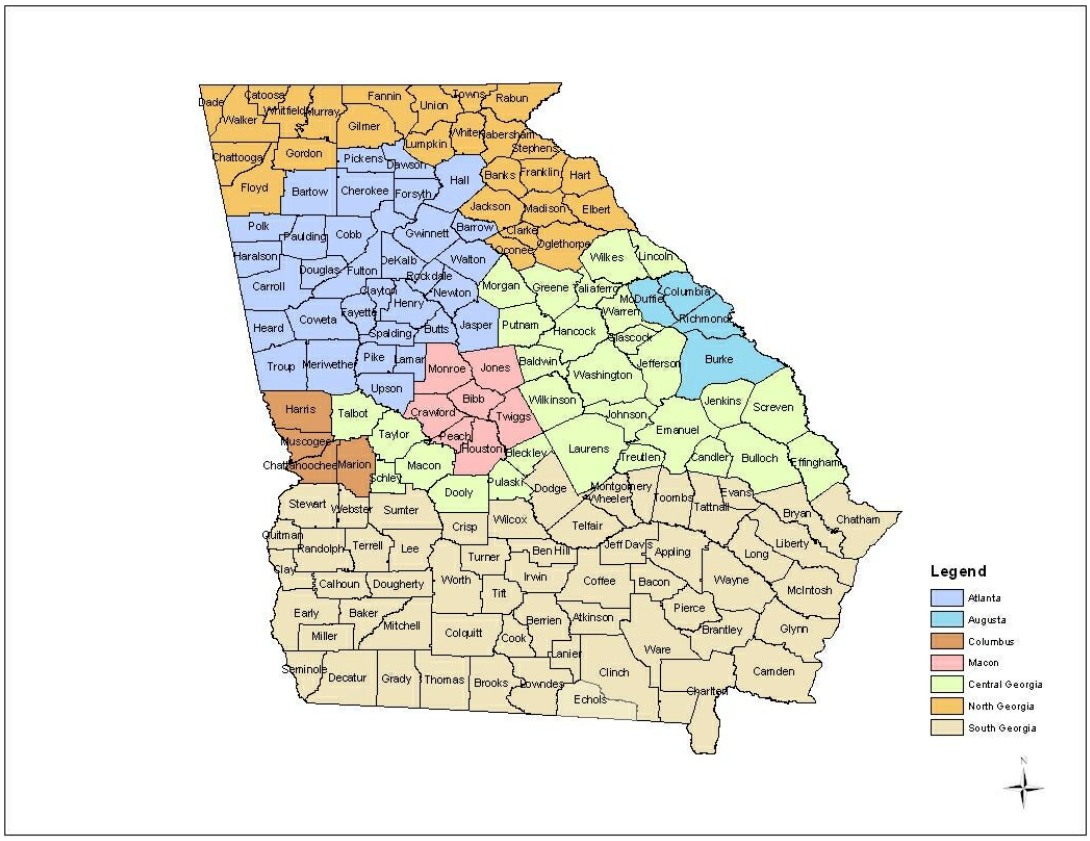

Figure C.1. Regions for sensitivity analysis.

Table C.1. Emission source regions for sensitivity analysis.

Atlanta (ATL)	**Macon (MAC)**	**Augusta (AUG)**	**Columbus (CBS)**	**North Georgia (N. GA)**	**Central Georgia (C. GA)**	**South Georgia (S. GA)**	
Atlanta - Sandy Springs - Gainesville CSA within GA	Macon - Warner Robins CSA	Augusta MSA within GA	Columbus MSA within GA				
Barrow	**Bibb**	Burke	Chatta-hoochee	Banks	Baldwin	Appling	Lee
Bartow	Crawford	Columbia	Harris	Catoosa	Bleckley	Atkinson	Liberty
Butts	Houston	McDuffie	Marion	Chattooga	Bulloch	Bacon	Long
Carroll	Jones	**Richmond**	Muscogee	Clarke	Candler	Baker	Lowndes
Cherokee	Monroe*			Dade	Dooly	Ben Hill	McIntosh
Clayton	Peach			Elbert	Effingham	Berrien	Miller
Cobb	Twiggs			Fannin	Emanuel	Brantley	Mitchell
Coweta				Floyd	Glascock	Brooks	Montgomery
Dawson				Franklin	Greene	Bryan	Pierce
De Kalb				Gilmer	Hancock	Calhoun	Quitman
Douglas				Gordon	Jefferson	Camden	Randolph
Fayette				Habersham	Jenkins	Charlton	Seminole
Forsyth				Hart	Johnson	Chatham	Stewart
Fulton				Jackson	Laurens	Clay	Sumter
Gwinnett				Lumpkin	Lincoln	Clinch	Tattnall
Hall				Madison	Macon	Coffee	Telfair
Haralson				Murray	Morgan	Colquitt	Terrell
Heard				Oconee	Pulaski	Cook	Thomas
Henry				Oglethorpe	Putnam**	Crisp	Tift
Jasper				Rabun	Schley	Decatur	Toombs
Lamar				Stephens	Screven	Dodge	Turner
Meriwether				Towns	Talbot	Dougherty	Ware
Newton				Union	Taliafero	Early	Wayne
Paulding				Walker	Taylor	Echols	Webster
Pickens				White	Treutlen	Evans	Wheeler
Pike				Whitfield	Warren	Glynn	Wilcox
Polk					Washington	Grady	Worth
Rockdale					Wilkes	Irwin	
Spalding					Wilkinson	Jeff Davis	
Troup						Lanier	
Upson							
Walton							

Counties in bold have been recommended by the State of Georgia as non-attainment for 8-hour ozone. The EPA has recommended that Monroe and Houston Counties also be designated non-attainment, and that Richmond County is now in attainment.

* NO_x emissions from Plant Scherer are excluded from the Macon region and considered separately.

** NO_x emissions from Plant Branch are excluded from the Central Georgia region and considered separately.

The counties comprising the four city regions are selected based on the June 2003 Office of Management and Budget definitions of combined statistical areas (CSAs) and metropolitan statistical areas (MSAs). Emissions from two power plants that are projected to be the largest point sources of NO_x in Georgia in 2007, Plant Scherer in Monroe County (Macon region) and Plant Branch in Putnam County (Central Georgia region), are considered separately. FAQS 2007 inventory projected NO_x emission rates (short tons per ozone season day) under planned federal controls show that the Atlanta source region has the highest emissions, and Columbus the lowest (Figure C.2). Projections for Georgia power plant NO_x emissions are based upon permitted emission rates (in lb/mmBtu). Because Plant Scherer switched to a cleaner-burning coal in 2003, and low-NO_x burners at Plant Branch have been more effective than anticipated, NO_x emissions at Scherer and Branch will be 25% and 18%, respectively, less than inventory projections if 2003 emission rates are maintained.

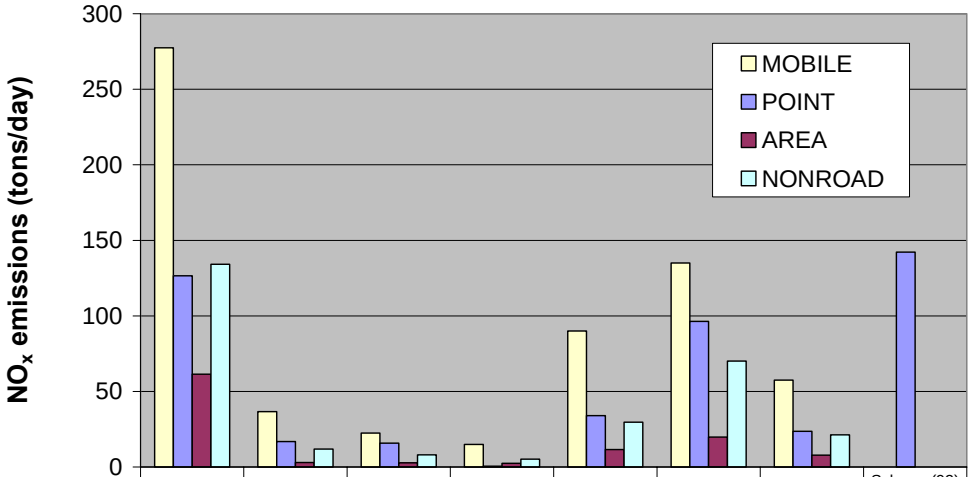

	Atlanta	Macon	Augusta	Columbus	N. Georgia	S. Georgia	C. Georgia	Scherer (92) + Branch (50)
MOBILE	277.4	36.7	22.5	14.9	90.1	135.0	57.6	
POINT	126.6	16.8	15.8	0.6	34.0	96.5	23.7	142.2
AREA	61.5	3.0	2.7	2.5	11.6	19.8	7.9	
NONROAD	134.2	11.9	8.2	5.2	29.6	70.1	21.3	

Figure C.2. NO_x emissions in 2007 by source region and category.

For the sensitivity analysis in this chapter, NO_x emissions from Atlanta, Macon, and Augusta are considered separately in three categories: (1) mobile sources, (2) point sources, and (3) area and non-road sources. Because area sources are the smallest category of NO_x emissions and have a similar spatial distribution to non-road emissions, combining the two categories is an appropriate way to reduce the number of sensitivity coefficients that must be computed.

The spatial distribution of anthropogenic NO_x emissions averaged over the 10-day episode highlights the locations of major cities and interstate highways (Figure C.3). Several large power plants emit more than 50 tons/day (tpd), an order of magnitude larger than the scale of the color scheme. By contrast, broad rural regions have daily NO_x emissions of only fractions of a ton.

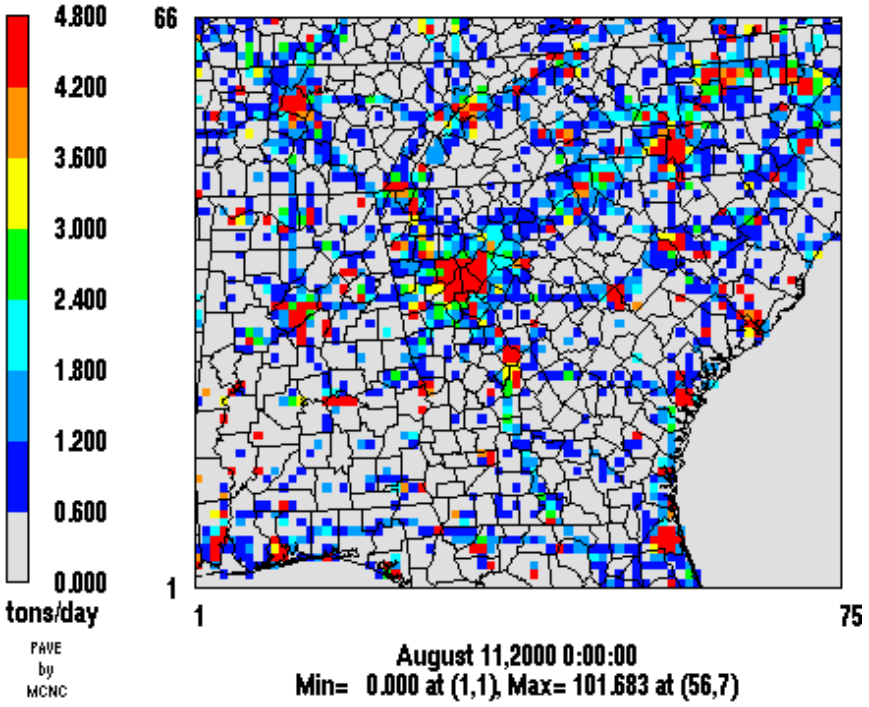

Figure C.3. Projected anthropogenic NO_x emissions in summer 2007.

C.3 Domain-wide results

Before examining sensitivity results, we present an overview of ozone conditions during the four-day period, August 15-18, when ozone concentrations were highest in Georgia (Figure C.4). Ozone concentrations throughout the domain are typically 0.010-0.020 ppmV lower than those modeled for Year 2000 emissions reflecting lower NO_x emissions throughout the Eastern United States projected for 2007. Even so, peak 8-hour ozone concentrations are modeled to exceed 0.085 ppmV in parts of the Atlanta and Macon regions throughout the 4-day period. August 15 and 17 are modeled to be days of elevated ozone concentrations near Columbus, and August 16 and August 17 are elevated days for Augusta. August 17 is modeled to be the peak day of the episode for most of Georgia, as it was in ozone observations in 2000.

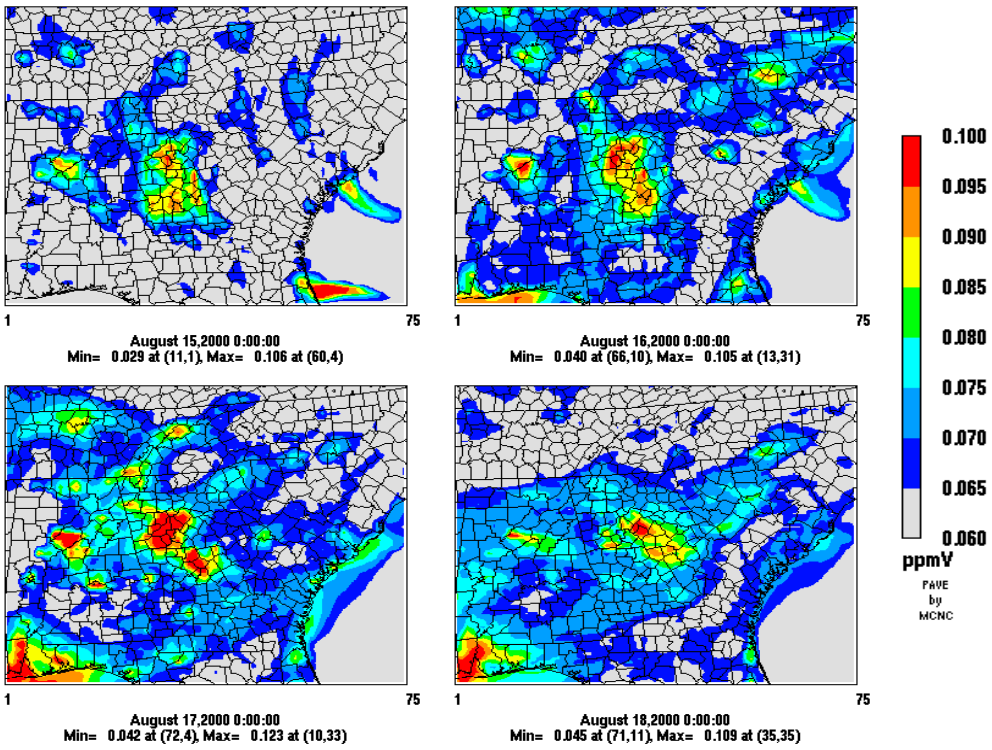

Figure C.4. Peak 8-hour ozone concentrations, Aug. 15-18, with Year 2007 emissions.

Sensitivity analysis of ozone to VOC and NO_x emissions domain-wide, using 2007 emissions, finds that a NO_x-limited ozone production regime dominates almost the entire Southeast throughout the air pollution episode (Figure C.5). VOC sensitivity on some less severe ozone days is slightly larger than on August 17, but is consistently dwarfed by NO_x sensitivity. This reflects the relative abundance of VOC emissions compared to NO_x emissions, and that biogenic sources dominate VOC emissions in much of the Southeast. Significant sensitivity to VOC emissions is isolated in Georgia to the center of the Atlanta region and to coastal outflow. Thus, an assessment of the sensitivity of ozone to its precursor gases can largely be simplified to elucidating the ozone-NO_x relationship. The remainder of this chapter focuses extensively on the response of ozone to NO_x emissions, with attention to VOC sensitivities where warranted.

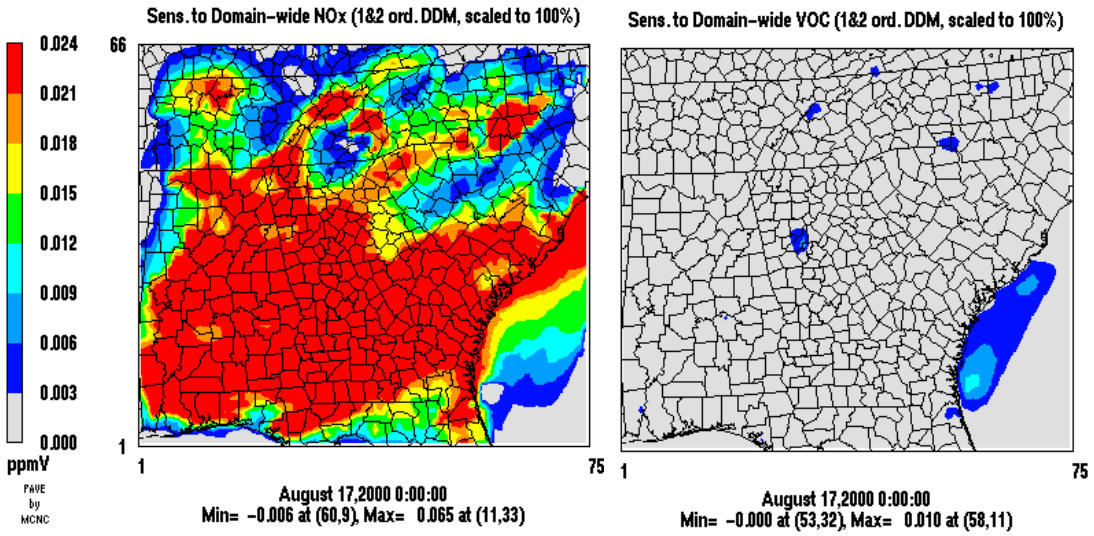

Figure C.5. Sensitivity of 8-hour ozone on Aug. 17 to domain-wide anthropogenic emissions of NO_x (L) and VOC (R).

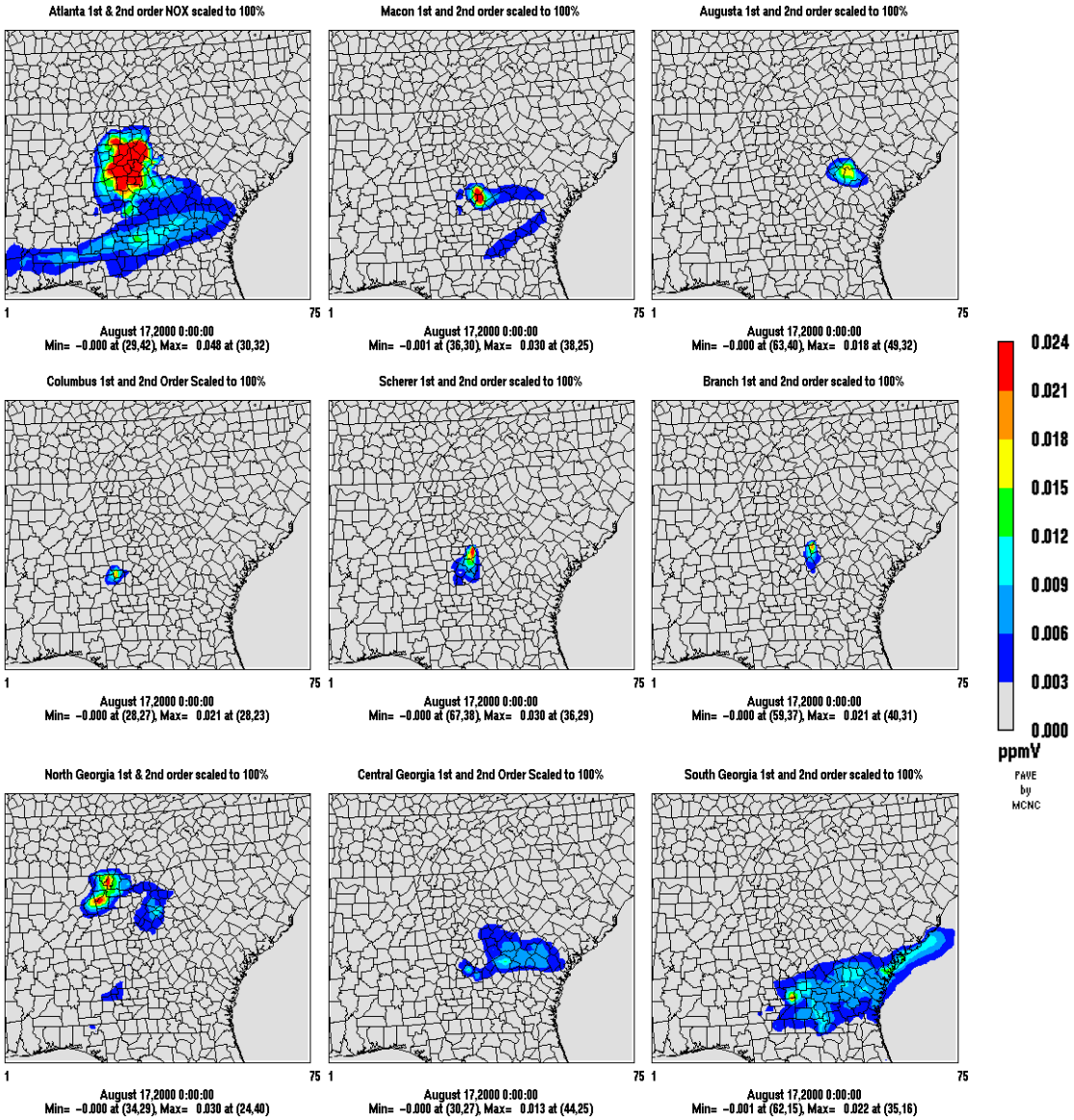

Figure C.6. Source contribution of NO_x emissions from Atlanta (top L), Macon (top C), Augusta (top R), Columbus (mid L), Scherer (mid C), Branch (mid R), N. Georgia (bottom L), C. Georgia (bottom C), and S. Georgia (bottom R) to peak 8-hr ozone on Aug. 17.

Figure C.6 shows the source contribution, computed by Equation C.2, of Year 2007 NO_x emissions from each region to peak 8-hour ozone concentrations on August 17. Similar plots for August 15, 16, and 18 are included as an appendix.

For each region, the impact of its NO_x emissions is most intense within the region itself, but evidence of inter-regional transport is also apparent. Atlanta, with nearly double the emissions of any other region, generates the most intense ozone plume and contributes to ozone concentrations throughout much of the state. Comparing modeled peak ozone concentrations to the regional source contributions (Figure C.4 and Figure C.6), highest ozone concentrations in Georgia coincide with the locations most affected by emissions from the Atlanta region, with secondary contributions from the Macon region and Plant Scherer.

C.4 Sensitivity in Georgia Cities

Much of the development of control strategies and implementation plans for ozone attainment occurs with respect to air quality within a metropolitan region, and the influence of emissions within and beyond that region. Thus, the following sections focus attention individually on sensitivity analysis of ozone in four metropolitan regions of Georgia: Atlanta, Macon, Augusta, and Columbus.

C.4.1 Atlanta

Efforts to control ozone in Georgia have historically focused on conditions in the Atlanta region. The region contains roughly half of the population of Georgia, and the most NO_x emissions of any Georgia region. Atlanta has violated the 1-hour federal

standard for ozone for over two decades, and the State of Georgia has recommended that 20 counties in the region be designated as non-attainment of the 8-hour ozone standard. Figure C.7 shows the distribution of Year 2007 NO_x emissions by source category within the counties of the Atlanta-Sandy Springs-Gainesville Combined Statistical Area, averaged over the 10-day air pollution episode.

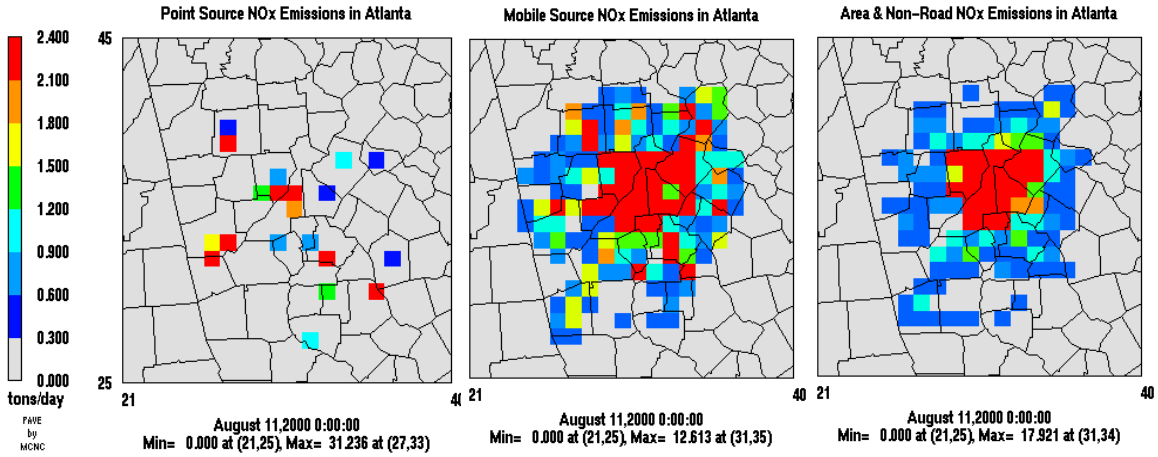

Figure C.7. Daily NO_x emissions from point (L), mobile (C), and area and non-road (R) sources within the Atlanta region.

More than 90% of Atlanta's point source NO_x emissions are contained within the six red-colored grid cells (the seventh and most south-easterly red grid cell contains Plant Scherer, and its point emissions are considered separately). Emissions from the other categories are more widely distributed, with highest emission rates in a multi-county area centered on downtown Atlanta and elevated mobile emissions along the Interstate 75 and Interstate 85 corridors.

Based on Figure C.7, one might ask whether Atlanta's point source NO_x, which originates primarily from a handful of elevated plumes, would exert similar influence as

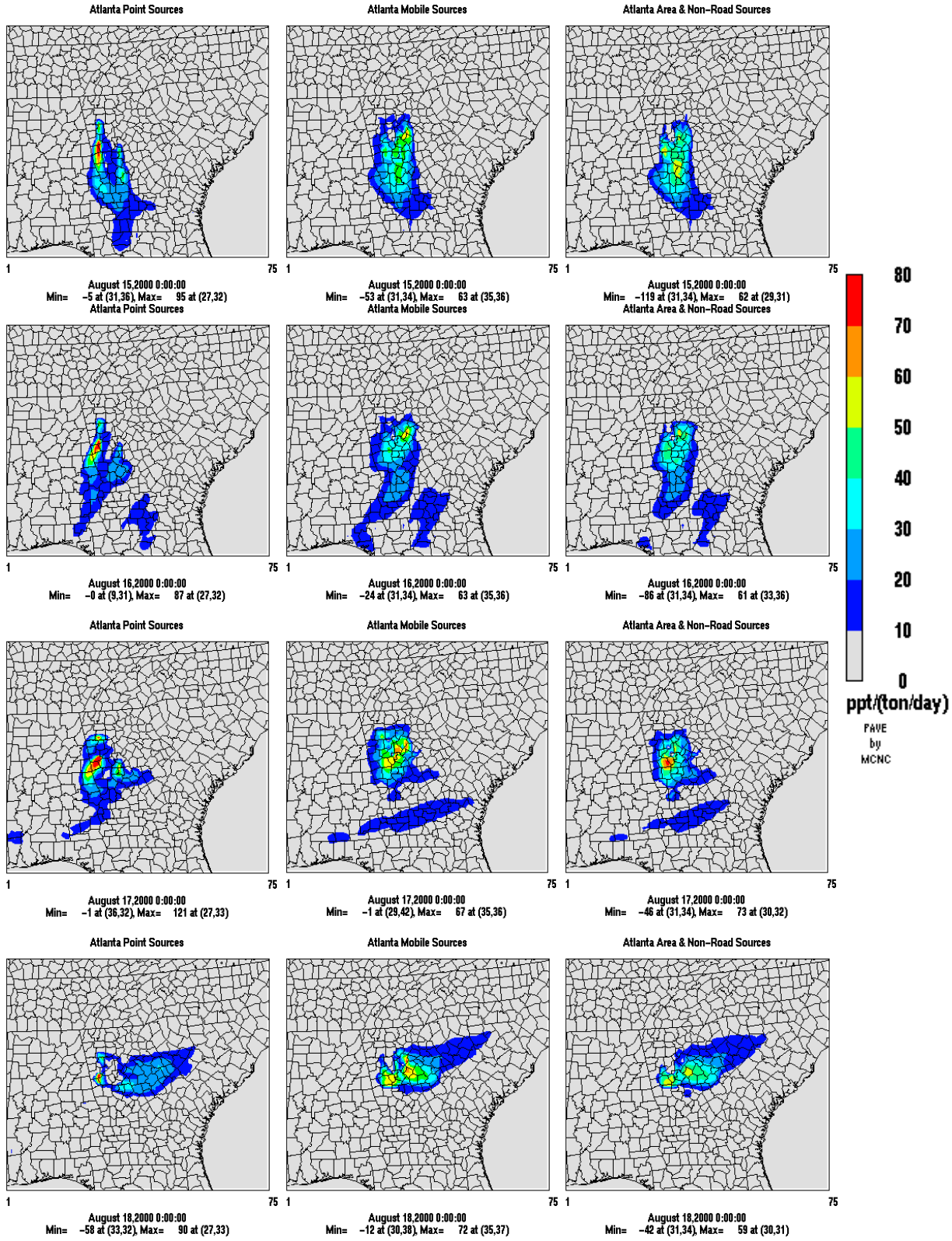

Figure C.8. Incremental sensitivity (pptV/ton/day) of 8-hour ozone to Atlanta point source (L), mobile source (C), and area & non-road (R) NO_x emissions, Aug. 15-18.

NO_x from the other categories, which originates from a broader emissions "footprint". In other words, is a ton of point source NO_x control equal to a ton of ground-level NO_x control for ozone strategy development? These questions can be addressed by examining the incremental sensitivity of ozone to emissions from each category (Figure C.8).

The patterns and magnitudes of sensitivity to point source emissions are distinct from those for mobile and area & non-road emissions. The sensitivity to point sources is characterized by the superposition of the several intense plumes of elevated emissions. The maximal sensitivity is typically greater for the point sources, whereas the mobile and area sources more uniformly impact a wide region. Strong negative sensitivity to NO_x is often observed in a single grid cell which contains Atlanta's Hartsfield-Jackson International Airport and the most area and non-road emissions of any cell. The source categories display roughly equal propensity to impact locations downwind, though the location of impact differs somewhat by category. Greater variability is observed between days, as the first three days are characterized by predominantly northerly wind flow but August 18 is characterized by westerly winds.

Table C.2. 8-hour ozone concentrations (ppm), averaged over Atlanta monitors, and their sensitivity (ppt/ton/day) to emissions.

		ATLANTA		ATL NO_x by category			NO_x Emissions from Other Regions							
DATE	O_3 Conc.	VOC	NO_x	MO	A,NR	PT	MAC	BRA	SCH	AUG	CBS	N. GA	C. GA	S. GA
8/13	0.062	2.63	8.01	8.72	10.26	2.92	0.00	0.00	0.00	0.00	0.00	4.60	0.00	0.00
8/14	0.080	5.18	26.55	30.06	32.45	8.66	0.00	1.04	0.01	4.10	0.00	8.25	3.25	0.00
8/15	0.080	3.67	17.16	19.86	21.51	4.83	0.00	0.01	0.00	0.08	0.00	10.33	0.10	0.00
8/16	0.086	2.18	20.13	23.65	24.76	5.35	0.00	0.00	0.00	0.00	0.00	17.78	0.00	0.00
8/17	0.096	2.10	35.30	43.21	38.84	11.56	0.00	0.00	0.00	0.00	0.00	11.86	0.12	0.00
8/18	0.081	1.24	22.26	28.06	22.67	8.25	0.03	0.00	0.11	0.00	0.78	11.47	0.05	0.01
8/19	0.081	3.19	19.07	19.60	22.29	11.89	0.00	0.00	0.00	0.00	0.00	12.78	0.03	0.00
7-day avg	**0.081**	**2.89**	**21.21**	**24.74**	**24.68**	**7.64**	**0.00**	**0.15**	**0.02**	**0.60**	**0.11**	**11.01**	**0.51**	**0.00**

Table C.2 presents peak 8-hour ozone concentrations, averaged over the 12 ozone monitors in the Atlanta region, and their incremental sensitivity to VOC emissions and to NO_x emissions by category and region. Complete tables of per-ton sensitivity of ozone at each Georgia monitor to each source region and category are included as an appendix.

On each day, ozone at Atlanta monitors is on average more sensitive to changes in emissions from the ground-level emissions categories (mobile, area, and non-road) than to point source emissions. This trend holds true at all of the Atlanta monitors except for the two located in: (1) Paulding County, which is one county south of Plant Bowen, and (2) central Fulton County, which most often experiences VOC-limited (NO_x-saturated) conditions and thus small or even negative sensitivity to nearby NO_x emissions. Ozone at all Atlanta area monitors exhibits very little sensitivity to changes in emissions from most other Georgia regions. The exception is emissions from North Georgia, whose influence is enhanced by proximity and by the northerly wind flow that predominates during much of the episode. Sensitivity to Atlanta VOC emissions primarily occurs at the Fulton, Fayette, and Dekalb county monitors and is strongest on August 14 and 15.

The magnitudes of sensitivities in Table C.2 indicate the relative effectiveness of controlling a ton of emissions from each region and category. For example, on average 1 tpd of mobile source NO_x control in Atlanta will reduce ozone in Atlanta by about three times as much as 1 tpd from point sources (25 pptV v. 8 pptV). By computing the reciprocal of the magnitudes, one could estimate the amount of NO_x reduction necessary to achieve a target reduction in ozone. By this method, an average of 47 tpd of controls would be needed to reduce Atlanta ozone by 0.001 ppmV. The geographic breadth of Atlanta emissions and monitors is the main reason for this relative insensitivity to

controls. Another reason is that intense NO_x emissions make Atlanta somewhat less sensitive to an incremental ton.

To assess the origin or source attribution of ozone, we must consider not only incremental sensitivity but also the size of each emission source and second-order responses by applying Equation C.2.. Figure shows the source contribution of each emissions category to peak 8-hour ozone concentrations, averaged over the 12 Atlanta area monitors. Only the contribution of Atlanta and North Georgia emissions are shown, because each other Georgia source region contributes less than 0.001 ppmV to average Atlanta ozone on each day of the episode.

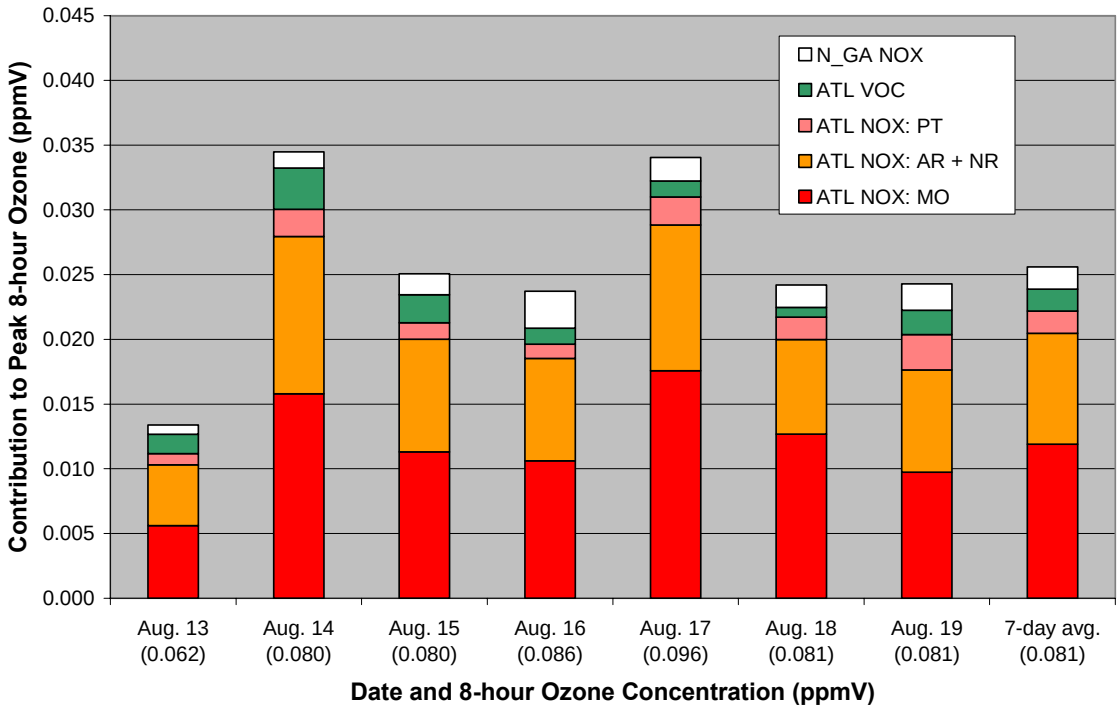

Figure C.9. Contribution of emissions to ozone, averaged over Atlanta monitors.

Mobile source NO_x emissions are the largest contributor to Atlanta ozone (0.012 ppmV), followed by non-road and area sources (0.009 ppmV). The average contribution of point sources is much smaller (0.002 ppmV), reflecting both the smaller size of point sources in the emissions inventory and the smaller per-ton impact of point sources in the Atlanta region. Note that the source contributions do not sum to the modeled ozone concentrations, which are significantly influenced by factors not considered in Figure C.9, including boundary conditions, emissions from other states, biogenic emissions, and non-linearities across source impacts (i.e., the presence of Source A influences the impact of Source B).

Taylor expansions of DDM-3D coefficients can also be used to estimate ozone concentrations for any percentage change in emissions (see Equation B.5 in previous appendix). Figure C.10 shows the ozone concentrations modeled to occur in Atlanta on August 15-18 under various levels of controls of total Atlanta NO_x emissions. The non-linear concave-down response, especially pronounced on August 17, implies that the marginal benefit of controls would increase as more controls are applied. Taylor expansions such as those in Figure C.10 can be a powerful tool in determining the size of emissions reduction needed to attain ozone standards; however, caution should be taken to compare the Year 2000 modeled concentrations with observations before applying projected 2007 concentration and sensitivity modeling results in attainment demonstrations.

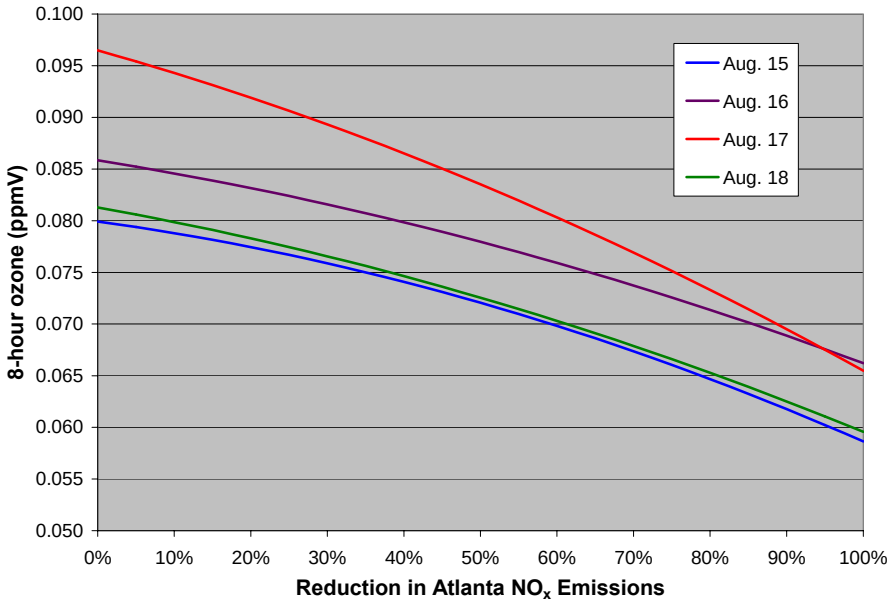

Figure C.10. Response of 8-hour ozone, averaged over Atlanta monitors, to controls of Atlanta NO_x emissions.

C.4.2 Macon

Macon has the highest ozone concentrations among Georgia cities other than Atlanta. The State of Georgia recommended that Bibb County be designated as non-attainment for the 8-hour ozone standard, and the Environmental Protection Agency has announced its intention to include neighboring Houston and Monroe Counties as well [state recommendations and EPA responses are available at www.epa.gov/air/oaqps/glo/designations/regions/region4t.htm]. Thus the sensitivity of ozone in the Macon area is of special interest to the development of control strategies for bringing the region back into attainment.

For the Macon-Warner Robins Combined Statistical Area, the "footprints" of the three emissions categories are fairly similar, with most emissions occurring near the

Interstate 75 corridor (Figure C.11). Plant Scherer NO_x emissions are considered separately from the rest of the Macon region for sensitivity calculations.

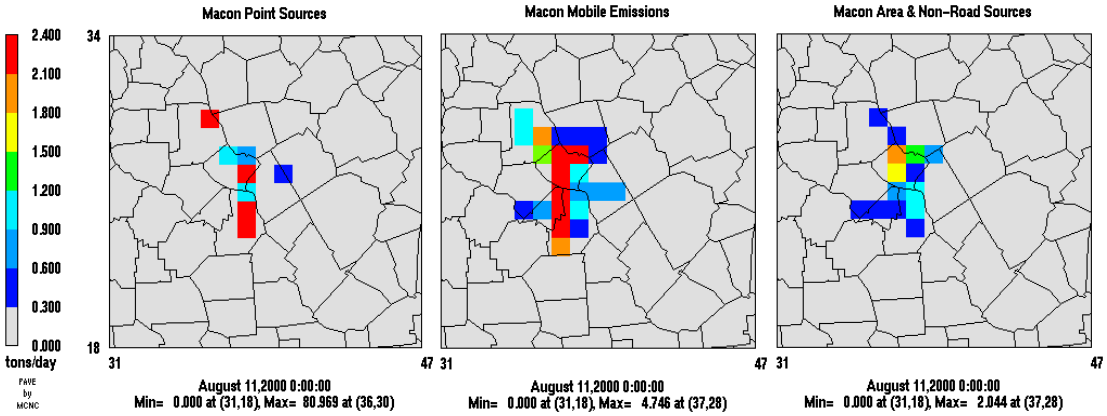

Figure C.11. Daily NO_x emissions from point (L), mobile (C), and area & non-road (R) sources within the Macon region.

On each day, the peak sensitivity to Macon emissions is either collocated with the footprint of emissions, or located one county downwind (Figure C.12). Note that the scale of the incremental sensitivity plots is a factor of 5 larger than that of the Atlanta plots. This primarily reflects that a one ton change in emissions from Atlanta would be spread over a much larger footprint than a one ton change in Macon emissions. In addition, the ozone production efficiency per ton of emissions would be expected to be higher in the more dilute NO_x conditions of the Macon plume.

The results reflect considerable day-to-day variability of the location and magnitude of sensitivity to Macon NO_x emissions. Strongest sensitivity is found on August 17, when hot and stagnant conditions led to increased biogenic emissions, reduced dispersion and facilitated ozone production. Spatial plots of sensitivity appear similar across source categories, but differences are suggested by the results at grid cells

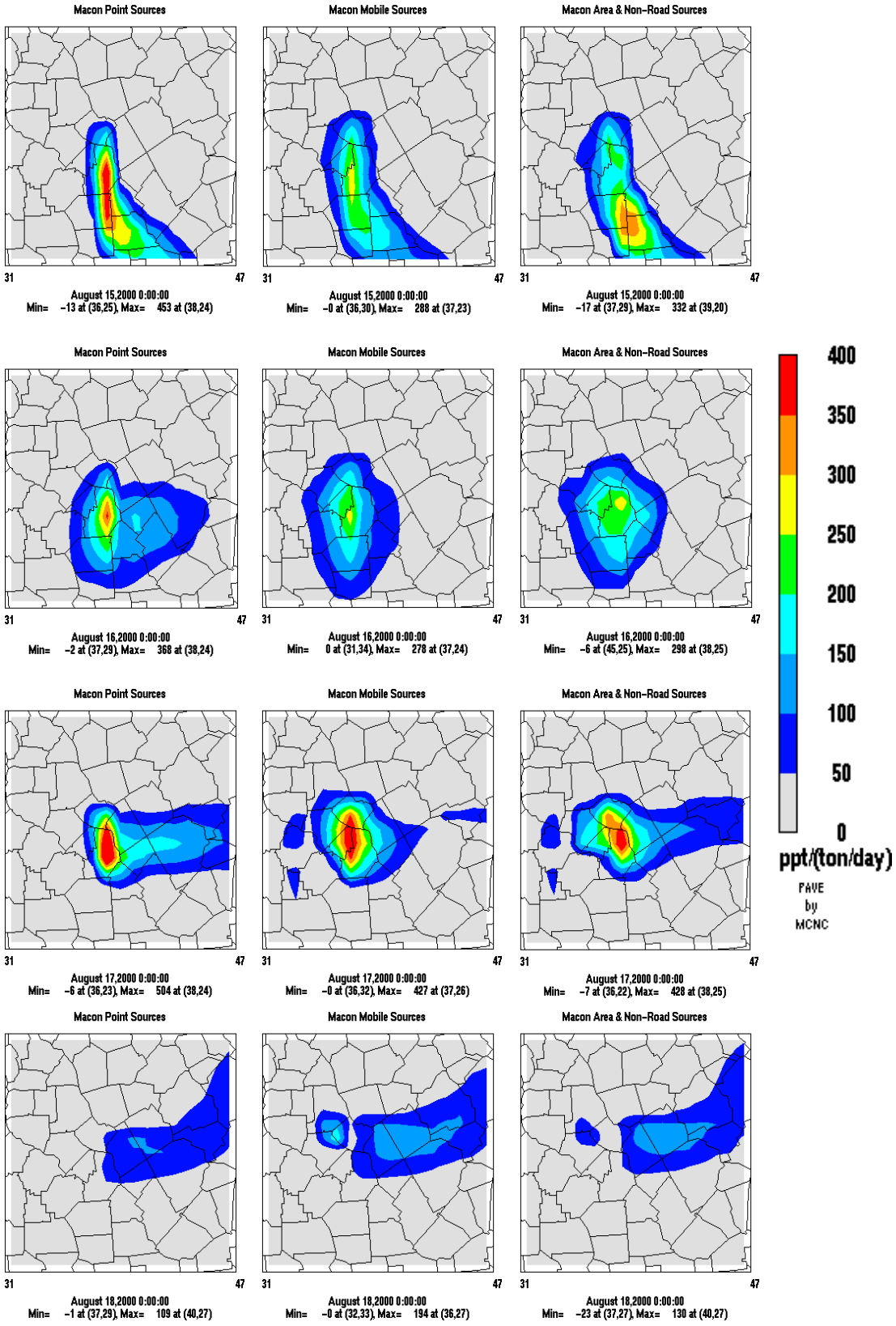

Figure C.12. Incremental sensitivity (pptV/ton/day) of ozone to Macon point (L), mobile (C), and area & non-road (R) NO_x emissions, Aug. 15-18.

containing two Macon area monitors (Table C.3 and Table C.4) and by the sensitivity of ozone spatially averaged across the Macon region (Table C.5).

Table C.3. Sensitivity (ppt/ton/day) of 8-hour ozone at the Macon EPD monitor to incremental emissions.

		MACON		MAC NO_x by category			NO_x Emissions from Other Regions							
DATE	O_3 Conc.	VOC	NOX	MO	A,NR	PT	ATL	BRA	SCH	AUG	CBS	N. GA	C. GA	S. GA
8/13	0.068	1.59	85.91	73.58	104.65	95.20	1.68	12.29	51.42	0.00	0.00	6.42	5.42	0.00
8/14	0.070	1.24	161.45	113.98	148.97	276.63	4.53	0.61	38.74	14.92	0.00	2.82	15.28	0.00
8/15	0.069	0.48	107.63	89.32	100.97	153.66	5.35	47.71	2.78	8.56	0.00	23.18	43.03	0.00
8/16	0.082	1.19	102.47	79.58	107.48	147.64	9.17	63.91	6.50	2.16	0.00	13.53	18.35	0.00
8/17	0.093	2.80	206.08	187.92	221.61	230.84	16.80	40.49	20.67	0.00	3.10	6.45	3.80	0.07
8/18	0.079	0.10	68.87	77.27	52.77	65.36	6.42	0.06	6.76	0.00	24.18	1.79	3.00	0.04
8/19	0.075	1.82	120.13	118.00	123.61	121.24	3.34	16.30	53.88	0.20	0.00	2.18	4.82	0.00
7-day avg.	**0.077**	**1.32**	**121.79**	**105.66**	**122.87**	**155.80**	**6.75**	**25.91**	**25.82**	**3.69**	**3.90**	**8.05**	**13.38**	**0.02**

Table C.4. Sensitivity (pptV/ton/day) of 8-hour ozone at the Macon Sandy Beach Park (FAQS) monitor to incremental emissions.

		MACON		MAC NO_x by category			NO_x Emissions from Other Regions							
DATE	O_3 Conc.	VOC	NOX	MO	A,NR	PT	ATL	BRA	SCH	AUG	CBS	N. GA	C. GA	S. GA
8/13	0.067	0.64	30.35	42.16	34.77	0.28	6.06	1.25	52.49	0.00	0.00	6.85	0.64	0.00
8/14	0.077	4.98	183.12	198.62	231.94	103.16	4.38	1.93	55.26	11.31	0.00	2.84	9.55	0.00
8/15	0.094	2.55	61.62	86.76	67.23	1.19	15.18	0.30	111.21	4.19	0.00	14.96	3.12	0.00
8/16	0.089	1.38	94.02	113.57	116.58	29.92	12.70	2.53	53.71	0.10	0.00	10.58	2.55	0.00
8/17	0.105	1.07	147.72	209.99	147.03	11.67	17.79	0.72	148.64	0.00	3.05	4.63	1.03	0.02
8/18	0.077	-1.44	136.72	194.30	100.19	44.42	10.60	2.48	89.02	0.01	10.93	1.76	8.88	1.56
8/19	0.063	1.33	29.25	42.02	22.97	7.10	3.67	12.59	25.98	0.04	0.00	2.35	1.89	0.00
7-day avg.	**0.082**	**1.50**	**97.54**	**126.77**	**102.96**	**28.25**	**10.05**	**3.11**	**76.61**	**2.24**	**2.00**	**6.28**	**3.95**	**0.23**

Table C.5. Sensitivity (ppt/ton/day) of 8-hour ozone, averaged over Macon region, to incremental emissions.

		MACON		MAC NO_x by category			NO_x Emissions from Other Regions							
DATE	O_3 Conc.	VOC	NOX	MO	A,NR	PT	ATL	BRA	SCH	AUG	CBS	N. GA	C. GA	S. GA
8/13	0.064	1.15	44.01	46.80	50.13	32.23	5.35	12.03	26.08	0.00	0.00	5.94	5.28	0.00
8/14	0.069	2.49	99.14	99.56	101.61	95.91	5.29	13.94	38.28	12.10	0.00	2.53	16.62	0.02
8/15	0.078	1.17	66.92	73.31	67.61	52.36	13.79	41.15	37.11	5.58	0.00	16.21	22.67	0.00
8/16	0.085	1.48	81.68	83.64	94.58	65.43	12.07	35.63	40.40	2.06	0.00	9.69	13.93	0.01
8/17	0.090	0.50	116.97	133.33	119.55	78.93	14.03	31.49	56.88	0.02	15.52	5.77	13.91	0.68
8/18	0.080	-0.02	40.87	52.95	31.74	23.05	9.59	0.38	31.33	0.00	31.51	1.30	7.31	0.31
8/19	0.068	0.87	53.66	59.56	54.52	40.00	7.18	13.42	32.06	0.58	0.52	2.77	6.92	0.01
7-day avg.	**0.076**	**1.09**	**71.89**	**78.45**	**74.25**	**55.41**	**9.61**	**21.15**	**37.45**	**2.91**	**6.79**	**6.32**	**12.38**	**0.15**

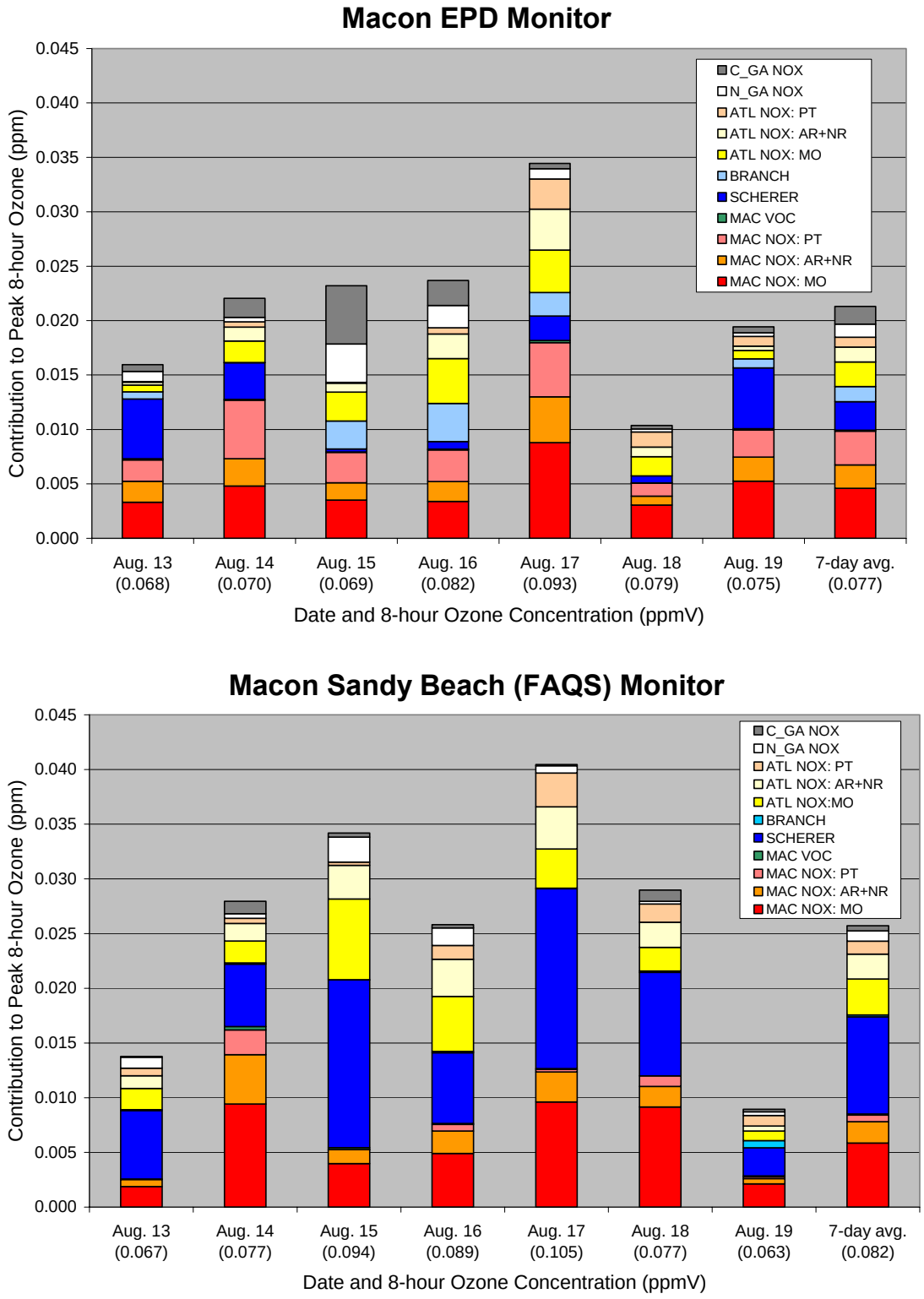

Figure C.13. Source attribution for 8-hour ozone concentrations at Macon's EPD monitor (top) and Sandy Beach monitor (bottom).

The Macon monitor in eastern Bibb County (Table C.3), operated by the Georgia Environmental Protection Division (EPD), is the regulatory monitor for the region. A second monitor was installed as part of FAQS at Sandy Beach Park in western Bibb County (Table C.4), and was operated by Georgia Tech during the FAQS monitoring campaign. The tables suggest ozone at the EPD monitor is most sensitive to local point source emissions whereas the Sandy Beach monitor is most sensitive to mobile sources; on a regional average basis, ozone is about one-fourth less sensitive to each ton of point sources than to mobile, area, and non-road sources. Close inspection of the emissions distribution in the Macon region (Figure C.11) reveals that the footprint of point sources (excluding Plant Scherer) is slightly to the east of those for other sources, and thus on average in closer proximity to the more easterly EPD monitor. Further, wind flow during the August 2000 episode was more often westerly than easterly.

While the tables present incremental (per-ton) sensitivities, Figure C.13 shows the source contribution of each emissions category to ozone concentrations at each Macon monitor, as computed by Equation C.2.

The results in Figure C.13 do not account for the reductions in NO_x emissions at Plant Scherer and Branch beyond Year 2007 inventory projections. The 25% reduction in NO_x emissions at Plant Scherer due to cleaner-burning coal reduces its average source contribution by 0.0006 ppmV at the EPD monitor and by 0.0019 ppmV at the Sandy Beach monitor. The 18% reduction at Plant Branch corresponds to 0.0002 ppmV less ozone at the EPD monitor, and a negligible impact at Sandy Beach.

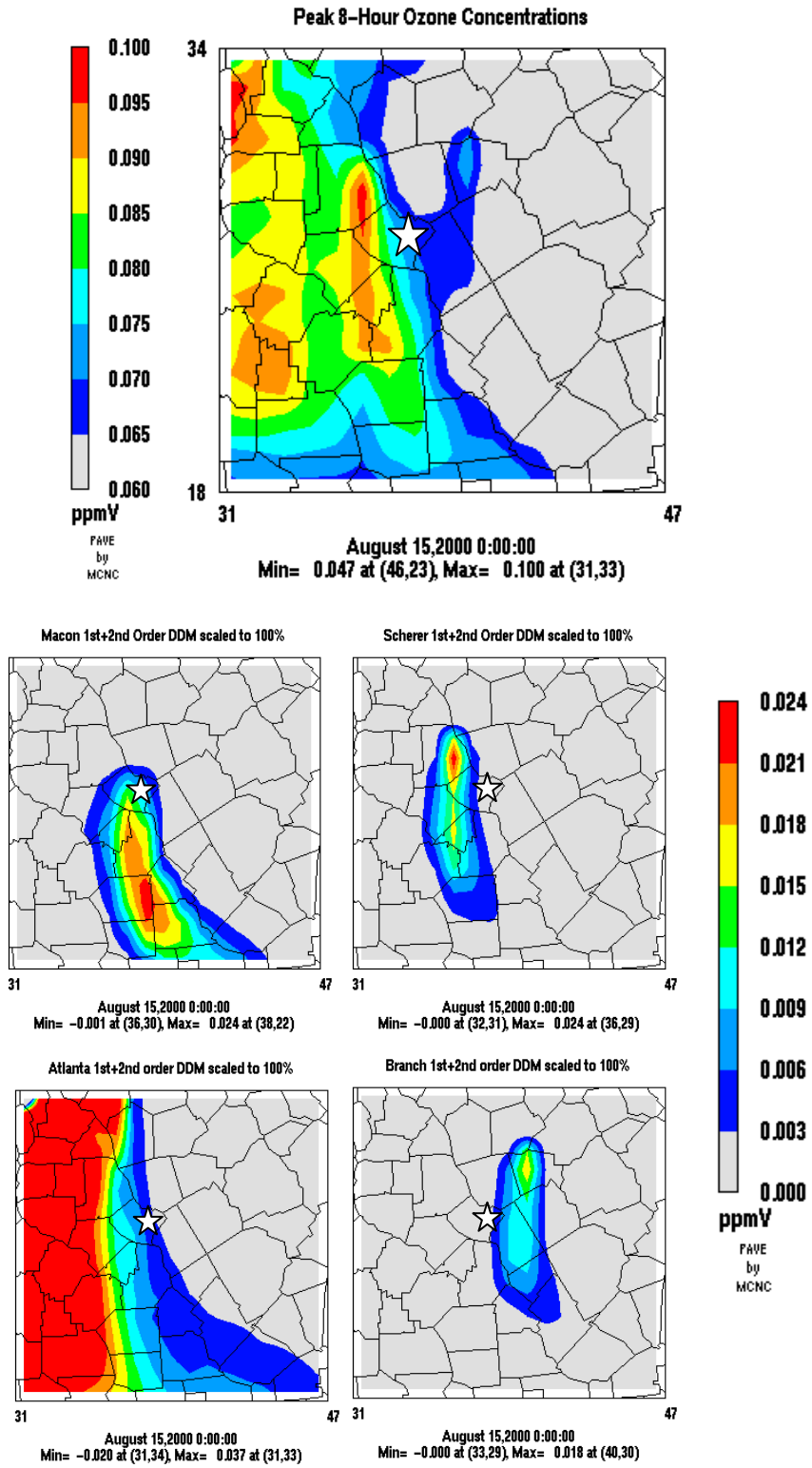

Figure C.14. Peak 8-hour ozone concentrations (top) on August 15, and the contribution from NO_x emissions from (clockwise from top, L) Macon, Scherer, Branch, and Atlanta. The star shows the location of the EPD monitor in eastern Bibb County.

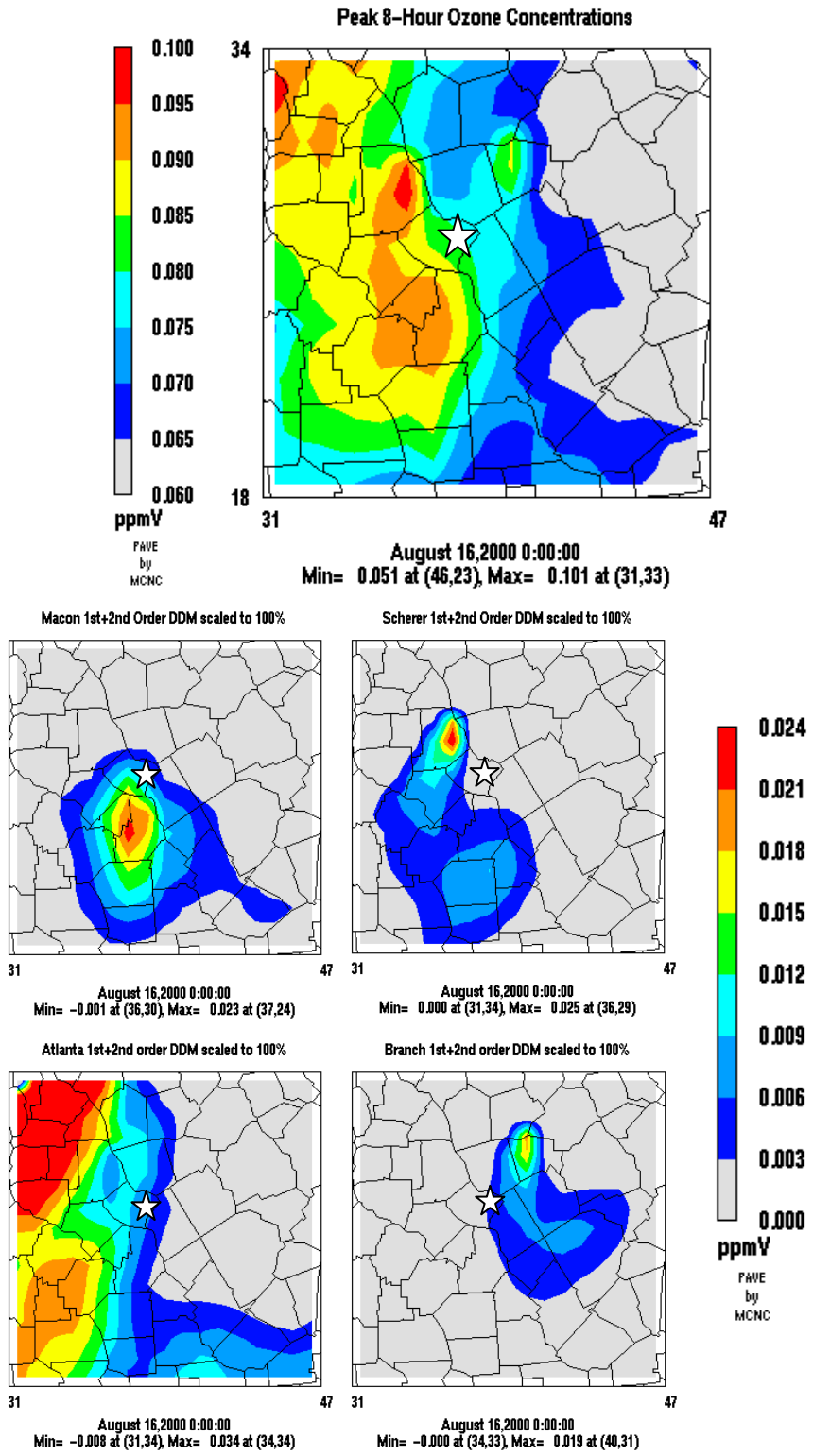

Figure C.15. Peak 8-hour ozone concentrations (top) on August 16, and the contribution from NO_x emissions from (clockwise from top, L) Macon, Scherer, Branch, and Atlanta.

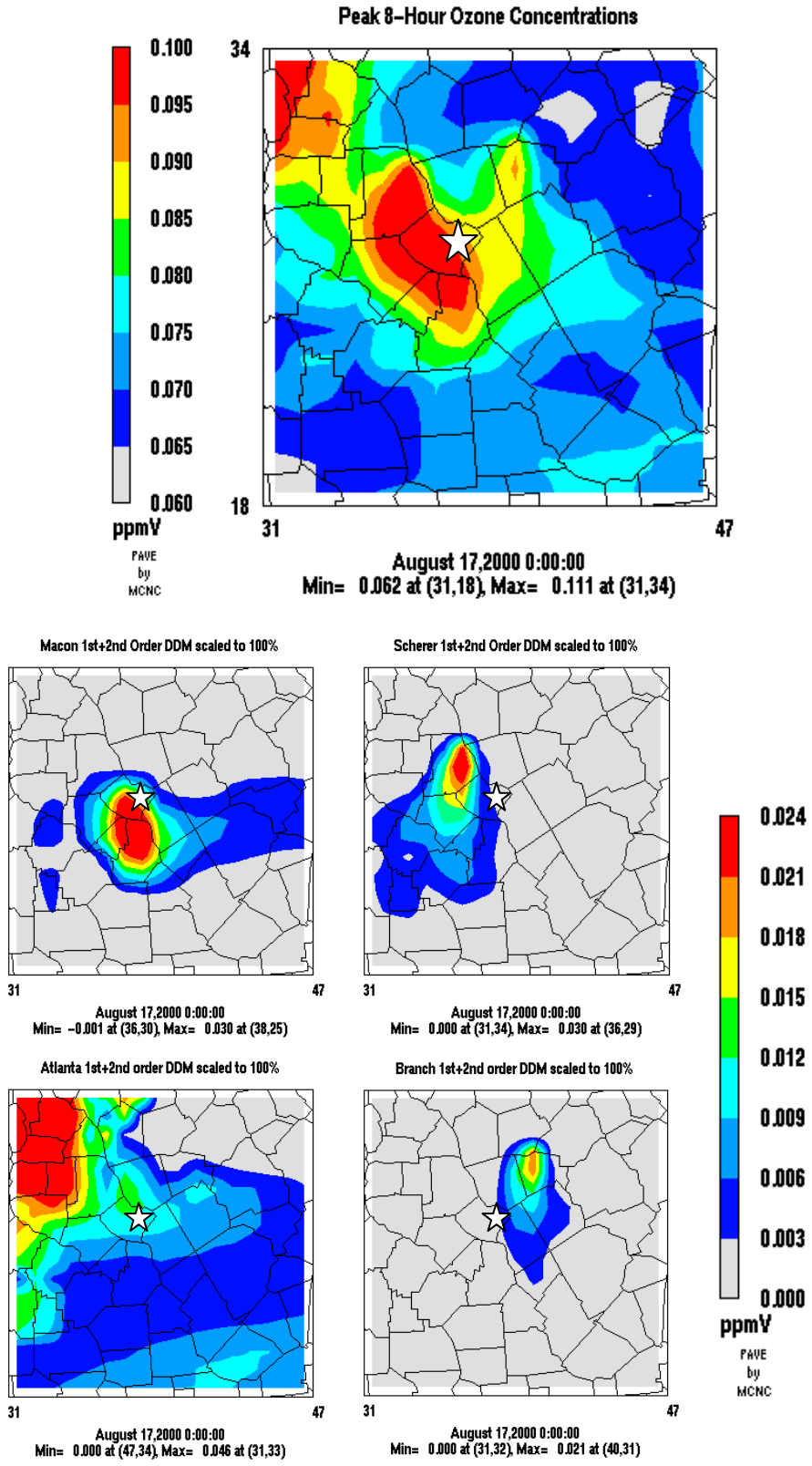

Figure C.16. Peak 8-hour ozone concentrations (top) on August 17, and the contribution from NO_x emissions from (clockwise from top, L) Macon, Scherer, Branch, and Atlanta.

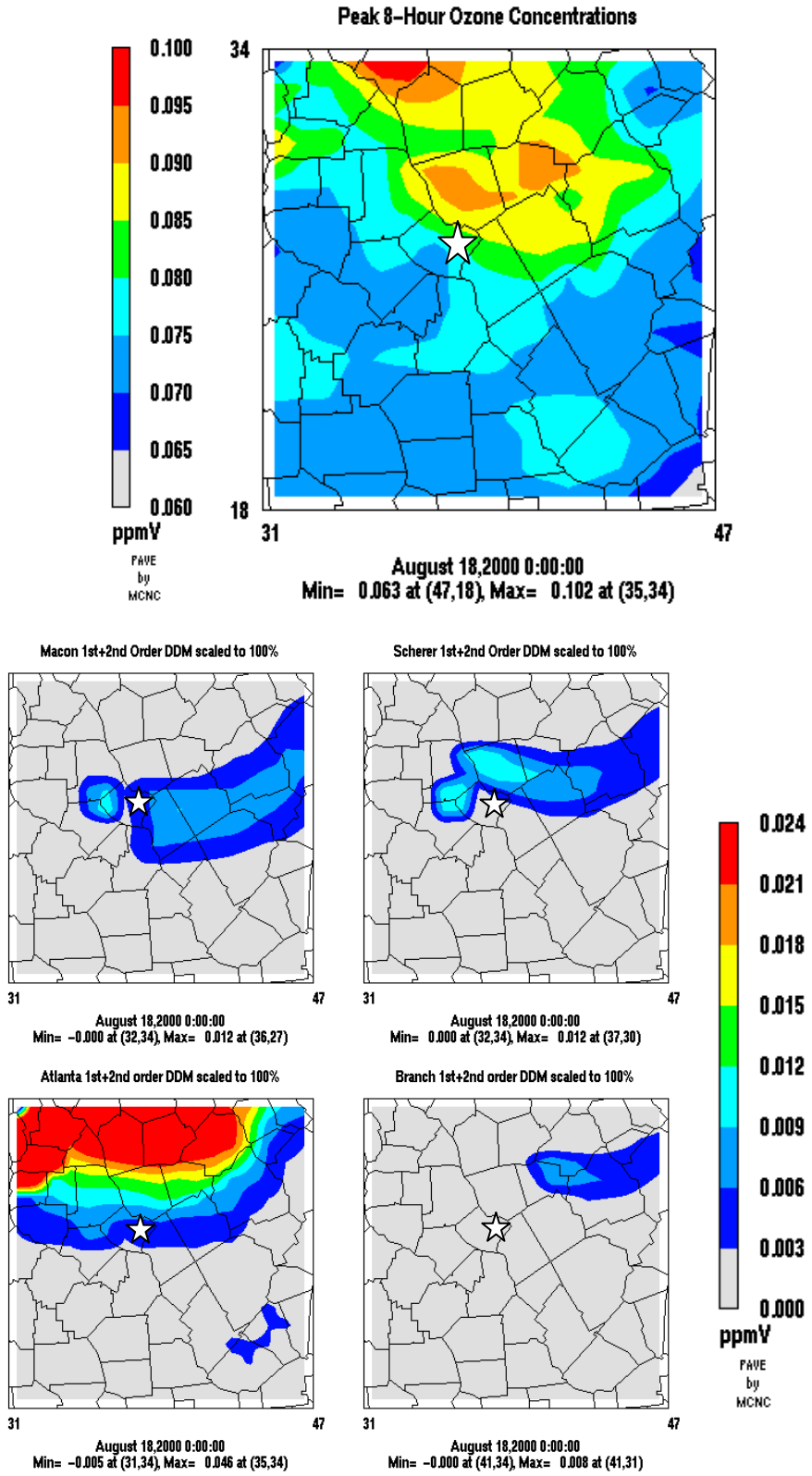

Figure C.17. Peak 8-hour ozone concentrations (top) on August 18, and the contribution from NO_x emissions from (clockwise from top, L) Macon, Scherer, Branch, and Atlanta.

DDM-3D results suggest that Plant Branch contributes to ozone at the Macon EPD monitor more often that at the Sandy Beach monitor, while the opposite holds true for Plant Scherer. The difference in contribution corresponds to the relative proximity of each power plant with each monitor. However, model results for individual point sources and receptors must be interpreted with caution since small errors in model wind fields can greatly influence modeled sensitivity. Sensitivity to a point source can vary greatly over short intervals of time and space and is critically dependent on whether a plume is passing over a given location at a given time. Particular caution is merited for August 17, a day when FAQS modeling for the Year 2000 underpredicted ozone concentrations observed at the Macon EPD monitor though accurately captured the peak ozone levels at Sandy Beach. The August 17 gap could be partially rectified if the Plant Scherer plume actually passed over the EPD monitor to a similar extent that the model indicates it passed over the Sandy Beach monitor or if Atlanta's plume had a more substantial impact. In any case, it is safe to say that each monitor is influenced by a three-part cocktail of NO_x emissions from (1) local sources, (2) nearby power plants, and (3) the Atlanta region, reacting with primarily biogenic VOC emissions to boost ozone concentrations above regional background levels. The spatial patterns of how NO_x from the major source regions contribute to ozone concentrations throughout central Georgia can be seen in Figures C.14 – C.17.

On each day in Figures C.14 – C.17, maximum ozone in the Macon-Warner Robins CSA is modeled to occur where the Atlanta plume overlaps with the Plant Scherer plume and the ozone from local emissions. The Plant Branch plume coincides with a secondary enhancement of ozone but not with the areas of maximum ozone each day. Thus while

both Plant Scherer and Plant Branch join Macon and Atlanta emissions as significant contributors to Macon ozone concentrations, DDM-3D results suggest Plant Branch plays a smaller role in contributing to ozone exceedances.

Are our conclusions, based on DDM-3D results for this single episode, indicative of typical origins of high ozone in Macon? This question can be explored by examining a wind rose comparing a three-year record of ozone observations at Macon's EPD monitor with local wind direction and speed (Figure C.18). All observations of 8-hour ozone higher than 0.085 ppmV occurred during stagnant or westerly winds. We would expect such winds to accentuate the impact of Macon region NO_x emissions sources, which are located primarily to the west of the eastern Bibb County monitor. Winds typically veer (turn clockwise) with height in the planetary boundary layer (e.g.Bluestein, 1992), so westerly winds would correspond to northwesterly flow aloft, facilitating inflow of ozone formed from Plant Scherer and Atlanta emissions. The observations are therefore consistent with DDM-3D in indicating that local, Plant Scherer, and Atlanta emissions are the dominant contributors to ozone on days with highest concentrations in Macon. The absence of high ozone observations on days with northerly and northeasterly flow reinforces the earlier suggestion that Plant Branch is not a dominant cause of ozone exceedances. The DDM-3D results and wind rose are both consistent with simple geographic considerations dictating that Plant Branch, located in an area of sparse emissions northeast of Macon, would contribute less to ozone exceedances than Plant Scherer, a much larger facility aligned between heavy NO_x emissions in Macon and Atlanta.

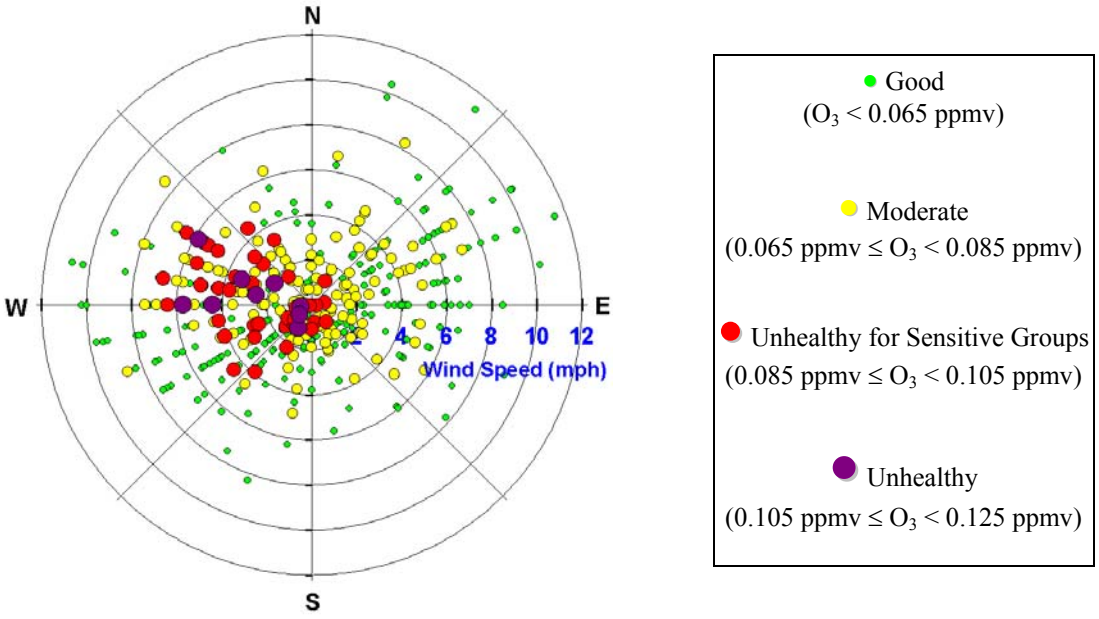

Figure C.18.: 8-hour ozone at Macon EPD monitor as a function of local resultant wind, 1997-1999 ozone seasons. Courtesy of Michael Chang, FAQS July 2001 report.

C.4.3 Augusta

Ozone concentrations near Augusta have hovered near the federal 8-hour standards in recent years. The State of Georgia recommended that Richmond County be designated as non-attainment based on ozone monitoring from 2000-2002 and agreed to develop an Early Action Compact to reduce ozone in the region. However, ozone concentrations in the cool, rainy summer of 2003 were sufficiently low to bring Augusta back into attainment. The sensitivity of ozone in Augusta remains of interest for identifying what sort of controls might be implemented to help ensure that the region does not regress to non-attainment in future years.

Within the Georgia counties of the Augusta MSA, point source emissions originate almost entirely from facilities along the Savannah River that forms the border with South

Carolina (Figure C.19). Mobile, area, and non-road sources are more widely distributed, with greatest emissions in the city of Augusta and along the Interstate 20 corridor.

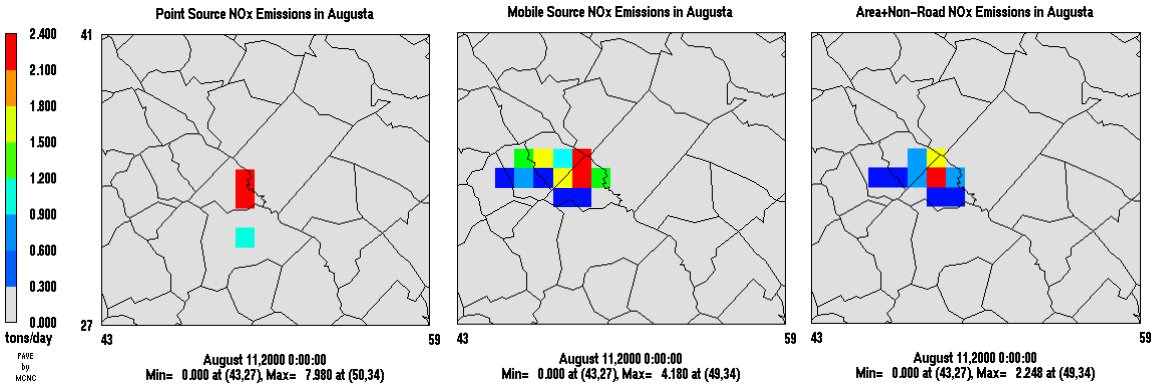

Figure C.19. Daily NO_x emissions from point (L), mobile (C), and area & non-road (R) sources within the Augusta region.

Sensitivity analysis shows that the more easterly and compact footprint of point source emissions is reflected in the incremental sensitivities of peak 8-hour ozone to Augusta NO_x emissions by category (Figure C.20). The peak impact of point source NO_x lies somewhat to the east of the peak impact of other categories.

Because all Augusta emissions footprints are relatively compact, differences between sensitivities among categories in Figure C.20 do not appear pronounced visually. However, the differences are more apparent in terms of the modeled per-ton impacts on the Augusta EPD monitor (Table C.6), located in north-central Richmond County.

Table C.6. Sensitivity (ppt/ton/day) of ozone at the Augusta EPD monitor.

		AUGUSTA		AUG NO_x by category			NO_x Emissions from Other Regions							
DATE	O_3 Conc.	VOC	NOX	MO	A,NR	PT	ATL	BRA	SCH	MAC	CBS	N. GA	C. GA	S. GA
8/13	0.058	4.37	33.48	42.75	62.18	2.51	0.00	0.00	0.00	0.00	0.00	0.00	0.02	0.00
8/14	0.070	14.28	169.96	222.10	200.19	82.77	0.35	0.00	0.00	0.00	0.00	2.50	0.16	0.00
8/15	0.076	6.92	144.05	210.11	168.48	42.79	0.00	0.00	0.00	0.00	0.00	0.08	0.01	0.00
8/16	0.082	13.77	324.39	507.43	417.33	27.05	0.00	0.01	0.00	0.00	0.00	0.81	4.75	0.00
8/17	0.085	4.00	148.33	201.88	171.80	63.82	0.00	0.08	0.00	0.00	0.00	0.09	0.43	0.00
8/18	0.078	0.41	69.16	129.83	50.04	3.71	8.13	43.51	27.54	44.43	20.49	5.40	39.62	5.75
8/19	0.066	2.66	79.91	63.33	80.17	101.08	1.80	1.78	1.73	2.58	1.27	4.79	4.03	1.03
7-day avg.	**0.074**	**6.63**	**138.47**	**196.78**	**164.31**	**46.25**	**1.47**	**6.48**	**4.18**	**6.72**	**3.11**	**1.96**	**7.00**	**0.97**

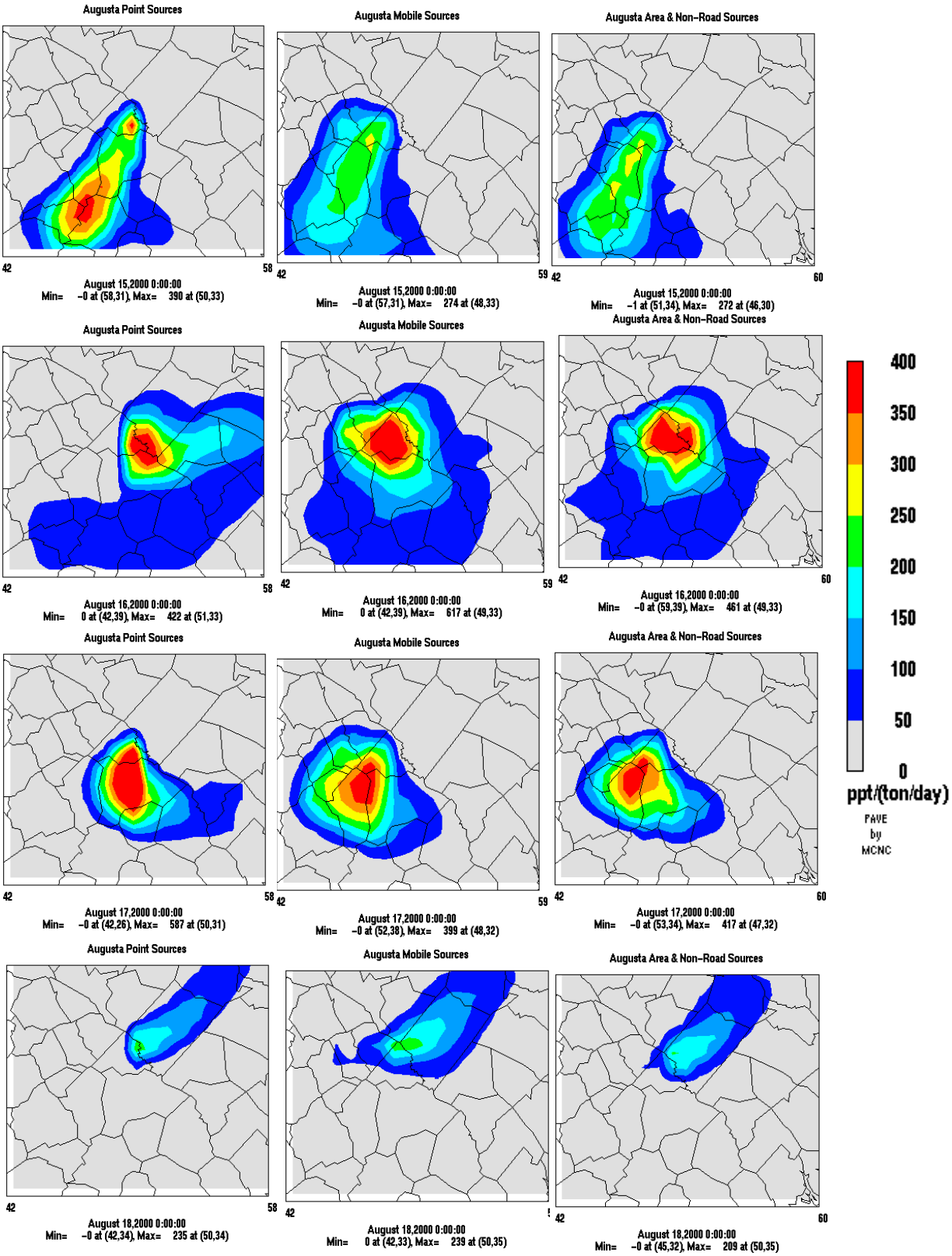

Figure C.20. Sensitivity (pptV/ton/day) of ozone to Augusta point (L), mobile (C), and area & non-road (R) NO_x emissions, Aug. 15-18.

On average, DDM-3D results suggest ozone concentrations at the Augusta EPD monitor could be reduced by about 138 pptV for each 1 tpd reduction in NO_x emissions from the region. However, at least for the episode modeled, Table C.6 suggests that on a per-ton basis, controls of mobile, area, and non-road emissions would be several times more effective than point source controls for reducing ozone concentrations at the monitor. The differences between categories are even more pronounced for the FAQS monitor located further to the west in Columbia County.

The origin of elevated ozone in Augusta varies depending on the day. Much of the time local emissions represent the single greatest source. Emissions from South Carolina have the next greatest impact. Only one day during the episode, Aug. 18, exhibits strong sensitivity of Augusta ozone concentrations to emissions from other Georgia regions (Figure C.21). On this day, winds shifted to be more westerly in contrast to the northerly and easterly winds that predominated near Augusta on other days. For all other days within the episode, Augusta is the dominant source region within Georgia for the formation of locally higher levels of ozone. NO_x emissions from South Carolina contribute significantly as well.

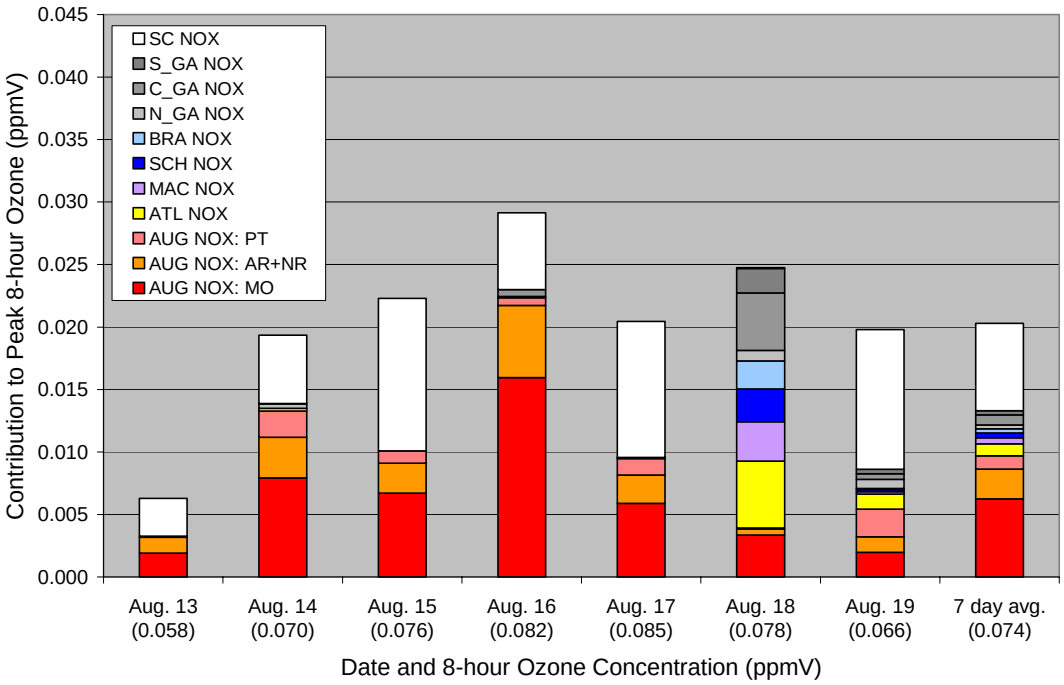

Figure C.21. Source attribution for 8-hour ozone at Augusta EPD monitor.

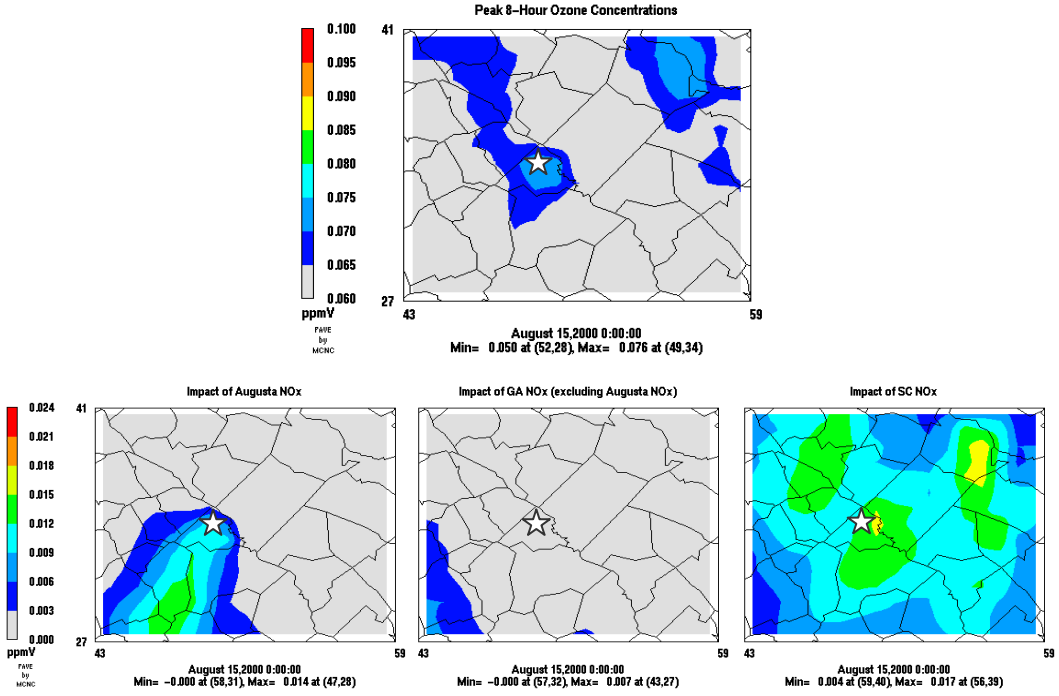

Figure C.22. 8-hour ozone on August 15 (top) and source contribution of NO_x emissions from Augusta (L), other Georgia regions (C), and South Carolina (R). Star shows location of EPD monitor in north-central Richmond County.

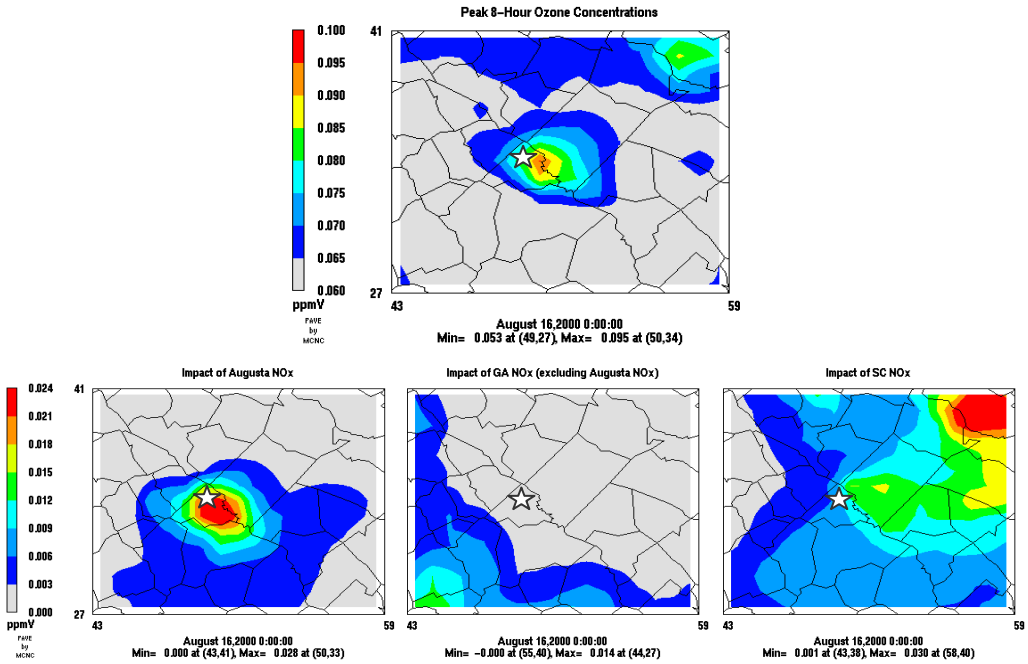

Figure C.23 8-hour ozone on August 16 (top) and source contribution of NO_x emissions from Augusta (L), other Georgia regions (C), and South Carolina (R).

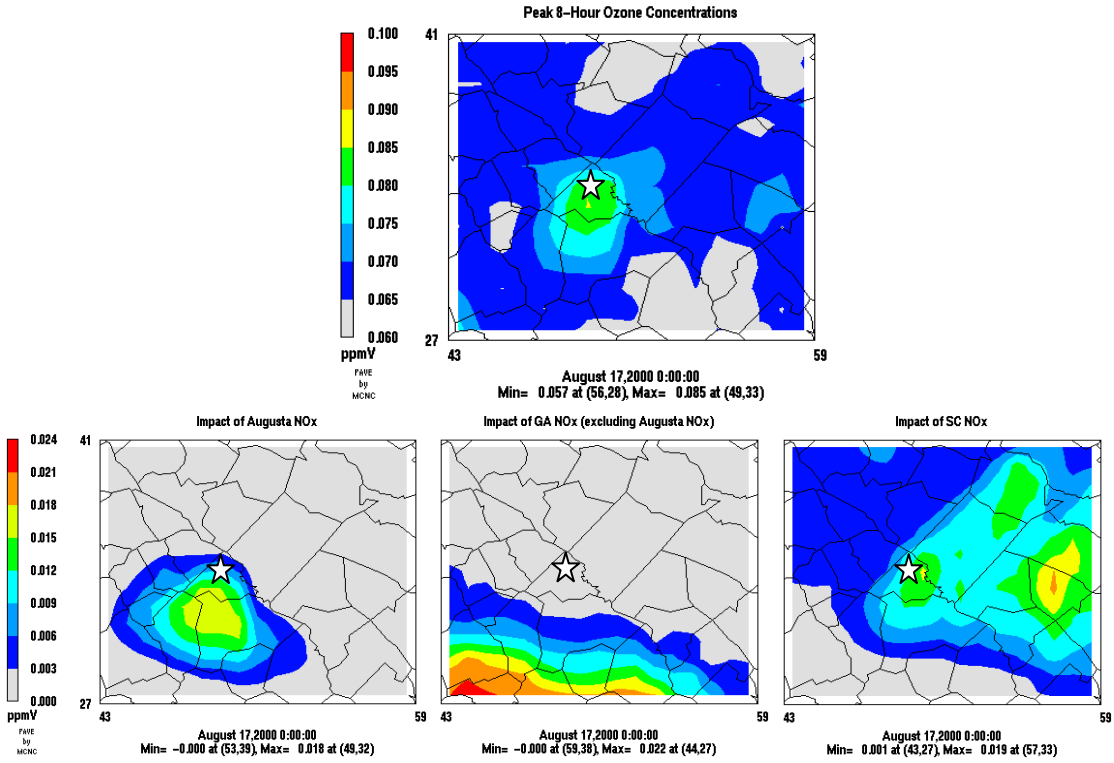

Figure C.24 8-hour ozone on August 17 (top) and source contribution of NO_x emissions from Augusta (L), other Georgia regions (C), and South Carolina (R).

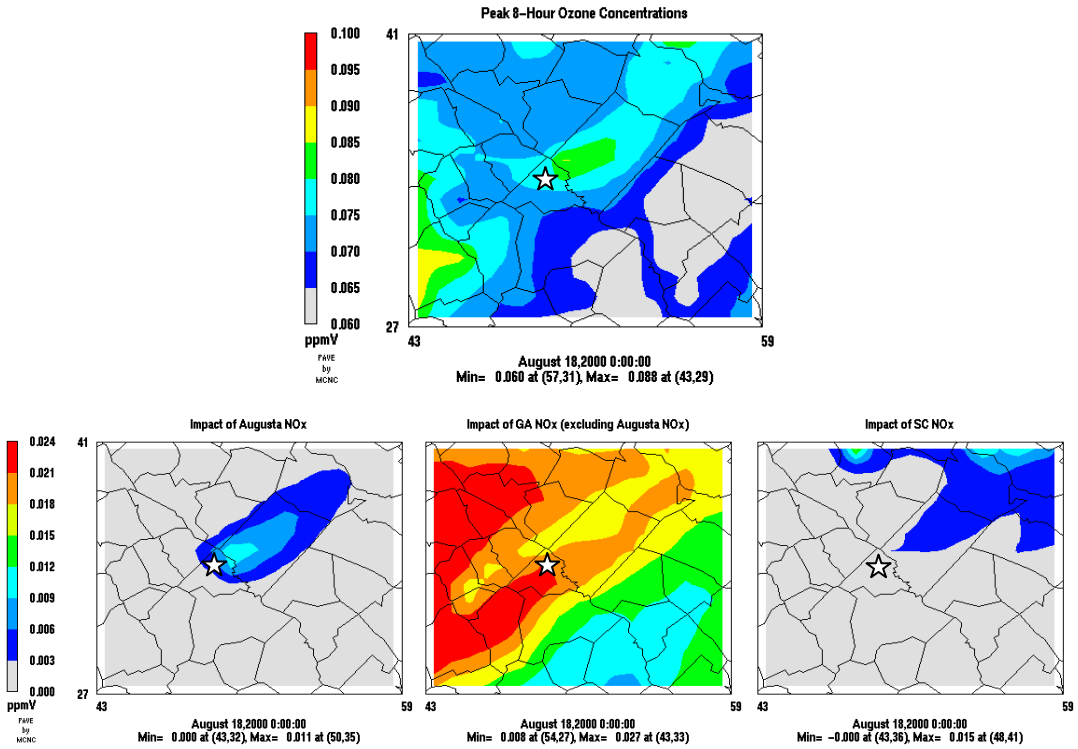

Figure C.25. 8-hour ozone on August 18 (top) and source contribution of NO_x emissions from Augusta (L), other Georgia regions (C), and South Carolina (R).

Spatial patterns of the ozone source contributions of NO_x emissions from Augusta, other Georgia regions, and South Carolina are shown in Figure C.22 Figure –Figure Figure C.25 for August 15-18. On the two days with highest concentrations, August 16-17, the local ozone peak corresponds to the areas influenced by emissions from Augusta and South Carolina. Emissions from elsewhere in Georgia have little influence on these days. When winds are sufficiently strong and westerly to transport outflow from major Georgia sources (Aug. 18), ozone concentrations are somewhat lower because the winds diminish the influence of Augusta and South Carolina emissions. Thus, at least for the episode modeled, it appears that emissions from elsewhere in Georgia can significantly influence ozone concentrations in Augusta on moderately polluted days, but that highest

concentrations are most likely to occur when stagnant or light north-easterly winds enhance the impact of nearby emissions.

That stagnant or northeasterly flow would generate the highest ozone concentrations can be understood by examining the spatial pattern of emissions near Augusta (Figure C.26). Augusta is closer to the South Carolina cities of North Augusta, Aiken and Columbia to its northeast than to any major Georgia city. Emissions from the most concentrated Georgia source regions such as Atlanta and the major power plants are likely to dilute significantly while passing over the sparsely emitting areas to the west of Augusta.

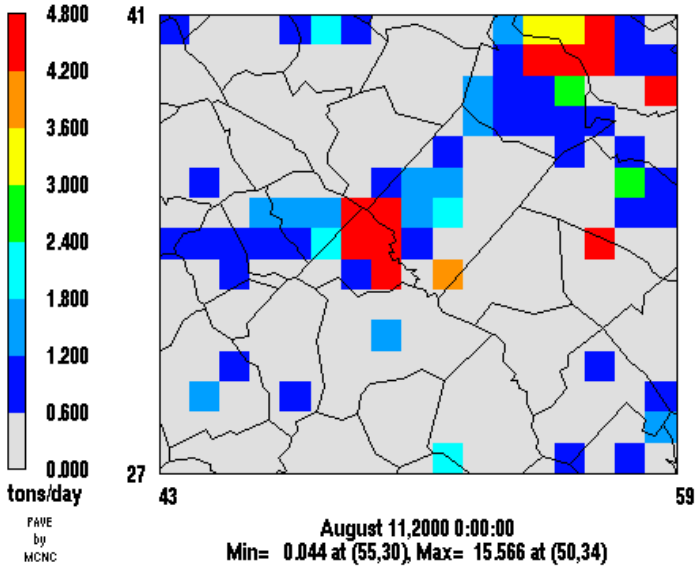

Figure C.26. Daily NO_x emissions near Augusta.

Again, we turn to a wind rose to examine whether conclusions suggested by DDM-3D results of a single episode are supported by a multi-year record of ozone observations (Figure C.27). Almost all observations of high ozone concentrations in Augusta are accompanied by light winds. These stagnant conditions would be most conducive to the

formation of ozone from nearby precursor emissions. On only one day in the three-year period did high ozone concentrations coincide with the strong westerly winds that would facilitate inflow from Atlanta and other Georgia source regions. The observational record is therefore consistent with the hypothesis that although emissions from a number of regions will exert a periodic impact, ozone exceedance conditions in Augusta will most often display a predominantly local character.

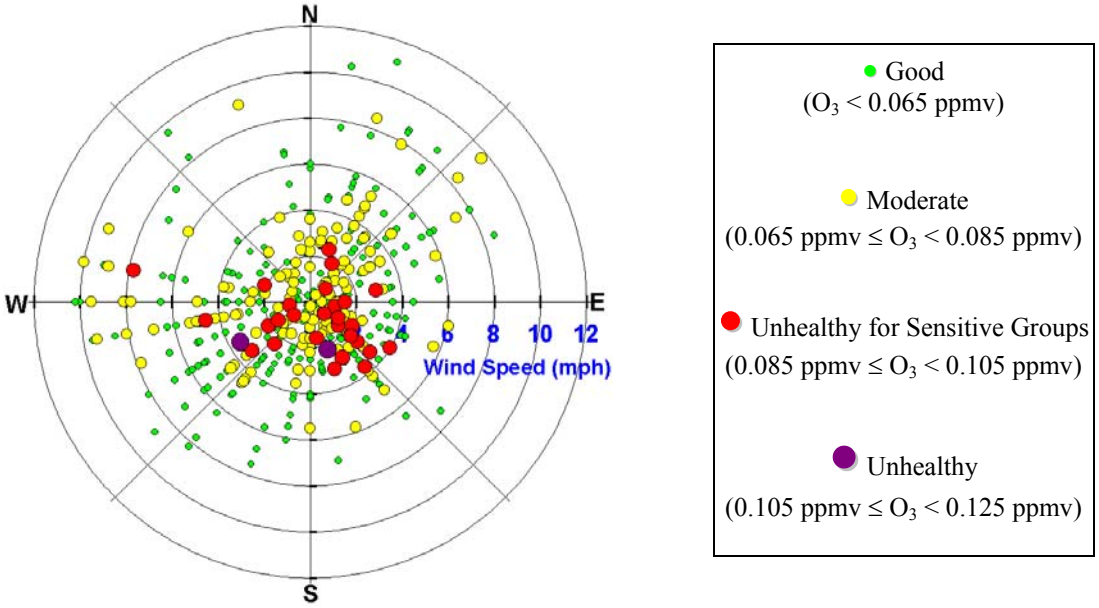

Figure C.27. 8-hour ozone at Augusta monitor as a function of local resultant wind, 1997-1999 ozone seasons. Courtesy of Michael Chang, FAQS July 2001 report.

C.4.4 Columbus

Columbus has the smallest NO_x emissions of the four Georgia cities examined in this report (Figure C.2), and also the lowest observed ozone concentrations. Columbus is currently attaining federal ozone standards. Given the small level of emissions and lack

of major point sources in Columbus, we group all local source categories together for sensitivity analysis. Emissions of NO_x in the Georgia portion of the Columbus MSA are concentrated in Muscogee County near the Alabama border (Figure C.28).

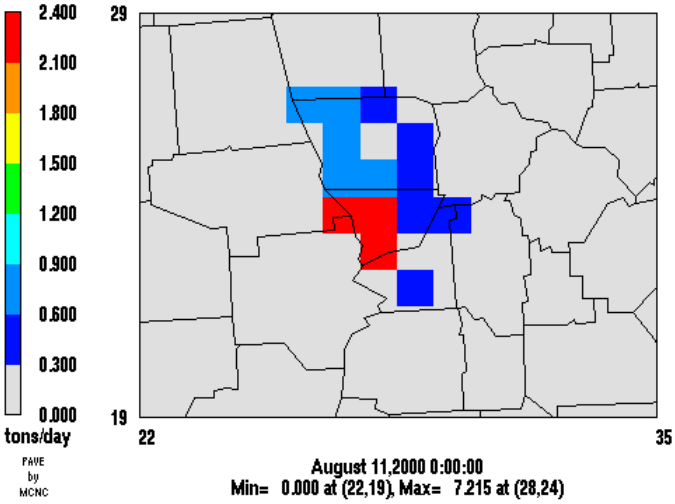

Figure C.28. Daily NO_x emissions within the Columbus region.

The compact nature of Columbus NO_x emissions, in close proximity to the EPD monitors, leads to strong per-ton sensitivity of ozone to local emissions (Table C.7). On average, 8-hour ozone during the episode could be reduced by 226 pptV for each 1 tpd of NO_x emissions reductions. Only slight sensitivity to VOC is observed. The two days with highest ozone concentrations in Columbus, August 15 and August 17, exhibit distinct patterns of sensitivity to emissions (Table C.7 and Figure C.29). These high ozone regimes can be termed "regional enhancement" and "locally sensitive," respectively.

Table C.7. Sensitivity (ppt/ton/day) of 8-hour ozone at the Columbus EPD monitors to incremental emissions (Crime Lab and Airport monitors reside in the same grid cell).

		COLUMBUS		NO_x Emissions from Other Regions							
DATE	Ozone Conc.	VOC	NOX	ATL	BRA	SCH	MAC	AUG	N. GA	C. GA	S. GA
8/13	0.067	4.18	130.28	12.76	0.00	0.00	0.00	0.00	2.46	0.10	0.00
8/14	0.076	13.30	298.02	15.38	0.00	0.01	0.03	0.00	6.21	0.54	0.00
8/15	0.088	5.66	129.76	25.96	0.01	0.00	0.00	0.15	17.58	0.49	0.00
8/16	0.080	2.34	224.81	10.38	0.00	0.00	0.00	0.00	12.40	1.46	0.00
8/17	0.088	3.65	686.05	7.26	0.00	0.00	0.00	0.00	13.07	0.95	0.01
8/18	0.077	1.90	84.80	1.17	2.86	1.56	1.57	0.01	0.94	0.73	0.02
8/19	0.062	3.23	31.30	5.09	0.00	0.05	0.06	0.00	3.07	0.27	0.00
7-day avg.	**0.077**	**4.89**	**226.43**	**11.14**	**0.41**	**0.23**	**0.24**	**0.02**	**7.96**	**0.65**	**0.00**

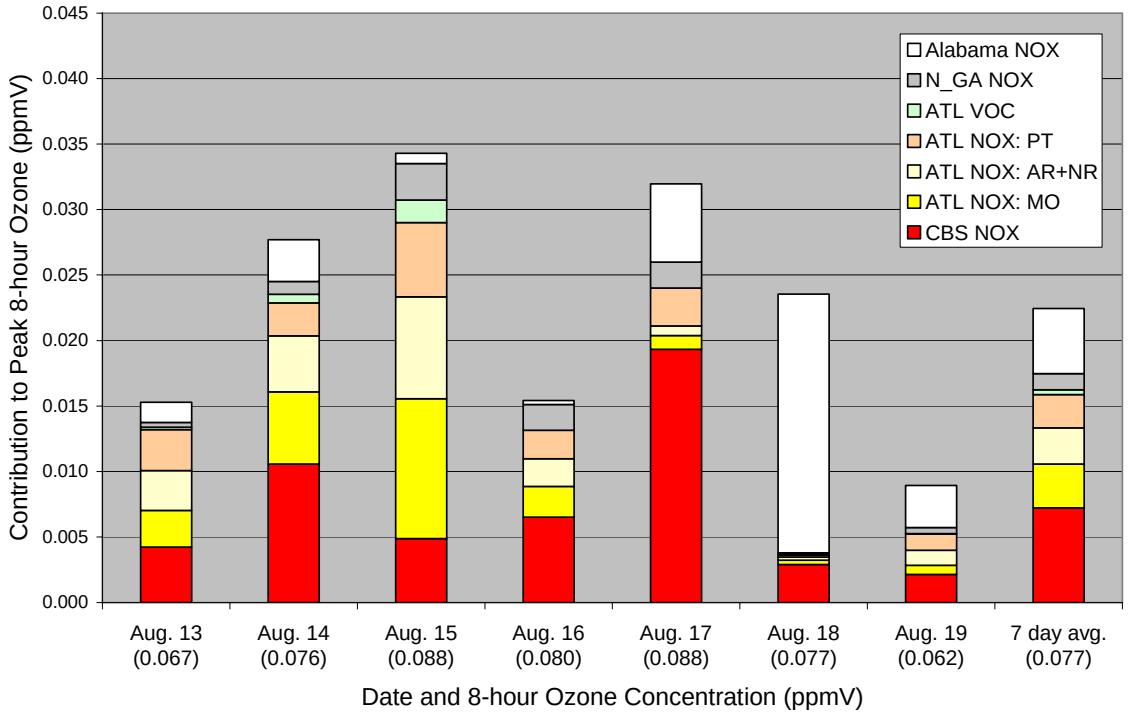

Figure C.29. Source attribution for 8-hour ozone concentrations at Columbus monitor.

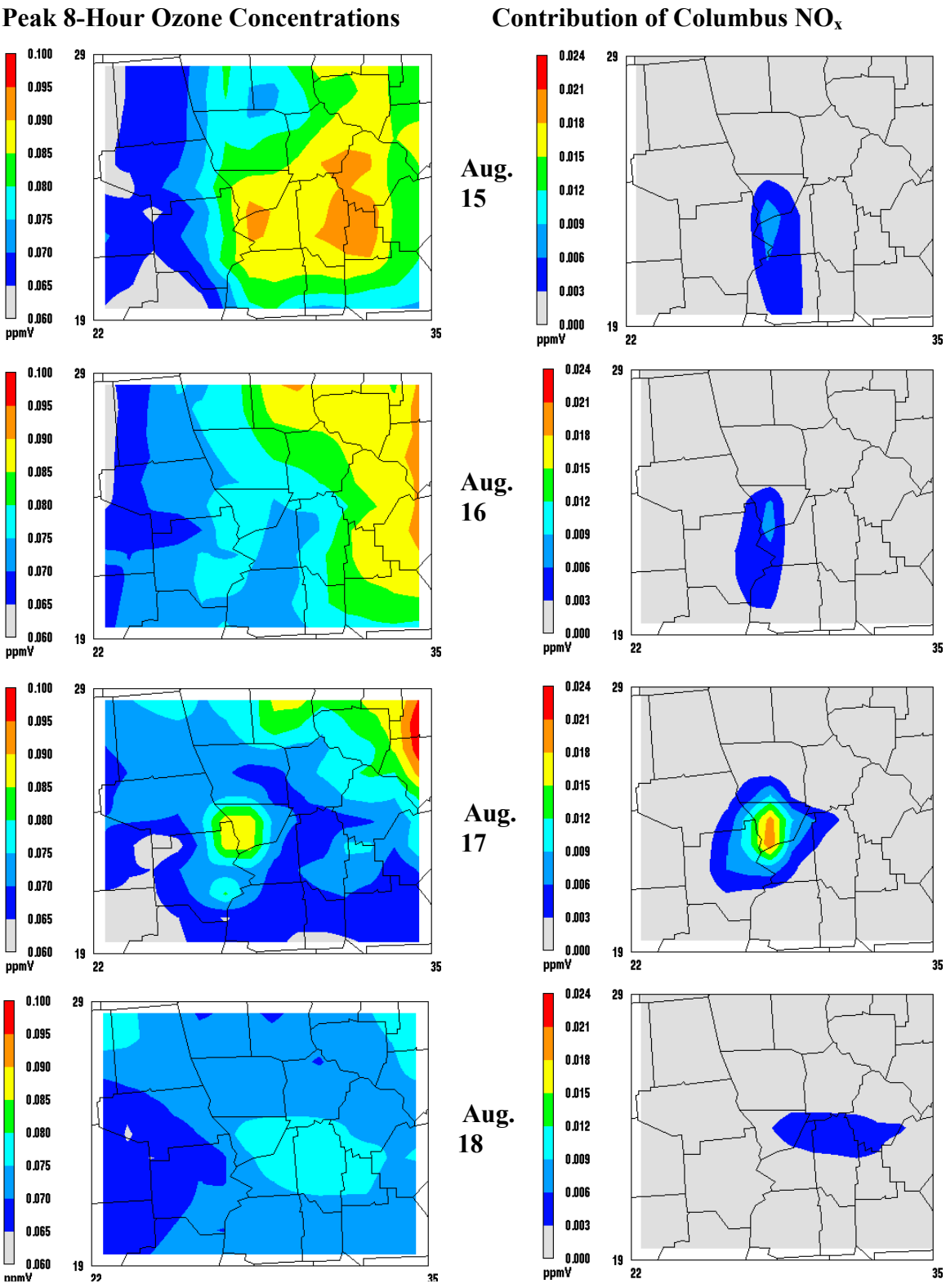

Figure C.30. 8-hour ozone concentrations near Columbus (L) and the contribution of Columbus NO_x emissions to ozone (R).

On August 15, Columbus is engulfed in a broad region of elevated ozone concentrations, slightly enhanced by local emissions (Figure C.4 and Figure C.30). Northerly winds disperse the Columbus emissions to downwind counties and bring in outflow from the western counties of the Atlanta region and rural North Georgia. The much larger size of the emissions in these neighboring regions means that even though the per-ton sensitivities are smaller, the source contribution can exceed that of emissions within Columbus itself. On August 17, stagnant and warmer conditions cause ozone to be much more sensitive to local emissions, which generate about 0.020 ppmV of the 8-hour ozone in Columbus on this day, while the inflow from other Georgia regions is diminished. Alabama NO_x emissions generate about 0.006 ppmV of Columbus' ozone on August 17 (Figure C.29).

The effectiveness of air pollution control strategies will depend on the meteorological regime generating high ozone in Columbus on a given day. The benefit of local emission controls will be greatest on "locally sensitive" days such as August 17, whereas the benefit from controls in neighboring regions will be strongest on "regional enhancement" days such as August 15. Our modeling suggests that either of these high ozone regimes could cause Columbus to exceed 0.085 ppmV ozone concentrations on a hot summer day, even with anticipated 2007 emission controls.

A wind rose of ozone observations suggests that both the local and regional regimes do in fact contribute to elevated ozone concentrations in Columbus. High ozone concentrations have been observed in Columbus during days with stagnant winds conducive to local ozone formation and days with stronger winds that could transport pollution from Atlanta, North Georgia, and Alabama. Low ozone concentrations

accompany winds from the east and southeast, where emissions are sparse. These observations agree with the DDM-3D source impact analysis.

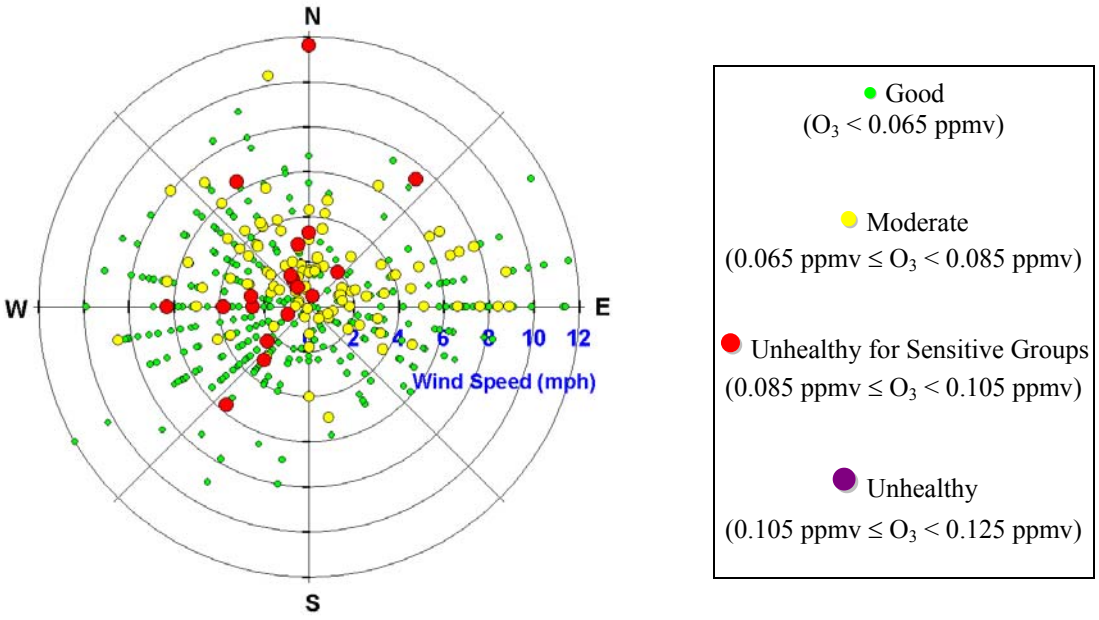

Figure C.31. 8-hour ozone at Columbus Airport monitor as a function of local resultant wind, 1997-1999 ozone seasons. Courtesy of Michael Chang, FAQS July 2001 report.

C.5 Conclusions

The sensitivity of ozone concentrations to precursor emissions has been examined for a projected Year 2007 scenario with meteorology from the August 11-20, 2000 episode. A NO_x-limited ozone production regime dominates Georgia throughout the episode, with significant sensitivity to VOC limited to central counties of the Atlanta region.

Ozone sensitivity has been considered via two metrics: (1) the incremental sensitivity per ton of change in emissions and (2) the overall contribution of each emissions source to ozone concentrations. Care has been taken to examine not only the average impact of

each emissions source during the episode, but also to distinguish between sources that tend to contribute most to exceedances of federal ozone standards and those whose impact is more often felt during cleaner conditions. For this purpose, DDM-3D modeling results have been supplemented with consideration of the observational record and the spatial distribution of emission sources.

Ozone in each of the four focus cities is found to be governed by a distinct set of source influences. In Atlanta, local emissions, particularly NO_x emissions from mobile and non-road sources, are the dominant origin for enhancements of ozone above regional background levels. Emissions from Atlanta frequently travel downwind to contribute to ozone in Macon, which is also strongly influenced by emissions from local sources and two nearby power plants. The geographic alignment of Plant Scherer between Atlanta and Macon makes it especially conducive to contributing to maximum ozone concentrations near Macon on high-ozone days. In Augusta, NO_x emissions from local sources and from nearby counties in South Carolina are major sources of ozone on most days. Days with significant inflow from other Georgia regions are unlikely to have especially high ozone because the associated strong westerlies tend to dilute ozone concentrations. By contrast, inflow from Atlanta and Alabama significantly contribute to some high ozone days in Columbus. In addition to these times of "regional enhancement," Columbus can also experience high ozone on "locally sensitive" days when stagnant conditions cause local emissions to play a more predominant role. In each Fall-Line city, the results of DDM-3D for the modeled episode are broadly consistent with a multi-year record of ozone observations with regards to the source regions and meteorological conditions most conducive to high ozone concentrations.

Sensitivity analysis has been shown to be a useful tool for informing the development of ozone control strategies. Because some degree of uncertainty is inherent in air pollution modeling and because only one episode has been presented in this chapter, caution should be taken to further consider observational evidence and other modeled episodes when developing control strategies.

REFERENCES

Altshuller, A. P. (1978). "Association of oxidant episodes with warm stagnating anticyclones." *Journal of the Air Polluion Control Association* 28: 152-155.

Ang-Olson, M. Fischer and R. Dulla (2000). "Land use as an air quality control measure." *Transportation Research Record* 1738: 33-38.

Baker, D. and J. P. Barrett (1999). The feasibility of pay by the mile automobile insurance. Economic Policy Institute Technical Paper No. 231.

Bell, M. and H. Ellis (2003). "Comparison of the 1-hr and 8-hr national ambient air quality standards for ozone using Models-3." *Journal of the Air and Waste Management Association* 53: 1531-1540.

Bergin, M. S., G. S. Noblet, K. Petrini, J. R. Dhieux, J. B. Milford and R. A. Harley (1999). "Formal uncertainty analysis of a Lagrangian photochemical air pollution model." *Environmental Science and Technology* 33: 1116-1126.

Bluestein, H. B. (1992). Synoptic-Dynamic Meteorology in Midlatitudes. Volume I: Principles of Kinematics and Dynamics. New York, Oxford University Press.

Brunekreef, B. and S. T. Holgate (2002). "Air pollution and health." *Lancet* 360: 1233-1242.

Byun, D. W. and J. K. S. Ching (1999). Science algorithms of the EPA Models-3 Community Multiscale Air Quality (CMAQ) Modeling System. U.S. EPA/600/R-99/030.

CARB (1995). (California Air Resources Board), "Controlling locomotive emissions in California: Technology, cost-effectiveness, and regulatory strategy. Final Report." Contract Nos. A032-169 and 92-917.

Carter, W. P. L. (2000). Documentation of the SAPRC-99 chemical mechanism for VOC reactivity assessment. Final Report to California Air Resources Board, Contract No. 92-329 and 95-308.

Chameides, W. L., F. Fehsenfeld, M. O. Rodgers, C. Cardelino, J. Martinez, D. Parrish, W. Lonneman, D. R. Lawson, R. A. Rasmussen, P. Zimmerman, J. Greenberg, P. Middleton and T. Wang (1992). "Ozone precursor relationships in the ambient atmosphere." *Journal of Geophysical Research* 97: 6037-6055.

Chang, M. E. (2001). "Air quality management in small markets." *EM*: 24-27.

Chock, D. P., S. L. Winkler and S. Pezda (1997). "Attainment flip-flops and the achievability of the ozone air quality standard." *Journal of the Air and Waste Management Association* 47: 620-622.

Chock, D. P., S. L. Winkler and P. Sun (2002). "Effect of grid resolution and subgrid assumptions on the model prediction of a reactive buoyant plume under convective conditions." *Atmospheric Environment* 36: 4649-4662.

Cohan, D., Y. Hu, A. Hakami and A. G. Russell (2003). Sensitivity analysis of ozone in the Southeast. Models-3 Users Workshop. www.cmascenter.org/2003_workshop/session2/cohan_abstract.pdf.

Cohan, D. S., Y. Hu, A. Hakami, M. T. Odman and A. G. Russell (2002). Implementation of a direct decoupled sensitivity method into CMAQ. 1st Models-3 Users Workshop. www.cmascenter.org/workshop/session5/cohan_abstract.pdf.

Davis, W. T. and T. L. Miller (2004). "Estimates of potential emissions reductions for the Nashville ozone early action compact area, Final Report," prepared for the Nashville Department of Environment and Conservation.

Dunker, A., G. Yarwood, J. Ortmann and G. Wilson (2002). "The decoupled direct method for sensitivity analysis in a three-dimensional air quality model - Implementation, accuracy, and efficiency." *Environmental Science and Technology* 36: 2965-2976.

Dunker, A. M. (1981). "Efficient calculation of sensitivity coefficients for complex atmospheric models." *Atmospheric Environment* 15: 1155-1161.

Dunker, A. M. (1984). "The decouple direct method for calculating sensitivity coefficients in chemical kinetics." *Journal of Chemical Physics* 81: 2385-2393.

Farrell, A. (2001). "Multi-lateral emission trading: lessons from inter-state NOx control in the United States." *Energy Policy* 29: 1061-1072.

Frey, H. C. and J. Zheng (2002). "Quantification of variability and uncertainty in air pollutant emission inventories: Method and case study for utility NOx emissions." *Journal of Air and Waste Management Association* 52: 1083-1095.

Fuhrer, J. (2002). "Ozone impacts on vegetation." *Ozone Science and Engineering* 24: 69-74.

GA-DNR (2001). (Georgia Department of Natural Resources), Georgia's State Implementation Plan for the Atlanta ozone non-attainment area.

Georgopoulos, P. G., S. Arunachalam and S. Wang (1997). "Alternative metrics for assessing the relative effectiveness of NO_x and VOC emission reductions in controlling ground-level ozone." *Journal of Air and Waste Management Association* 47: 838-850.

Gillani, N. V. and J. E. Pleim (1996). "Sub-grid-scale features of anthropogenic emissions of NOx and VOC in the context of regional Eulerian models." *Atmospheric Environment* 30: 2043-2059.

Grell, G., J. Dudhia and D. Stauffer (1994). A description of the Fifth-Generation Penn State/NCAR Mesoscale Model (MM5). NCAR Technical Note, NCAR/TN 398+STR.

Guenther, A., C. Geron, T. Pierce, B. Lamb, P. Harley and R. Fall (2000). "Natural emissions of non-methane volatile organic compounds; carbon monoxide, and oxides of nitrogen from North America." *Atmospheric Environment* 34: 2205-2230.

Guenther, A., P. Zimmerman, L. Klinger, J. Greenberg, C. Ennis, K. Davis, W. Pollock, H. Westberg, G. Allwine and C. Geron (1996). "Estimates of regional natural volatile organic compound fluxes from enclosure and ambient measurements." *Journal of Geophysical Research* 101: 1345-1359.

Hahn, R. W. (1995). "An economic analysis of scrappage." *RAND Journal of Economics* 26: 222-242.

Hakami, A. (2003b). Direct sensitivity analysis in air quality models, Georgia Institute of Technology. Ph.D. Dissertation.

Hakami, A., M. T. Odman and A. G. Russell (2003a). "High-order, direct sensitivity analysis of multidimensional air quality models." *Environmental Science and Technology* 37: 2442-2452.

Hanna, S. R., J. C. Chang and M. E. Fernau (1998). "Monte Carlo estimates of uncertainties in predictions by a photochemical grid model (UAM-IV) due to uncertainties in input variables." *Atmospheric Environment* 32: 3619-3628.

Hanna, S. R., Z. Lu, H. C. Frey, N. Wheeler, J. Vukovich, S. Arunachalam, M. Fernau and D. A. Hansen (2001). "Uncertainties in predicted ozone concentrations due to input uncertainties for the UAM-V photochemical grid model applied to the July 1995 OTAG domain." *Atmospheric Environment* 35: 891-903.

Henderson, J. V. (1996). "Effects of air quality regulation." *American Economic Review* 86: 789-813.

Hu, Y., D. S. Cohan, M. T. Odman and A. G. Russell (2004). Air quality modeling of the August 11-20, 2000 episode for the Fall Line Air Quality Study. Prepared for Environmental Protection Division, Georgia Department of Natural Resources.

Hu, Y., M. T. Odman and A. G. Russell (2003). Meteorological modeling of the first base case episode for the Fall Line Air Quality Study. Prepared for Environmental Protection Division, Georgia Department of Natural Resources.

ICF-SAI (2002). (ICF Consulting/Systems Applications International). "Ozone episode selection analysis for urban areas in northern Georgia and northern Alabama (1995-2001)." Prepared for John J. Jansen, Southern Company.

IPCC (2001). (Intergovernmental Panel on Climate Change). Climate change 2001: The Scientific Basis. Cambridge, Cambridge University Press.

Jacob, D. J., L. W. Horwitz, J. W. Munger, B. G. Heikes, R. R. Dickerson, R. S. Artz and W. C. Keene (1995). "Seasonal transition from NO_x- to hydrocarbon-limited

conditions for ozone production over the eastern United States in September." *Journal of Geophysical Research* 100: 9315-9324.

Jang, J.-C. C., H. E. Jeffries, D. Byun and J. E. Pleim (1995a). "Sensitivity of ozone to model grid resolution - I. Application of high-resolution regional acid deposition model." *Atmospheric Environment* 29: 3085-3100.

Jang, J.-C. C., H. E. Jeffries and S. Tonnesen (1995b). "Sensitivity of ozone to model grid resolution - II. Detailed process analysis for ozone chemistry." *Atmospheric Environment* 29: 3101-3114.

Kasibhatla, P., W. L. Chameides, R. D. Saylor and D. Olerud (1998). "Relationships between regional ozone pollution and emissions of nitrogen oxides in the eastern United States." *Journal of Geophysical Research* 103: 22,663-22,669.

Kleinman, L. I. (2000). "Ozone process insights from field experiments - part II: Observation-based analysis for ozone production." *Atmospheric Environment* 34: 2023-2033.

Kleinman, L. I., P. H. Daum, J. H. Lee, Y.-N. Lee, L. J. Nunnermacker, S. R. Springston, L. Newman, J. Weinstein-Lloyd and S. Sillman (1997). "Dependence of ozone production on NO and hydrocarbons in the troposphere." *Geophysical Research Letters* 24: 2299-2302.

Koren, H. S. (1995). "Associations between criteria air pollutants and asthma." *Environmental Health Perspectives* 103: 235-242.

Kuzmyak, J. R. (2002). "Cost-effectiveness of congestion mitigation and air quality strategies," in The Congestion Mitigation and Air Quality Improvement Program: Assessing 10 years of experience, Transportation Research Board Special Report 264, Washington, DC: National Academy Press.

Liang, J. and M. Z. Jacobson (2000). "Effects of subgrid segregation on ozone production efficiency in a chemical model." *Atmospheric Environment* 34: 2975-2982.

Lin, C. Y. C., D. J. Jacob and A. M. Fiore (2001). "Trends in exceedances of the ozone air quality standard in the continental United States, 1980-1998." *Atmospheric Environment* 35: 3217-3228.

Lin, X., M. Trainer and S. C. Liu (1988). "On the nonlinearity of the tropospheric ozone production." *Journal of Geophysical Research* 93: 15,879-15,888.

Litman, T. (1997). "Distance-based insurance as a TDM strategy." *Transportation Quarterly* 51: 119-137.

Liu, L., G. H. Huang, Y. Liu, G. A. Fuller and G. M. Zeng (2003). "A fuzzy stochastic robust programming model for regional air quality management under uncertainty." *Engineering Optimization* 35: 177-199.

Liu, S. C., M. Trainer, F. C. Fehsenfeld, D. D. Parrish, E. J. Williams, D. W. Fahey, G. Hübler and P. C. Murphy (1987). "Ozone production in the rural troposphere and the implications for regional and global ozone distributions." *Journal of Geophysical Research* 92: 4191-4207.

Lu, C.-H. and J. S. Chang (1998). "On the indicator-based approach to assess ozone sensitivities and emission features." *Journal of Geophysical Research* 103: 3453-3462.

Martin, R. V., A. M. Fiore and A. Van-Donkelaar (2004). "Space-based diagnosis of surface ozone sensitivity to anthropogenic emissions." *Geophysical Research Letters* 31: doi:10.1029/2004GL019416.

McConnell, R., K. Berhane, F. Gilliland, S. J. London, T. Islam, W. J. Gauderman, E. Avol, H. G. Margolis and J. M. Peters (2002). "Asthma in exercising children exposed to ozone: a cohort study." *Lancet* 359: 386-391.

McKeen, S. A., E. Y. Hsie and S. C. Liu (1991). "A study of the dependence of rural ozone on ozone precursors in the eastern United States." *Journal of Geophysical Research* 96: 15,377-15,394.

Meagher, J. F., E. B. Cowling, F. C. Fehsenfeld and W. J. Parkhurst (1998). "Ozone formation and transport in the southeastern United States: Overview of the SOS Nashville Middle Tennessee Ozone Study." *Journal of Geophysical Research* 103: 22213-22223.

Mendelsohn, R. (1986). "Regulating heterogeneous emissions." *Journal of Environmental Economics and Management* 13: 301-312.

Nobel, C. E., E. C. McDonald-Buller, Y. Kimura and D. T. Allen (2001). "Accounting for spatial variation of ozone productivity in NOx emission trading." *Environmental Science and Technology* 35: 4397-4407.

Nobel, C. E., E. C. McDonald-Buller, Y. Kimura, K. E. Lumbley and D. T. Allen (2002). "Influence of population density and temporal variations in emissions on the air quality benefits of NOx emission trading." *Environmental Science and Technology* 36: 3465-3473.

NRC (1991). Committee on Tropospheric Ozone Formation and Measurement. Rethinking the ozone problem in urban and regional air pollution, National Academy Press.

NRC (2004). Air quality management in the United States. Washington, DC, National Academies Press.

Pansing, C. E., N. Schreffler and M. A. Sillings. (1998). "Comparative evaluation of the cost-effectiveness of 58 transportation control measures." *Transportation Research Record* 1641: 97-104.

Paulson, S. E., R. C. Flagan and J. H. Seinfeld (1992). "Atmospheric photooxidation of isoprene. 1. The hydroxyl radical and ground-state atomic oxygen reactions." *International Journal of Chemical Kinetics* 24: 79-101.

Pechan, E. H. (2002). "Control strategy cost analyses for the Southern Appalachian Mountain Initiative." Pechan Rpt. No. 02.07.003/9405.000, prepared for Southern Appalachian Mountain Initiative.

Pechan, E. H. (2003a). "AirControlNET Version 3.2 Development Report," prepared for U.S. EPA.

Pechan, E. H. (2003b). "AirControlNET Version 3.2 Documentation Report," prepared for U.S. EPA.

Roselle, S. J. and K. L. Schere (1995). "Modeled response of photochemical oxidants to systematic reductions in anthropogenic volatile organic compound and NOx emissions." *Journal of Geophysical Research* 100: 22,929-22,941.

Russell, A. G. and R. Dennis (2000). "NARSTO critical review of photochemical models and modeling." *Atmospheric Environment* 34: 2283-2324.

Ryerson, T. B., M. Trainer, J. S. Holloway, D. D. Parrish, L. G. Huey, D. T. Sueper, G. J. Frost, S. G. Donnelly, S. Schauffler, E. L. Atlas, W. C. Kuster, P. D. Goldan, G. Hubler, J. F. Meagher and F. C. Fehsenfeld (2001). "Observations of ozone formation in power plant plumes and implications for ozone control strategies." *Science* 292: 719-723.

Shoup, D. C. (1997). "Evaluating the effects of cashing out employer-paid parking: Eight case studies." *Transport Policy* 4: 201-216.

Sillman, S. (1999). "The relation between ozone, NOx and hydrocarbons in urban and polluted rural environments." *Atmospheric Environment* 33: 1821-1845.

Sillman, S. (2000). " Ozone production efficiency and loss of NOx in power plant plumes: Photochemical model and interpretation of measurements in Tennessee." *Journal of Geophysical Research* 105: 9189-9202.

Sillman, S., K. I. Alwali, F. J. Marsik, P. Nowacki, P. J. Samson, M. O. Rodgers, L. J. Garland, J. E. Martinez, C. Stoneking, R. Imhoff, J. H. Lee, L. Newman, J. Weinstein-Lloyd and V. P. Aneja (1995). "Photochemistry of ozone formation in Atlanta, GA: Models and measurements." *Atmospheric Environment* 29: 3055-3066.

Sillman, S. and D. He (2002). "Some theoretical results concerning O3-NOx-VOC chemistry and NOx-VOC indicators." *Journal of Geophysical Research* 107: doi: 10.1029/2001JD001123.

Sillman, S., J. A. Logan and S. C. Wofsy (1990). "The sensitivity of ozone to nitrogen oxides and hydrocarbons in regional ozone episodes." *Journal of Geophysical Research* 95: 1837-1851.

Stauffer, D. R. and N. L. Seaman (1994). "Multiscale four-dimensional data assimilation." *Journal of Applied Meteorology* 33: 416-434.

Tang, Y. (2002). "A case study of nesting simulation for the Southern Oxidants Study 1999 at Nashville." *Atmospheric Environment* 36: 1691-1705.

Tian, D., Y. Hu and A. G. Russell. (2004). "Meteorological modeling of the 1999 August episode for the Fall-Line Air Quality Study." Prepared for Environmental Protection Division, Georgia Department of Natural Resources.

Tietenberg, T. H. (1980). "Transferable discharge permits and the control of stationary source air pollution: A survey and synthesis." *Land Economics* 56: 391-416.

Tolley, G. and B. Smith (2001). "Clearing Houston's Air: An Economic Evaluation of Clean Air Act Compliance Strategy Alternatives," (unpublished). Available at www.tppf.org/environment/clearing/clearing.pdf.

Trainer, M., D. D. Parrish, M. P. Buhr, R. B. Norton, F. C. Fehsenfeld, K. G. Anlauf, J. W. Bottenheim, Y. Z. Tang, H. A. Weibe, J. M. Roberts, R. L. Tanner, L. Newman, V. C. Bowersox, J. T. Meagher, K. J. Olszyna, M. O. Rodgers, T. Wang, H. Berresheim, K. L. Demerjian and U. K. Roychowdhury (1993). "Correlation of ozone with NOy in photochemically aged air." *Journal of Geophysical Research* 98: 2917-2925.

Trainer, M., D. D. Parrish, P. D. Goldan, J. Roberts and F. C. Fehsenfeld (2000). "Review of observation-based analysis of the regional factors influencing ozone concentrations." *Atmospheric Environment* 34: 2045-2061.

Trainer, M., E. J. Williams, D. D. Parrish, M. P. Buhr, E. J. Allwine, H. H. Westberg, F. C. Fehsenfeld and S. C. Liu (1987). "Models and observations of the impact of natural hydrocarbons on rural ozone." *Nature* 329: 705-707.

U.S.-EIA (2004). (U.S. Energy Information Administration), Monthly Energy Review (Table 1.9, p. 17).

U.S.-EPA (1997). "Opportunities to improve air quality through transportation pricing programs." Prepared by ICF Incorporated.

U.S.-EPA (1998). "Finding of significant contribution and rulemaking for certain states in the Ozone Transport Assessment Group region for purposes of reducing regional transport of ozone, FRL-6171-2." *Federal Register* 63 (207).

U.S.-EPA (1999). "Draft guidance on the use of models and other analyses in attainment demonstrations for the 8-hour ozone NAAQS." EPA-454-R-99-004.

U.S.-EPA (2001). "Cost of selective catalytic reduction (SCR) application for NOx control on coal-fired boilers." EPA-600/R-01-087.

U.S.-EPA (2004a). "Interstate Ozone Transport: Response to Court Decisions on the NOx SIP Call, NOX SIP Call Technical Amendments, and Section 126 Rules; Final Rule." *Federal Register* 69: 21603-21648.

U.S.-EPA (2004b). "8-hour ozone National Ambient Air Quality Standards; Final Rules." *Federal Register* 69: 23,858-23,951.

Unal, A., D. Tian, Y. Hu and A. G. Russell (2003). 2000 August Emissions Inventory for Fall Line Air Quality Study (FAQS). Prepared for Environmental Protection Division, Georgia Department of Natural Resources.

Wang, L. and J. B. Milford (2001). "Reliability of optimal control strategies for photochemical air pollution." *Environmental Science and Technology* 35: 1173-1180.

Wilkinson, J. G. and Y.-J. Yang (2000). Area of influence: Identifying regions whose sources potentially impact downwind air quality. Air Pollution Modeling and Its Application XIII, ed. S.-E. Gryning and E. Batchvarova, Kluwer Academic/Plenum Publishers, 127-135.

Yang, Y.-J., J. Wilkinson and A. Russell (1997). "Fast, direct sensitivity analysis of multidimensional photochemical models." *Environmental Science and Technology* 31: 2859-2868.

VITA

Daniel Cohan was born in Washington, D.C., in September 1976 and grew up in Dallas, Texas. He received his B.A. in Applied Mathematics from Harvard University, where his interest in atmospheric chemistry was sparked under the guidance of Professor Daniel Jacob. Daniel then served as a Fulbright Scholar to Australia, conducting atmospheric research at the Cooperative Research Centre for Southern Hemisphere Meteorology. He began graduate studies at Georgia Institute of Technology's School of Earth and Atmospheric Sciences (EAS) in 1999, studying initially under the advisement of Professor Bill Chameides before joining the research group of Professor Ted Russell to work on the Fall-Line Air Quality Study. During his Ph.D. studies, Daniel was the recipient of a National Science Foundation Graduate Research Fellowship, a Georgia Tech Presidential Scholarship, a Georgia Air & Waste Management Association Scholarship, and EAS Best Paper and Best Speaker awards. The author of three scientific papers and numerous conference presentations on topics including methyl iodide, pollutant-vegetation interactions, and regional air pollution, Daniel also has worked extensively with regional panels and lay audiences to promulgate understanding of the atmosphere. His implementation of a sensitivity analysis method into a regional air quality model has been adopted by numerous atmospheric research groups. Daniel married Sandi Kaye in 2002, and they live in Atlanta, Georgia.